A mechanistic link between histone mRNA homeostasis and piRNA biogenesis

Dissertation

Zur Erlangung des Grades

Doktor der Naturwissenschaften

Am Fachbereich Biologie

Der Johannes Gutenberg-Universität Mainz

Joana Sofia Costa Pereirinha

geboren am 1 Juni 1994 in Benavente, Portugal

Mainz, 2024

Dekan: Prof. Dr. Eckhard Thines

1.Berichterstatter: Prof. Dr. René F. Ketting

2.Berichterstatter: [redacted]

Tag der mündlichen Prüfung: 11 April 2025

Table of contents

List of abbreviations

Ago	argonaute protein
APA	alternative polyadenylation
AP-MS	affinity purification followed by mass spectrometry
ARE	AU rich element
Bb	Balbiani body
bp	base pair
CPM	counts per million mapped
CPS	cleavage and polyadenylation site
CPSF	cleavage and polyadenylation specificity factor
CTD	C-terminal domain
DNA	deoxyribonucleic acid
DoG	difference of Gaussian
dsRNA	double strand DNA
eAgo	eukaryotic argonaute protein
eIF	eukaryotic initiation factor
EJC	exon junction complex
EMS	ethyl methanesulfonate
EMSA	electrophoretic mobility shift assay
Endo-siRNA	endogenous short interfering RNA
ERH	enahncer of rudimentary
eTUDOR	extended TUDOR
Exo-siRNA	exogenous short interfering RNA
FDR	false discovery rate
FT	flow-through
gDNA	genomic DNA
GO	gene ontology
HCC	histone cleavage complex
HDE	histone downstream element
HLB	histone locus body
iCLIP	individual-nucleotide resolution UV crosslinking and immunoprecipitation
ICM	integrator cleavage module
IEI	intergenerational epigenetic inheritance
IP	immunoprecipitation
lncRNA	long non-coding RNA
m7G	7-methylguanosine
Mel	maternal effect lethal
MID	middle
miRNA	micro RNA
mRNA	messenger RNA
Mrt	mortal germline
MZT	maternal-to-zygotic transition

N/C	nuclear-to-cytoplasmic
NA	numerical aperture
ncRNA	non-coding RNA
NGM	nematode growth medium
NLS	nuclear localisation signal
NMD	non-mediated decay
nt	nucleotide
pAgo	prokaryotic argonaute protein
PAS	poly-adenylation signal
PFA	paraformaldehyde
PGC	primordial germ cell
PIC	pre-initiation complex
piRNA	PIWI-interaction RNAs
PPCF	protein production core facility
PUP	poly U polymerase
RACE	rapid amplification of cDNA ends
RBD	RNA-binding domain
RBP	RNA-binding protein
RD	replication-dependent
RISC	RNA-induced silencing complex
risiRNA	ribosomal short interfering RNA
RNA	ribonucleic acid
RNAe	RNA-induced epigenetic silencing RNAi
RNAi	RNA interference
RNP	ribonucleoprotein
ROI	region of interest
RPM	reads per million
RRM	RNA recognition motif
rRNA	ribosomal RNA
SD	standard deviation
sec	second
siRNA	short interfering RNA
SL	stem-loop
SLBP	stem-loop binding protein
SLIM	site-directed, ligase-independent mutagenesis
snoRNA	small nucleolar RNAs
SNP	single nucleotide polimorphisms
snRNA	small nuclear RNA
SOSS	sensor of single-stranded DNA
TEI	transgenerational epigenitc inheiritance
TENT	terminal nucleotidyltransferases
TF	transcription factor
TMG	2,2,7-trimethylguanosine
tRNA	transfer RNA

ts	temperature sensitive
tSAM	*t*-statistical analysis of microarrays
tsRNA	transfer RNA-derived small RNAs
TUT	terminal uridylytransferases
U snRNA	uridine-rich small nuclear RNAs
USTC	upstream sequene transcription complex
wt	wild type
Y2H	yeast-two-hybrid
ZGA	zygotic genome activation

List of figures

List of tables

Contribution to the thesis

The term ‘we’ is generally used throughout this thesis. Individual contributions to the work presented include iCLIP sequencing analysis performed by Anke Bush, and RNA sequencing analyses performed by Emil Karalaunov and Ann-Sophie Seistrup. Svenja Hellmann performed all *C. elegans* injections for the generation of new alleles and provided technical support. Rene Ketting contributed the AlphaFold3 predictions. Karim AboShawish assisted with the Y2H experiments. Carolina Ruivinho and Vindhya Jaya contributed with technical support in the EMS mutagenic screen. iCLIP sequencing, whole genome sequencing, and RNA sequencing were performed by the IMB Genomics Core Facility. Whole genome sequence analysis was performed by Nastasja Kreim. Mass-spectometry and data analysis were performed by the IMB Proteomics Core Facility. IMB Microscopy Core facility contributed greatly with technical assistance. Finally, ChatGPT (v3) was used for grammatical correction of the text. All other experiments were executed and analysed by me.

Summary

Germ cells play a fundamental role in evolution by containing all the necessary information for the development of a new organism. Numerous mechanisms have evolved to protect germ cells from unwanted changes, ensuring the correct transmission of information to the progeny. One such mechanism is the piRNA pathway, a highly conserved small RNA pathway best known for silencing transposable elements (TEs) in germ cells. In *C. elegans*, piRNAs predominantly target germline mRNAs and have only a modest effect on TEs regulation. Unlike other species, the loss of the piRNA pathway in *C. elegans* does not lead to acute sterility. piRNAs precursors are stabilised by binding to a complex known as PETISCO, which stimulates piRNA production. Surprisingly, although piRNAs are not essential for *C. elegans* development, PETISCO is crucial for their embryonic development. This apparent dual functionality is reflected by PETISCO's two interacting proteins: PID-1 and TOST-1. While *pid-1* mutants lack piRNAs and are viable, *tost-1* mutants have piRNAs but are embryonic lethal.

In this work, I found that PETISCO binds replication-dependent (RD) histone mRNAs and is essential for their homeostasis in the adult germline. This function depends on TOST-1, not PID-1, reflecting the dual functionality of PETISCO through its interacting proteins. Using various transgenic constructs, I found that histone expression is tightly regulated by the unique features of their transcripts, which complicates the investigation of their expression. Nonetheless, I demonstrated that altering histone concentrations, either through genetic depletion or by impairing degradation pathways, regulates embryogenesis and influences the fate of development or arrest. I propose that the maternal effect lethal phenotype of PETISCO mutants is a result of histone mRNA loss. Additionally, I found that PETISCO mutants exhibit widespread gene expression misregulation in early embryos and premature gene activation. I propose that PETISCO stabilizes maternal histone mRNA in the germline, ensuring their proper deposition into embryos, where they are essential for the earliest cell divisions.

Overall, this study, combined with our previous work, proposes that PETISCO functions to stabilise inherently unstable transcripts: in the germ cells, piRNA precursors are stabilized to enable processing into piRNAs, while maternal RD histone mRNAs are stabilized to provide the early embryo with sufficient histone proteins. Evolutionary analysis of PID-1 and TOST-1 indicates that the RD histone mRNA stabilization function likely pre-dates PETISCO's role in piRNA production. Hence, piRNA biogenesis may have evolved from a maternal mRNA stabilisation mechanism.

Zusammenfassung

Keimzellen spielen eine grundlegende Rolle in der Evolution, da sie alle notwendigen Informationen für die Entwicklung eines neuen Organismus enthalten. Zahlreiche Mechanismen haben sich entwickelt, um Keimzellen vor unerwünschten Veränderungen zu schützen und die korrekte Weitergabe von Informationen an die Nachkommen sicherzustellen. Einer dieser Mechanismen basiert auf piRNAs, konservierte, kurze RNAs, die vor allem für die Stilllegung von Transposon-Elementen (TEs) in Keimzellen bekannt sind. In *C. elegans* regulieren piRNAs überwiegend Boten-RNAs (mRNAs) der Keimbahn und haben nur einen geringen Einfluss auf TEs. Im Gegensatz zu anderen Arten führt der Verlust von piRNAs in *C. elegans* nicht zu akuter Sterilität. piRNA-Vorläufer werden durch Bindung an einen Komplex namens PETISCO stabilisiert, der die piRNA-Produktion stimuliert. Obwohl piRNAs nicht essenziell für die Entwicklung von *C. elegans* sind, ist PETISCO überraschenderweise entscheidend für die embryonale Entwicklung. Diese scheinbare doppelte Funktionalität spiegelt sich in den beiden interagierenden Proteinen von PETISCO wider: PID-1 und TOST-1. Während *pid-1*-Mutanten keine piRNAs haben, aber lebensfähig sind, weisen *tost-1*-Mutanten piRNAs auf, zeigen jedoch embryonale Letalität.

In dieser Arbeit habe ich herausgefunden, dass PETISCO replizierungsabhängige (RD) Histon-mRNAs bindet und für deren Homöostase in der Keimbahn adulter Tiere essenziell ist. Diese Funktion hängt von TOST-1 ab, jedoch nicht von PID-1, was die doppelte Funktionalität von PETISCO durch seine interagierenden Proteine widerspiegelt. Mithilfe verschiedener transgener Konstrukte konnte ich zeigen, dass die Histonexpression durch die einzigartigen Eigenschaften ihrer Transkripte streng reguliert wird, was die Untersuchung ihrer Expression erschwert. Dennoch konnte ich nachweisen, dass Veränderungen der Histonkonzentration, entweder durch genetische Depletion oder durch Beeinträchtigung von Abbauwegen, die Embryogenese regulieren und den Entwicklungsprozess oder Stillstand beeinflussen. Ich präsentiere ein Model, indem der maternal-letale Phänotyp von PETISCO-Mutanten eine Folge des Verlustes von Histon-mRNAs ist.

Darüber hinaus habe ich festgestellt, dass PETISCO-Mutanten eine weit verbreitete Fehlregulation der Genexpression in frühen Embryonen sowie eine vorzeitige Genaktivierung aufweisen. Ich postuliere, dass PETISCO maternale Histon-mRNAs in der Keimbahn stabilisiert, um ihre ordnungsgemäße Einlagerung in Embryonen zu gewährleisten, wo sie für die frühesten Zellteilungen essenziell sind.

Insgesamt zeigt diese Studie, zusammen mit unseren früheren Arbeiten, dass PETISCO dazu dient, von Natur aus instabile Transkripte zu stabilisieren: In Keimzellen werden piRNA-Vorläufer stabilisiert, um deren Verarbeitung zu piRNAs zu ermöglichen, während maternale RD-Histon-mRNAs stabilisiert werden, um dem frühen Embryo ausreichende Histonproteine bereitzustellen. Eine evolutionäre Analyse von PID-1 und TOST-1 deutet darauf hin, dass die Funktion von PETISCO bei der Stabilisierung von RD-Histon-mRNAs wahrscheinlich der Rolle bei der piRNA-Produktion vorausgeht. Somit könnte die piRNA-Biogenese aus einem Mechanismus zur Stabilisierung von maternalen mRNAs hervorgegangen sein.

INTRODUCTION

General introduction

Embryogenesis is the key process in establishing animal life, transforming a single-celled zygote into a mature organism. This dynamic and intricate process is tightly regulated by maternal and paternal cues, with control gradually shifting to the embryo's own regulatory systems as development progresses. Germ cells, specialized haploid cells, fuse to form the zygote, transmitting not only genetic information but also gene-regulatory elements, which are not encoded in the genome, and the necessary material to support the early stages of embryonic development.

RNA is a crucial molecule in life cycle and development, beyond serving as the intermediary between genes and proteins, RNA is integral to gene regulation and transmission. RNA molecules exist in many sizes and structures, with diverse roles, ranging from catalytic activity to regulatory functions. A common feature among many RNA molecules is their specific association with a vast array of RNA-binding proteins (RBPs), forming ribonucleoproteins (RNPs) that are essential in many pathways within the organism.

In this introduction, I will provide a brief overview of RNPs, focusing specifically on Argonaute proteins and their co-factors, small RNAs, and their role in epigenetic inheritance. I will highlight PETISCO, an RNP complex in *Caenorhabditis elegans*, the model organism used in this work. I will discuss the processes involved in the oocyte-to-embryo transition, emphasizing the central role RNPs play in regulating these events. I will also describe the mRNA life cycle, which is not only tightly regulated during this transition but throughout the organism's life. Following this, I will focus specifically on replication-dependent (RD) histone mRNAs, which are a unique class of mRNAs with distinct structural features and specialized regulatory mechanisms. While I will introduce these mechanisms broadly, based on studies in various model organisms, I will also focus on what is known specifically in *C. elegans*. Finally, I will briefly describe *C. elegans* early embryogenesis and germline development.

Ribonucleoprotein complexes

RNA has increasingly proven that the biology central dogma of - DNA to RNA to Protein - is just a small part of RNA's diverse functions. RNA exists in many different forms, such as messenger RNA

(mRNA), transfer RNA (tRNA), ribosomal RNA (rRNA), small nuclear RNA (snRNA), micro RNA (miRNA), long non-coding RNA (lncRNA), PIWI-interacting RNA (piRNA), etc, each playing active or regulatory roles in gene expression. For most of their functions, RNAs need to bind to proteins known as RNA-binding proteins (RBPs). RBPs are present throughout the entire life-cycle of RNA, from synthesis to processing and decay, and they typically function within multi-protein complexes called ribonucleoproteins (RNPs). Most RBPs do not possess intrinsic enzymatic activity; instead, their assembly with RNA and other proteins primarily mediates the recruitment of effectors or triggers certain reactions. RBPs can bind to specific RNA sequences and/or structural motifs in RNA via a set of structurally well-defined RNA-binding domains (RBDs) such as the RNA recognition motif (RRM), hnRNP K homology domain, DEAD box helicase domain or zinc-finger domain. An RBP can interact with RNA to regulate RNA function and metabolism (Lee & Lykke-Andersen, 2013). Conversely, some RNAs can also regulate the function of RBPs (Hentze et al., 2018). Two of the best-characterized RNP complexes are the ribosome (Ramakrishnan, 2014) and the spliceosome (Matera & Wang, 2014). However, there has been increasing effort to identify and describe smaller RNPs and novel RBPs, collectively referred to as the RNA interactome (Hentze et al., 2018). Beyond mRNAs, rRNAs and snRNAs, which are part of these well-known RNPs, other categories of non-coding RNAs (ncRNAs), such as miRNAs, piRNAs, lncRNAs also interact with RBPs to form RNPs (Gerstberger et al., 2014).

Although RBPs are often categorized based on the class of RNA they bind to, some RBPs can interact with and regulate multiple RNA classes. For example, the RNA exosome is involved in general RNA turnover (Kilchert et al., 2016), while the LIN28 protein binds to let-7 pre-miRNAs, mRNAs and small nucleolar RNAs (snoRNAs) (Mayr & Heinemann, 2013). RBP families are well-conserved across eukaryotes, with some orthologous groups traceable to the last universal common ancestor (Anantharaman et al., 2002; Kerner et al., 2011). While ribosomal proteins are amongst the most conserved RNPs, ncRNA-binding proteins exhibit the lowest levels of conservation (Gerstberger et al., 2014).

RNPs are dynamic and complex structures that involve multivalent interactions including protein-protein, protein-RNA and RNA-RNA interactions. Under specific conditions, some of these assemblies promote the formation of membraneless organelles called RNP granules. RNP granules are present in both the cytoplasm and the nucleus and play an essential role in various cellular processes, such as stress response (stress granules), gene expression and regulation (Cajal bodies) and RNA metabolism (P-bodies) (Ripin & Parker, 2023). They can either be ubiquitously present within the cell or appear transiently and some can be cell-type specific, such

as neuronal granules and germ cell granules. In contrast, other RNPs, such as the spliceosome or translation initiation complexes, operate in the nucleoplasm or cytoplasm without forming granules.

Argonaute proteins and small RNAs complexes

Argonaute proteins (Agos) are a large family of RBPs that assemble with a class of ncRNAs, known as small RNAs, forming an ncRNP complex called RNA-induced silencing complex (RISC), which is involved in target silencing through a mechanism called RNA interference (RNAi) (Fire et al., 1998; Iwakawa & Tomari, 2022; R. F. Ketting, 2011). These complexes, via base pairing of the small RNA, can regulate gene expression and mediate post-transcriptional and/or transcriptional silencing. Argonaute proteins are highly conserved and can be found in nearly all eukaryotes, and many prokaryotes, and archaea. While eukaryotic Agos (eAgos) and prokaryotic Agos (pAgos) have low sequence homology, their structure and function are remarkably conserved across organisms (Olina et al., 2018; Swarts, Makarova, et al., 2014). Most Agos are guided by a small RNA to regulate gene silencing but some pAgos use DNA as a guide (Swarts, Jore, et al., 2014; Wang et al., 2008). The number of Agos varies considerably between species, with one present in the fission yeast *Schizosaccharomyces pombe*, four in humans, and 19 in the nematode *Caenorhabditis elegans.* Based on their domain structure, the eAgo protein family is divided into four subfamilies based on their similarity to specific and well-studied Argonaute proteins of various model organisms: the AGO, giving their similarity to AGO1 of *Arabidopsis thaliana*; the PIWI, giving their close similarity to PIWI of *Drosophila melanogaster;* the worm-specific WAGO and the Trypanosoma Ago subfamilies. All eAgos share four main domains: the N-terminal domain, the PAZ domain, the MID domain and the PIWI domain. The N-terminal domain unwinds small RNA duplexes during RISC assembly, the PAZ domain contains a specific binding pocket that anchors the 3'end overhang produced during the processing of small RNAs; the MID domain binds the 5' phosphate characteristic of small RNAs; and the PIWI domain exhibits catalytic activity similar to RNase H (P. B. Kwak & Tomari, 2012; J. B. Ma et al., 2005; Parker et al., 2004, 2005; Rashid et al., 2007; Song et al., 2004; Yuan et al., 2005).

Small RNAs can be divided into different families including miRNAs, piRNAs and small-interfering RNAs (siRNAs), each of these assembling with specific Agos. However, the mechanisms of small RNA biogenesis and amplification vary greatly between organisms (Carthew & Sontheimer, 2009; Ozata et al., 2019). miRNAs and siRNAs are generated from double-stranded RNA (dsRNA) precursors that are cleaved by RNase III family enzymes, Drosha and/or Dicer. piRNAs on the

other hand, are produced from single-stranded RNAs, independent of Dicer and Drosha, mainly acting in germ cells to protect against invasive genomic elements. Interestingly, there is growing evidence that piRNAs also regulate endogenous genes (Ozata et al., 2019).

The specific combination of a small RNA with a particular eAgo determines the biological function of the RNP complex. These mechanisms can be cytoplasmic or nuclear and include the regulation and silencing of endogenous and exogenous genetic elements. Functions range from RNA degradation via cleavage or deadenylation, and translation inhibition, to chromosome structure modification or DNA methylation (Czech & Hannon, 2010; Nazer et al., 2022; J. Wu et al., 2020). The effector activity of Ago varies, as not all miRNA::AGO complexes possess catalytic activity or cleave their targets. On the other hand, complexes involving siRNAs or piRNAs with their respective Agos often exhibit endonuclease activity (Faehnle et al., 2013; Hauptmann et al., 2013, 2014; Nakanishi et al., 2013). In *C. elegans*, however, the PIWI protein has lost its cleavage activity and instead it makes their targets as templates for RNA-dependent RNA polymerases (RdRPs) to produce secondary small RNAs. These secondary small RNAs, in turn, work with a secondary Argonaute to drive the effector response (Ketting & Cochella, 2020).

Interestingly, small RNAs can also be inherited, perpetuating gene silencing across generations—one of the mechanisms of epigenetic inheritance. Mechanisms such as RNA interference in *C. elegans* or maternal piRNAs in *Drosophila* are two examples of heritable propagation of small RNA responses (Quarato et al., 2022), which, among others, are described in more detail below.

PETISCO - an RNP complex involved in piRNA biogenesis

PETISCO is a cytoplasmic multi-subunit complex that binds piRNA precursors in *C. elegans* (Cordeiro Rodrigues et al., 2019; Zeng et al., 2019). The biogenesis of *C. elegans* piRNAs differs significantly from that in mice and *Drosophila*; thus, they are referred to as 21U-RNAs. Mature 21U-RNAs are 21 nucleotides long, have a uracil bias at the 5' end, and associate with the *C. elegans* PIWI protein, PRG-1 (Batista et al., 2008; Das et al., 2008; G. Wang & Reinke, 2008). 21U-RNAs can be divided into type I and type II, based on their transcription mechanism. Type I 21U-RNAs precursors are transcribed from tens of thousands of miniature genes clustered on chromosome IV, with each gene located downstream of a specific sequence motif called the Ruby-motif (Ruby et al., 2006). The USTC protein complex recognizes this motif and stimulates transcription by RNA polymerase II (RNA pol II) (Weng et al., 2019). USTC contains the transcription factor SNPC-4, part of the snRNA-activating complex (Kasper et al., 2014), PRDE-1, a nuclear germline-expressed protein specifically found in piRNAs clusters (Weick et al., 2014),

and TOFU-4 and TOFU-5, initially identified in a genome-wide RNAi screen as being required for piRNAs expression (Goh et al., 2014). Type II 21U-RNAs are much less abundant and are transcribed from protein-coding genes and other RNA pol II transcripts that lack the Ruby-motif (Gu et al., 2012). Each 21U-RNA precursor has a 7-methylguanosine (m7G) cap and is approximately 28 nucleotides long (Gu et al., 2012). Transcript termination is regulated by the Integrator complex, which controls promoter-proximal Pol II pausing and cleaves the nascent precursors (Beltran et al., 2020; Berkyurek et al., 2021).

PETISCO stabilizes 21U-RNAs precursors for 5' end processing by the recently identified endoribonuclease complex PUCH, creating the 5' monophosphate end (Podvalnaya et al., 2023). Afterwards, the 21U-RNA intermediates are loaded onto PRG-1, and the 3' ends are trimmed and 2′-O-methylated by PARN-1 and HENN-1 respectively (Billi et al., 2012; Kamminga et al., 2012; T. A. Montgomery et al., 2012; Tang et al., 2016). These modifications stabilize small RNAs and prevent their degradation (Ameres et al., 2010; Pastore et al., 2021, 2024).

PETISCO structure

PETISCO is composed of the subunits PID-3, ERH-2, TOFU-6, and IFE-3 (Cordeiro Rodrigues et al., 2019; Zeng et al., 2019). It forms a dimer of tetramers, with a total molecular weight of 230 kDa, where dimerization is mediated by both PID-3 and ERH-2 (Figure I1) (Perez-Borrajero et al., 2021; X. Wang et al., 2021). Interestingly, PETISCO has two effector proteins, PID-1 and TOST-1, which control its function. These proteins lack identifiable domains, and their mechanism of action as effector proteins is still unknown. However, it is speculated that their function may be related to their differential expression throughout germline development.

PID-3 and TOFU-6 are specific to the nematode phylum, PID-3 has an RRM domain and a MID domain, similar to those found in Agos, while TOFU-6 has an RRM domain, an extended TUDOR (eTUDOR) domain, and a C-terminal eIF4E interaction motif. The RRM domains of PID-3 and TOFU-6 mediate their interaction, where both sides of the symmetric PID-3 RRM dimer interface recruit a single TOFU-6 RRM (Perez-Borrajero et al., 2021; X. Wang et al., 2021). IFE-3 is one of the five highly conserved *C. elegans*' eIF4E homologs, known for binding m7G caps (Jankowska-Anyszka et al., 1998; Keiper et al., 2000). Finally, ERH-2 is one of two "enhancer of rudimentary" (Erh) homologs in *C. elegans*, a highly conserved protein across eukaryotes. ERH has been implicated in the RNA decay pathway in *Schizosaccharomyces pombe* (Sugiyama et al., 2016), the processing of miRNAs (Chul Kwon et al., 2020; Fang & Bartel, 2020), and the regulation of gene expression in human cells (Katznelson et al., 2024; McCarthy et al., 2021). ERH-2 binds to PID-3

and to PID-1 or TOST-1. The latter interactions are bound via a shared sequence motif in both proteins and they mutually exclusively bind to ERH-2. TOST-1 binds more strongly to ERH-2 than PID-1 does (Perez-Borrajero et al., 2021). The RNA binding site of PETISCO has not yet been identified, but it is possible that the RRM domain of TOFU-6 and/or the cap-binding protein IFE-3 are responsible for this function.

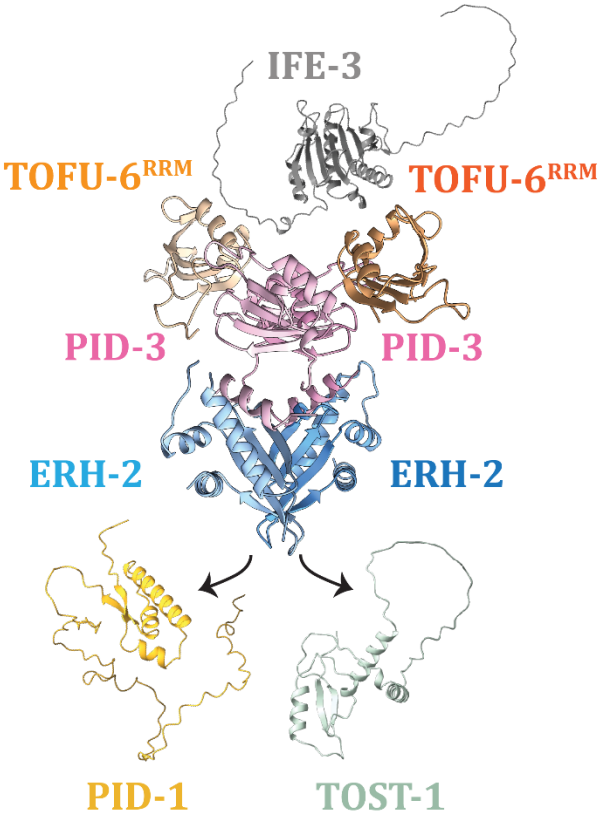

Figure I1 | Structure of PETISCO. Modelling of the PETISCO core complex by combining the crystal structures of PID-3^{RRM}/TOFU-6^{RRM} and ERH-$^{2\Delta C}$/PID-3^{pep} subcomplexes. TOFU-6 is coloured in orange, PID-3 in pink and ERH-2 in blue (Perez-Borrajero et al., 2021). Alphafold2 predictions of IFE-3 (grey), PID-1 (yellow) and TOST-1 (green).

PETISCO localisation and further functions

PETISCO associates with P granules in germ cells but is also found in the cytoplasm of oocytes and embryos (Cordeiro Rodrigues et al., 2019; Zeng et al., 2019). Interestingly, when the interaction between ERH-2 and PID-3 is abolished, ERH-2 localises to the nucleus and the same is observed for TOST-1 in oocytes of *erh-2* mutants (X. Wang et al., 2021). PID-3, however, retains its cytoplasmic location even when it is not bound to ERH-2, but it becomes nuclear when losing the interaction with TOFU-6 (Perez-Borrajero et al., 2021; X. Wang et al., 2021). These results indicate that the interplay between the different components of PETISCO is essential for ensuring

proper localisation and function within the cell, and reveal inherent nuclear localisation of some of the PETISCO subunits. The relevance of this has remained unclear.

As previously shown by Cordeiro Rodrigues et al. and Zeng et al., PETISCO's functions depend on the effector proteins PID-1 and TOST-1. TOST-1 is not required for 21U-RNA processing but is crucial for embryonic development. Mutants for PETISCO proteins exhibit a maternal-effect embryonic lethality (Mel) phenotype, meaning that while the first-generation homozygous mutants develop to adulthood, their progeny arrests development during embryogenesis. F1 embryos show defects in chromosome segregation during cell division, which ultimately leads to embryonic arrest (Zeng et al., 2019). This phenotype was previously observed in *tofu-6* mutants (Minasaki & Streit, 2007).

Additionally, PETISCO was reported to interact with a type of snRNAs, the splice-leader 1 (SL1), involved in *trans*-splicing in *C. elegans* (Cordeiro Rodrigues et al., 2019). Mutants of *erh-2*, *tost-1* and *ife-3* show an accumulation of both splice leader RNAs of *C. elegans*, SL1 and, to a lesser extent, SL2 (Cordeiro Rodrigues et al., 2019). IFE-3 was also found to interact with components of the SMN complex, a key processor of snRNAs into snRNPs and involved in SL1 *trans*-splicing (Philippe et al., 2017). These results highlight a potential, and previously hypothesized, parallel between snRNAs and piRNAs in *C. elegans*, where PETISCO, together with TOST-1 or PID-1, may play a dual role (Beltran et al., 2019, 2020; Kasper et al., 2014; Weng et al., 2019).

Epigenetic inheritance

Apart from DNA sequences, gene regulatory determinants are transmitted from parental gametes to the zygote. This mechanism, known as epigenetic inheritance, can persist for one or two generations, depending on whether it is paternal or maternal, a phenomenon termed intergenerational epigenetic inheritance (IEI). Alternatively, it can extend over multiple generations, known as transgenerational epigenetic inheritance (TEI). The factors involved in epigenetic inheritance are transmitted across generations and can regulate gene expression, either silencing or activating it, without altering the DNA sequence. This allows future generations to inherit the induced phenotypic trait without exposure to the initial environmental cause. Because these changes are highly dynamic and flexible, organisms can adapt their genetic output without permanent changes to the DNA. Epigenetic inheritance derived from gametes involves various mechanisms such as DNA methylation, histone post-translational modifications,

and the transfer of ncRNAs (Santilli & Boskovic, 2023; Skvortsova et al., 2018). For the purpose of this study, I will focus on the inheritance of small ncRNAs.

Epigenetic inheritance of small RNAs

RNAi inheritance is the most well-studied mechanism of TEI in *C. elegans* and can last for many generations (Vastenhouw et al., 2006). For example, worms expressing a GFP::H2B reporter in the germline and exposed to *gfp* dsRNA show silencing of the *gfp* transcript until the generation F2, which was not exposed to the *gfp* dsRNA. The exogenous dsRNA, introduced via feeding with bacteria expressing dsRNA, triggers the RNAi response in P0 through exogenous siRNA (exo-siRNAs), leading to the amplification of secondary siRNAs. These secondary siRNAs, produced by RdRPs, are inherited to subsequent generations, ensuring the continuity of the response (Almeida et al., 2019; F. R. Ketting & Cochella, 2020). The target genes are silenced through the formation of heterochromatin domains and inhibitions of RNA Pol II but also via post-transcriptional mechanisms (Frolows & Ashe, 2021).

Similar responses are observed when the initial trigger are endogenous siRNAs (endo-siRNAs) (Alcazar et al., 2008) or piRNAs/21U-RNAs (H. C. Lee et al., 2012; Luteijn et al., 2012; Shirayama et al., 2012). Silencing triggered by piRNAs produced from endogenous loci is called RNA-induced epigenetic silencing (RNAe). RNAe can persist for many generations, and although it needs piRNAs for *de novo* establishment, the silencing of the target transcripts is maintained in their absence (Ashe et al., 2012; Luteijn et al., 2012; Shirayama et al., 2012). In fact, RNAe can become permanent if piRNAs are lost, as they prevent germline-expressed mRNAs from entering self-perpetuating silencing pathways (Shukla et al., 2021). Maternally provided piRNAs in *C. elegans* are sufficient to trigger the silencing of their targets in embryos and are necessary to prevent silencing of non-targets (de Albuquerque et al., 2015; Placentino et al., 2021)

The inheritance of some populations of endo-siRNAs is crucial for embryonic development (Gerson-Gurwitz et al., 2016; Quarato et al., 2021). In *C. elegans*, the Argonaute protein CSR-1 binds to secondary siRNAs that are generated from germline mRNAs. The loading and activity of CSR-1 with the small RNAs, in embryos, are required for the clearance of untranslated maternal mRNAs (Quarato et al., 2021). Besides CSR-1 and its cognate siRNAs are also hypothesized to license the expression of self-transcripts by protecting them from piRNAs-dependent silencing (Seth et al., 2013; Wedeles et al., 2013).

In mouse embryos, maternal Ago2 is essential for embryonic development and it might also be required for the degradation of maternal mRNAs (Svoboda & Flemr, 2010; J. M. Zhang et al., 2020). Additionally, transfer RNA-derived small RNAs (tsRNAs) are emerging as potential inherited small RNAs via sperm in mammals (Q. Chen et al., 2021). In *Drosophila*, piRNAs and PIWI proteins are maternally inherited to silence TEs in the embryo (Brennecke et al., 2008). The silencing is maintained in the germline of adult flies and transmitted to the next generation (Fabry et al., 2021). The inheritance of maternal piRNAs is essential for their development, as piRNA-defective embryos result in female sterility (Akkouche et al., 2017).

Contrary to *Drosophila* and many other animals, *C. elegans* lacking piRNAs are initially fertile but they gradually lose their fertility across generations until becoming completely sterile (Simon et al., 2014). This phenomenon is called mortal germline (Mrt) phenotype. The cause for this defect is unknown, but it is not clearly related to transposon reactivation (Barucci et al., 2020; Reed et al., 2019; Simon et al., 2014; Spichal et al., 2021). Recent studies attribute the loss of fertility to a stochastic activation of secondary small RNAs, causing aberrant target silencing, mainly of histones and rRNAs. Once initiated, this silencing occurs consistently across generations (Barucci et al., 2020; B. E. Montgomery et al., 2021; Reed et al., 2019; Wahba et al., 2021).

Germ granules in early development

Germ granules are defined as a collection of dynamic, germline-specific, membrane-less organelles. Some models propose that their function is to bring specific proteins and nucleic acids together in space and time, promoting their activity (Ripin & Parker, 2023). Germ granules are also responsible for transmitting specific components, such as small RNAs, mRNAs or proteins, to the zygote and preventing premature translation of maternally provided mRNAs (C.-Y. S. Lee et al., 2020; Mukherjee & Mukherjee, 2021; Phillips & Updike, 2022; Scholl et al., 2024; Voronina et al., 2011).

Drosophila has a great variety of germ granules involved in RNA storage, transport, and regulation, germline specification, and defence against transposons. Structures like nuage, sponge bodies, Balbiani body (Bb), and cytoplasmic polar granules are necessary for the transport and deposition of maternal mRNAs and proteins from the oocyte to the embryo (Mukherjee & Mukherjee, 2021). Interestingly, the Balbiani body is responsible for incorporating mitochondria into the germline and is thought to be needed for its inheritance (Bilinski et al., 2017; R. T. Cox & Spradling, 2003). The Bb is a highly conserved structure found from insects to humans. In *Xenopus* and zebrafish, it is also essential for germplasm assembly, germ cell

specification and ultimately, embryo development. Mammalian oocytes also contain a Bb that is important for organelle distribution and RNA regulation (Jamieson-Lucy & Mullins, 2019). The germ granules in mammalian oocytes are known to dissolve in mature oocytes and to re-establish *de novo* in primordial germ cells (Voronina et al., 2011). In male germ cells of mammals, a distinct type of granule known as chromatoid bodies is present. These structures are enriched with mRNAs and proteins, including histones and Argonautes. However, they disintegrate as sperm mature (Chuma et al., 2009).

In *C. elegans*, P granules were the first germ granules discovered (Strome & Wood, 1982). They segregate with the P lineage throughout embryogenesis and are visualized at every stage of germline development (Phillips & Updike, 2022). P granules are heterogeneous structures, and their composition of proteins and RNAs differs depending on the developmental stage. Unlike in *Drosophila*, P granules in *C. elegans* are not required for germ cell specification but only later in development to keep germ cell identity (Seydoux, 2018; D. Updike & Strome, 2010). P granules house a repertoire of small endogenous RNAs as well as Argonaute proteins and other proteins involved in small RNA biogenesis. During most stages of germline development, P granules associate with the nuclear pore. It is thought that, due to this association, P granules sort and select transcripts for translation, based on the small RNA machinery within them (Campbell & Updike, 2015; Gerson-Gurwitz et al., 2016; D. L. Updike et al., 2011). Later in germline development, P granules divide into substructures, such as *Mutator* foci, Z granules and SIMR granules, which contain different components and have distinct functions in the small RNA pathways. However, both components and functions are thought to be interchangeable (Phillips & Updike, 2022).

Maternal-to-zygotic transition

At the beginning of animal development, differentiated mature germ cells are reprogrammed to create a totipotent zygote. This allows the zygotic to subsequently drive the differentiation of all necessary adult cell types. This reprogramming is possible by the accumulation of maternal mRNAs and proteins in the oocyte. The development of early embryos requires specific maternal products that are regulated in three mechanisms: direct movement of the maternal material, localised stabilization of maternal proteins, or localised stabilization and translation of maternal

mRNAs. This coordination of events is called maternal-to-zygotic transition (MZT), and although the mechanisms vary across organisms, it can be divided into two major phases: the degradation of maternal gene products and the onset of transcription from the zygote's genome.

Maternal deposition in the embryo

All animal oocytes are loaded with mRNAs to be deposited in the embryo. Global analyses suggest that the proportion of maternal transcripts relative to the zygote protein-coding transcriptome ranges from about one-third in the mouse (Q. T. Wang et al., 2004) and *C. elegans* (Baugh et al., 2003; Stoeckius et al., 2014) to three-quarters in *Drosophila* (Thomsen et al., 2010) and zebrafish (Aanes et al., 2011; Harvey et al., 2013).

In *C. elegans*, many of the maternal mRNAs are deposited via RNP granules and encode RBPs that are essential in the specification of early blastomere fates (Schisa et al., 2001). Additionally, the 3' UTRs of many maternally supplied mRNAs contain specific signals for RNP binding, allowing precise and strict control of the spatiotemporal expression pattern of these maternal mRNA (Robertson & Lin, 2015).

Regulation of mRNA stability and clearance

Although the deposition of maternal material is essential for embryo development, some products become harmful after fertilization and need to be cleared rapidly (G. Yang et al., 2024). Maternal mRNAs are degraded in the embryo in a phased manner, and the scale and dynamics of these phases vary among species. However, in general, the first phase is directed by maternally provided elements, while the later phases depend on zygotic elements (Vastenhouw et al., 2019). Maternal mRNAs can remain stable for long periods in the oocytes but are rapidly degraded in the embryos. These processes are regulated by RBPs, small non-coding RNAs, RNA modifications, and other mechanisms (Figure I2) (Despic & Neugebauer, 2018). The RBPs that regulate maternal transcripts appear to vary across species. For example, Y-box proteins in zebrafish and mouse translationally repress and stabilize maternal transcripts in oocytes (Medvedev et al., 2011; Sun et al., 2018). In *Drosophila* and *C. elegans*, Y-box proteins are expressed in oocytes but do not seem to play a role in transcript stabilization; instead, a Dead-box helicase has been implicated in this function (A. Arnold et al., 2014; Boag et al., 2005; M. Wang et al., 2017). miRNAs also influence maternal transcript decay in multiple species, including *C. elegans* (Giraldez, 2010; Svoboda & Flemr, 2010). In *Drosophila,* it was also found that piRNAs and the PIWI protein bind

to maternal mRNAs in the early embryo and are involved in the decay of one of them (Barckmann et al., 2015; Rouget et al., 2010). Additionally, endo-siRNAs are suggested to be involved in the depletion of a subset of maternal mRNAs in *C. elegans* embryos (Stoeckius et al., 2014). RNA modifications, such as m6A or m5C, and the uridylation of poly(A) tails on maternal mRNAs, are also involved in maternal transcripts decay in vertebrates (Chang et al., 2018; Y. Yang et al., 2019; B. S. Zhao et al., 2017).

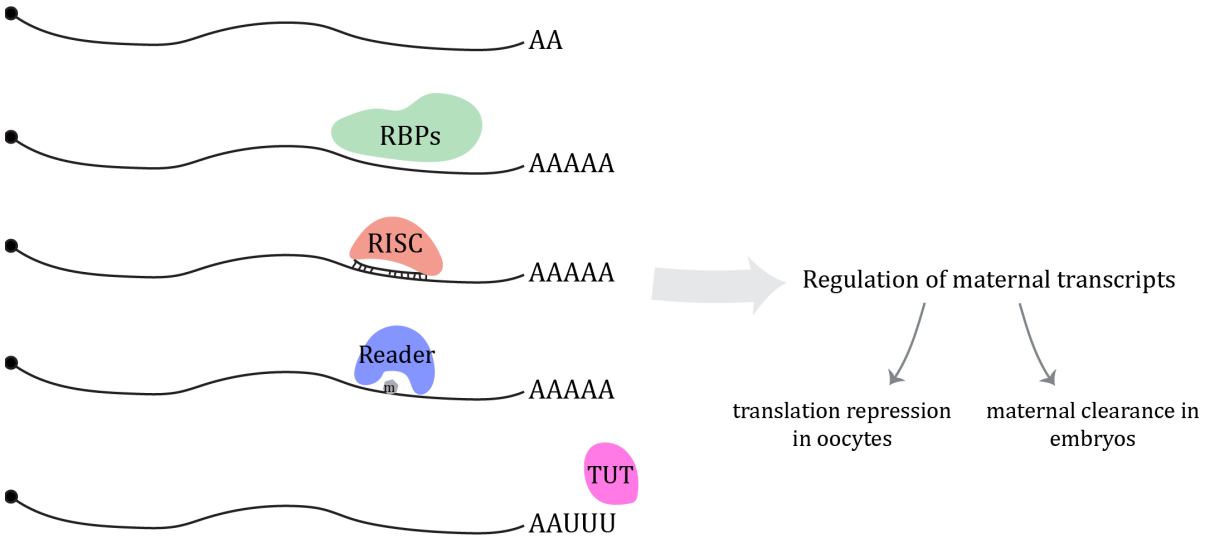

Figure I2 | Mechanisms of maternal transcript regulation. Organisms utilise various mechanisms to regulate maternal transcripts in the germline and later in the zygote. Short poly(A) tails typically lead to rapid degradation or translational repression. Different RNA-binding proteins (RBPs) have been reported to repress translation or to trigger transcript degradation via deadenylation. MicroRNAs and endo-siRNAs mediate maternal transcript decay via the RISC. RNA modifications, such as m5C and m6A, along with their respective reader proteins, play roles in stabilizing or degrading maternal transcripts. Additionally, terminal uridylation by TUT proteins is implicated in targeted degradation of maternal transcripts during MZT. Schematic illustration adapted from (Vastenhouw et al., 2019; G. Yang et al., 2024).

Translational control of maternal mRNAs

Most maternal mRNAs destined for the embryos are transcribed in the germ cells during mitosis or early meiosis and become repressed during oocyte development. In embryos, the early cell cycles are rapid, and the cell polarization (in some species, such as *C. elegans*) occurs in the first two cycles; therefore, the control of the maternal mRNAs needs to be precise. In most cases, translational regulation is dependent on the 3' UTR of maternal mRNAs, which is sufficient to confer the correct temporal and special expression patterns (Merritt et al., 2008). The poly(A) tail may play a role in the regulation of translation during MZT. In several organisms, like

zebrafish or frog, there is a correlation between the length of poly(A) tails and translation efficiency in early embryos, which is not found in non-embryonic tissues (Subtelny et al., 2014).

In *C. elegans*, the cytoplasmic polyadenylation and deadenylation are also involved in mRNA stability and translation during MZT (Tsukamoto et al., 2017). Maternal mRNA translational regulation is based on distinct elements, such as GLD-1, MEX-3 or POS-1, which can repress translation in the germline and/or activate it in the embryos (Evans & Hunter, 2005). During the first few embryonic divisions, MZT is driven primarily by maternal mRNA translation. This is evidenced by the observation that inhibition of zygotic transcription by knocking down RNA Pol II results in no observable phenotype until the 28-cell stage, when gastrulation begins (Powell-Coffman et al., 1996).

Post-translational regulation of maternal proteins

The maternal proteome is highly regulated in oocytes and embryos. A conserved mechanism of phosphorylation and ubiquitin-dependent proteolysis occurs during MZT in diverse organisms, such as *C. elegans*, *Drosophila* and mice (Toralova et al., 2020; Vastenhouw et al., 2019). Other protein degradation pathways, such as autophagy and endocytosis, are also involved in maternal protein degradation (Toralova et al., 2020).

In *C. elegans* early embryos, for instance, the maternally provided OMA-1 and OMA-2 proteins are phosphorylated and sequester a general transcription factor TAF-4 in the cytoplasm, preventing its import into the nucleus. By the four-cell stage, the OMAs are ubiquitylated and degraded, releasing TAF-4 to initiate zygotic transcription (Guven-Ozkan et al., 2008).

Zygotic genome activation

The onset of zygotic transcription involves a gradual activation, and the timing of the cell cycles and the first zygotic transcripts differs depending on the organism. In humans and mice, the first zygotic transcripts are produced at the one-cell stage, while in *C. elegans*, zebrafish and *Drosophila*, zygotic transcription begins at cell cycles 2, 6 and 8, respectively (Figure I3) (Schulz & Harrison, 2019). During zygotic genome activation (ZGA), a significant fraction of genes are transcribed (between 5% and 35%, depending on the organism) but the specific set of genes differs in different species (Vastenhouw et al., 2019). Some of the genes transcribed during ZGA encode transcription factors and other development regulators, such as miRNAs that are important for the clearance of maternally loaded RNAs (Bushati et al., 2008; De Renzis et al.,

2007; M. T. Lee et al., 2013). Although some of the genes expressed during ZGA are exclusively zygotic, many are also maternally loaded, which can reinforce the expression of specific genes. Additionally, some genes encode distinct mRNA isoforms compared to the maternal ones, leading to changes in gene expression patterns (Aanes et al., 2013; Xing et al., 2020).

ZGA is a complex process regulated at multiple levels, transitioning from transcriptional repression to transcriptional activation (Figure I3). It has been suggested that the cell cycle length can influence the timing of transcription onset (Collart et al., 2013) while other studies indicate that the lengthening of the cell cycle is a consequence of zygotic transcription (Farrell & O'Farrell, 2013; M. Zhang et al., 2014). Interestingly, the length of the cell cycle affects both the length and the number of transcripts produced. In *Drosophila* and zebrafish, the first genes expressed are short and have few or no introns (Heyn et al., 2014; Kwasnieski et al., 2019). Another model explaining the timing of the ZGA is the nucleocytoplasmic ratio (N/C ratio). In many species, the volume of the embryo remains constant during MZT, but the nuclear volume and content increase with each division cycle, leading to a progressive increase in the N/C ratio. This model, proposed in frogs, suggests that increasing nuclear content can cause premature ZGA (Newport & Kirschner, 1982; Prioleau et al., 1994). However, similar effects on global transcription have not been observed in *Drosophila* or mice (Edgar et al., 1986; D. R. Lee et al., 2001; X. Lu et al., 2009).

Transcriptional repressors also play a role in regulating ZGA. Many specific repressors are maternally loaded to support the embryo development, while general transcriptional repressors, such as histones, are also important. Histones are present in large amounts in early embryos and bind to DNA, blocking transcriptional machinery (Amodeo et al., 2015). In *Drosophila* and zebrafish, the concentration of soluble histone in the nucleus decreases near the time of genome activation (Anderson & Lengyel, 1980; Joseph et al., 2017). Altering the concentration of maternal histones affects ZGA timing, with lower histone concentration leading to earlier ZGA and higher concentrations causing delays (Chari et al., 2019). Additionally, the availability of the transcriptional machinery also influences the onset of transcription, as illustrated by the role of OMA-1 and OMA-2 and the transcription factor TAF-4 (Guven-Ozkan et al., 2008).

Chromatin accessibility is another critical level of ZGA regulation. Generally, the genome of early embryos is relatively open during the transcriptionally inactive period and becomes more compact during ZGA. However, local genome accessibility increases during genome activation, accompanied by specific histone modifications and histone variants (Eckersley-Maslin et al., 2018).

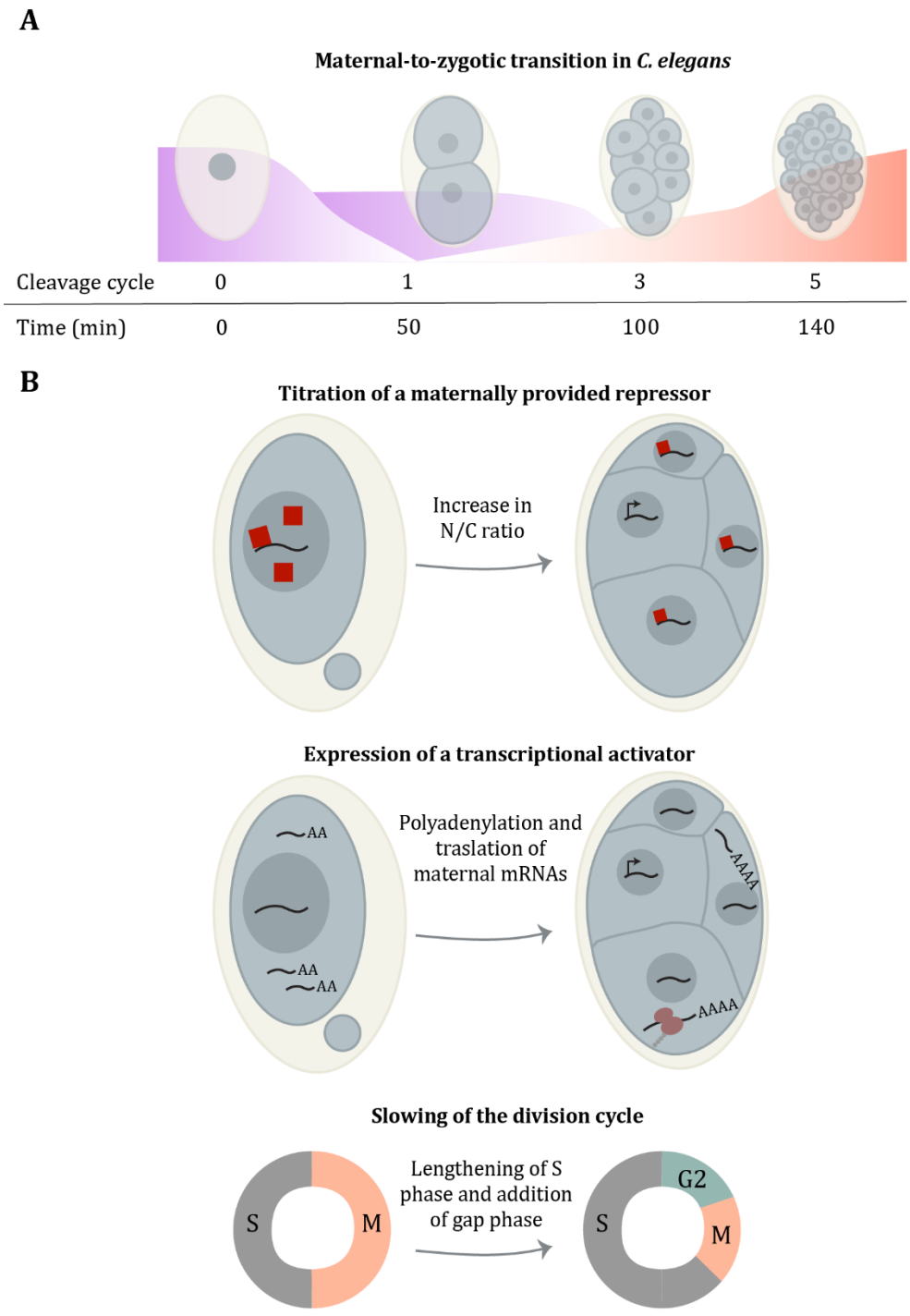

Figure I3 | Mechanisms regulating zygotic genome activation. A. Maternal-to-zygotic transition in *C. elegans*. The pink curves represent the decay of maternal transcripts, while the pink gradients indicate the timing of the multiple phases of transcript degradation. The orange curve represents transcription from the zygotic genome, and the orange gradient illustrates the gradual increase in genes transcribed during ZGA. B. Several mechanisms regulate the timing of ZGA. Maternal repressors (red square) prevent transcription in early embryos. As the nuclear-to-cytoplasmic (N/C) ratio increases, these repressors are diluted, enabling transcription to initiate in cells with reduced repressor levels. Polyadenylation and translation of maternal mRNAs lead to the expression of transcription activators that are absent in early embryos, allowing the activation of their target genes. The lengthening of the S phase and the introduction of

a gap phase slow down the cell cycle, further influencing the timing of ZGA. Schematic illustration adapted from (Vastenhouw et al., 2019; G. Yang et al., 2024).

During ZGA, some canonical histone proteins are replaced by histone variants which have specific functions. For example, the germline-specific linker histone H1 is replaced by a somatic embryonic H1 variant in flies, frogs and mice (Fu et al., 2003; Pérez-Montero et al., 2013; Smith et al., 1988). The histone variant H2A.Z is essential for transcription regulation in zebrafish, *Drosophila* and *C. elegans* early embryos (Ibarra-Morales et al., 2021; Murphy et al., 2018; Whittle et al., 2008). Additionally, the histone variant H3.3 plays an important role in DNA replication during early embryogenesis in *C. elegans* and other organisms (Malik & Henikoff, 2003; Strobino et al., 2020; Szenker et al., 2011).

In *C. elegans*, ZGA occurs initially in the somatic blastomeres. In contrast, the germline precursors (P lineage) and primordial germ cells (PGCs) remain transcriptionally silent, with the somatic sisters undergoing rapid transcriptional activation. The PGCs become transcriptionally active only at later stages. This is a common characteristic of PGCs in all animals (Lesch & Page, 2012). This silencing is maintained by OMA proteins in the 1-cell zygote, and later by PIE-1, which is expressed in the P-lineage to inhibit RNA Pol II (Batchelder et al., 1999; Ghosh & Seydoux, 2008). Transcription is activated in the germ lineage around the 100-cell stage.

mRNA regulation and stability

Similar to the processes occurring during MZT, mRNA molecules must be carefully regulated and stabilized. They undergo various mechanisms, including synthesis, processing and degradation, to establish a specific and precise gene expression pattern.

mRNA transcription initiation and elongation

In eukaryotes, mRNA transcription is mediated by RNA Pol II, which associates with transcription factors and other protein complexes at the core promoter of protein-coding genes (Blackwell & Walker, 2006; Reinke et al., 2013). RNA Pol II activity is tightly regulated during three distinct phases: initiation, elongation, and termination. During transcription, serine residues 5 and 2 of the conserved domain C-terminal domain (CTD) are phosphorylated for transcription initiation and elongation, respectively (Phatnani & Greenleaf, 2006; Zaborowska et al., 2016). This

transition is an important checkpoint in metazoans, allowing fine-tuning of gene expression (Adelman & Lis, 2012; Fuda et al., 2009; H. Kwak & Lis, 2013).

Following transcription initiation, RNA Pol II pauses at the promoter-proximal region. This arrest is mediated by the DSIF complex (SPT4/SPT5) and the NELF complexes, where DSIF bridges the interaction between NELF and RNA Pol II (Core & Adelman, 2019). NELF components are conserved only in higher eukaryotes, where promoter-proximal pausing is common, including in *Drosophila* and mammals (Chivu et al., 2023; Diao et al., 2024; Narita et al., 2003). However, promoter-proximal pausing events are rare in *C. elegans*, which is consistent with the absence of NELF proteins (Kruesi et al., 2013; Narita et al., 2003). SPT4 and SPT5, on the other hand, are highly conserved proteins from yeast to humans (Werner, 2012).

The DSIF complex and RNA Pol II CTD are involved in recruiting the 5'-end capping machinery (Adelman & Lis, 2012; Cho et al., 1997; Ho & Shuman, 1999; H. Kwak & Lis, 2013). Eukaryotic mRNAs are modified at the 5'-end by the addition of an m7GpppN cap. This is the first step in pre-mRNA processing, protecting the mRNA from exonucleases and promoting its processing, nuclear export and translation initiation (Ramanathan et al., 2016). Elongation is restored when RNA Pol II CTD, SPT5 and NELF are phosphorylated, leading to the dissociation of NELF (Bowman & Kelly, 2014). In *C. elegans*, productive elongation is similarly regulated by homologous kinases that phosphorylate RNA Pol II CTD and possibly SPT5 (Bowman & Kelly, 2014).

Cis-splicing and *trans*-splicing

RNA splicing is a highly conserved mechanism responsible for the removal of introns and ligation of exons in pre-mRNA. It is catalysed by a multi-megadalton RNP complex called spliceosome, which is composed of 80-200 proteins and five uridine-rich small nuclear RNAs (U snRNAs), conserved throughout eukaryotes (Sharp et al., 2017). The 5' splice donor site and 3' splice acceptor site have consensus sequences recognized by the spliceosome.

A peculiarity of *C. elegans* is that its introns are relatively short compared to other metazoan introns (Spieth et al., 2014), and these introns are also important for preventing gene silencing by Argonaute proteins and small RNAs in the *C. elegans* germline (Makeyeva et al., 2021). Moreover, it has been shown in plants, *C. elegans* and human cells that there is a connection between Argonaute proteins, small RNAs and the splicing machinery (Akay et al., 2017; Guidi et al., 2023; Makeyeva et al., 2021; Meng et al., 2022; Newman et al., 2018).

In addition to *cis*-splicing, *C. elegans* employs a process called *trans*-splicing (**Figure I4**) (Blumenthal, 2005). *Trans*-splicing is common in nematodes and was originally found in the protozoan *Trypanosoma* (Sutton & Boothroyd, 1986). During *trans*-splicing, one of two extragenically derived 22-nucleotide sequences called spliced leader (SL1 and SL2) is added to the 5'-end of the pre-mRNA (Allen et al., 2011). This type of SL-derived *trans*-splicing has not been found in plants, fungi, insects or vertebrates (Lei et al., 2016). SL1 and SL2 are provided by SL1 or SL2 RNA molecules assembled into snRNPs, and the process is catalysed by the spliceosome (Hannon et al., 1991; Van Doren & Hirsh, 1988). Unlike U snRNPs, SL RNA is consumed in each *trans*-splicing event (Van Doren & Hirsh, 1988). SL1 RNA genes are found in 110-150 tandem repeats, while SL2 RNA is derived from 18 SL2 RNA genes. More than 85% of *C. elegans* mRNAs begin with SL1 or SL2 (Bernard et al., 2023; Tourasse et al., 2017). SL1 is present in the majority of *C. elegans* mRNAs and is dependent on the presence of an outron, while SL2 trans-splices exclusively between genes found in operons (Allen et al., 2011; Blumenthal, 2005; Blumenthal et al., 2002). Like U snRNAs, the co-transcriptionally added m7G cap of SL RNAs is modified to a 2,2,7-trimethylguanosine (TMG) cap in the cytoplasm, resulting in the fact that mRNAs processed by trans-splicing also possess a TMG cap (Allen et al., 2011; Van Doren & Hirsh, 1988).

Interestingly, PETISCO interacts with capped SL1 snRNAs and loss of PETISCO leads to their accumulation (Cordeiro Rodrigues et al., 2019). Furthermore, components of the SMN complex, which is a core component of the U snRNPs and SL RNA, are found to interact with IFE-3, the m7G cap-binding protein of PETISCO (Cordeiro Rodrigues et al., 2019). This suggests that PETISCO, or only IFE-3, may be important for the homeostasis of these snRNPs.

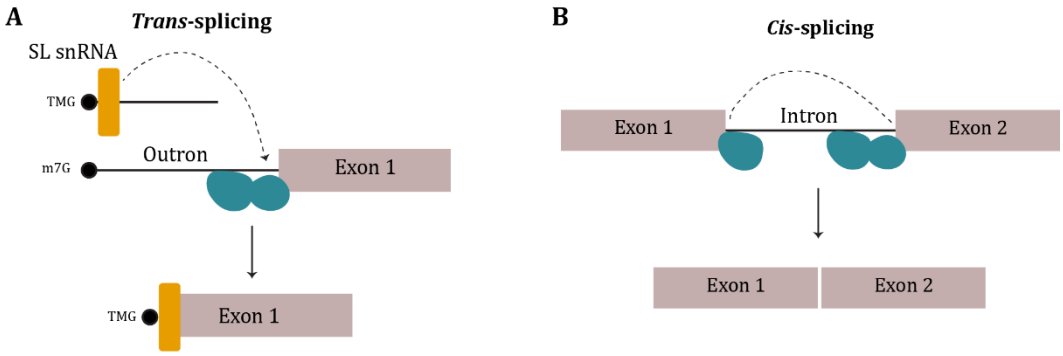

Figure I4 | Schematic representation of *trans*-splicing and *cis*-splicing in *C. elegans*. A. In *trans*-splicing a 2,2,7-trimethylguanosine (TMG)-capped spliced leader (SL) sequence, derived from an SL snRNA in SL snRNP, replaces the 7-methylguanosine (m7G)-capped outron in a pre-mRNA. B. In *cis*-splicing, an intron is excised and the upstream and downstream exons are ligated. Boxes represent exons, and solid lines indicate introns and outrons. Dashed lines

connect exons that are ligated in the splicing reactions. Cap structures are indicated as black circles, and blue circles represent proteins involved in splice-site recognition. Schematic illustration adapted from (Arribere et al., 2020).

Canonical 3' end formation of mRNAs

In general, when the RNA Pol II complex reaches the end of the gene, an endonucleolytic cleavage event releases the nascent transcript from RNA Pol II and generates a free 3' end that serves as the substrate for the addition of a poly(A) tail. The poly(A) tail is important for nuclear export, translation and stability of mRNAs (Passmore & Coller, 2021). These processes are well-conserved among eukaryotes (Rodríguez-Molina & Turtola, 2023). Transcription termination is not required for mRNA 3' end formation, rather efficient transcription termination depends on the processing of 3' ends, as these processes are functionally coupled. In *C. elegans* operons, 3' end formation is coupled to *trans*-splicing rather than transcription termination (Blumenthal, 2005).

Specifically, cleavage and polyadenylation require a cleavage and polyadenylation specificity factor (CPSF) complex that binds to a consensus hexameric polyadenylation signal (PAS) sequence upstream of the cleavage and polyadenylation site (CPS) (Kumar et al., 2019). The canonical PAS sequence is present in only 50% of the PAS sites, and other PAS sequences contribute to the regulation of 3' end processing (Kumar et al., 2019; Rodríguez-Molina & Turtola, 2023). The CPS defines the end of the 3'UTR of the mature mRNA.

The 3' UTR regulates many processes, including mRNA stability, localisation, and activity of its protein product (Merritt et al., 2008; Passmore & Coller, 2021). For example, the presence of AU-rich elements (AREs) in the 3' UTRs promotes mRNA decay, as do miRNAs binding sites (Bartel, 2018). Genes can have multiple CPSs and PAS sequences, leading to alternative polyadenylation (APA) and variability in the 3' ends of the same mRNA. APA can regulate the spatial and temporal pattern of protein translation based on cell type, developmental stage, and cellular conditions (Tian & Manley, 2016). APA can also occur in regions upstream of the 3' UTR, resulting in the production of different protein isoforms (Tian & Manley, 2016). Co-transcriptional splicing and 3' end processing are tightly connected, representing an additional level of regulation of gene expression (Feng et al., 2024; M. Wang et al., 2023).

Promoter-proximal termination

As explained previously, RNA Pol II pausing and release into productive elongation are major points of gene regulation (Adelman & Lis, 2012; Core & Adelman, 2019). Recently, there has been

increasing evidence of an alternative fate for paused RNA Pol II: premature termination. Promoter-proximal termination is mediated by a complex called Integrator (Wagner et al., 2023). Integrator consists of 15 subunits and associates with the RNA Pol II CTD (Baillat et al., 2005; J. Chen et al., 2012; Fianu et al., 2024). It has endonuclease activity to cleave and degrade nascent RNA, along with a module that interacts with PP2A phosphatase (Fianu et al., 2024; Fujiwara et al., 2023; Hu et al., 2023; H. Zheng et al., 2020). The phosphatase activity is important in antagonizing the phosphorylation of the RNA Pol II, DSIF and NELF, thereby preventing the transition into productive elongation (Huang et al., 2020). Integrator is divided into modules based on its function: the backbone, the auxiliary module, the cleavage module, and the phosphatase module. The proteins in the Integrator cleavage module (ICM) are paralogous to the endonucleases (CPSF100 and CPSF73) in the CPSF complex, which is part of the canonical poly(A) termination pathway (Dominski, Yang, Purdy, Wagner, et al., 2005). INTS3 and INTS6, two components of the phosphatase module, also interact in an Integrator-independent manner with the sensor of single-stranded DNA (SOSS) complex (Ren et al., 2014), which is involved in the repair of DNA double-stranded breaks (Skaar et al., 2009; F. Zhang et al., 2013). Recent results also indicate that the Integrator-SOSS complex is involved in removing RNA Pol II after pausing (Fianu et al., 2024). Despite the close association between Integrator subunits and paused RNA Pol II, these subunits can remain bound to the polymerase as it enters the gene body (Dasilva et al., 2021; Rosa-Mercado et al., 2021). Integrator plays a role in transcription termination of snRNAs (Baillat et al., 2005), piRNAs (Beltran et al., 2020) and other ncRNAs (Welsh & Gardini, 2022). It has also been suggested to act in the processing and termination of mRNAs (Dasilva et al., 2021; Rosa-Mercado et al., 2021; Skaar et al., 2015; Tatomer et al., 2019). Integrator is implicated in gene regulation by attenuating the expression of protein-coding genes in *Drosophila* and *C. elegans* through premature transcription termination (Elrod et al., 2019; Fujiwara et al., 2023; Gómez-Orte et al., 2019; Tatomer et al., 2019).

Interestingly, not all Integrator subunits are required for every function, as the depletion of specific subunits produces different effects (Ezzeddine et al., 2011). Defects in the Integrator complex result in abnormalities during early development and lethality in various species, including mice, *Drosophila*, zebrafish and *C. elegans* (Mendoza-Figueroa et al., 2020). The specificity of Integrator binding is not fully understood (Hu et al., 2023; Jonkers et al., 2014). Some studies suggest that it can bind indiscriminately to all active transcription units, acting as a quality control mechanism to terminate elongation-incompetent RNA Pol II (Lykke-Andersen et al., 2021; Rohban et al., 2023; Rouvière et al., 2022).

In *C. elegans*, Integrator is composed of 13 subunits, as opposed to at least 15 subunits in the human complex, and it is essential for embryonic development (Gómez-Orte et al., 2019). Downregulation of different Integrator subunits leads to varying levels of defects in cell fate during embryogenesis (Green et al., 2024). Similar to other organisms, Integrator is responsible for snRNAs transcription termination, but it also affects the termination of SL snRNAs (Gómez-Orte et al., 2019). Downregulation of Integrator causes RNA Pol II read-through downstream of snRNAs loci, leading to dramatic alterations in the transcriptomic profile (Gómez-Orte et al., 2019). Additionally, Integrator acts on transcription termination of motif-dependent piRNA, producing ~48 nt precursors at one of the two known RNA Pol II pausing sites (Beltran et al., 2020). This function depends on RNA Pol II and the conserved transcription elongation factor TFIIS (Beltran et al., 2020; Berkyurek et al., 2021). Finally, Integrator is regulated by one isoform of CSR-1, as shown by CSR-1 loss, which negatively affects the translation efficiency of multiple Integrator subunits, resulting in snRNAs misprocessing (Waddell & Wu, 2024).

mRNA regulation by the 3' end

mRNA molecules undergo constant surveillance and regulation, with 3' UTR processing being one key method the cell uses to regulate and stabilize RNA. Terminal nucleotidyltransferases (TENTs) are conserved enzymes that add non-templated nucleotides to the RNA 3'-end. For instance, non-canonical poly(A) polymerases are involved in cytoplasmic polyadenylation, which promotes mRNA stability or enhances translation. Alternatively, terminal uridylytransferases (TUTases) add untemplated uridines, forming poly(U) tails (Liudkovska & Dziembowski, 2021; Yu & Kim, 2020). While the lengthening of the poly(A) tails stabilizes transcripts, the addition of poly(U) tails generally signals RNA degradation (Lim et al., 2014). After uridylation, the Sm-like proteins (Lsm1-7) complex binds to the U tail and promotes decapping by the DCP1–DCP2 complex (Montemayor et al., 2020; Tharun et al., 2000). Once decapped, mRNAs are degraded 5'-3' by exoribonucleases, while the uridylated tails can be recognized by 3'-5' exoribonucleases, such as the exosome (Yu & Kim, 2020). Uridylation also plays a role in innate immune responses. In human cells, TUT4/7-mediated uridylation restricts retrotransposition (Warkocki et al., 2018).

Similarly, in *C. elegans,* the TUT4/7 homolog CDE-1, also known as poly(U) polymerase (PUP)-1, uridylates viral transcripts and promotes their degradation (Le Pen et al., 2018). Additionally, CDE-1 uridylates endo-siRNAs to prevent their aberrant accumulation and subsequent erroneous gene silencing (van Wolfswinkel et al., 2009), and it also targets ribosomal siRNAs (risiRNAs) (Y.

Wang et al., 2020). *C. elegans* has two additional PUPs, PUP-2 and PUP-3, and the balance between the activities of CDE-1, PUP-2 and PUP-3 is critical for proper germline development (Y. Li & Maine, 2018).

Besides poly(U) tails, recent studies have uncovered mixed tailing events, where combinations of nucleotides are added to mRNA tails. These mixed tails are proposed to have roles in mRNA regulation (Lim et al., 2018; Shukla et al., 2020). TENTs also regulate other types of RNAs, such as rRNAs, tRNAs, snRNAs, and small RNAs (Liudkovska & Dziembowski, 2021).

mRNA translation and quality control mechanisms

Ribosomes translate mRNA into proteins through a series of regulated steps: scanning, initiation, elongation, and termination. Alongside this, ribosomes play a crucial role in mRNA stability and quality control (Q. Wu & Bazzini, 2023). Beyond the influence of the 3' UTR, as previously discussed, codon optimality is a key factor in mRNA stability and influences translation efficiency (Peng et al., 2024; Presnyak et al., 2015; Q. Wu & Bazzini, 2023).

During initiation, eukaryotic initiation factors (eIF) regulate ribosome recruitment to the mRNA. Proteins from the eIF4 group bind the initiation codon, the 5' cap and the poly(A) binding protein on the mRNA, while other eIFs bind the ribosomal subunits (Hinnebusch & Lorsch, 2012). One component of PETISCO, IFE-3, is an isoform of eIF4E, the cap-binding protein of the eIFs (Cordeiro Rodrigues et al., 2019; Zeng et al., 2019). *C. elegans* has five eIF4E isoforms, (IFE-1-5), and IFE-3 is predominantly expressed in the germline, where it binds exclusively m7G cap (Keiper et al., 2000; Stachelska et al., 2002). IFE-3 also promotes oocyte cell fate and development through the translational control of germline sex determination genes (Huggins et al., 2020). Translation elongation is influenced by codon optimality, thereby affecting mRNA stability. Finally, translation termination occurs when the ribosome recognizes a stop codon and releases the mRNA.

The canonical mRNA decay pathway in the cytoplasm often begins with deadenylation, followed by either decapping or the activity of 5'-to-3' exonucleases, or by 3'-to5'- decay via a multi-subunit complex, the RNA exosome (Deng et al., 2023). However, several other mRNA decay pathways exist to correct a variety of errors in a translational-dependent manner (Arribere et al., 2020). These pathways include nonsense-mediated mRNA decay (NMD), which targets mRNAs containing a premature stop codon; nonstop decay, which targets mRNAs lacking a stop codon; and no-go decay, which targets mRNAs with stalled translation elongation. NMD also plays an

essential role in regulating error-free mRNAs (Kishor et al., 2019). The core components of the NMD pathway are widely conserved among eukaryotes. They include the RNA helicase UPF1 (SMG-2 in *C. elegans*), the UPF1 activator UPF2 (SMG-3), and UPF3 (SMG-4). UPF1 requires phosphorylation by SMG-1 to induce NMD. SMG-5/7 are also necessary interactors of UPF1 for NMD and, SMG-6 contains an endonuclease domain that may cleave the targets to initiate degradation (Eberle et al., 2008; Gatfield & Izaurralde, 2004; Glavan et al., 2006; Huntzinger et al., 2008). Additionally, NMD components can recruit the deadenylase complex, decapping factors, and promote both 5'-3' and 3'-5' exonucleases activity (Kishor et al., 2019). UPF1/SMG-2 also functions in other pathways besides NMD, such as staufen-mediated mRNA decay and RD histone mRNA decay (Kim & Maquat, 2019).

Interestingly, in contrast to other species, depletion of NMD components in *C. elegans* results in relatively mild phenotypes (Pulak & Anderson, 1993), whereas NMD is essential in most other eukaryotes (Metzstein & Krasnow, 2006; Wittkopp et al., 2009). In *C. elegans*, NMD substrates include alternative-spliced variants, pseudogenes, and recently expanded gene families (Muir et al., 2018). In other species, long 3'UTRs, transposons, and association with the exon junction complex (EJC) are also recognized as NMD targets (Kishor et al., 2019; Mendell et al., 2004). The no-go and nonstop decay pathways are also conserved in *C. elegans* but remain less studied (Arribere et al., 2020). These pathways regulate endogenous mRNAs, including those undergoing RNAi or the clearance of NMD degradation products (Arribere & Fire, 2018; Hashimoto et al., 2017; Pule et al., 2019).

Histone mRNA regulation

Eukaryotes condense their genomic DNA into a highly repetitive structure called chromatin. Histones are the main protein component of chromatin and are among the most evolutionary conserved proteins in eukaryotes. Histone proteins can be extensively modified and play a crucial role in gene expression regulation. There are two major classes of histone proteins: canonical RD histones and histone variants.

Histones form an octameric core complex, composed of two copies of each of the four canonical histone proteins H2A, H2B, H3 and H4, which packages the chromosomal DNA to form nucleosomes (Campos & Reinberg, 2009). Histone H1 serves as the linker between nucleosomes. With only slight amino acid changes, histone variants with specific functions exist, such as H3.3, H2a.Z, CENPA, and macro-H2A (Henikoff & Ahmad, 2005). Canonical histone proteins are

encoded by a family of RD histone genes, synthesized during the S-phase, and must be maintained at high levels throughout this phase to coincide with the replication of DNA (Marzluff & Koreski, 2017). Metazoan RD histone mRNAs are unique in that they are the only known eukaryotic mRNAs that are not polyadenylated. Instead, they end with a conserved 3' stem-loop sequence (Marzluff et al., 2008). Additionally, they also do not contain introns. In contrast, histone variants are not cell-cycle regulated and contain poly(A) tails and introns.

Histone gene organization

In metazoans, the genes for the RD histone proteins are tightly linked and organized into clusters, which vary in size and distribution across chromosomes. For example, *Drosophila* has ~ 100 RD histone genes arranged in tandem repeats, while humans have at least 72 genes organized in jumbled clusters without repeating organization (Adams et al., 2000; Albig et al., 1997; Pardue et al., 1977; R. Singh et al., 2018). The *C. elegans* genome contains 62 RD histone genes organized into seven clusters of different sizes distributed across different chromosomes (Roberts et al., 1987, 1989). Typically, within these clusters, the genes for H2A and H2B, as well as H3 and H4, are paired and divergently transcribed. In addition, there are two pairs of RD histones on chromosomes I and X (**Figure I5**). Interestingly, *C. elegans* has two genes coding for the H3.3 variant (*his-69* and *his-73*) which possess hallmark features of RD histones, such as the absence of introns and a conserved stem-loop downstream the stop-codon (Pettitt et al., 2002). In *C. elegans*, there are also eight genes coding for the linker histone H1 family, which are not organized into clusters and do not have the structural features typical of RD histone genes (Jedrusik & Schulze, 2001). This contrasts with H1 genes in other species, such as *Drosophila* and mammals, where H1 genes exhibit the characteristics of RD histones. *C. elegans* also has a few core histone genes - coding for H2A, H2B and H4 - with introns, alongside five additional genes coding for the H3.3 variant (Pettitt et al., 2002). Similarly, both *Drosophila* and humans have core histone genes without RD features, and some are located individually on different chromosomes (Albig et al., 1997; Pardue et al., 1977).

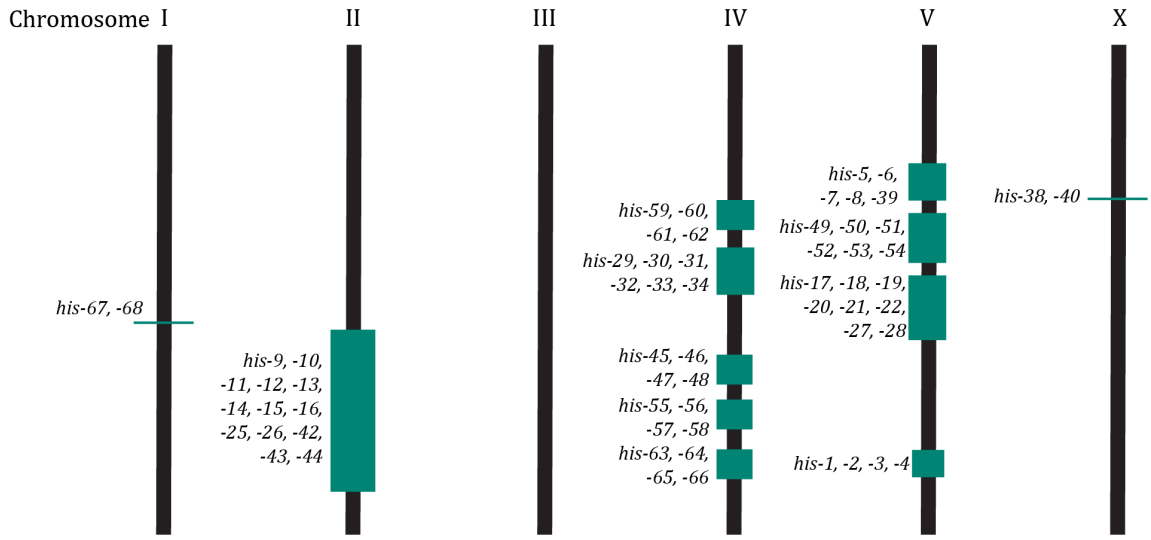

Figure I5 | Schematic representation of replication-dependent (RD) histone gene organization in *C. elegans* genome. The *C. elegans* genome contains 62 RD histone genes, defined by the presence of a stem-loop structure in their 3' UTR. These genes are organized in clusters (green boxes) distributed across the chromosomes (black lines).

Histone mRNA biogenesis

Histone genes are constitutively transcribed by RNA Pol II, and their rate of transcription increases during the S phase of the cell cycle (DeLisle et al., 1983). The protein NPAT (or Mxc in *Drosophila*) is essential for the expression of all five classes of histone genes and is necessary for the assembly of the membrane-less subnuclear compartment known as the histone locus body (HLB) (Terzo et al., 2015; Ye et al., 2003). HLBs are specialized nuclear domains that create an optimal environment for efficient transcription and histone mRNA processing (Geisler et al., 2023). At the onset of the S phase, cyclin E/CDK2 phosphorylates NPAT, which is bound to the promoters of RD histone genes within these bodies, leading to an increase in histone transcription (T. Ma et al., 2000; White et al., 2007; J. Zhao et al., 2000). NPAT oligomerizes and binds to the pre-mRNA processing factor FLASH, both of which are required for the assembly of the HLB (Armstrong et al., 2023; Barcaroli et al., 2006; Terzo et al., 2015; X. C. Yang et al., 2014). In a mutually exclusive manner, another protein called YARP (or Mute in *Drosophila*) binds NPAT at the same region as FLASH (Bulchand et al., 2010). YARP acts as a negative regulator of histone gene expression. Other components involved in histone pre-mRNA processing, such as the U7 snRNP, are also found in HLBs (White et al., 2007).

Throughout the RD histone mRNA metabolism, the conserved stem-loop binding protein (SLBP) binds to the stem-loop structure on the histone mRNA (Brooks et al., 2015; F. Martin et al., 1997). SLBP is necessary for histone mRNA transcription, processing, nuclear export, translation and

degradation, and it is essential for metazoan development (D. R. Arnold et al., 2008; Kodama et al., 2002; Pettitt et al., 2002; E. Sullivan et al., 2001). Inhibition of histone expression in embryos results in mitotic defects, such as decondensed chromosomes and chromosome bridges, and embryonic arrest (Ghule et al., 2016; Kodama et al., 2002; E. Sullivan et al., 2001), while inhibition in post-embryonic stages leads to sterility (Pettitt et al., 2002).

Histone mRNA 3' end processing

Because RD histone genes lack introns, their pre-mRNAs undergo only a single processing step - endonucleolytic cleavage - to produce the 3' end, forming mature histone mRNA. The 3' end of canonical RD histone mRNAs is evolutionary conserved in metazoans and consists of a 25-26 nt sequence, including 5 nt before the stem-loop, a 16 nt stem-loop and 4-5 nt after it (Marzluff et al., 2008). The 3' end processing is a co-transcriptional reaction that requires two *cis*-elements: the conserved stem-loop and a purine-rich sequence downstream of the cleavage site called Histone Downstream Element (HDE), where the 5' end of U7 snRNP base-pairs, stabilized by SLBP (Mowry & Steitz, 1987; Skrajna et al., 2017; Strub & Birnstiel, 1986). The U7 snRNP, similar to spliceosomal snRNPs, contains U7 snRNA and a heptameric Sm ring made of five Sm proteins (common with spliceosomal snRNAs) and two Lsm, Lsm10 and Lsm11 (Pillai et al., 2001, 2003). Lsm11 interacts with FLASH, promoting the recruitment of the histone cleavage complex (HCC) (X.-C. Yang et al., 2013). The HCC includes factors from the polyadenylation complex, such as symplekin, CPSF100 and the endonuclease CPSF73 (Kolev & Steitz, 2005; K. D. Sullivan et al., 2009). Interestingly, in some organisms like *Drosophila* and humans, a PAS sequence is found downstream of the conserved HDE (Keall et al., 2007; Lanzotti et al., 2002; López & Samuelsson, 2008). However, cleavage by CPSF73 occurs 3-6 nt after the stem-loop and before the PAS sequence (Dominski, Yang, Purdy, & Marzluff, 2005; Keall et al., 2007; Scharl & Steitz, 1994).

Histone mRNA 3' end cleavage shares similarities with the cleavage of polyadenylated mRNAs, where the two *cis*-elements: hexanucleotide sequence consensus and the GU-rich element downstream are required. Both cleavage reactions typically occur after the dinucleotide CA, producing a 3′-hydroxyl (3′-OH) (Scharl & Steitz, 1994). Moreover, both pathways share components of the CPSF complex (Dominski, Yang, & Marzluff, 2005). In *Drosophila* and mammalian cells, the absence of SLBP leads to polyadenylation of some RD histone pre-mRNAs (Lanzotti et al., 2002; Saldi et al., 2018). Similarly, inserting an intron into a histone gene results in polyadenylated histone mRNA (Pandey et al., 1990).

In RD histone mRNAs, the processing and transcription termination are also coupled mechanisms but they are regulated differently (Chodchoy et al., 1991). In histone mRNAs, RNA Pol II is released much more quickly compared to poly(A) mRNAs (Anamika et al., 2012). In mammalian cells, NELF and Integrator subunits, involved in RNA Pol II pausing and promoter-proximal termination of canonical mRNA, also participate in RD histone mRNA transcription and processing (Narita et al., 2007; Skaar et al., 2015). NELF and the Nuclear Cap-Binding Complex associate with SLBP in HLBs, and the knockdown of these components leads to the accumulation of polyadenylated RD histone mRNAs (Narita et al., 2007). Similarly, the depletion of INTS3 and INTS9 and the SOSS complex (NABP1 and NAPBP2), produces similar results and leads to the accumulation of soluble histone proteins (Skaar et al., 2015). A recent preprint indicates that Integrator also regulates RD histone transcription in a cell cycle-dependent manner and is present in HLBs (F. Lu et al., 2024). Mediator, a regulator of RNA Pol II transcription elongation, also affects RD histone mRNA termination and processing (Takahashi et al., 2020). Additionally, the rate of transcription elongation influences RD histone pre-mRNA 3' end formation (Saldi et al., 2018). The ncRNA, Y3** (stem-bulge RNA in *C. elegans* (Kowalski et al., 2015)), involved in DNA replication, associates with CPSF components in HBLs and promotes histone pre-mRNA 3' end processing (Köhn et al., 2015).

In *C. elegans*, RD histone mRNA 3' end processing contains some conserved elements, such as the SLBP (called CDL-1 in *C. elegans*), but it lacks other components, including the HLB organization and proteins like NPAT, FLASH and U7 snRNP (López & Samuelsson, 2008). At the sequence level, *C. elegans* also seems to have lost the HDE, where the U7 binds (López & Samuelsson, 2008). However, the PAS sequence is still present downstream of the stem-loop, similar to other species (Keall et al., 2007; Mangone et al., 2010). An alternative processing mechanism involving CSR-1b, expressed in late oocytes and early embryos (Charlesworth et al., 2021), and the RdRP EGO-1, has been identified (Avgousti et al., 2012). CSR-1 endo-siRNAs bind RD histone 3'-UTR between the stem-loop and PAS sequence. Depletion of *csr-1* and *ego-1* leads to the accumulation of unprocessed histone mRNAs and a reduction of mature histone mRNA and histone proteins (Avgousti et al., 2012). Depleting both proteins causes sterility and chromosome segregation defects in early embryos (Claycomb et al., 2009). However, overexpression of transgenic mature RD histone mRNAs rescues the viability of the progeny of treated animals (Avgousti et al., 2012). The precise cleavage mechanism and whether other components are involved remain known.

Translation of RD histone mRNAs

Similar to canonical mRNAs, where the poly(A) tail is required for nuclear export, in RD histone mRNAs, the stem-loop and the SLBP are necessary for transport (Eckner et al., 1991; Sànchez & Marzluff, 2002). In the cytoplasm, SLBP interacts with the translation initiation factor EIF4G, mediated by SLIP1, to circularize the histone mRNA, promoting translation (Cakmakci et al., 2008). Despite the differences in the 3' ends between RD histone mRNAs and canonical mRNAs, the translation regulation is conserved (Hayek et al., 2021). However, the region of the SLBP involved in translation and interaction with SLIP1 is not conserved in *C. elegans,* and there are no known SLIP-1 orthologues in nematodes. Therefore, the role of CDL-1 in translation remains unclear (Cakmakci et al., 2008).

Histone mRNA degradation

As cells approach the end of the S phase, the need for new canonical histone proteins decreases, leading to the degradation of their mRNAs and SLBP (Whitfield et al., 2000). The stem-loop at the 3' end and SLBP are required not only for translation but also for the mRNA degradation process (Slevin et al., 2014; Whitfield et al., 2000). RD histone mRNA is degraded bidirectionally like other mRNAs, but without deadenylation due to the absence of a poly(A) tail. Instead, the histone mRNA stem-loop is uridylated by TUT7 in response to the end of DNA synthesis (Lackey et al., 2016; Mullen & Marzluff, 2008). This process resembles that of canonical mRNAs, where uridylation accelerates degradation (Lim et al., 2014).

After RD histone pre-mRNA processing, the mature mRNA is exported from the nucleus. The stem-loop features an ACCCA tail that is shortened by 2-3 nt by the exonuclease 3'hExo/ERI1 (Hoefig et al., 2012). ERI1, in a complex with SLBP, is essential for the initial steps of RD histone mRNA degradation (Tan et al., 2013; X. C. Yang et al., 2006). Following trimming, the stem-loop is uridylated by TUT7 to restore its length during the S phase (Lackey et al., 2016; Welch et al., 2015). SLBP's binding requirements for the stem-loop are not fully understood in the context of trimming and uridylation (Battle & Doudna, 2001). However, SLBP dephosphorylation weakens its interaction with the stem-loop, and together with uridylation, promotes ERI1 activity (Shine et al., 2023). ERI1 and TUT7 cooperate to maintain histone mRNA during the S phase and initiate its degradation at the end of the phase (Holmquist et al., 2022).

As DNA synthesis concludes, ERI1 degrades the mRNA into the stem-loop, leaving 2-4 nt from the 3' end, which are then reuridylated before further degradation (Hoefig et al., 2012). This 3' to 5'

initial degradation and uridylation depends on translation and occurs on polyribosomes (Slevin et al., 2014). The number of nucleotides removed and the length of the poly(U) tails added vary, resulting in intermediates with different stem-loop and poly(U) tail lengths (Slevin et al., 2014). Other exonucleases may also initiate digestion into the stem-loop, promoting uridylation (Holmquist et al., 2022). The longer U-tails, generated after initial digestion, are bound by the Lsm1-7 ring, triggering rapid degradation (Lyons et al., 2014; Slevin et al., 2014). Lsm4 directly binds to ERI1 and SLBP (Hoefig et al., 2012; Lyons et al., 2014).

During this process, the NMD components UPF1 and SMG1 are recruited to the histone mRNA, likely due to inefficient translation, and are necessary for its degradation (Kaygun & Marzluff, 2005; Meaux et al., 2018). After the histone mRNA is released from polyribosomes, UPF1 binds to the 3' UTR just upstream of the stem-loop, where it interacts with SLBP (Brooks et al., 2015; Kaygun & Marzluff, 2005). The UPF1 Lsm1-7 complex likely participates in SLBP removal and recruits the exosome for further 3' to 5' degradation (Meaux et al., 2018; Slevin et al., 2014). Lsm1-7, bound to the poly(U) in the 3' UTR, also recruits the decapping machinery for 5' to 3' degradation (Mullen & Marzluff, 2008; Su et al., 2013). Alternatively, UPF1 recruits other NMD components, such as SMG5, which interacts with SLBP and promotes 5' to 3' degradation (Choe et al., 2014) (**Figure I6**).

Most studies on histone mRNA degradation have been conducted *in vitro*, in *Drosophila* embryos, or mammalian cells. While many of the proteins mentioned above have homologs in *C. elegans*, their involvement in histone mRNA degradation has not yet been demonstrated. Instead, some have been described to function in other processes. Specifically, *C. elegans* ERI1 homolog forms a complex with Dicer to generate siRNAs and is also involved in the depletion of other siRNAs (Thomas et al., 2014). Additionally, CDE-1, the homolog of TUT7, is involved in uridylation of small RNAs and mRNAs (Kelley et al., 2024; van Wolfswinkel et al., 2009; Vieux et al., 2021; Y. Wang et al., 2020).

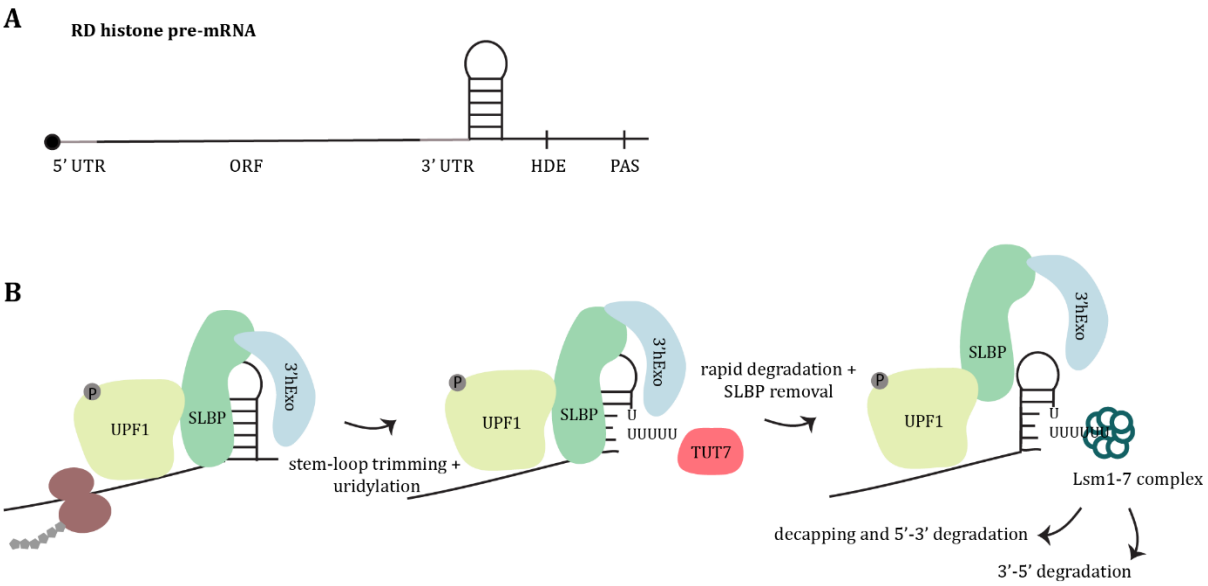

Figure I6 | Models of RD histone mRNA structure and degradation. A. Structure of a metazoan RD histone pre-mRNA. These genes lack introns and have short 5' and 3' UTRs. The distance from the stop codon to the start of the conserved stem-loop varies from 25 to 50 nucleotides. The stem-loop consists of a 6-base stem and a 4-nucleotide loop. The region encompassing the stem-loop is highly conserved across metazoans and spans a 25-26 nucleotide sequence, including 5 nucleotides upstream, the 16-nucleotide stem-loop, and 4-5 nucleotides downstream. Downstream the stem-loop lies the histone downstream element (HDE), which serves as a binding site for the U7 small nuclear RNP, a component essential for pre-mRNA processing. Further downstream, multiple poly-adenylation signals (PAS) are present (Marzluff & Koreski, 2017). B. Following histone mRNA processing, the 3' UTR is trimmed by 3'hExo and repaired by TUT7 to maintain the proper length. When DNA replication is inhibited or at the end of the S phase, UPF1 is recruited to the histone mRNA, possibly through ribosome (brown circles) recognition of the stop-codon, and interacts with SLBP. The 3'hEXo can degrade the stem, and the mRNA is extensively uridylated by TUT7. Lsm1-7 complex is proposed to bind the oligo(U) tail, initiation degradation and leading to the removal of SLBP. The decapping machinery and the exosome are subsequently recruited, resulting in bidirectional degradation (Marzluff & Koreski, 2017).

Regulation of histone expression during cell-cycle

Histone mRNAs are among the most tightly cell-cycle regulated mRNAs, expressed only during the S phase and rapidly degraded at its end. To accumulate enough histone proteins during DNA replication, cells employ distinct regulatory mechanisms to maintain the stoichiometry between histones and DNA. The two key strategies for histone biosynthesis are the activation of histone genes transcription and the processing of histone pre-mRNAs during the S phase (Armstrong et al., 2023; Duronio & Marzluff, 2017). These processes are in part driven by Cyclin E/Cdk2, a complex that controls progression through the G1/S transition by phosphorylating and activating factors such as NPAT, which promotes histone gene transcription (T. Ma et al., 2000; Ye et al., 2003; J. Zhao et al., 2000). The newly transcribed mRNAs are rapidly translated and degraded at the end of the S phase.

Producing histones outside of the S phase is highly toxic (R. K. Singh et al., 2009), while a shortage of the histones during the S phase can slow DNA synthesis and extend the length of the S phase (Günesdogan et al., 2014; X. Zhao et al., 2004). Conversely, the presence of excess non-nucleosomal histones inhibits DNA synthesis and triggers histone mRNA degradation (Armstrong et al., 2023). In *S. cerevisiae*, a mechanism has been identified to degrade excess histones at the end of the S phase through Rad53 kinase-mediated histone phosphorylation (Gunjan & Verreault, 2003). An imbalance between histone proteins and DNA is detrimental to the cell and leads to genetic instability, as observed from yeast to humans. This instability manifests as DNA damage, hyper-recombination, and checkpoint activation (Ghule et al., 2014; Prado et al., 2017; Prado & Aguilera, 2005).

Additionally, the eukaryotic translational initiation factor eIF4B, was found to bind and stabilize RD histone mRNAs, potentially through interactions with UPF1. This stabilization promotes cell cycle progression, as eIF4B depletion in cells results in delayed S-phase progression (Quintas et al., 2013). While eIF4B typically binds directly to the 5' UTRs of mRNAs, it was unexpectedly discovered to bind upstream of the stem-loop of RD histone mRNAs.

SLBP regulation is also cell cycle-dependent, though the molecular signals governing it differ. Inhibition of the DNA replication during the S phase rapidly degrades RD histone mRNAs, yet has no effect on SLBP levels (Whitfield et al., 2004). SLBP undergoes multiple modifications throughout the cell cycle that regulate its transport, activity and degradation (Dankert et al., 2016; Koseoglu et al., 2008; Lanzotti et al., 200the 2). Specifically, at the end of the S phase, certain residues are phosphorylated while others are dephosphorylated (Koseoglu et al., 2008; M. Zhang et al., 2012). These modifications promote the dissociation of SLBP from the stem loop, facilitating histone mRNA degradation and SLBP ubiquitination (Borchers et al., 2006; Krishnan et al., 2012; M. Zhang et al., 2012). SLBP is degraded by the ubiquitin-proteasome system, which is activated through different mechanisms in a cell cycle-dependent manner (Dankert et al., 2017; Djakbarova et al., 2014; L. Zheng et al., 2003).

Histone expression regulation by small RNAs

In *C. elegans* small RNAs are prone to silencing genes with few or no introns (Aljohani et al., 2020; Makeyeva et al., 2021; Newman et al., 2018). However, RD histone mRNAs manage to evade targeting by small RNA pathways through unknown mechanisms (Makeyeva et al., 2021). Notably, the loss of PRG-1, a PIWI protein in *C. elegans*, leads to the accumulation of secondary si-RNAs that target RD histone mRNAs, resulting in downregulation of RD histone expression

(Barucci et al., 2020; Reed et al., 2019). This effect does not extend to H1 linker and histone variants (Reed et al., 2019), consistent with these genes being spliced.

So far, a U7 snRNA homolog has not been identified in *C. elegans*, raising questions about how histone pre-mRNAs are cleaved during transcription (Marzluff et al., 2008). CSR-1, which interacts with SLBP/CDL-1, has been implicated in this process (Avgousti et al., 2012). Furthermore, the accumulation of histone siRNAs in *prg-1* mutants decreases when CSR-1 is catalytically inactive and when CDL-1 is downregulated (Barucci et al., 2020). This suggests that an interplay between CSR-1 and CDL-1 may be involved in the production of these small RNAs in the absence of PIWI.

The reasons behind the heightened susceptibility of histone mRNAs to trigger siRNAs in the absence of piRNAs remain unclear (Barucci et al., 2020; B. E. Montgomery et al., 2021; Reed et al., 2019). However, RD histone mRNAs are substrates for RDE-3-dependent pUGylation in *prg-1* mutants (Shukla et al., 2021). The addition of poly(UG) tails to RNAs converts them into templates for siRNAs synthesis and silencing via RNAi (Shukla et al., 2020), although the mechanism behind the targeting of histone mRNAs by RDE-3 is not yet understood. However, the susceptibility to poly(UG) tailing suggests that perhaps it is the absence of a poly(A) tail rather than the absence of splicing that makes histone mRNAs susceptible to siRNA production.

Histones in early development

In many organisms, early development is characterized by a rapid series of nuclear replication, which exponentially increase the amount of chromatin. These cell cycles typically alternate between S and M phases, without the gap phases (Robertson & Lin, 2015). As there is no transcription during these initial cell cycles, all components, including histones, must be stored in the gametes (Adamson & Woodland, 1977; Woodland & Adamson, 1977). Different organisms employ distinct strategies to transfer and regulate histone metabolism in the embryo to meet developmental demands.

In *D. melanogaster*, a large production of histone mRNAs occurs during oogenesis, followed by translation and storage in the egg. This transcription stage requires high levels of SLBP (Potter-Birriel et al., 2021). Histone proteins, stored alongside chaperones, are present in sufficient quantities to support development through several thousand cell stages (Ruddell & Jacobs-Lorena, 1985; Walker & Bownes, 1998). RD histone mRNAs, together with SLBP, are also stored and transmitted to the embryo (Godfrey et al., 2006; Walker & Bownes, 1998).

In *Xenopus laevis*, a significantly larger amount of histone proteins is produced in two phases during oogenesis. Later, upon oocyte maturation, SLBP binds histone mRNAs, activating translation (Sánchez & Marzluff, 2004; Turner & Woodland, 1983; Z.-F. Wang et al., 1999). In mammals, RD histones are stored as mRNAs in the growing oocyte and only during oocyte maturation does SLBP get translated, activating RD histone translation (Allard et al., 2005). Thus, SLBP is necessary for oocyte maturation and early embryonic development (Allard et al., 2005; D. R. Arnold et al., 2008).

Similar to other mRNAs, histones need to be stabilized in the oocyte and regulated when deposited in the embryo. For canonical mRNAs, the poly(A) tail is a major regulatory element (Subtelny et al., 2014). However, due to the lack of poly(A) tails, RP histone mRNAs depend on different regulatory factors (Marzluff et al., 2008). In zebrafish, one eIF4E1 paralogue specifically binds to transcripts with short or no poly(A) tail, such as RD histones. These transcripts are translationally repressed in embryos, and downregulation occurs in *eif4e1* mutants, suggesting that the eIF4E1 paralogue might play a role in stabilizing maternal histone mRNAs (Lorenzo-Orts et al., 2024). Interestingly, the *C. elegans* eIF4E homologue, IFE-3 interacts with IFET-1, a protein that negatively regulates translation of maternally inherited mRNAs (Boag et al., 2008; Cordeiro Rodrigues et al., 2019).

The concentration of histones in the early embryo influences cell cycle progression and the onset of zygotic transcription in flies, zebrafish and frogs (Amodeo et al., 2015; Chari et al., 2019; Joseph et al., 2017). Depleting histones results in earlier ZGA and longer cell cycles (Chari et al., 2019). This effect on cell cycle lengthening appears to depend on soluble histones rather than nucleosome-incorporated histones (Shindo & Amodeo, 2021).

In *C. elegans*, RD histone genes are organized into seven clusters, with genes from different clusters exhibiting distinct expression patterns during embryogenesis (Boeck et al., 2016; Gleason et al., 2023). RD histone genes from clusters located on chromosome IV show substantial expression at the 4-cell stage, peaking around 200-250 minutes into embryogenesis (Boeck et al., 2016). The expression of these genes in the adult gonad is also notably high, indicating a maternal origin in the embryos (Boeck et al., 2016). In contrast, histone genes from clusters on chromosomes I and III show minimal expression at the beginning of embryogenesis but peak around 200-300 minutes (Boeck et al., 2016). The expression of genes from different clusters rapidly declines after this peak (Boeck et al., 2016).

Development of *C. elegans* germline

C. elegans has a rapid life cycle of approximately 4 days at 20°C. It primarily exists as a self-fertilizing hermaphrodite, although males arise at a low frequency of about 0.2%. Hermaphrodites have five pairs of autosomes and two sex chromosomes (XX), while males have a single sex chromosome (XO). Embryogenesis lasts around 16 hours at 20°C, with embryos retained within the hermaphrodite until the 24-cell stage. Upon hatching, the embryos contain 558 nuclei, marking the first larval stage (Corsi et al., 2015).

During embryogenesis, cells divide asymmetrically, forming both the P cell lineage and the somatic cell lineage. At the 24-cell stage, the P4 cell undergoes symmetric division to generate the primordial germ cells Z2 and Z3 (Sulston et al., 1983). These cells do not divide further until the organism reaches the first larval stage (L1). The *C. elegans* life cycle consists of four larval stages (L1 – L4) followed by adulthood.

Hermaphrodites develop two gonadal arms, while males develop only one. During the L2 and L3 stages, germ cells are allocated to anterior and posterior populations, each of which contributes to forming one of the two gonadal arms. Early in the L3 stage, the gonadal arms rapidly expand, as germ cells proliferate. As the L3 stage progresses, the most proximal germ cells stop proliferating and enter meiosis, establishing a distal-proximal polarity in the developing germline. During the L4 stage and adulthood, germ cell proliferation continues in the distal mitotic zone, maintained by signals from the distal part of the somatic gonad, called the distal tip cell. As germ cells exit the mitotic region they enter meiosis in the transition zone, where chromosomes pair and undergo homologous recombination. Germ cells continue to advance through meiosis as they move through the gonad. Throughout these stages, the nuclei share a common cytoplasm, the rachis, and cellularisation into individual germ cells only occurs late during meiosis. In hermaphrodites, the germ cells that mature during the L4 stage enter spermatogenesis, with the resulting sperm being stored in the spermatheca. Starting during late L4 stage, hermaphroditic spermatogenesis halts and oogenesis begins, and the production of oocytes continues throughout adult life. In males, spermatogenesis continues throughout the lifespan of the animal. Oogenesis requires a significant increase in cytoplasmic volume to produce a maternally provisioned cell capable of supporting early embryogenesis. The most proximal oocyte enters the spermatheca, where it is fertilized and undergoes early embryogenesis in the uterus until it is laid (Hubbard & Greenstein, 2005).

Aim of this thesis

Germ cells have the extreme functions of producing, stabilizing and transmitting all the necessary and correct genetic and epigenetic information required for the early stages of an embryo. In this work, I aim to understand how a complex named PETISCO, known to be involved in the germline defence mechanism of piRNAs, is important in the embryogenesis of *Caenorhabditis elegans,* focusing on the early-stages when the maternal elements are most needed. This question is interesting for us because the piRNA pathway is not required in these early stages, suggesting additional functions for PETISCO. I want to dissect PETISCO's role during embryonic development, as well as its RNA targets.

MATERIALS AND METHODS

C. elegans culture and strains

All *C. elegans* strains were maintained under standard laboratory conditions at 20°C on Nematode Growth Medium (NGM) plates (90 mm) seeded with *Escherichia coli* OP50 (Brenner, 1974). Strains used for MosSCI transgenesis were cultured on NGM plates seeded with *Comamonas sp*. (DA1877). For iCLIP experiments, animals were grown on egg plates (Schweinsberg & Grant, 2013) for one generation, synchronized via hypochlorite treatment, and embryos were subsequently harvested. For IP/MS experiments, animals were first grown on egg plates for one generation, synchronized by hypochlorite treatment, and then transferred to NGM plates seeded with OP50 for one additional generation before harvest. Egg plates were prepared by thoroughly mixing egg yolk with 50 ml LB medium per egg. The mixture was incubated at 65°C for 2-3 hours and cooled to room temperature before adding 10 ml OP50 culture per egg. Approximately 10 ml of the prepared mixture was poured onto standard NGM plates and incubated at room temperature overnight. Excess liquid was decanted the next day, and the plates were incubated at room temperature for an additional two days before use. Bristol N2 strain was used as reference wild-type strain.

The list of strains used in this study is provided in Table 1.

Table 1 | Strains used in this study.

Strain	**Genotype**
FAS26	*ugeDf12 II*
FX17314	*pid-3(tm2417) I/hT2[bli-4(e937) let-?(q782) qIs48](I;III)*
JCP378	*jcpSi19[eft-3p::ints-6::3xFLAG::eGFP::ints-6 3'UTR + unc-119(+)] II; unc-119(ed3) III*
KK359	*tofu-6(it20) unc-4(e120)/mnC1 dpy-10(e128) unc-52(e444) II*
N2	*C. elegans* wild isolate var Bristol
NL5100	*cde-1(tm1021) III*
RFK1244	*ugeDf12 II; tost-1(xf196/+) oxTi615[eft-3p::tdTomato::H2B::unc-54 3'UTR + Cbr-unc119(+)]/+ III*
RFK1260	*mut-16(xf142) I; tost-1(xf196 ts) oxTi615[eft-3p::tdTomato::H2B::unc-54 3'UTR + Cbr-unc119(+)] III*
RFK1265	*mut-16(xf142) I; tost-1(xf194/+) oxTi615[eft-3p::tdTomato::H2B::unc-54 3'UTR + Cbr-unc119(+)]/+ III*
RFK1303	*xfSi254[his-67p::GFP::his-67::his-67 3'UTR + Cbr-unc-119(+)] II*
RFK1305	*xfSi255[his-67p::GFP::his-67::tbb-2 3'UTR + Cbr-unc-119(+)] II*
RFK1315	*tost-1(xf263[2Xflag::tost-1]) III*
RFK1339	*xfSi268[his-67p::GFP-CDS::his-67::his-67 3'UTR + Cbr-unc-119(+)] II*
RFK1341	*xfSi269[his-67p::GFP-CDS::his-67::tbb-2 3'UTR + Cbr-unc-119(+)] II*
RFK1345	*xfSi306[his-67p::sv40-NLS::GFP-CDS::egl13-NLS::his-67 3'UTR + Cbr-unc-119(+)] II*
RFK1347	*xfSi307[his-67p::sv40-NLS::GFP-CDS::egl13-NLS::tbb-2 3'UTR + Cbr-unc-119(+)] II*

RFK1443	*tost-1(xf196) oxTi615[eft-3p::tdTomato::H2B::unc-54 3'UTR + Cbr-unc119(+)] cde-1 (tm1021) III*
RFK1532	*cde-1(xf319), tost-1(xf194) oxTi615[eft-3p::tdTomato::H2B::unc-54 3'UTR + Cbr-unc119(+)] III*
RFK1533	*cde-1(xf319), tost-1(xf194) oxTi615 [eft-3p::tdTomato::H2B::unc-54 3'UTR + Cbr-unc119(+)] III*
RFK1534	*smg-2(r908) I; tost-1(xf196) oxTi615[eft-3p::tdTomato::H2B::unc-54 3'UTR + Cbr-unc119(+)] III*
RFK1535	*tofu-6(it20) unc-4(e120) II; cde-1(tm1021) III*
RFK1536	*pid-3(tm2417) I; cde-1(tm1021) III*
RFK1568	*xfSi268[his-67p::GFP-CDS::his-67::his-67 3'UTR + Cbr-unc-119(+)] II; tost-1(xf196) oxTi615 [eft-3p::tdTomato::H2B::unc-54 3'UTR + Cbr-unc119(+)] cde-1(tm1021) III*
RFK1569	*xfSi268[his-67p::GFP-CDS::his-67::his-67 3'UTR + Cbr-unc-119(+)] II; cde-1(tm1021) III*
RFK1570	*tost-1(xf196) oxTi615[eft-3p::tdTomato::H2B::unc-54 3'UTR + Cbr-unc119(+)] III; his-61(ne4846[gfp::his-61]) IV*
RFK1571	*tost-1(xf196) oxTi615[eft-3p::tdTomato::H2B::unc-54 3'UTR + Cbr-unc119(+)] III; his-61(ne4847[intronless gfp::his-61]) IV*
RFK1694	*mut-7(xf125) III; his-61(ne4847[intronless gfp::his-61]) IV*
RFK1695	*tost-1(xf196) oxTi615[eft-3p::tdTomato::H2B::unc-54 3'UTR + Cbr-unc119(+)] mut-7 (xf125) III; his-61(ne4846[gfp::his-61]) IV*
RFK1698	*pid-1(xf35) II; tost-1(xf196) oxTi615[eft-3p::tdTomato::H2B::unc-54 3'UTR + Cbr-unc119(+)] III*
RFK1699	*cde-1(xf360) erh-2(xf168) oxTi615[eft-3p::tdTomato::H2B::unc-54 3'UTR + Cbr-unc119(+)] III/ qC1 [dpy-19(e1259) glp-1(q339) qIs26] III*
RFK1718	*jcpSi19[eft-3p::ints-6::3xFLAG::eGFP::ints-6 3'UTR + unc-119(+)] II; tost-1(xf263[2xflag::tost-1]) III*
RFK1719	*smg-2(xf368) I*
RFK1721	*smg-1(xf369) I; tost-1(xf196) oxTi615[eft-3p::tdTomato::H2B::unc-54 3'UTR + Cbr-unc119(+)] III*
RFK1722	*smg-1(xf369) I*
RFK1724	*smg-1(xf370) I; tost-1(xf196) oxTi615[eft-3p::tdTomato::H2B::unc-54 3'UTR + Cbr-unc119(+)] III*
RFK1725	*smg-1(xf370) I*
RFK1727	*tost-1(xf196) oxTi615[eft-3p::tdTomato::H2B::unc-54 3'UTR + Cbr-unc119(+)] III; C14C10.5(xf371) V*
RFK1728	*C14C10.5(xf371) V*
RFK1800	*C14C10.5(xf387) V*
RFK1801	*tost-1(xf196) oxTi615[eft-3p::tdTomato::H2B::unc-54 3'UTR + Cbr-unc119(+)] III; C14C10.5(xf387) V*
RFK1813	*xfSi268[his-67p::GFP-CDS::his-67::his-67 3'UTR + Cbr-unc-119(+)] II; tost-1(xf196) oxTi615[eft-3p::tdTomato::H2B::unc-54 3'UTR + Cbr-unc119(+)] III*
RFK1814	*xfSi254[his-67p::GFP::his-67::his-67 3'UTR + Cbr-unc-119(+)] II; tost-1(xf196) oxTi615[eft-3p::tdTomato::H2B::unc-54 3'UTR + Cbr-unc119(+)] III*
RFK1815	*xfSi269[his-67p::GFP-CDS::his-67::tbb-2 3'UTR + Cbr-unc-119(+)] II; tost-1(xf196) oxTi615[eft-3p::tdTomato::H2B::unc-54 3'UTR + Cbr-unc119(+)] III*
RFK1816	*smg-2(xf368) I; tost-1(xf196) oxTi615[eft-3p::tdTomato::H2B::unc-54 3'UTR + Cbr-unc119(+)] III*
RFK1817	*tofu-6(it20) unc-4(e120) II; mut-7(xf125) cde-1(tm1021) III*
RFK1818	*tost-1(xf196) oxTi615[eft-3p::tdTomato::H2B::unc-54 3'UTR + Cbr-unc119(+)] III; C14C10.5(xf389) V*
RFK1819	*C14C10.5(xf389) V*
RFK182	*pid-1(xf35) II*
RFK1821	*smg-3(xf391) IV*
RFK1822	*tost-1(xf196) oxTi615 [eft-3p::tdTomato::H2B::unc-54 3'UTR + Cbr-unc119(+)] III; smg-3(xf391) IV*
RFK691	*mut-16(xf142) I*
RFK905	*tost-1(xf194) oxTi615[eft-3p::tdTomato::H2B::unc-54 3'UTR + Cbr-unc119(+)] III/qC1[dpy-19(e1259) glp-1(q339) qIs26] III*
RFK912	*tost-1(xf196) oxTi615[eft-3p::tdTomato::H2B::unc-54 3'UTR + Cbr-unc119(+)] III*
SX523	*prg-1(n4357) I*
TR1421	*smg-2(r908) unc-54(r293) I*

WM748	*his-61(ne4846[gfp::his-61]) IV*
WM749	*his-61(ne4847[intronless gfp::his-61]) IV*

MosSCI Transgenesis

The MosSCI system was used to introduce transgenes for ectopic expression in the germline (Frøkjær-Jensen et al., 2008, 2012). The transgenic alleles *xfSi254, xfSi255, xfSi268, xfSi269, xfSi306, xfSi307* were inserted into the ttTi5605 locus on chromosome II. The *gfp* coding sequence, including three introns, was amplified from pDD282 (Addgene plasmid # 66823. All plasmids used for microinjection were purified from 5 ml bacterial culture using NucleoSpin® Plasmid (Art. No. 740588.50, Macherey-Nagel®), eluted in sterile water and verified by PCR and Sanger sequencing. To generate transgenic lines, DNA mixes containing 50 ng/µl pCFJ601, 10 ng/µl pMA122, 10 ng/µl pGH8, 5 ng/µl pCFJ104, 2.5 ng/µl pCFJ90 and 50 ng/µl of pRFK3105 (*xfSi254*) or pRFK3118 (*xfSi268),* pRFK3124 *(xfSi255)*, pRFK3126 *(xfSi269)*, pRFK3132 *(xfSi306)*, pRFK3133 *(xfSi307)* were injected in both gonads of 50 young adult EG6699 worms (carrying the *ttTi5605* insertion site on chromosome II). The progeny was screened for successful transgene integration as previously described (Frøkjær-Jensen et al., 2008, 2012). Insertion events were confirmed by Sanger sequencing, and all newly generated strains were out-crossed twice before any additional crosses or analysis.

The plasmids pCFJ601, pMA122, pGH8, pCFJ90 and pCFJ104 were obtained from Addgene (Addgene plasmid #: 34874; 34873; 19359; 19327; 19328) (Frøkjær-Jensen et al., 2008, 2012).

CRISPR/Cas9-mediated genome editing

Protospacer sequences were selected using CRISPOR (http://crispor.tefor.net) (Concordet & Haeussler, 2018) and cloned into pRK2411 (plasmid expressing Cas9 + sgRNA(F+E) (B. Chen et al., 2013); derived from pDD162) via site-directed, ligase-independent mutagenesis (SLIM) (Chiu et al., 2004, 2008). pDD162 (Peft-3::Cas9 + Empty sgRNA) (Addgene plasmid # 47549) (Dickinson et al., 2013). SLIM reactions were transformed into Subcloning Efficiency™ DH5α™ Competent Cells (Art. No. 18265017, Invitrogen™) and plated on LB agar plates supplemented with 100 µg/ml ampicillin. All protospacer sequences used in this study are listed in Table 2. Genome editing was performed using either *dpy-10(cn64)* or *unc-58(e665)* co-conversion strategies (Arribere et al., 2014). DNA injection mixes were injected into both gonad arms of one

to 20 young adult N2 hermaphrodites maintained at 20°C, unless otherwise stated. Selected F1 progeny were screened for edits using PCR, and successful editing events were confirmed by Sanger sequencing. All generated mutant strains were out-crossed at least twice before additional crosses or analysis. All CRISPR/Cas9-generated alleles are listed in Table 3.

Table 2 | Protospacer sequences used for CRISPR/Cas9-mediated genome editing.

Gene	Allele	Sequence (5' to 3')
cde-1	*xf319 / xf361*	AGCAAAGGTCTGGAAGTAGG
		TTCGTATTGCTTAAAGATTG
		GTGTGATCTCGATTCATCGG
		TTCAAAAATGGAGAGGAAGG
smg-2	*xf368*	TCTTCCAGTAATGGACGATT
		CGGGGAAACCCTCACATTTG
		GACGGCGTTGGTCACCACGG
		ACATTTGCTGCTGAGAGTTG
smg-1	*xf369 / xf370*	TGACACGCCACAGAAGGAA
		TATTGGGAACCTGATAGAAC
		CGTGTTGAACGGCGTCTCAA
		AAATTGTCTCCTCGCGAAG
C14C10.5	*xf371 / xf387 / xf389*	GCTCGATGAGGACATTGATA
		ACAAGTACGAACCATCACTG
		TATTGTGGCACTCTTGTCAG
		GCATGAGCAACAATTCAACG
smg-3	*xf391*	GTTGAGGAAATGGCGTCGGT
		CTTCAGTGAACAGATGGCTG
		ACTGTTCAACGATGCCAACA
		CACCATTCTCCTTCGAGGTG

Table 3 | Description of CRISPR/Cas9-generated alleles used in this study.

Gene	Allele	Details
cde-1	*xf319*	Deletion of 5887 bp & insertion of 749 bp, 24 bp from ATG (GAGCAAAGGTCTGGAAGT - Indel[CTCTCCATTTTTG - GCGATCGTCTGACTT] – AGGTGGCGATCGTCTG). First 9 amino acids from *cde-1* followed by newly added aminoacids and premature stop codon.
	xf361	Deletion of 5856 bp & insertion of 38 bp, 25 bp from ATG (AGCAAAGGTCTGGAAGTA - deletion + CGCCTTGAGATGTGTGGACGCAAGATCCACGCACATAT - deletion – ATCGTCTGACTTATCACAA)
smg-2	*xf368*	Deletion of 12624 bp, 13 bp upstream ATG (aaaacccctcaaaaacgcac - deletion – AACGCCGTCCTCCTCCACAA)
smg-1	*xf369*	Deletion of 11211 bp, 116 bp from ATG (ACGTGACACGCCACAGAAG - deletion – aatttttttaagatttagtt)
	xf370	Deletion of 11386 bp & insertion of 12 bp, 112 bp from ATG (AACGTGACACGCCACA - deletion + AAAAAAAAAAAG – AGTTTTTGATTTTGAAAA)
C14C10.5	*xf371*	Deletion of 290 bp, 115 bp from ATG (AGAGCTCGATGAGGACA - deletion – AGCCAATCAGCACTTTTT)
	xf387	Deletion of 6448 bp, 117 bp from ATG (taagaaaaataaaaATG - deletion – aACGAGGATCAACTCATG)
	xf389	Deletion of 6284 bp, 159 bp from ATG (ACTTGAAAATCTCCA - deletion – CGGgtaaattcgatagt)

smg-3	*xf391*	Deletion of 6579 bp & insertion of 7 bp, 256 bp from ATG (GTTGAGGAAATGGCGT – deletion + GAAATGT – gaaatgcccct)

RNAi experiments

HT115(DE3) bacteria carrying Timmons and Fire L4440 RNAi feeding vector (Timmons & Fire, 1998) were grown for 16 hours and directly seeded onto RNAi plates (standard NGM; 1mM IPTG and 50µg/m L ampicillin). HT115(DE3) bacteria containing the *tost-1, tofu-6, his-65, his-66* or *cde-1* targeting RNAi constructs were obtained from the Ahringer RNAi library (Kamath et al., 2003; Kamath & Ahringer, 2003). The control treatment used HT115(DE3) with the empty L4440 vector. To generate a new RNAi vector targeting *tost-1,* its cDNA was cloned into the L4440 vector, using the plasmid pRFK3133. This plasmid was subsequently transformed into HT115(DE3) bacteria and used as described above.

For all RNAi treatments, worms were synchronized by hypochlorite treatment, and L1 larvae were seeded onto RNAi plates containing induced bacteria.

Embryonic viability experiments

All mutant strains were confirmed and outcrossed two times before the experiments. Worms were synchronized using the hypochlorite treatment and allowed to hatch in M9 buffer (22mM KH_2PO_4, 42mM Na_2HPO_4, 85mM NaCl, 1mM $MgSO_4$) for 16h. Synchronized L1 larvae were grown to the L4 stage, after which individual worms were transferred to NGM plates (60 mm) and placed at the appropriate temperature (15°C, 20°C or 25°C) depending on the experimental conditions. Worms were allowed to reproduce for 24-48 hours, after which the adult progenitors were removed from the plates, and the embryos were counted. Plates were incubated for an additional 48-72 hours, after which the number of hatched larvae was recorded. Embryonic viability was calculated as the proportion of hatched larvae to the total number of embryos.

RNA extraction and sequencing

<u>RNA extraction from embryos</u>

To extract RNA from embryos, synchronized gravid adults were washed with M9 buffer and subjected to hypochlorite treatment to isolate embryos. The recovered embryos were washed

four times with cold M9 buffer and then frozen in “worm balls” using liquid nitrogen. The frozen ”worm balls” were ground with a mortar and a pestle, and five volumes of TRIzol™ LS Reagent (Art. No. 10296010, Invitrogen™) were added. RNA extraction was performed using the Direct-zol RNA Microprep kit (Art. No. R2060, Zymo Research™), following the manufacturer’s protocol, with an additional TURBO DNAse treatment (Art. No. AM2208, Invitrogen™) to remove residual genomic DNA. The extracted RNA was resuspended in nuclease-free water.

RNA extraction from larvae

For RNA extraction from larvae, animals were harvested in cold M9 buffer and added with ten volumes of TRIzol LS Reagent (Art. No. 10296010, Invitrogen™). The mixture was flash-frozen in liquid nitrogen to facilitate cell lysis. Subsequent RNA isolation steps were carried out as described for embryos.

Library preparation and RNA sequencing

NGS library prep was performed with Illumina's Stranded mRNA Prep Ligation Kit following Stranded mRNA Prep Ligation ReferenceGuide (June 2020) (Document # 1000000124518 v00). Libraries were prepared with a starting amount of 1000 ng and amplified in 10 cycles. For normalization, 2µl of a 1:100 dilution of ERCC spike-ins (Ambion) were added to the starting material. Libraries were profiled in a DNA 1000 chip on a 2100 Bioanalyzer (Agilent technologies) and quantified using the Qubit dsDNA HS Assay Kit, in a Qubit 2.0 Fluorometer (Life technologies).

All 12 samples were pooled in equimolar ratio and sequenced on 1 NextSeq500 Highoutput FC, SR for 1x 80 cycles plus 10 cycles for the index read plus 1 dark cycle upfront Read.

Read processing and mapping

Sample demultiplexing and FastQ file generation were performed using Illumina's bcl2fastq Conversion Software (v.2.19.1.403). The raw sequence reads were quality assessed using FastQC (v.0.11.8) (https://www.bioinformatics.babraham.ac.uk/projects/fastqc), aligned to the *C. elegans* genome (WBcel235/ce11 assembly) with gene annotation from Ensembl release 104 using STAR (v.2.7) (https://github.com/alexdobin/STAR) with parameter "--outFilterMismatchNoverLmax 0.04" and all secondary alignments were removed with Samtools v.1.9 (http://www.htslib.org).

The mapped sequence data was quality assessed using QualiMap (v.2.2.1) (http://qualimap.conesalab.org) and dupRadar (v.1.37.0) (https://bioconductor.org/packages/dupRadar). Coverage tracks of aligned reads were produced with deepTools bamCoverage (v.3.1) (https://deeptools.readthedocs.io) using Counts Per Million mapped reads (CPM) normalisation. Read counts were summarised on the gene level using Subread featureCounts (v.1.6) (https://subread.sourceforge.net). Differential gene expression analysis was performed with DESeq2 (v.1.26.0) (https://bioconductor.org/packages/DESeq2) following the recommended analysis workflow with independent gene filtering and using 1% FDR significance threshold.

5' Rapid Amplification of cDNA Ends (RACE) PCR

RNA was purified from mixed-stage wild-type worms as described above, and cDNA was synthesized using the ProtoScript First Strand cDNA Synthesis Kit (Art. No. E6300, NEB). The 5' RACE was performed using the FirstChoice® RLM-RACE Kit (Art. No. AM1700, Invitrogen™), following the manufacturer's instructions. Specific oligonucleotides targeting *his-67, his-46* and *tost-1* 5'UTRs were used to assess *trans*-splicing events (Table 4). The resulting 5' RACE products were cloned using TOPO™ TA Cloning™ kit (Art. No. K4575J10) and transformed into One Shot™ TOP10 chemically competent cells (Art. No. C404003, Invitrogen). Successful clones were confirmed by Sanger sequencing.

Table 4 | Oligos used in the RACE PCR experiment

Name	Gene	Sequence 5' – 3'
JP105	*his-67*	TGTGACGGTCTTCCTCTTGG
JP106		ACACCTTGAGAACTCCACGA
JP107		GTGGAAAGGGAGGAAAAGGC
JP122	*his-46*	GAGTTCTTCCTTGGCGCTTC
JP123		GTCTTTCTCTTGGCGTGCTC
JP108	*tost-1*	CGAATTCAAGTTCCGGTCGT
JP109		CGTTAAGCGCTTAGAGCCGAATG

iCLIP

Samples and library preparation

iCLIP in *C. elegans* embryos was performed as described in (Buchbender et al., 2020). Wild-type worms were grown on egg plates, and embryos were harvested via bleaching as described above. Unless otherwise stated, embryos were cross-linked four times using 100 mJ/cm2 in a Stratalinker 2400 at 254 nm. Cross-linking was performed in Worm Lysis Buffer (25mM Tris HCl pH7.5, 150mM NaCl, 1.5mM $MgCl_2$, 1mM DTT, 0.1% Triton X-100), and samples were snap-frozen in liquid nitrogen as "worm balls". 100 µl of Novex™ DYNAL™ Dynabeads™ Protein G (Art. No. 10004D, Invitrogen™) were conjugated with 2 µg of TOFU-6 antibody for 1h at room temperature, followed by two washes with Worm Lysis Buffer. Embryo extracts were prepared by grinding as described above, and 1 mg of total protein was used per replicate. Extracts were incubated for 3 minutes at 37°C with specified concentrations of RNase I (Art. No. AM2295, Ambion) and TURBO DNase (Art. No. AM2208, Invitrogen™), then cooled on ice for 3 minutes. Lysates were clarified by centrifugation at 4°C for 11 minutes and filtered using Proteus Clarification Mini Spin Columns (Art. No. GEN-MSF500, Generon). The lysates were incubated with antibody-conjugated beads for 2 hours at 4°C, followed by washes with high-salt buffer and PNK buffer. RNA-protein complexes on beads were treated with T4 PNK enzyme and RNase inhibitor for RNA 3'end dephosphorylating for 20 min at 37°C. After additional washed, L3-App adapter ligation was performed using T4 RNA ligase overnight at 16°C. Beads were washed, and RNA 5'-end labelling was performed with 32P-γ-ATP at 37°C for 5 minutes. Samples were washed, mixed with 1x NuPAGE loading buffer (Art. No. NP0008, Novex), boiled at 70°C for 10 minutes, and supernatants were collected and run on a 4-12% NuPAGE Bis-Tris gel (Art. No. NP0321PK2, Invitrogen). The RNA-protein complexes were transferred to a Protan BA85 Nitrocellulose Membrane (Whatman), visualised using a phosphoimager (GE Typhoon FLA9500), and the protein-RNA complexes were isolated from the membrane according to the autoradiograph mask.

Membrane fragments were treated with Proteinase K, and RNA was extracted using phenol/chloroform (Art. No. P3803, Sigma) and 2 ml Phase Lock Gel Heavy tube (Art. No. 713-2536, VWR). RNA was precipitated with GlycoBlue (Art. No. 9510, Ambion), 3M sodium acetate pH 5.5, and 100% ethanol. Reverse transcription was performed using RToligo and SuperScript III (Art. No. 18080093 , Invitrogen) as described in the manuscript. RNA clean-up was performed using MyONE Silane beads (Art. No. 37002D, Invitrogen). A second adapter was ligated using High

concentration RNA Ligase (Art. No. M0437M, NEB), followed by another clean-up using MyONE Silane beads. cDNA was amplified with the primer mix P5Solexa/P3Solexa for 18-24 cycles, depending on the sample. Primer dimers were removed using ProNex Chemistry (Art. No. NG2001, Promega). Library size distribution was assessed with High Sensitivity D1000 Kit on the TapeStation system, and library concentration was quantified using Qubit High Sensitivity D1000 Kit. All 4 samples were pooled in equimolar ratio and the library was diluted to 4nM further sequenced.

The experiment was performed using 4 replicates and 2 replicates for negative control without antibody.

RNA sequencing and read processing and mapping

The iCLIP libraries were sequenced on an Illumina NextSeq 500 sequencing machine as 150 nt single-end reads including a 6 nt sample barcode as well as 5+4 nt unique molecular identifiers (UMIs).

Basic quality controls were done with FastQC (v0.11.9) (https://www.bioinformatics.babraham.ac.uk/projects/fastqc/) and reads were filtered based on sequencing qualities (Phred score) in the barcode and UMI regions using the FASTX-Toolkit (v0.0.14) (http://hannonlab.cshl.edu/fastx_toolkit/) and seqtk (v1.3) (https://github.com/lh3/seqtk/). Reads with a Phred score below 10 in the considered regions were removed from further analysis. The remaining reads were de-multiplexed based on the sample barcode on positions 6 to 11 of the reads using Flexbar (v3.5.0) (Roehr et al., 2017). Barcode and UMI regions as well as adapter sequences were trimmed from read ends using Flexbar requiring a minimal overlap of 1 nt of read and adapter. UMIs were added to the read names and reads shorter than 15 nt were removed from further analysis.

Duplicated reads were defined as identical reads including identical UMIs. They were removed from the de-multiplexed and trimmed reads of each sample using basic Bash commands. De-duplicated reads were mapped using STAR (v2.7.3a) (Dobin et al., 2013) and genome assembly WBcel235 and annotation of Ensembl release 108 (Harrison et al., 2024). During mapping, up to 4% of the bases were allowed to be mismatched (--outFilterMismatchNoverReadLmax 0.04 --outFilterMismatchNmax 999), a splice junction overhang of 134 nt (--sjdbOverhang 134) was used and soft-clipping at the 5' end (--alignEndsType Extend5pOfRead1) was prohibited. Since many reads were expected to map to multiple locations, the maximally accepted number of

locations was set to 999 (--outFilterMultimapNmax 999) and the maximal number of loci anchors are allowed to map to was set to 100 (--winAnchorMultimapNmax 100). Multiple alignments of reads were output in random order and the choice of the primary alignment from the highest scoring alignments was made at random (--outMultimapperOrder Random). Secondary hits were removed using Samtools (v1.10) (Danecek, 2021) (samtools view -F 256) keeping only one hit per multi-mapping read. The resulting BAM files were sorted using Samtools (v1.10). Reads directly mapped to the chromosome ends were removed since they do not have an upstream position and, thus, no crosslink position can be extracted.

The position upstream of mapped reads was extracted using BEDTools (v2.29.2) (Quinlan & Hall, 2010) bamtobed, shift (with parameters -m 1 -p -1) and genomecov (with parameters -bg -strand + -5 for reads on the forward strand and with parameters -bg -strand - -5 for reads on the reverse strand). The resulting bedGraph files were converted to bigWig files using bedGraphToBigWig of the UCSC tool suite (v385) (Kent et al., 2010).

In addition to the position upstream of mapped reads, the last position of mapped reads, which were trimmed at the 3' end by at least 6 nt, was extracted as well using BEDTools (v2.29.2) bamtobed and genomecov (with parameters -bg -strand + -3 for reads on the forward strand and with parameters -bg -strand - -3 for reads on the reverse strand). Requiring at least 6 nt to be trimmed ensures that the last position of the reads is indeed the end of the RNA insert. The resulting bedGraph files were converted to bigWig files using bedGraphToBigWig of the UCSC tool suite (v385).

Exonic reads per gene were counted using featureCounts from the Subread tool suite (v2.0.0) (Liao et al., 2014) with non-default parameters --donotsort -M -s1. Raw counts per gene were normalized to reads per million (RPM). The normalized data were visualized using scatter plots, where the log-transformed mean RPM values were compared between specific conditions: Cnt vs TOFU6 rep1-6 and TOFU6 rep1+2 vs TOFU6 rep3-6. In these plots, replication-dependent (RD) histone genes were highlighted in blue, replication-independent (RI) histone genes in brown, and all other genes in light pink.

Genes differentially bound between TOFU-6 iCLIP and control iCLIP samples were detected using the R package DESeq2 (v1.38.1) (Love et al., 2014) in an R/Bioconductor environment (v3.16/ v4.2.2 (Huber et al., 2015; R Core Team, 2019). As control iCLIP samples only differ from TOFU-6 iCLIP samples by not using the TOFU-6 antibody, we are confident that the differences we see are due to different binding behaviour and not due to different expression. However, to be sure, this would require expression data in addition to the iCLIP data to be confirmed.

Results from DESeq2 were visualized as a volcano plot comparing log2 FC of normalized counts of Cnt iCLIP and TOFU-6 iCLIP conditions. A false discovery rate (FDR) threshold of ≥ 1e-5 and the negative log10 of the adjusted p-values (corrected for multiple testing) were used to identify significant changes. Genes below the log2 FC threshold were shown in light pink, with RD histone genes highlighted in blue, RI histone genes in brown, and other gene categories represented in distinct colours.

Using bigWig coverage tracks of either positions upstream of mapped reads or last positions of trimmed mapped reads, we extracted the coverage +/-100 nt around the start and stop codons as well as around the stem-loop regions of selected histone genes using R packages rtracklayer (v1.58.0) (Lawrence et al., 2009), GenomicRanges (v1.50.1) (Lawrence et al., 2013), stringr (v1.5.0) (Wickham, 2022), Biostrings (v2.66.0) (Pagès et al., 2022), and BSgenome (v1.66.1) (Pagès, 2022) in an R/Bioconductor environment (v4.2.2/v3.16) (Huber et al., 2015; R Core Team, 2019). Histone genes were selected based on the presence of the conserved stem-loop (Pettitt et al., 2002). Start and stop codon locations were taken from WBcel235 annotation of Ensembl release 108 (Harrison et al., 2024). Per histone gene, the coverage of each position was normalised by dividing it by the sum of the coverage of all positions in the respective region in the respective gene. All normalised coverages are between 0 and 1 and can be compared between the genes. The average normalised coverage of all selected histone genes is plotted as blue bars in Figure R4 using the R package ggplot2 (v3.4.0) (Wickham et al., 2016). Average normalised coverages shown in Figure R4.A-C are based on positions upstream of mapped reads, while coverages shown in Figure R4.D-F are based on last positions of trimmed mapped reads. The black line shows the rolling mean of the position-wise average normalised coverage using a window size of 20. It was calculated using the R package RcppRoll (v0.3.0) (Ushey, 2022).

In addition to extracting coverages around start and stop codons as well as stem-loop regions separately, we extracted the coverage of the complete gene starting 100 nt upstream of the start codon and ending 100 nt downstream of the stem-loop region using bigWig coverage tracks of positions upstream of mapped reads and R packages rtracklayer (v1.58.0), GenomicRanges (v1.50.1), stringr (v1.5.0), Biostrings (v2.66.0), and BSgenome (v1.66.1) in an R/Bioconductor environment (v4.2.2/v3.16). Start and stop codons as well as stem loop regions were kept as anchor points in order to be able to compare different genes. Since genes have different lengths (CDS region) and also different distances between the stop codon and the stem-loop sequence, these regions have to be made equally long in all genes in order for them to be averaged and shown in the same plot. This was done by equal binning in these regions, i.e. the same number of

bins was used for every gene. Since the region between start and stop codon is typically several 100 nt long, this region was split into 100 equal sized bins and the average position-wise coverage per bin was calculated. The region between the stop codon and the stem-loop sequence varies between 31 and 57 nt. It was split into 31 bins for all considered genes and the average position-wise coverage per bin was calculated. The regions upstream of the start codon as well as downstream of the stem-loop sequences were not binned, but kept as 100 individual positions. The coverage of all bins and positions was normalised by dividing it by the sum of the coverage of all bins and positions. The average normalised coverage of all selected histone genes was calculated per sample, smoothed using a rolling mean as implemented in the R package RcppRoll (v0.3.0) with a window size of 5 and visualized in Figure R3.B using the R package ggplot2 (v3.4.0). Figure R3.C shows the normalized coverage of all positions of histone gene *his-11*. Here, no binning was done and individual positions were visualized. The coverage in TOFU-6 iCLIP replicates is shown as stacked bars.

RT-qPCR

Cultured worms and RNA samples were prepared as described above. Reverse transcription was performed for each sample using a normalised amount of total RNA using the ProtoScript First Strand cDNA Synthesis Kit (Art. No. E6300, NEB) and qPCR Random Primer Mix. qPCR 10µl reactions were set up using PowerUp™ SYBR™ Green Master Mix (Art. No. A25742, Applied Biosystems), 500mM primer concentration and cDNA diluted to approximately 1 ng/µL (1:10 of total PCR volume). Amplifications were performed on Applied Biosystems ViiA7 Real Time PCR System (ThermoFisher Scientific) with cycling conditions as recommended by the manufacturer: Standard run, initial hold at 95°C for 10 minutes, followed by temperature increments of 1,6°C/s; 40 cycles of 95°C for 15 seconds and 60°C for 1 minute; melt curve calculation: 15 seconds at 95°C, 1 minute at 60°C, temperature increments of 0,05°C/s to 95°C and hold for 15 seconds. Technical triplicates and biological duplicates or triplicates, as indicated for each experiment, were used. The ΔΔCT method was applied for data analysis (Schmittgen & Livak, 2008), with *pmp-3* serving as the reference gene for normalization (Hoogewijs et al., 2008). Error bars represent the standard deviation of three technical replicates. Used primers are listed below (Table 5).

Table 5 | qRT-PCR oligonucleotides.

Target	Sequence 5' – 3'
pmp-3_control_Fw	GTTCCCGTGTTCATCACTCAT
pmp-3_control_Rev	ACACCGTCGAGAAGCTGTAGA
his-66_Fw	CAAGCAAGTTCACCCAGACA
his-66_Rev	TCTCCTGGGAGAATCAAACG
his-65_Fw	GTCGGTCGTCTTCACCGTAT
his-65_Rev	AGCTTGTTGAGCTCCTCGTC

Embryo extracts

Synchronized gravid adults were bleached and washed three times with cold M9 buffer, followed by two times with Worm Lysis Buffer (25mM Tris HCl pH7.5, 150mM NaCl, 1.5mM MgCl2, 1mM DTT, 0.1% Triton X-100). Embryo pellets were flash-frozen with liquid nitrogen as "worm balls" and kept at -80°C until usage. Frozen embryo pellets were ground using a pre-chilled mortar and pestle, followed by homogenization with a Dounce homogenizer (40 strokes). The lysates were centrifuged at 21,000 x g for 10 minutes at 4°C. Supernatants were carefully collected into a fresh tube, avoiding contamination from the pellet. Protein concentration of embryo lysates was quantified using the Pierce BCA Protein Assay Kit (Art. No. 23225, ThermoFisher Scientific) according to the manufacturer's instructions, and measurements were performed on an Infinite® M200 Pro plate reader (Tecan).

Immunoprecipitation

Protein extracts were normalised to total protein concentration and diluted with 1x Worm Lysis Buffer to a final volume of 500 µl. 50 µl of each extract were mixed with 1x Novex™ NuPAGE™ LDS sample buffer supplemented with 100 mM DTT and served as input controls.

For TOFU-6 IP, 50 µl Novex™ DYNAL™ Dynabeads™ Protein G (Art. No. 10004D, Invitrogen™) were washed three times with 500 µl 1x wash buffer (25 mM Tris HCl pH 7.5, 150 mM NaCl, 1.5 mM MgCl2, 1 mM DTT, cOmplete™ Mini EDTA-free Protease Inhibitor Cocktail). The washed beads were conjugated with 2 µg antibody (TOFU-6 in-house antibody (Podvalnaya, 2023)) and then incubated with 450 µl of the diluted protein extract for 1 h at 4°C with rotation. After three washes with 500 µl 1x wash buffer, the beads were resuspended in 25 µl 1.2x Novex™ NuPAGE™

LDS sample buffer supplemented with 120 mM DTT. The samples were heated at 70°C for 10 minutes, and the beads were pelleted using the magnetic stand, with the supernatant collected for further analysis.

For 2xFLAG::TOST-1 IP, 30 µl Anti-FLAG® M2 Magnetic Beads (Art. No. M8823, Millipore) were washed three times with 500 µl 1x wash buffer. The beads were then incubated with 450 µl of the diluted protein extract for 1 h at 4°C with rotation. 50 µl of the sample were separated as flow-through. Following the incubation, the beads were washed three times with 500 µl 1x wash buffer and resuspended in 50 µl of 25 mM Tris-HCl pH 8.0 + 1%[w/v] SDS. The samples were heated at 70°C for 10 minutes, and the beads were pelleted using the magnetic stand, with the supernatant collected for further analysis.

For INTS-6::3xFLAG::eGFP IP, 15 µl of GFP-Trap® Magnetic Agarose (Art. No. gtma, Chromotek) or in-house Magnetic GFP binder beads (PPCF) were washed three times with 500 µl of 1x wash buffer and incubated with 450 µl of protein extracts. The remaining steps were performed as described above, except that the beads were resuspended in 1x Novex™ NuPAGE™ LDS sample buffer, boiled for 5 minutes at 95°C, supplemented with 100 mM of DTT and boiled for another 5 minutes at 95°C.

Western-blot

Embryo extracts were prepared and normalised to total protein concentration as described previously. For immunoprecipitation experiments, equal amounts of input samples, flow-through and IP samples were adjusted to the same volume with 1x Novex™ NuPAGE™ LDS sample buffer (Art. No. NP0007, Invitrogen™) supplemented with 100 mM DTT and incubated for 10 min at 95°C.

Samples were loaded onto 4-12% gradient gels (Art. No. NP0321BOX, ThermoFisher,) and separated using 1x NuPAGE MES SDS Running Buffer (Art. No. NP0002, ThermoFisher,) for INTS-6::3xFLAG::eGFP IP or 1x NuPAGE MOPS SDS Running Buffer (Art. No. NP0001, ThermoFisher,) for TOFU-6 IP. Proteins were transferred to Protan BA85 Nitrocellulose Membrane (Art. No. 10600002, Amersham) for 1h at 120 V using a Mini Trans-Blot® Cell (Art. No. 1703930, Bio-Rad) using 1x NuPAGE™ Transfer Buffer (Art. No NP0006, Invitrogen™) supplemented with 10 % methanol. Membranes were blocked in 1x PBS containing 5 % skim milk and 0.1 % Tween®20 for 1 h, then sectioned as necessary based on protein molecular weights. Each section was incubated overnight at 4°C in 1x PBS containing 5 % skim milk, 0.1 % Tween®20, and the

appropriated primary antibody: in-house anti-TOFU-6; anti-FLAG (rabbit, 1:1000, F7425-2MG, Sigma), anti-α Tubulin (mouse, 1:1000, ab7291, Abcam). Membranes were washed three times for 10 minutes each with 0.1% PBS-T (1× PBS + 0.1% Tween®20), incubated for 1 h in 0.1% PBS-T with the secondary antibody (1:2500 anti-rabbit IgG HRP-linked, Art. No. 7074, Cell Signaling Technology®; or 1:2500 anti-mouse IgG HRP-linked, Art. No. 7076, Cell Signaling Technology®), and washed three additional times with 0.1% PBS-T. Protein detection was carried out using Amersham™ ECL Select™ Western Blotting Detection Reagent (Art. No. RPN2235, GE Healthcare) and imaged on a LI-COR Odyssey M Western blot imager.

Mass-spectrometry

Enzymatic protein digestion

Immunoprecipitation experiments associated with mass spectrometry were performed as explained above, in quadruplicates.

All samples were processed using the SP3 approach (Hughes et al., 2019). The proteins were reduced in DTT and alkylated by iodoacetamide in the dark. Enzymatic protein digestion was performed using trypsin overnight at 37°C. The resultant peptide solution was purified by solid phase extraction in C_{18} StageTips (Rappsilber et al., 2003).

Liquid chromatography tandem mass spectrometry

Peptides were separated via an in-house packed 30-cm analytical column (inner diameter: 75 µm; ReproSil-Pur 120 C18-AQ 1.9-µm silica particles, Dr. Maisch GmbH) on an EASY-nLC 1000 UHPLC system (Thermo Scientific). The online reversed-phase chromatography separation was conducted through a 105-min non-linear gradient of 1.6-32% acetonitrile with 0.1% formic acid at a nanoflow rate of 225 nl/min. The eluted peptides were sprayed directly by electrospray ionization into a Q Exactive Plus Orbitrap mass spectrometer (Thermo Scientific). Mass spectrometry was conducted in data-dependent acquisition mode using a top10 method with one full scan (mass range: 300 to 1,650 m/z; resolution: 70,000, target value: 3 × 106, maximum injection time: 20 ms) followed by 10 fragmentation scans via higher energy collision dissociation (HCD; normalised collision energy: 25%, resolution: 17,500, target value: 1 × 105, maximum injection time: 120 ms, isolation window: 1.8 m/z). Precursor ions of unassigned or +1 charge

state were rejected. Additionally, precursor ions already isolated for fragmentation were dynamically excluded for 20 seconds.

Mass spectrometry data processing and statistical analysis

Mass spectrometry raw data were processed by MaxQuant software package (v 2.1.3.0) (J. Cox & Mann, 2008) using its built-in Andromeda search engine (J. Cox et al., 2011). Spectral data were searched against a target-decoy database consisting of the forward and reverse sequences of the 3XFLAG::TOST-1 bait protein, the UniProt *C. elegans* (release 2023_02; 28,540 entries) and E*. coli* (release 2023_01; 5,064 entries) reference proteomes and a list of common contaminants. Trypsin/P specificity was assigned. A maximum of 2 missed cleavages were tolerated. Carbamidomethylation of cysteine was set as fixed modification. Methionine oxidation and protein N-terminal acetylation were chosen as variable modifications. The "second peptides" option was switched on. The "match between runs" function was activated. The minimum peptide length was set to 7 amino acids. False discovery rate (FDR) was set to 1% at both peptide and protein levels.

The MaxLFQ algorithm (J. Cox et al., 2014) was employed for label-free protein quantification without using its default normalization option. Minimum LFQ ratio count was set to be one. Both the unique and razor peptides were used for quantification. Detected *E. coli* proteins, reverse hits, potential contaminants and "only identified by site" protein groups were filtered out. Data normalisation was performed on the log-transformed data. Under the assumption that the majority of the detected proteins were non-specific background binders, the distribution of protein LFQ intensities was assessed using kernel density estimation to find the peak density (A. K. Rai et al., 2018). The LFQ intensities of each pull-down were then normalised by adjusting to the point at which the peak density was found. Proteins were further filtered to retain only those detected in at least two out of the four replicates in either group of each comparison. Following imputation of the missing LFQ intensity values, the statistical significance of the difference between the two groups was assessed using a modified *t*-statistic (*t*(SAM, statistical analysis of microarrays) (Tusher et al., 2001) and visualized on a volcano plot. The combined significance threshold (hyperbolic curve) was defined as t_0 = 1.4 and s_0 = 1.5.

Wide-field microscopy

Adult hermaphrodites were prepared by washing 20 – 30 animals in a drop of 100 µl M9 buffer, followed by transfer to a 50 µl drop of M9 buffer supplemented with 40 mM sodium azide on a coverslip. After incubating for 15 to 30 min, excess buffer was removed, and a glass slide with a freshly prepared agarose pad (2 % (w/v) in water) was placed over the coverslip. For imaging embryos, adult hermaphrodites were washed and dissected in M9 buffer before mounting.

Imaging was performed using a Leica DM6000B or Leica DMi8 wide-field microscope. For embryo imaging, a 63× objective (NA 1.43) was used, and a 40× objective (NA 1.25) was used for larvae. Images were processed and analysed using Fiji software.

Spinning disk microscopy

Adult hermaphrodites were washed and dissected in M9 buffer to isolate embryos, which were then mounted as previously described. Time-lapse imaging of embryos was performed over 66 minutes with a 3-minute interval using a spinning disk confocal microscope from Visitron Systems (VisiSope 5Elements) based on a Nikon Ti-2E stand and a spinning disk from Yokogawa (CSU-W, 50 µm pinhole) controlled by the VisiView® software. The microscope was equipped with a 60x plan apochromatic water immersion objective (NA 1.49), a twofold magnification lens in front of the sCMOS camera (BSI, Photometrics), and a stage-top incubation chamber for live imaging (20°C, ambient CO_2). Embryos were excited by an argon laser at λ_{ex} = 488 nm (200 mW, power set to 20 %) and the emission was detected in a range of λ_{em} = 500 - 550 nm (ET525/50m, Chroma). Z stacks were acquired with 5 µm step size.

Image processing and quantification

Microscopy images were processed using Fiji. For measuring the GFP mean intensity in embryo nuclei, background subtraction was first applied to the images. Regions of interest (ROIs) for nuclei were defined using the Difference of Gaussian (DoG) filter (sigmas set to 11 and 7), followed by thresholding with the Otsu method. In each embryo, the average GFP mean intensity was calculated from three nuclei that were in focus. For embryos where GFP expression in nuclei was absent, ROIs were manually defined using the brightfield channel. In addition to GFP mean intensity, the nuclear area was quantified

For time-lapse experiments (Figure R22), z-stacks were combined using the Sum Z projection in Fiji. GFP mean intensity and standard deviation across the entire embryo were calculated after background subtraction. ROIs for this analysis were manually defined based on the brightfield channel. For the nuclei counting (Figure R23), the same procedure described above for defining ROIs and quantifying nuclear GFP intensity was applied.

smFISH

Sample preparation and imaging

Single-molecule FISH probes (Table 6) targeting the *gfp* sequence present in the alleles *ne4846* and *ne4847* (Makeyeva et al., 2021) were designed using the Sterallis Probe designer. *C. elegans* embryos were harvested three days after bleaching, as described previously. To slow developmental progression, all buffers and centrifugations were performed at 4°C. Embryos were fixed in 4% paraformaldehyde (PFA) in 1x PBS for 15 minutes at room temperature. The samples are vortexed and immediately subjected to freeze-cracking by immersion in liquid nitrogen for one minute, followed by thawing in water at room temperature. After thawing, the samples were vortexed again, placed on ice for 20 minutes, and washed twice with 1x PBS. For permeabilization, the embryos were resuspended in 70% ethanol and stored overnight at 4°C. Hybridization was performed by mixing the probes in hybridization buffer (100 mg/mL Dextran sulfate, 1 mg/mL E. coli tRNA, 2 mM Vanadyl ribonucleoside complex, 0.2 mg/mL RNase-free BSA, 10% (v/v) Formamide (deionized)) at a final concentration of 125 nM. After washing the embryos with wash buffer (10% (v/v) Formamide (deionized), 1X SSC buffer), the hybridization buffer was added, and the samples were incubated overnight at 30°C. The samples were subsequently washed twice for 30 minutes at 37°C, with DAPI added to the final wash at a concentration of 5 ng/ml to stain the nuclei. After a final 5-minute wash with 2x SSC at room temperature, the embryos were mounted in Ibidi mounting medium (Art. No. 50001, Ibidi) and directly imaged using a Spinning Disc Confocal Microscope BC43 (Andor) and the objective 100x (NA 1.45). Z-stacks were acquired with 0.5 µm intervals.

Table 6 | Probes used in smFISH experiment.

Probe name	Sequence
his-61_GFP_1	aagttcttctcctttactgg
his-61_GFP_2	gaattgggacaactccagtg

his-61_GFP_3	cccattaacatcaccatcta
his-61_GFP_4	cctctccactgacagaaaat
his-61_GFP_5	gtaagttttccgtatgttgc
his-61_GFP_6	gtagttttccagtagtgcaa
his-61_GFP_7	acaagtgttggccatggaac
his-61_GFP_8	ggtatctcgagaagcattga
his-61_GFP_9	tcatgccgtttcatatgatc
his-61_GFP_10	gggcatggcactcttgaaaa
his-61_GFP_11	ttctttcctgtacataacct
his-61_GFP_12	gttcccgtcatctttgaaaa
his-61_GFP_13	tgacttcagcacgtgtcttg
his-61_GFP_14	taacaagggtatcaccttca
his-61_GFP_15	atacctttaactcgattct
his-61_GFP_16	gtgtccaagaatgtttccat
his-61_GFP_17	gtgagttatagttgtattcc
his-61_GFP_18	gtctgccatgatgtatacat
his-61_GFP_19	ctttgattccattcttttgt
his-61_GFP_20	ccatcttcaatgttgtgtct
his-61_GFP_21	atggtctgctagttgaacgc
his-61_GFP_22	cgccaattggagtattttgt
his-61_GFP_23	gtctggtaaaaggacagggc
his-61_GFP_24	aagggcagattgtgtggaca
his-61_GFP_25	tcttttcgttgggatctttc
his-61_GFP_26	tcaagaaggaccatgtggtc
his-61_GFP_27	aatcccagcagctgttacaa
his-61_GFP_28	tatagttcatccatgccatg

Image analysis and quantification

smFISH image analysis were performed using Imaris software (v 10.1). The "Spots" function within the software was used to detect and quantify individual fluorescent molecules. The detection of smFISH molecules was guided by the "Quality" threshold parameter, which determines the minimum signal intensity required for a spot to be considered. This parameter was optimized to minimize background detection while ensuring accurate identification of true smFISH signals. For each detected spot, the maximum fluorescence intensity was also measured to assess variability in signal strength. This experiment was performed in two independent times.

EMS screening

Mutagenesis

The protocol used was based on (Brenner, 1974; Jorgensen & Mango, 2002). Mix stage plates of the RFK912 strain, containing a large number of early L4 larvae, were washed with M9 buffer.

The worms were collected in 15 ml sterile plastic centrifuge tube, and the supernatant was discarded following centrifugation. The worm pellet was then resuspended in 3 ml of M9 buffer and transferred to a new tube containing diluted EMS (Art. No M0880, Sigma) in M9 buffer to a final concentration of 47mM. The worms were incubated at 20°C for 4 hours on a spinning wheel. After incubation, the worms were pelleted again, the supernatant removed, and the worms were washed twice with M9 buffer. The treated worms were then transferred to NGM plates (90 mm) seeded with OP50 and incubated at 15°C. Seven days later, 1100 F1 offspring were singled onto new NGM plates (60 mm), with 5 worms per plate, and incubated at 15°C. After five days, when the F1 generation reached the L4 stage, the worms were transferred to 25°C. After an additional five days, plates were screened for F3 suppressors, which were then singled onto individual plates. F3 plates were incubated at 25°C to confirm homozygosity of the suppressor mutation for one more generation. F4 animals with viable progeny were selected and backcrossed twice to the original RFK912 strain. The clonal population from the F4 generation of the outcrossed strains was expanded until the plates were starved for genomic DNA extraction. The RFK912 strain was used as the reference genome for subsequent analyses.

Genomic DNA extraction and library preparation

Genomic DNA (gDNA) was extracted using the Gentra Puregene Tissue Kit (Art. No. 158667, Qiagen), according to the manufacturer's instructions. A total of 1.5 µg of gDNA was diluted to a final volume of 55 µl using TE buffer and fragmented using a Covaris S2 sonicator, using the following parameters: Intensity: 5; Duty Cycle: 10%; Cycles/burst: 200; Time (sec): 120; Number of cycles: 2.; Power mode: Frequency sweeping.; Degassing mode: Continuous. The fragmented gDNA was pooled and analysed using the Tape Station with High Sensitivity D1000 ScreenTape.

Library preparation was performed using NEBNext Ultra II DNA Library Prep Kit for Illumina Version 7.0_9/22. Libraries were prepared with a starting amount of 10ng of fragmented DNA and were amplified in 9 PCR cycles. Libraries were profiled in a High Sensitivity DNA on a 2100 Bioanalyzer (Agilent technologies) and quantified using the Qubit 1x dsDNA HS Assay Kit, in a Qubit 4.0 Fluorometer (Invitrogen by Thermo Fisher Scientific). All 22 samples were pooled together in equimolar ratio and sequenced on 1 NextSeq2000 P2 FC,PE for 2x 100 cycles plus 2x 8 cycles for the dual index read.

Sequencing and analysis

Libraries were sequenced on a NextSeq2000 with a read length of 100 base pairs in paired end mode. Reads were trimmed for sequencing adapters using Cutadapt (M. Martin, 2011) (v4.4) and mapped against the C.elegans genome (WBcel235) using BWA-MEM2 (H. Li, 2013) (v2.2.1), read duplicates were removed using Picard ('Picard Toolkit', 2019) (v3.0.0). Tracks were generated using bamCoverage (Ramírez et al., 2016) (v3.5.1). The variants were called using GATK Haplotypecaller (Poplin et al., 2018) (v4.4.0.0) and subsequently filtered using GATK's SelectVariants tool for SNPs, Indels and mixed variants. The identified variants were ten filtered filtered for variants present in the TOST sample using vcftools (Danecek et al., 2011) (v0.1.16). The TOST sample serves as the background of the used strain towards the reference strain. Additional filtering was done for standard quality and a minimal depth of 6 (parameter "–filter +/d=6") by vcftools. The variants were then classified as homozygous and heterozygous calls using GATKs SelectVariants and VariantFilteration tools. Afterwards vcf files were converted to maf (Mayakonda et al., 2018) (v1.6.21) and annotated using VEP (McLaren et al., 2016) (v110.1). The expected transitions from G to A and C to T were selected, using bcftools (Danecek et al., 2021) (v1.17). The filtered vcf files for homozygous calls were then converted to XLSX format using R/Bioconductor (Huber et al., 2015) (v3.16) and a range of R/Bioconductor packages (Maftools (Mayakonda et al., 2018) v2.16, VariantAnnotation (Obenchain et al., 2014) v1.46, openxlsx (Schauberger et al., 2024) v4.2.5.2, tidyr (Wickham et al., 2024) v1.3.0, purrr (Wickham & Henry, 2024) v1.0.1, dplyr (Wickham et al., 2023) v1.1.2 , tibble (Müller & Wickham, 2024) v3.2.1).

Y2H

Two-hybrid assays were performed using the haploid *Saccharomyces cerevisiae* strains PJ69-4a and PJ70-4α, along with the pGAD and pGBD plasmid series, as described previously in (James et al., 1996). Briefly, plasmids were constructed by cloning the cDNA of the respective gene into the appropriate plasmid vector using restriction enzymes (Table 7). The resulting plasmids were then transformed into one of the two yeast strains and allowed to grow on –Trp or –Leu YPD plates to select for successful transformation. Colonies carrying the pGAD plasmid were then pooled with colonies carrying the pGBD plasmid and allowed to mate at 37°C overnight. The mating solution was spotted onto –Trp –Leu YPD plates, and the plates were incubated for 3 days at 30°C to confirm successful mating. A colony from each mating pair was subsequently used for

pinning onto selection plates [a) –Leu –Trp; b) -Leu –Trp –His; c) -Leu –Trp –His –Ade]. These plates were incubated for three days, and interactions were scored based on growth. Cell pinning was performed using the Rotor HAD (Singer Instruments, ROT-001).

Table 7 | List of plasmids used in the Y2H experiment.

Plasmid number	Construct/Backbone	Plasmid number	Construct/Backbone
pRFK1394	pGAD	pRFK3186	ints3a in pGAD
pRFK1395	pGBD	pRFK3187	ints3c in pGAD
pRFK1396	ife-3 in pGAD	pRFK3188	ints3d in pGAD
pRFK1397	ife-3 in pGBD	pRFK3189	ints6a in pGAD
pRFK1398	erh-1 in pGAD	pRFK3190	spt5 in pGAD
pRFK1399	erh-1 in pGBD	pRFK3191	spt4 in pGAD
pRFK2100	pid-1 in pGAD	pRFK3192	nabp1a in pGAD
pRFK2101	pid-1 in pGBD	pRFK3193	nabp1b in pGAD
pRFK2102	tost-1 in pGAD	pRFK3194	ints3a in pGBD
pRFK2103	tost-1 in pGBD	pRFK3195	ints3c in pGBD
pRFK2104	tofu-6 in pGAD	pRFK3196	ints3d in pGBD
pRFK2105	tofu-6 in pGBD	pRFK3197	ints6a in pGBD
pRFK2106	pid-3 in pGAD	pRFK3198	spt5 in pGBD
pRFK2107	pid-3 in pGBD	pRFK3199	spt4 in pGBD
pRFK2115	erh-2 in pGAD	pRFK4500	nabp1a in pGBD
pRFK2116	erh-2 in pGBD	pRFK4501	nabp1b in pGBD

Statistics

Statistical analyses of microscopy data and viability assays were performed using RStudio (v 4.2.2). Normality of the data distribution was assessed using the Shapiro-Wilk test. Homogeneity of variance for normally distributed data was evaluated using Levene's test. For normally distributed data with equal variances, an unpaired Student's t-test was used for comparisons between two groups. For non-normally distributed data, the Mann-Whitney U test was used for comparisons between two groups. For multiple group comparisons of non-normally distributed data, the Kruskal-Wallis test followed by Dunn's post-hoc test with Benjamini-Hochberg correction was applied to adjust p-values. A p-value < 0.05 was considered statistically significant. All experiments were performed at least twice.

Online resources

All databases, predictors and other online resources are listed in Table 8.

Table 8 | List of online resources used in this study.

Name	**URL**	**Reference**
BLAST®	https://blast.ncbi.nlm.nih.gov/Blast.cgi	(Camacho et al., 2009)
Clustal Omega	https://www.ebi.ac.uk/Tools/msa/clustalo/	(Madeira et al., 2019)
CRISPOR	http://crispor.tefor.net/	(Haeussler et al., 2016)
IDT™ OligoAnalyzer	https://eu.idtdna.com/calc/analyzer	-
Omero	https://www.openmicroscopy.org/	(Allan et al., 2012)
Primer3web v4.1.0	http://primer3.ut.ee/	(Untergasser et al., 2012)
UniProt	https://www.uniprot.org/	(Bateman, 2019)
Stellaris Probe Designer v 4.2	https://www.biosearchtech.com/stellaris-designer	-
Wormatlas	https://www.wormatlas.org/	-
Wormbase	https://wormbase.org/	-
Wormbook	http://wormbook.org/	-

RESULTS

TOFU-6 binds specifically RD histone mRNAs in embryos

Our group, along with others, previously identified the PETISCO complex, which includes the proteins TOFU-6, PID-3, ERH-2 and IFE-3 (Cordeiro Rodrigues et al., 2019; Zeng et al., 2019). PETISCO interacts with two distinct small ligand proteins, PID-1 and TOST-1, which appear to direct the complex towards different RNA targets. In the presence of PID-1, PETISCO associates specifically with piRNAs precursors. However, the RNA targets of PETISCO in the presence of TOST-1 remain unknown. Importantly, both PETISCO and TOST-1 are essential for early embryogenesis; loss of either result in a maternal-effect embryonic lethality (Mel) phenotype. PID-1 on the other hand, is not necessary for embryonic development.

TOFU-6 iCLIP optimization

To identify the RNA targets of PETISCO in embryos, we optimized Individual-nucleotide resolution UV crosslinking and immunoprecipitation (iCLIP) on endogenous TOFU-6, a 41 kDa protein with an RRM domain, making it well-suited for RNA binding experiments. Using an anti-TOFU-6 antibody, we detected a distinct, specific band in immunoprecipitated (IP) samples from embryos (**Figure R1.A**). We optimized the iCLIP protocol across several parameters, such as UV-C irradiation intensity, antibody concentration, and RNase concentration, each tested sequentially to determine optimal TOFU-6/RNA complex formation, monitored via phosphoimaging (**Figure R1.B**). UV-crosslinking confirmed that TOFU-6 associates with RNA *in vivo,* as indicated by a clear band in UV-treated samples (**Figure R1.B**, sample 1) that was absent in untreated samples (**Figure R1.B**, sample 3). We tested two antibody concentrations (2 µg and 10 µg) and found that 2 µg provided the best specificity (**Figure R1.B**, samples 5, 6); thus, we proceeded with this concentration. Next, we optimized the UV-C dose and observed that 400 mJ/cm^2 produced the most stable protein-RNA complexes (**Figure R1.B**, samples 7-10). Adjustments in RNase concentration generated RNA fragments of various sizes, with lower RNase levels producing more diffused signal due to longer protein-RNA complexes (**Figure R1.B**, samples 11-14). Using an RNase inhibitor instead of RNase resulted in a highly diffuse signal, indicating the presence of untrimmed RNA (**Figure R1.B**, sample 15).

Based on these optimizations, we used 2 µg of anti-TOFU-6 antibody, an RNase dilution of 1:300, and 400 mJ/cm^2 UV-C irradiation for all subsequent library preparations. Immunoprecipitations and RNA extractions were performed in two separate batches, resulting in six biological

replicates for TOFU-6 iCLIP (samples 1 to 6) along with two negative controls lacking anti-TOFU-6 antibody (Cnt1 and Cnt2) (**Figure R1.C**).

After RNA purification and cDNA synthesis, we amplified the libraries using varying PCR cycles to maintain optimal yield: 21 cycles for replicate 1, 19 cycles for replicate 2, and 24 cycles for the remaining samples. We assessed the library size distribution using a TapeStation (**Figure R1.D**). All samples, including the negative controls, showed prominent bands at approximately 50 bp and 70-80 bp, which likely corresponded to primer dimers. However, only TOFU-6 iCLIP samples showed diffuse signal spanning from 70 bp to 150 bp and from 200 bp upwards, which was absent in Cnt1 and Cnt2. The libraries were pooled, and excess primers were removed through two rounds of ProNex size selection (**Figure R1.E**).

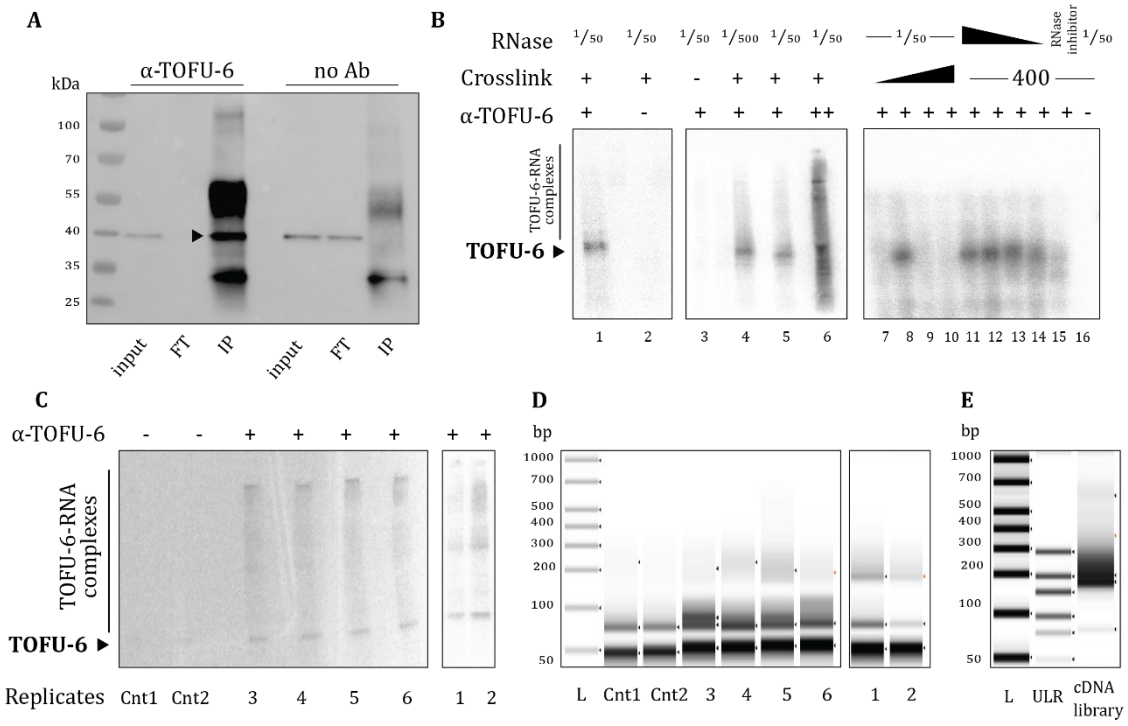

Figure R1 | TOFU-6 iCLIP optimization in *C. elegans* embryos. A. Immunoprecipitation (IP) experiment using embryo lysates incubated with beads conjugated to anti-TOFU-6 antibody (α-TOFU-6) or unconjugated beads (no Ab). Input, IP and flow-through (FT) fractions were analysed by western blot. The predicted TOFU-6 protein is indicated by the arrow. B. Autoradiographs showing radioactively labelled TOFU-6-RNA complexes from optimization steps for α-TOFU-6 specificity (left panel), antibody concentration (middle panel), and UV-C crosslink intensity and RNase concentration (right panel). In the left panel (lanes 1 and 2), embryos were UV-treated with 400 mJ/cm2 (+), followed by IP with α-TOFU-6 conjugated beads (+) or unconjugated beads (-), and treatment with RNase at a 1:50 dilution. In the middle panel (lanes 3 - 6), embryos were either untreated (-) or treated with UV-B 400 mJ/cm2 (+), followed by IP with beads conjugated to either 2 µg (+) or 10 µg (++) of α-TOFU-6, with RNase diluted at either 1:50 or 1:500. In the right panel (lanes 7 - 16), embryos were treated with increasing UV-B energies (200 mJ/cm2, 400 mJ/cm2, 600 mJ/cm2, 800 mJ/cm2) (lanes 7-10), followed by IP with beads conjugated to 2 µg of α-TOFU-6 and RNase treatment at 1:50. In lanes 11 – 14, embryos were treated with UV-B 400 mJ/cm2, IP was done with 2 µg α-TOFU-6 conjugated beads, and RNase was diluted at 1:50, 1:300, 1:500, or 1:1000. Lane 15, shows a sample treated with RNase inhibitor instead of RNase. Lane 16 shows embryos treated with UV-B and subjected to IP with unconjugated beads (-). C.

Autoradiographs of final TOFU-6-RNA complexes used for library preparation (replicates 1 - 6). Samples prepared with unconjugated beads were used as negative controls (Cnt1 and Cnt2). D. Tape-station profile of PCR fragments extracted from RNA samples (from samples shown in C), amplified using a different number of cycles: 21 cycles for replicate 1, 19 cycles for replicate 2, and 24 cycles for the remaining samples. E. Tape-station profile of the final pooled library after size-selection treatment.

RD-histone mRNAs are enriched in TOFU-6 iCLIP

In standard iCLIP analysis, a read is classified as a technical duplicate of another read, if both map to the same genomic position and strand with identical random barcodes (unique molecular identifiers, or UMIs) (Busch et al., 2020). However, for this experiment, we adjusted the protocol by defining technical duplicates as reads with identical sequences, including matching UMIs, before mapping. This modification allowed for the removal of duplicated reads prior to alignment, which was critical given our expectation of enrichment in genes with high sequence similarity. Such enrichment typically results in multi-mappers, which are usually excluded. In our analysis, we obtained ~20-30% uniquely mapped reads and ~60-70% multi-mapped reads, and we retained multi-mappers for further analysis.

We observed a significant enrichment of replication-dependent (RD) histone genes in TOFU-6 iCLIP samples compared to the two negative control samples (Cnt iCLIP), with an FDR < 0.01 (**Figure R2.A**). This enrichment is specific to RD histones, as replication-independent (RI) histones showed no significant increase. The classification of these histone classes is based on the presence of a conserved stem-loop structure, as described in Pettitt et al., 2002. To confirm that variability between the two sets of replicates (rep 1-2 and rep 3-6) did not affect our findings, we compared normalized RD histone read counts across the sets and found no major differences (**Figure R2.B**). Differential expression analysis between TOFU-6 iCLIP and Cnt iCLIP further confirmed a significant and specific enrichment for RD histones (**Figure R2.C**).

Beyond RD histones, we also detected a significant enrichment for several other RNA types, including tRNAs, the ncRNAs *Y105C5A.1284* and *CD4.17*, the snoRNA *W03B1.17*, as well as two protein-coding genes *C08F8.2* and *W09H1.4* and the RI histone *his-39*. In order to see why these non-RD histone mRNAs were identified, we analysed these in further detail. For *W09H1.4*, read mappings were localized in the 5' UTR, which overlaps with the coding sequence of *his-73,* an RD histone gene encoding an H3-like protein with a distinctive stem-loop (Pettitt et al., 2002). In contrast, *his-39,* while classified as an RI histone coding for the variant H2B.K, also possesses a conserved stem-loop structure. This gene includes an intron in the *C. elegans* genome assembly WBcel235, which is absent in WBcel245. It is tentatively described as RD histone by (Pettitt et al., 2002). The gene *C08F8.2* encodes an ortholog of the human Suv3-like RNA helicase. Read

alignments to *C08F8.2* began in the last 8 bp of its sixth intron and extended over a span of 250.000 bp, terminating in the 3'UTR of *his-63* and *his-64* genes. This means that even the mRNA targets that are not RD histones, are still likely to be genomically related to them.

On the other hand, two other genes encoding canonical histone proteins, *his-41* and *his-37,* were expected to be enriched in the TOFU-6 iCLIP experiment. These genes encode canonical H2B and H4 histone proteins, respectively. However, we did not observe significant enrichment for these targets. Despite their canonical roles, these genes are spliced and lack the conserved stem-loop structure, which likely explains their absence from the TOFU-6 iCLIP-enriched targets.

Overall, we conclude that TOFU-6 specifically binds to RD-histone mRNAs. The presence of the conserved stem-loop structure or the absence of splicing in these genes likely contributes to this specificity.

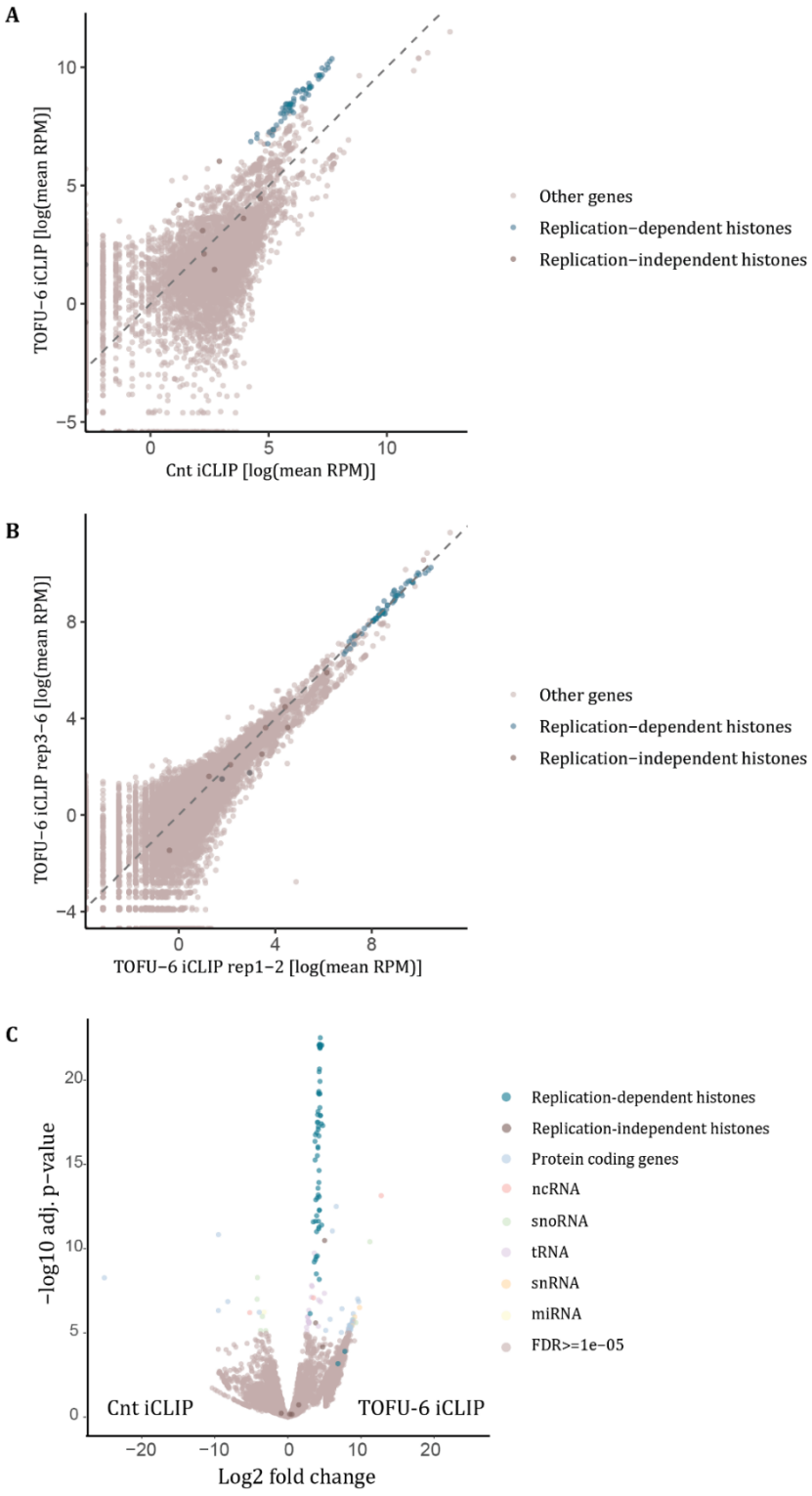

Figure R2 | Replication-dependent (RD) histones are specifically enriched in TOFU-6 iCLIP. A. Scatter plot comparing the mean of normalised reads per million (RPM) between TOFU-6 iCLIP (replicates 1 - 6) and control iCLIP (Cnt1 and Cnt2). RD histone genes are highlighted in one colour, while RI histone genes are shown in another. B. Scatter plot comparing the mean of normalised reads (RPM) between TOFU-6 iCLIP replicates 1 and 2 with replicates 4 to 6. RD histone genes are highlighted in one colour, while RI histone genes are shown in another. C. Volcano plot displaying

the results of differential expression analysis (DESeq2) for all tested genes, depicting their expression fold change vs. statistical significance. All significantly changed genes (FDR<0.00001) are coloured according to their gene biotype, with histone genes specifically labelled as either replication-dependent (RD) or replication-independent (RI).

TOFU-6 binds the 3'UTR of RD histone mRNAs

Crosslinking events detected in histone genes are distributed throughout the transcripts (**Figure R3.A**). Using the iCLIP protocol, crosslinking events can be identified at nucleotide resolution (König et al., 2010). To analyse TOFU-6 binding patterns across all RD histone transcripts, we generated a metagene coverage plot by aligning sequences 100 bp upstream of each start codon through 100 bp downstream of each stem-loop structure. For each RD histone gene, we calculated the mean of the normalised coverage, obtained by calculating the absolute coverage per histone gene (number of iCLIP reads mapped starting at each position) divided by the total coverage across the respective gene. To account for variability in transcript lengths, we binned regions instead of using absolute base-pair positions (**Figure R3.B**). Our results show that TOFU-6 binding on histone transcripts is enriched towards the 3' end, with two main peaks directly upstream and downstream of the stop codon, along with a larger peak located just upstream of the stem-loop (**Figure R3.B**). Using *his-11* as a representative example, we observe numerous crosslinking events just upstream of the stop codon, between the stop codon and the stem-loop, and a final peak immediately upstream of the stem-loop (**Figure R3.C**).

A

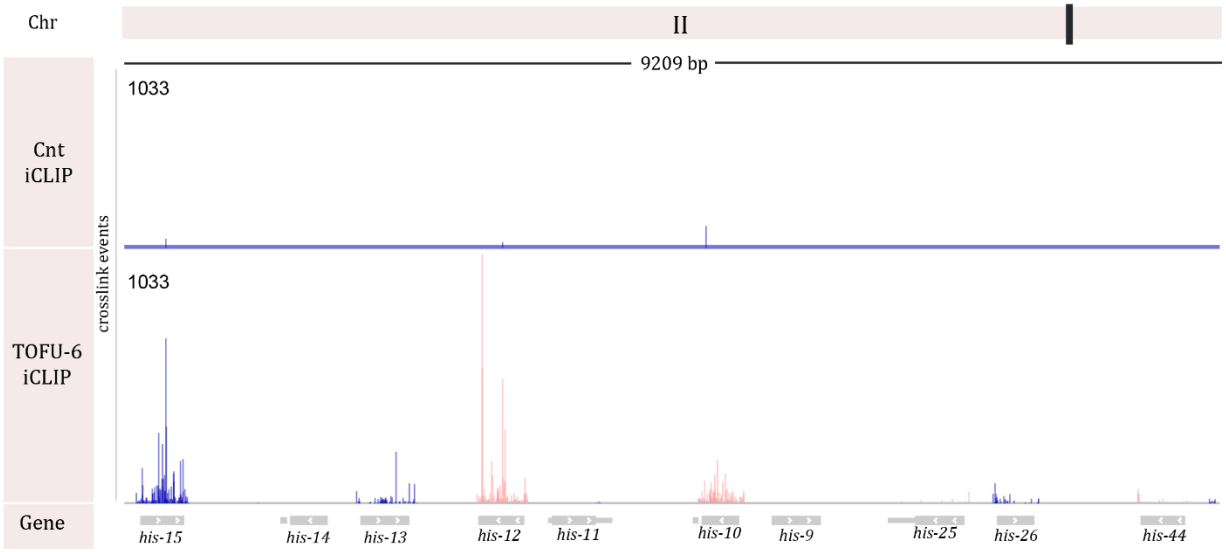
Chr
II
9209 bp
Cnt iCLIP
1033
crosslink events
TOFU-6 iCLIP
1033
Gene
his-15
his-14
his-13
his-12
his-11
his-10
his-9
his-25
his-26
his-44

B

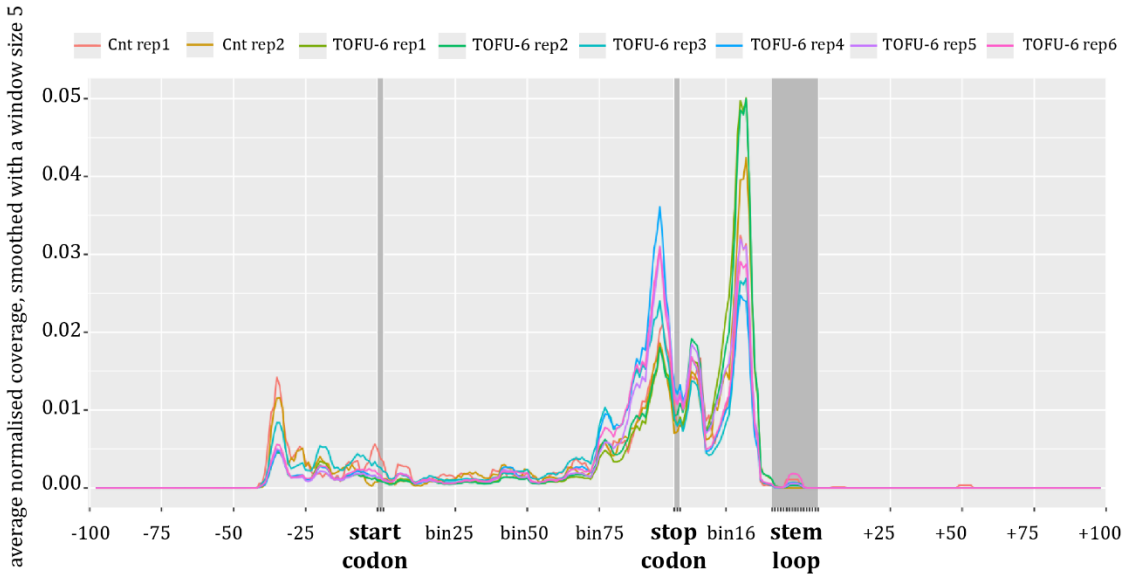
Cnt rep1
Cnt rep2
TOFU-6 rep1
TOFU-6 rep2
TOFU-6 rep3
TOFU-6 rep4
TOFU-6 rep5
TOFU-6 rep6
average normalised coverage, smoothed with a window size 5
0.05
0.04
0.03
0.02
0.01
0.00
-100
-75
-50
-25
start codon
bin25
bin50
bin75
stop codon
bin16
stem loop
+25
+50
+75
+100

C

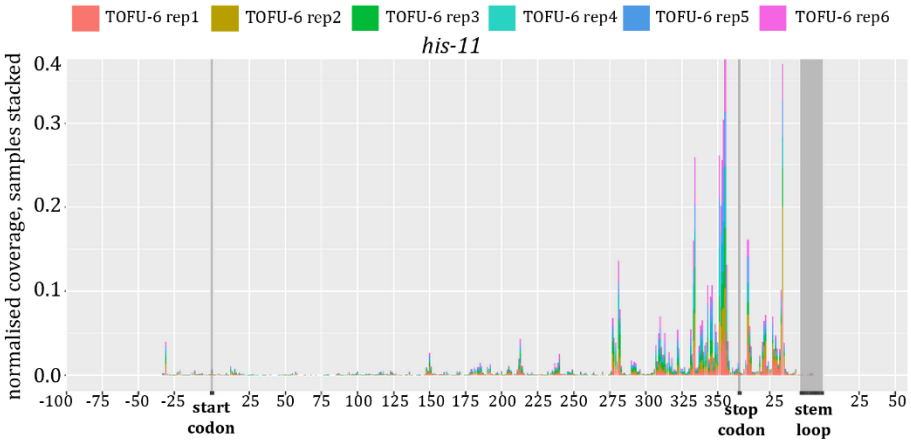
TOFU-6 rep1
TOFU-6 rep2
TOFU-6 rep3
TOFU-6 rep4
TOFU-6 rep5
TOFU-6 rep6
his-11
normalised coverage, samples stacked
0.4
0.3
0.2
0.1
0.0
-100
-75
-50
-25
start codon
25
50
75
100
125
150
175
200
225
250
275
300
325
350
stop codon
25
stem loop
25
50

Figure R3 | TOFU-6 binding is enriched in the 3'-end of RD histone transcripts. A. Genome browser view showing a cluster of histone genes on chromosome II, highlighting crosslinking events detected in TOFU-6 iCLIP and Cnt iCLIP. B. Meta coverage plot illustrating the average normalised coverage of the first position upstream of each read of all RD histone transcripts, averaged across replicates. The coding sequence (CDS) region, located between the start and stop codons, is divided into 100 bins, with bin sizes adjusted to gene length. The region between the stop codon and the stem-loop sequence is split into 31 bins. C. Example of a meta coverage plot for *his-11*, displaying the normalised coverage of the first positions upstream each read in *his-11*.

To examine binding specificity around the start codon, the stop codon and the stem-loop, we generated separate metagene coverage plots for each region (**Figure R4.A-C**). While no distinct patterns emerged around the start and stop codons, a prominent peak consistently appeared 12 bp upstream of the stem-loop across all enriched RD histone genes. This peak marks the beginning of a specific sequence conserved in all *C. elegans* RD histone genes (**Figure R4.G**). This finding is intriguing, as RD histone genes are highly similar in sequence, yet their 3' UTR are quite variable, and even the conserved stem-loop shows nucleotide variability (Keall et al., 2007). However, this specific sequence upstream of the stem-loop is present across all RD histone genes enriched in our iCLIP data.

Furthermore, analysis of the final mapped positions of trimmed reads shows a similar accumulation around the stop codon and a unique peak just downstream of the stem-loop (**Figure R4.D-F**). This peak marks the end of the stem-loop, with no reads detected beyond two nucleotides downstream (**Figure R4.F, G**). Given that RD histone mRNAs are initially synthetized with longer 3' UTR that are subsequently processed to the stem-loop (Keall et al., 2007), these findings suggest that PETISCO binds only the mature forms of RD histone mRNAs.

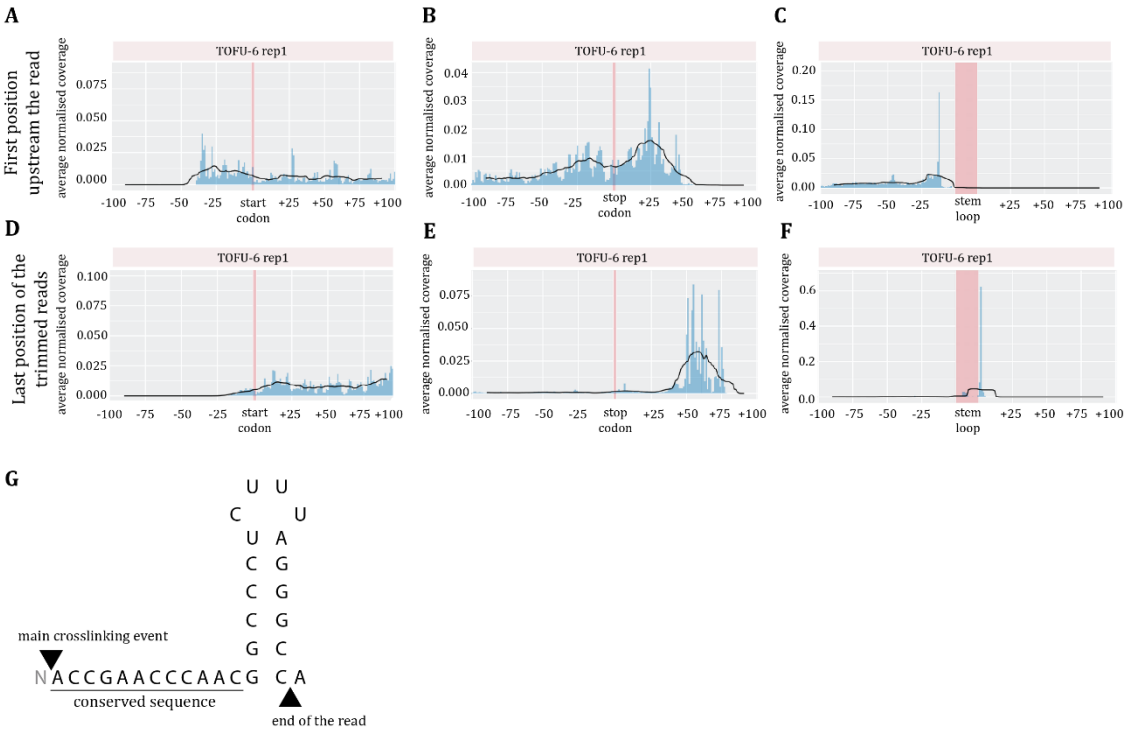

Figure R4 | TOFU-6 binds a conserved motif upstream of the stem-loop in processed RD histone transcripts. A-C. Meta gene coverage analysis of TOFU-6 iCLIP replicate 1, showing average normalised coverage based on the first positions upstream of each read relative to key transcript regions: the start codon (A), the stop codon (B), and the stem-loop (C) for all RD histone transcripts. D-E. Meta gene coverage analysis of TOFU-6 iCLIP replicate 1, showing average normalised coverage based on the last position of the trimmed reads relative to the start codon (D), the stop codon (E), and the stem-loop (F) of all RD histone transcripts. G. Representation of a canonical RD histone stem-loop, with an upstream conserved sequence across *C. elegans* RD histone genes. Arrowheads indicate the position of the starting of the majority of the reads before the stem-loop, and where the reads end immediately after the stem-loop.

In conclusion, TOFU-6, and by extension PETISCO, binds specifically to all mature RD histone mRNAs in *C. elegans* embryos, with a preference for the conserved region directly upstream of the stem-loop. Interestingly, CDL-1, the *C. elegans* homolog of the human SLBP, also binds the conserved region encompassing the stem-loop, with binding dependent on the stem-loop sequence (Kodama et al., 2002). Altering the stem-loop sequence or just the first nucleotide in the loop interferes with CDL-1 binding (Kodama et al., 2002; Michel et al., 2000). Although PETISCO and CDL-1 bind similar regions in RD histone mRNAs, CDL-1 has not been identified as a PETISCO interactor (Cordeiro Rodrigues et al., 2019; Zeng et al., 2019), leaving any potential interplay between these two complexes an open question.

RD histone mRNAs are not *trans*-spliced

One component of PETISCO, IFE-3, is a *C. elegans* eIF4E homolog known to bind preferentially to m7G cap structures (Keiper et al., 2000; Miyoshi et al., 2002). In *C. elegans*, mRNAs that undergo *trans*-splicing have TMG cap structures due to the addition of a SL sequence (Allen et al., 2011). Given that RD histone mRNAs bind to PETISCO, we sought to determine whether they are *trans*-spliced.

To investigate this, we performed 5' RLM-RACE PCR to sequence the 5' ends of histone transcripts (**Figure R5.A**). We used two primer sets targeting different histone genes, *his-67* and *his-46*. Due to the high sequence similarity among histone genes, these primers could also amplify cDNAs from other RD histone transcripts. In the resulting sequences, we observed the endogenous 5' UTR sequences of *his-67* and *his-46,* confirming the expected 5' histone mRNA sequence without evidence of an added SL sequence (**Figure R5.B, C**). We also obtained clones with endogenous sequences of other RD histone genes (*his-10, his-14, his-26*). To verify that our method can detect *trans*-spliced sequences, when present, we analysed *tost-1* cDNA as a control. Consistent with expectations, we identified the SL1 sequence upstream of *tost-1* start codon, confirming the successful detection of *trans*-splicing events (**Figure R5.D**).

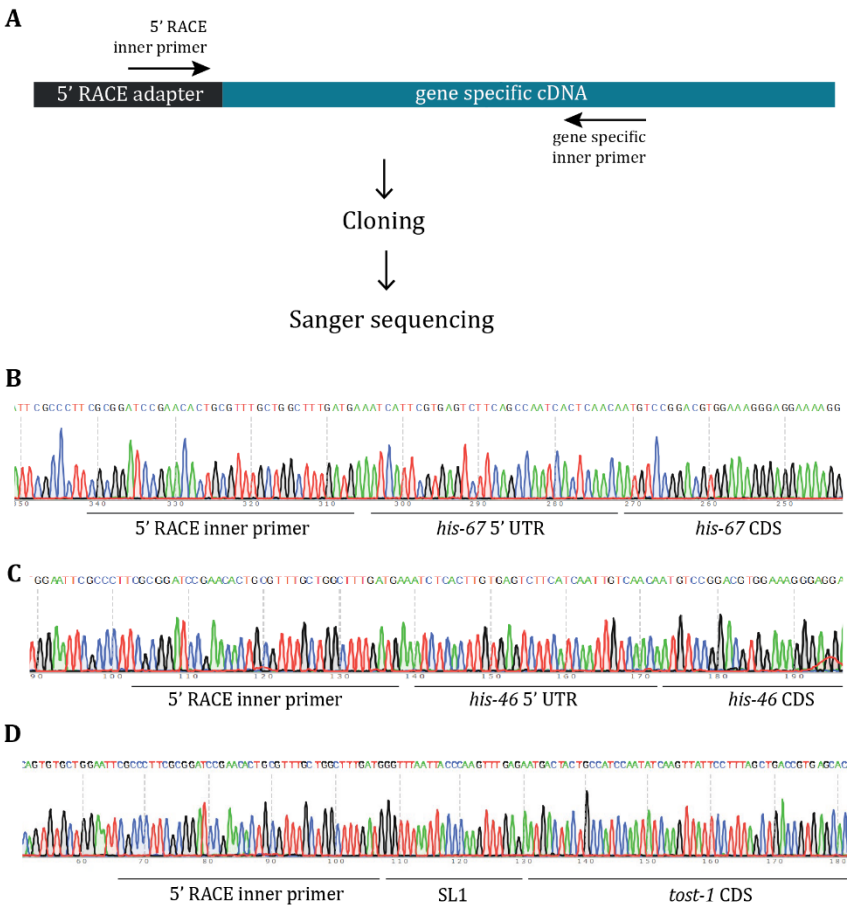

Figure R5 | RD histone transcripts are not *trans*-spliced. A. Schematic illustration of 5'RACE-RLM PCR amplification process, cloning and sequencing steps of the genes of interest. B-D. Sanger sequencing results of representative clones from *his-67* gene (B), *his-46* gene (C), and *tost-1* gene (D). Each sequence shows the position of the 5'RACE inner primer located upstream of the 5' sequence, which includes either the endogenous 5' UTR or the splice leader SL1 sequence, followed by the start of the coding sequence (CDS) of the cloned cDNA.

A prior meta-analysis of RNA-seq datasets indicated that at least 84% of *C. elegans* genes undergo *trans*-splicing, although SL1 or SL2 addition to histones genes was not conclusively detected (Tourasse et al., 2017). A more recent study using Nanopore direct-cDNA sequencing aligned with our findings, also reporting an absence of *trans*-splicing in RD histone transcripts (Bernard et al., 2023). These findings support the conclusion that RD histone mRNAs are not *trans*-spliced in *C. elegans.*

Histone mRNAs are affected in PETISCO mutants

PETISCO is essential for multiple RNA-based processes in *C. elegans*. While PETISCO with PID-1 facilitates piRNA precursor biogenesis independently of TOST-1 (Cordeiro Rodrigues et al., 2019;

Zeng et al., 2019), PETISCO's association with TOST-1 is critical for embryonic development (Cordeiro Rodrigues et al., 2019; Zeng et al., 2019). Loss of PETISCO or TOST-1 leads to a fully penetrant Mel phenotype, characterized by chromosome segregation defects and developmental arrest prior to gastrulation (Cordeiro Rodrigues, 2019; Zeng et al., 2019). Intriguingly, RNAi depletion of histone mRNAs results in similar developmental defects in *C. elegans* (Kodama et al., 2002), suggesting that histone mRNA misregulation may contribute to the embryonic arrest observed in PETISCO and *tost-1* mutants.

Embryonic defects in *tost-1* mutants

Since PETISCO, possibly in association with TOST-1, binds to histone mRNAs, we investigated the effects of TOST-1 loss on embryonic development and RD histone mRNA expression.

In *tost-1(xf194)* mutants, the Mel phenotype is fully penetrant, resulting in the arrest of all embryos from mutant mothers (**Figure R6.A**). The *tost-1(xf194)* allele includes a 445 bp deletion that disrupts the first exon and removes residues essential for ERH-2 binding (Cordeiro Rodrigues et al., 2019; Perez-Borrajero et al., 2021). We further examined a hypomorphic allele *tost-1(xf196 ts),* which contains a deletion affecting the splice acceptor site of the third exon but retains the ERH-2 interaction site (Cordeiro Rodrigues et al., 2019). Animals with *tost-1(xf196 ts)* display a temperature-sensitive (ts) phenotype: they are viable at 15°C and 20°C but their embryos arrest at 25°C, mirroring the embryonic lethality seen in *tost-1(xf194)* mutants (Cordeiro Rodrigues et al., 2019) (**Figure R6.B**). Notably, at 20°C, the phenotype is intermediate, with partial fertility defects observed (**Figure R6.B**).

PID-1 and TOST-1 share little sequence similarity, except for the conserved residues required for ERH-2 binding, suggesting that the two proteins may compete for PETISCO binding (Cordeiro Rodrigues et al., 2019; Perez-Borrajero et al., 2021). In *tost-1(xf194)* mutants, there is a modest increase in piRNA expression and enhanced silencing of a piRNA activity sensor upon *tost-1* RNAi (Cordeiro Rodrigues et al., 2019), implying that PETISCO becomes more available to bind PID-1 and engage in piRNA processing when TOST-1 is absent. To explore the impact of combined *pid-1* and *tost-1* mutations on embryogenesis, we generated *pid-1;tost-1* double mutants. The *pid-1(xf35);tost-1(xf194)* double mutant exhibited complete Mel, similar to *tost-1(xf194)* alone. However, in *pid-1(xf35);tost-1(xf196 ts)* animals, we observed a significant increase in viability at 25°C and moa dest but no significant increase at 20°C (**Figure R6.C, D**). These findings suggest that the hypomorphic *tost-1(xf196 ts)* allele allows PETISCO to functionally compensate in the absence of PID-1, potentially due to altered availability or competitive interactions within the

complex. For instance, in the absence of PID-1, more PETISCO::TOST-1*(xf196)* may be present, resulting in some level of rescue of the phenotype.

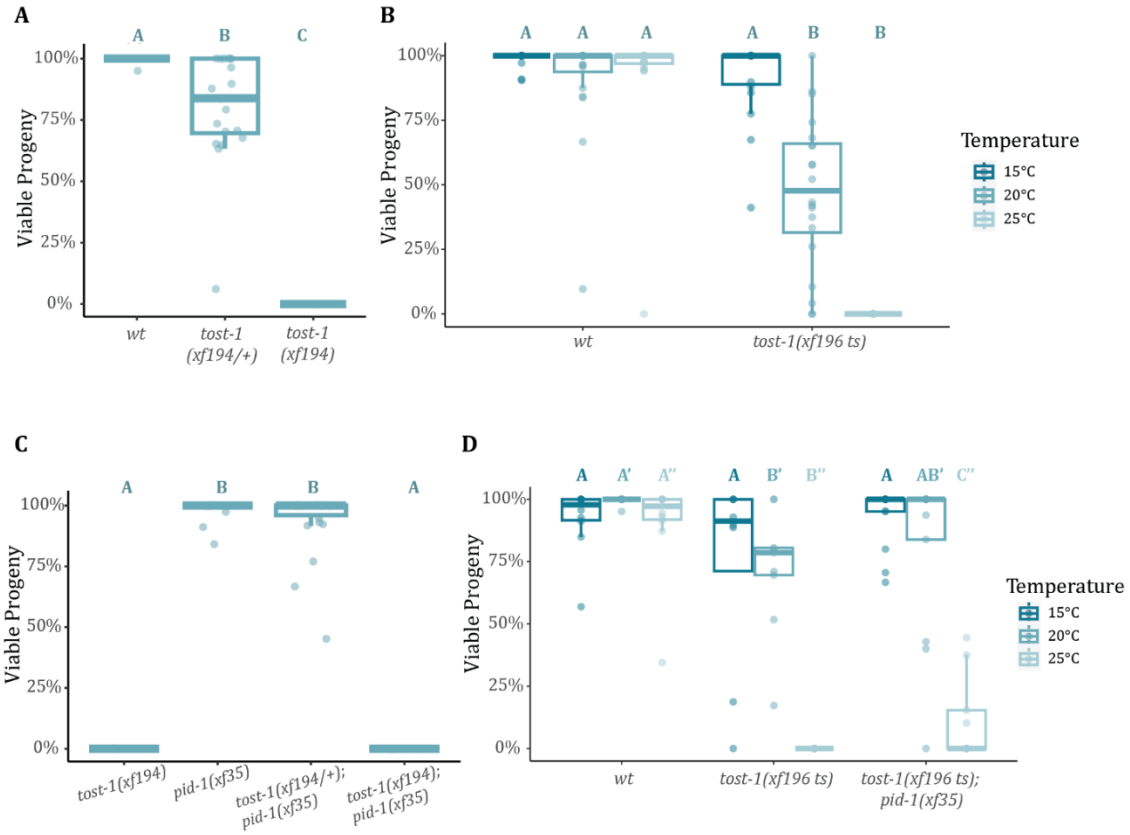

Figure R6 | *tost-1* mutants display a maternal effect lethality phenotype. A-D. Percentage of viable progeny from animals with the indicated genotype. Each data point represents an individual worm. A, C. Strains were synchronized and cultured at 20°C, and F1 embryos and larvae were counted from individual worms. B, D. Strains were synchronized and cultured at the indicated temperature, and F1 embryos and larvae were counted from individual worms. P-values were calculated using the pairwise Dunn test and adjusted with Holm–Bonferroni method for multiple comparisons. Different letters indicate p-value < 0.05. In D, pairwise comparisons were performed within each temperature condition.

RD histone mRNAs are downregulated in *tost-1* mutants

To evaluate the impact of TOST-1 on RD histone mRNA levels, we quantified *his-65* and *his-66* mRNA levels (coding H2B and H2B, respectively) in gravid adults of *tost-1(xf194)* mutants using RT-qPCR. Strikingly, *his-65* and *his-66* were expressed at levels sixteen times lower than in wild-type animals, with fold-changes of 0,02 and 0,05, respectively (**Figure R7.A**). In contrast, *pid-1(xf35)* and *prg-1(n4357)* mutants - both essential for piRNA formation (Batista et al., 2008; de Albuquerque et al., 2014) – showed no change in histone mRNA expression (**Figure R7.A**). These

results support a dual role for PETISCO, wherein TOST-1, but not PID-1, is critical for RD histone mRNA regulation.

In *tost-1(xf196 ts)* mutants, we observed a temperature-sensitive effect, with *his-65* and *his-66* levels reduced by half at 15°C (fold-changes of 0,4 and 0,5, respectively), and by threefold at 25°C (fold-change of 0,3) (**Figure R7.B**), confirming a hypomorphic effect for *tost-1(xf196 ts)* in histone mRNA regulation. Given the developmental defects observed in embryos from *tost-1* mutant mothers, we hypothesized that maternal TOST-1 is essential for RD histone mRNA regulation in the embryo.

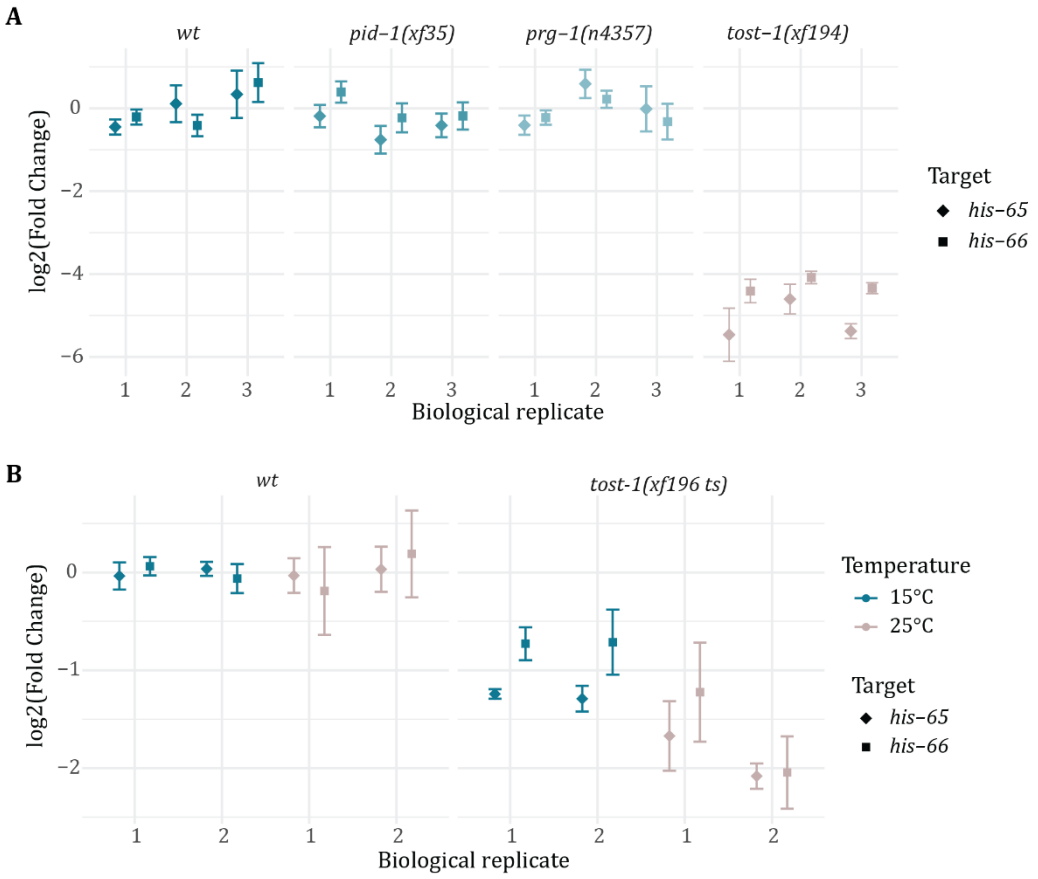

Figure R7 | Relative expression of RD histone mRNAs. A. Quantitative RT-PCR analysis of *his-65* (H2A) and *his-66* (H2B) expression levels in *wild type* (*wt*), *pid-1(xf35), prg-1(n4357),* and *tost-1(xf194)* gravid adults cultured at 20°C. B. Quantitative RT-PCR analysis of *his-65* (H2A) and *his-66* (H2B) expression in *wild type* (*wt*) and *tost-1(xf196 ts)* gravid adults cultured at 15°C and 25°C. A, B. The gene *pmp-3* serves as reference gene. Each bar represents an individual biological replicate, each measured in three technical replicates. Fold change calculations were calculated based on the mean expression of *wt* samples at each respective temperature. Error bars represent standard deviation across technical replicates within each biological replicate.

TOST-1 role in maternal RD histone mRNA stability in embryos

In the previous experiments, we found that PETISCO binds RD histone mRNAs in embryos, that their expression is impaired in adults, and that PETISCO mutants fail to complete embryogenesis. Given that the first mutant generation does not exhibit developmental defects, but their progeny does, we hypothesize that the defect originates maternally. Because RD histone mRNAs are depleted in adult hermaphrodites, we infer that their deposition in early embryos is also affected in *tost-1* mutant, resulting in reduced expression, at least until the onset of zygotic transcription. We propose that PETISCO, together with TOST-1, plays a critical role in maintaining RD histone mRNAs stability during oogenesis and early embryogenesis.

To investigate the role of TOST-1 in maternal histone mRNAs stability, we used single-molecule FISH (smFISH) to assess RD histone mRNA expression in *wild-type* and *tost-1* mutant embryos (**Figure R8, 9**). Due to technical limitations, we were unable to use probes targeting endogenous wild-type histone transcripts. Instead, we utilized two strains with endogenously gfp-tagged *his-61* gene (Makeyeva et al., 2021), using probes designed to target the *gfp* sequence. The two strains differ by the following alleles: *ne4846(gfp::his-61)*, containing introns in the *gfp* sequence, and *ne4847(gfp**::his-61), with *gfp* as a single exon and therefore not spliced (**Figure R8.A**). From this point forward, non-spliced *gfp* will be referred to as *gfp**. These strains have different expression patterns in the germline and embryos, allowing us to assess whether each tag closely replicates wild-type *his-61* regulation. To ensure probe specificity we included controls with wild-type embryos lacking the *gfp* sequence. Additionally, the allele *ne4847,* which contains intronless *gfp*,* was previously identified as a target of siRNAs, leading to its silencing in the germline (Makeyeva et al., 2021). To understand whether siRNA-induced silencing also affects the expression of the alleles in the embryos, we crossed the endogenously tagged *his-61* strains with *mut-7* mutants, which are defective in RNAi-mediated silencing (R. F. Ketting et al., 1999), and assessed *gfp* expression.

In animals expressing *ne4846(gfp::his-61),* we observed no significant difference in *gfp::his-61* RNA expression between *tost-1(xf196 ts)* mutants and *wild-type* embryos (**Figure R8.B**). Similarly, *mut-7(xf125);tost-1(xf196 ts)* double mutant, which lacks endo-siRNA function, showed no substantial change in *gfp::his-61* RNA expression. However, we detected tdtomato::H2B signal (transgene present in the background of the *tost-1(xf196 ts)* mutant strain) in the same channel as the *gfp* probes. This transgene may be silenced in *wild-type* early embryos but became expressed in the absence of siRNA-mediated silencing in *mut-7* mutants.

Similarly, smFISH analysis of *ne4847*(*gfp*::his-61)* embryos, containing the intronless *gfp**, revealed no significant difference in expression between *tost-1* mutants and *wild-type*. Loss of MUT-7 also had no effect on *gfp*::his-61* RNA expression in these embryos (**Figure R8.C**). We conclude that neither transcript is affected in embryos at these stages. Therefore, we decided to investigate early embryos to analyse the maternal provided transcripts.

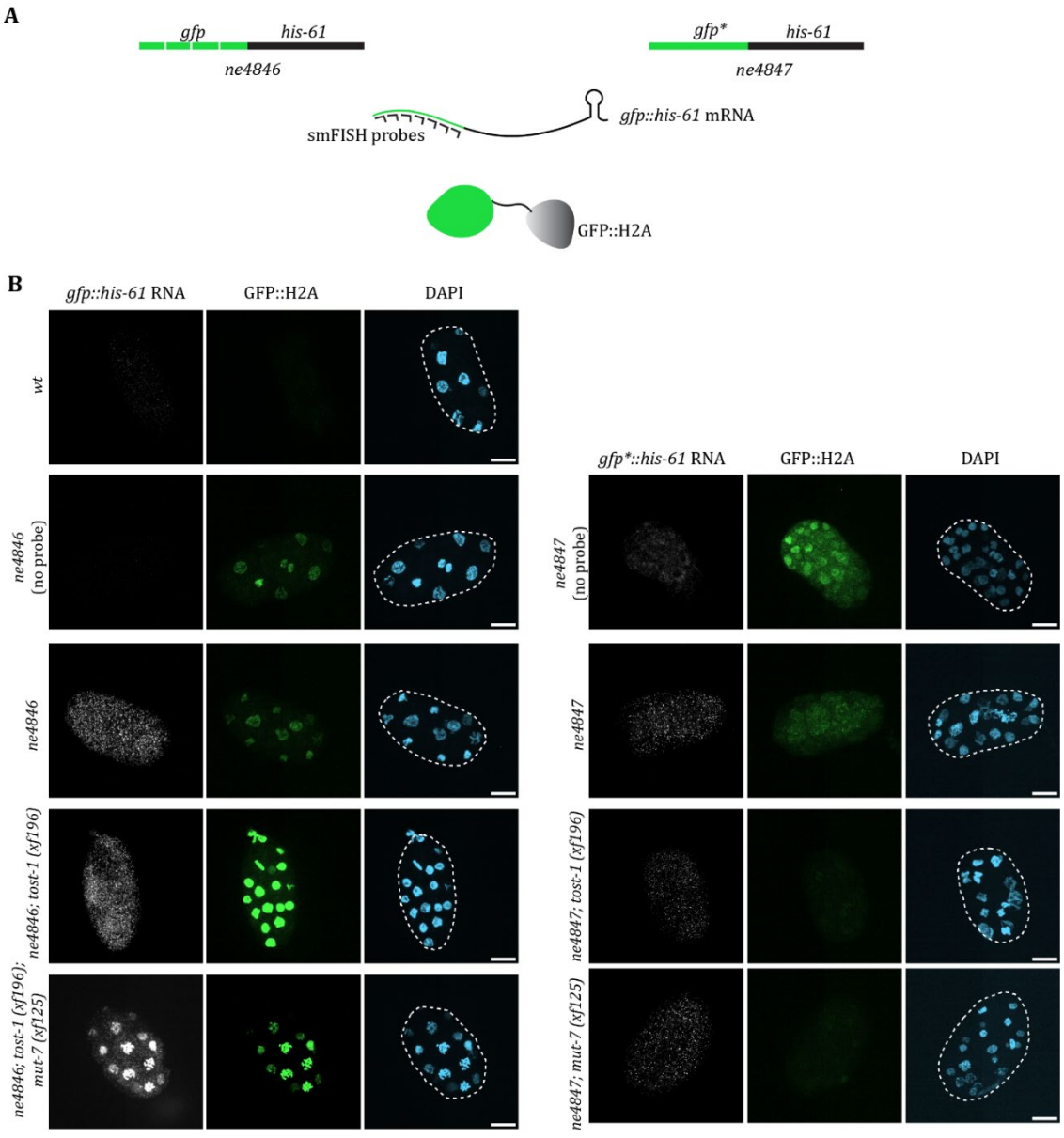

Figure R8 | Expression patterns of *gfp::his-61* mRNA in embryos. A. Schematic representation of the two *gfp::his-61* alleles (*ne4846*, containing introns in the *gfp* sequence, and *ne4847*, lacking introns in the *gfp* sequence), showing the probes targeting the *gfp* and the resulting fused GFP::H2A protein. B. Confocal maximum intensity projections of single molecule (sm) FISH of *gfp::his-61* RNA (grey), combined with imaging of GFP::H2A (green) in dissected embryos. DNA was stained with DAPI (blue). Scale bars = 10 µm.

To explore maternal RD histone transcript stability in early embryos, we analysed *gfp::his-61* expression between one- and four-cell stages, prior to ZGA (**Figure R9**). At these stages, most histone transcripts are largely maternally inherited, therefore we are able to see the effect of TOST-1 in maternally provided RD histone transcripts. We utilized two independent datasets from embryos expressing either the *ne4846* or *ne4847* allele in both *wild-type* and *tost-1(xf196 ts)* mutant backgrounds. Using the image analysis software Imaris (Oxford Instruments, v10.1), we quantified fluorescent spots corresponding to *gfp::his-61* transcripts in each sample. To understand and distinguish background signal from specific signal we plotted the distribution of maximum intensity values of the identified spots (**Figure R9.A, D**). Notably, while *wild-type* embryos (without *gfp* expression) and embryos containing both versions of *gfp* inserted in the *his-61* locus (*gfp/gfp*::his-61)* showed similar distributions, the latter demonstrated a higher accumulation of spots with maximum intensities exceeding 270 a.u. This suggests that the signals detected below this threshold may represent background noise rather than specific transcript detections.

However, due to uncertainty regarding the specificity of the signal, we opted for a conservative approach in our analysis. Accordingly, we retained all acquired data for further analyses, including spots with lower maximum intensities. For each dataset, we calculated the number of spots per embryo independently. Interestingly, the results for *ne4846* samples were inconsistent (**Figure R9.B, C**). In dataset 1, no difference in the number of spots per embryo was observed between *tost-1* wild type and mutant backgrounds. Conversely, in dataset 2, the *tost-1(xf196 ts)* mutant exhibited a significant reduction in number of spots. The results do not change if we remove the spots with lower maximum Intensity (data not shown). This variability indicates that the regulation of this mRNA may not be directly dependent on TOST-1 and suggests that additional replicates are necessary for conclusive results.

In contrast, with respect to the *ne4847* allele, we observed a reduction in spot counts in *tost-1(xf196 ts)* mutant animals across both datasets, however only in dataset 4 the difference was statistically significant (**Figure R9.E, F**). This suggests that TOST-1 may indeed stabilize maternal *gfp*::his-61* transcripts in the early embryo. However, due to the unique regulatory mechanism surrounding RD histone genes, we remain cautious in extending this conclusion to untagged histone transcripts. It is still unclear whether the *gfp* fusions behave as the endogenous wild-type RD histone transcripts. This is particularly relevant considering that RD histone transcripts are hypothesized to terminate via a promoter-proximal transcription termination complex, Integrator, rather than the canonical termination machinery (Skaar et al., 2015). The size of these

transcripts may therefore influence their transcriptional regulation, which is clearly affected by the addition of the *gfp* sequence at the N-terminus. In addition, the inserted *gfp* sequences may interfere with PETISCO binding to the histone transcripts.

In conclusion, our findings suggest that histone mRNAs may indeed be stabilized in early embryos through TOST-1. However, these experiments will need to be repeated on untagged histone transcripts.

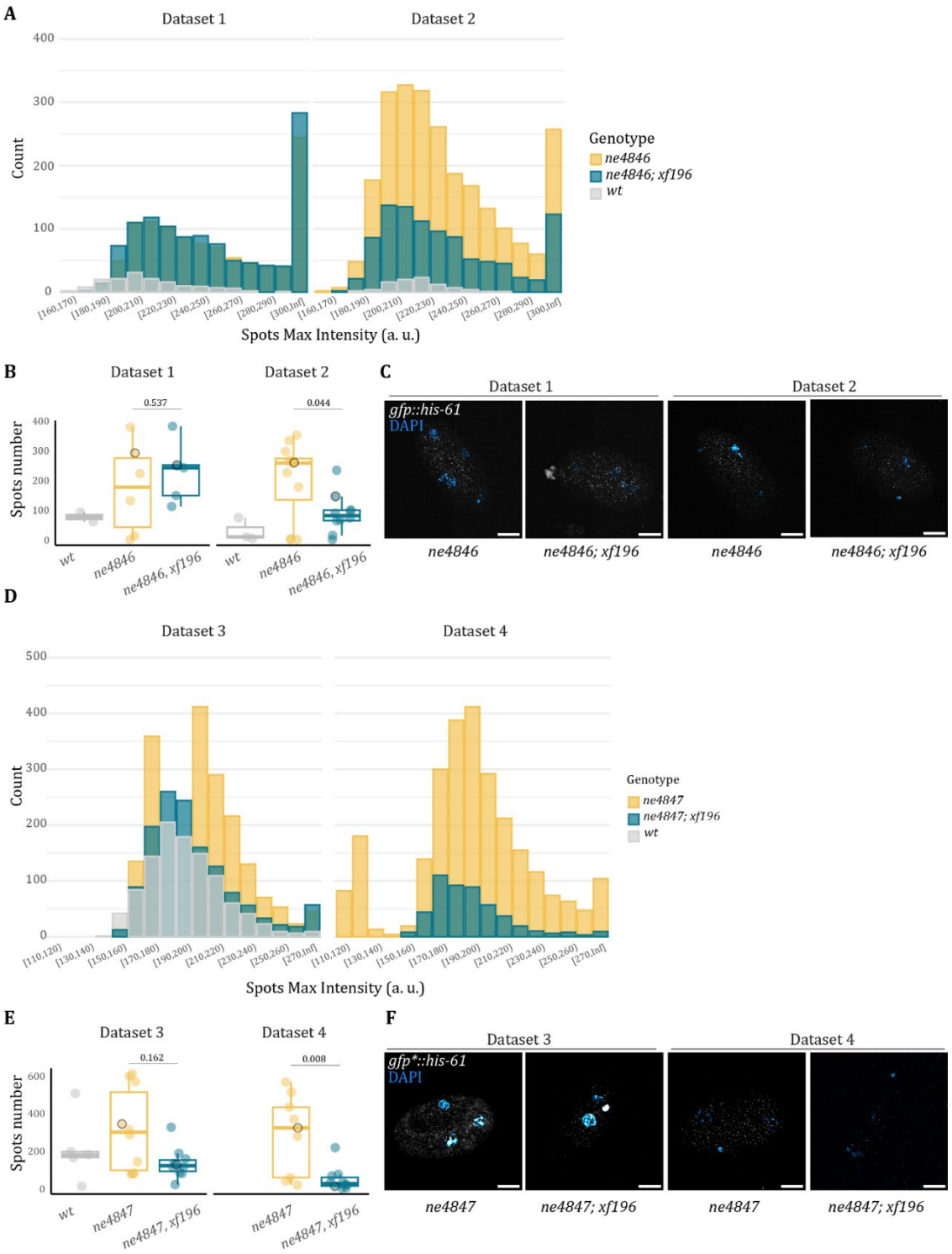

Figure R9 | *gfp::his-61* mRNA expression in early embryos. A. Distribution of *gfp::his-61* mRNA smFISH spots identified with Imaris software, categorized by their maximum (Max) intensity in *wt* (no *gfp*), *ne4846[gfp::his-61]* and *ne4846[gfp::his-61];tost-1(xf196 ts)* embryos. Each dataset (Dataset 1 and Dataset 2) represents two independent experiments. B. Quantification of *gfp::his-61* mRNA smFISH spots per embryo. Each data point represents an individual embryo. C. Representative images showing one embryo per condition from B, highlighted by darker outline. D. Distribution of *gfp*::his-61* mRNA smFISH spots identified with Imaris software, categorized by their Max intensity in *wt* (no *gfp*), *ne4847[gfp*::his-61]* and *ne4847[gfp*::his-61];tost-1(xf196 ts)* embryos. Each dataset (Dataset 3 and

Dataset 4) represents two independent experiments. E. Quantification of *gfp*::his-61* mRNA smFISH spots per embryo. Each data point represents an individual embryo. F. Representative images showing one embryo per condition from E, highlighted by darker outline. B, E. P-values were calculated using the Mann-Whitney U test.

tost-1 mutant phenotype is independent on small RNAs

smRNAs do not target RD histones in the absence of TOST-1

RD histone mRNAs are susceptible to targeting by small RNAs. Previous studies have shown that loss of PRG-1 results in accumulation of secondary siRNAs, which target RD histone mRNAs, leading to their overall downregulation (Barucci et al., 2020; Reed et al., 2019). The authors suggest that the epigenetic silencing of RD histone mRNAs is a major contributor to the loss of fertility observed over generations in *prg-1* mutants (Barucci et al., 2020). In contrast, *tost-1* mutants show a mild upregulation of piRNAs/21U RNAs (Cordeiro Rodrigues et al., 2019). To investigate whether there is an accumulation of small RNAs targeting histones in *tost-1* mutants, we re-analysed the small RNA sequencing dataset from (Cordeiro Rodrigues et al., 2019), specifically examining the small RNAs targeting histone mRNAs (**Figure R10.A**). Our analysis revealed no significant differences in the levels of piRNAs (21U RNA) and secondary siRNAs (22G RNA) in *tost-1(xf194)* mutants compared to wild type (Figure R10.A).

Depletion of 22G RNAs does not rescue *tost-1* Mel

While we did not observe an accumulation of small RNAs targeting RD histones in *tost-1* mutants, it is important to note that the samples used were from gravid adults. Given that TOST-1 is primarily required during embryogenesis, we next assessed whether reducing endo-siRNAs/22G RNAs levels would affect embryonic development in *tost-1* mutants. We did this by using *mut-16* mutants, which have a severe 22G RNA biogenesis phenotype (C. Zhang et al., 2011). We found that depletion of 22G RNAs did not rescue embryonic arrest in *tost-1(xf194)* mutants. In hypomorphic *tost-1(xf196 ts)* mutant animals, only 4 out of 13 animals produced viable progeny, but this difference is not statistically significant (**Figure R10.B**).

Additionally, RD histone mRNAs are substrates for RDE-3-dependent pUGylation in *prg-1* mutants, which can mark them for siRNA-dependent silencing (Shukla et al., 2020, 2021). To determine if this degradation mechanism contributed to the downregulation of RD histone mRNAs observed in *tost-1* mutants, we crossed *rde-3(ne298)* mutants with *tost-1(xf194)* and *tost-*

1(xf196 ts). However, we did not observe a rescue of the Mel phenotype in these crosses, although this experiment was not quantified.

In summary, our findings indicate that the loss of TOST-1 does not lead to the aberrant accumulation of small RNAs targeting RD histone mRNAs. Furthermore, 22G RNAs and histone pUGylation do not appear to be the primary causes of embryonic arrest seen in *tost-1* mutants.

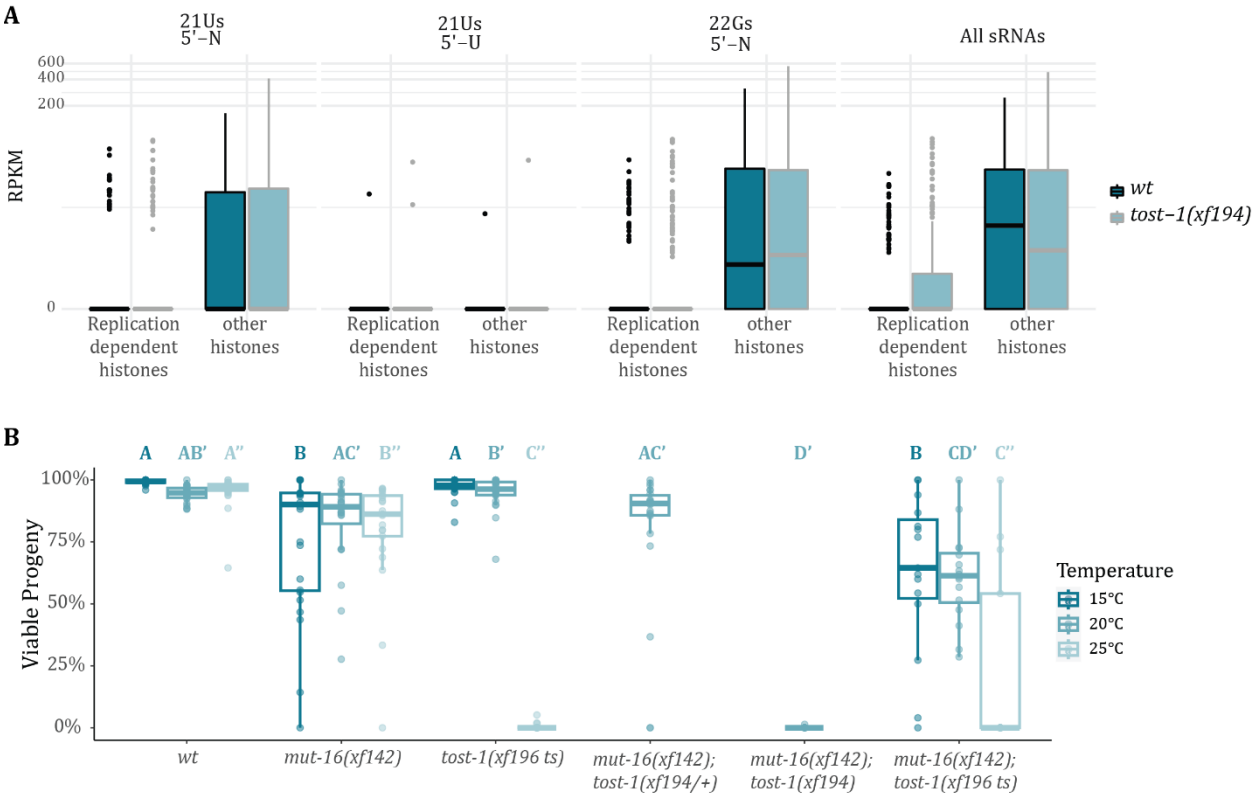

Figure R10 | *tost-1* mutants do not accumulate RD histone-targeting 22G RNAs. A. Reads per kilobase per million (RPKM) of small RNAs from *wt* and *tost-1(xf194)* gravid adults (Cordeiro Rodrigues et al., 2019) were aligned to RD histone genes and histone variants. Mapped reads were categorized into three subgroups: i) 21Us with a hard U-bias (reads exactly 21nt in length with a U at the 5'-position), ii) 21Us with no hard U-bias (reads exactly 21nt in length with any nucleotide at the 5'-position), and iii) 22Gs (reads ranging in length from 20-23nt with any nucleotide at the 5'-position. B. Percentage of viable progeny from animals with the indicated genotype. Each data point represents an individual worm. P-values were calculated using the pairwise Dunn test (within each temperature condition) and adjusted with Holm–Bonferroni method, after failing the Shapiro-Wilk normality test. Different letter indicate p-value < 0.05.

Characterization of histone GFP::H4 transgenes expression

To investigate how the loss of PETISCO may affect RD histone expression in the adult germline and embryos, we assembled a series of histone transgene constructs. Using the coding sequence

of *his-67*, we varied regulatory elements, including the endogenous *his-67* 3' UTR, the *tbb-2* 3' UTR, and a codon-optimized *gfp* sequence, with (referred as *gfp*) or without (referred as *gfp**) introns. These transgenes were integrated into chromosome II via MosSCI transgenesis (Frøkjær-Jensen et al., 2008, 2012). By testing different constructs, we aimed to mimic the regulatory mechanisms of endogenous RD histone transcripts, which are unique due to their lack of splicing and presence of a 3'UTR stem-loop.

Our experiments showed that both transgenic strains, *xfSi254[gfp::his-67]* and *xfSi255[gfp::his-67::tbb-2 3'UTR]* – where the 3' UTR is either from the endogenous *his-67* gene or the *tbb-2* gene - expressed GFP::H4 across the adult hermaphrodite gonad and throughout all embryonic stages (**Figure R11**). This expression pattern is consistent with that of endogenous *his-67* gene, which is expressed in the adult germline and in embryos (Boeck et al., 2016), and the different 3' UTR does not affect its expression pattern.

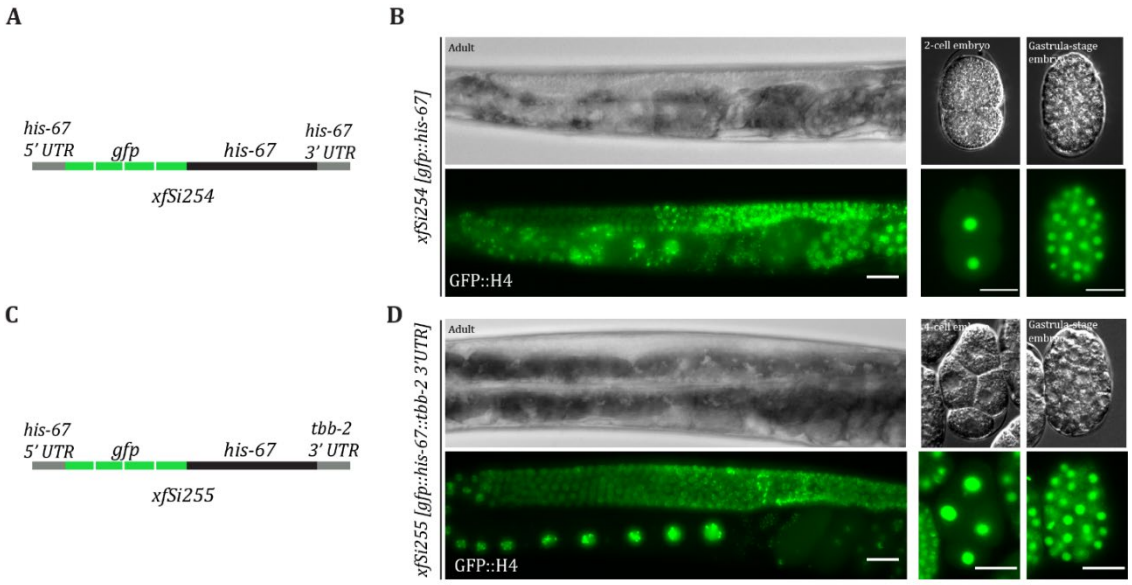

Figure R11 | Expression pattern of *xfSi254* and *xfSi255* carrying transgenes expressing GFP::H4. A, C. Schematic illustrations of the assembled transgenes *xfSi254* and *xfSi255*. B, D. Wide-field micrographs showing maximum projections of adult gonads and single optical sections of dissected embryos expressing GFP::H4. Scale bars = 20 µm.

Since RD histone genes lack introns and are not spliced, we generated additional transgenic lines using only the *gfp* coding sequence without introns (referred to as *gfp**), fused to the *his-67* coding sequence and integrated into the same locus in chromosome II (**Figure R12.A, C**). In contrast to the intron-containing transgenic strains showed above, GFP*::H4 was not expressed in the adult gonad or early embryonic stages in animals with *xfSi268[gfp*::his-67]* and *xfSi269[gfp*::his-67::tbb-2 3'UTR]* transgenes (**Figure R12.B, D**). The absence of GFP expression

in these stages aligns with previous observations that intronless transgenes are often silenced in the *C. elegans* germline, likely due to the unique genome defence mechanisms in this tissue (Aljohani et al., 2020; Frøkjær-Jensen, 2019). Moreover, the lack of expression in early embryos is likely due to the absence of maternal deposition of mRNA and protein in the embryo. Interestingly, despite this general germline silencing, animals carrying the *xfSi269* transgene still expressed GFP::H4 in sperm (**Figure R12.B**).

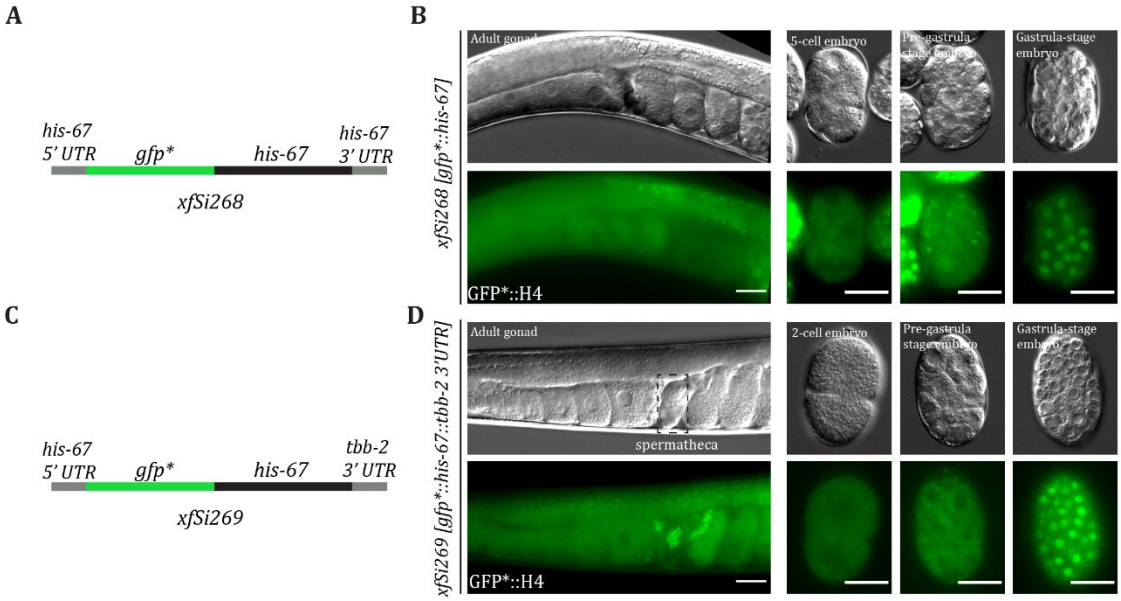

Figure R12 | Expression pattern of *xfSi268* and *xfSi269* carrying transgenes expressing GFP*::H4. A, C. Schematic illustrations of the assembled transgenes *xfSi268* and *xfSi269*. B, D. Wide-field micrographs showing single optical sections of adult gonads and dissected embryos expressing GFP*::H4. Scale bars = 20 µm.

We also investigated whether the transgene size could influence its expression. Given that histones are small, nuclear-localized proteins, we created additional constructs using the *his-67* promoter and *his-67* or *tbb-2* 3' UTR. In these constructs, we substituted the *his-67* coding sequence with intronless *gfp**, adding the nuclear localization signals SV40 and EGL-13 (Lyssenko et al., 2007) (**Figure R13.A, C**). Similar to the *xfSi268* and *xfSi269* transgenic animals, strains carrying *xfSi306[NLS^{SV40}::gfp*::NLS^{EGL-13}::his-67 3'UTR]* and *xfSi307[NLS^{SV40}::gfp*::NLS^{EGL-13}::tbb-2 3'UTR]* were silenced in the germline and only showed expression later during embryogenesis, as observed in later-stage embryos still within the uterus (**Figure R13.A, B**).

In conclusion, these findings suggest that the presence or absence of introns is a critical regulator of transgene expression in the germline. Additionally, the GFP tag leads to a distinct expression

profile compared to the endogenous *his-67* gene, indicating that such transgenes are not ideal for studying the behaviour of histone genes. Furthermore, our results demonstrate that simply adding a *gfp* sequence—whether in combination with histone regulatory sequences (5' UTR and 3' UTR) at a different genomic locus or directly tagging an endogenous histone locus—results in similar expression profiles, as observed with the allele *ne4847* (**Figure R8**). This finding underscores that the *gfp* sequence itself significantly disrupts the regulation of these genes, making it unsuitable for reliably addressing histone gene expression.

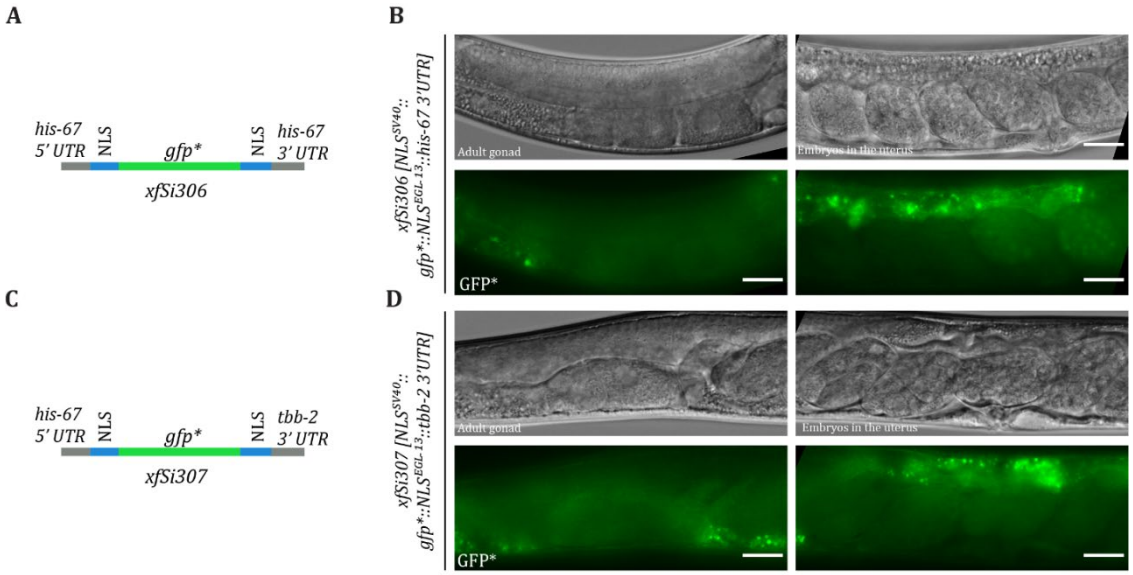

Figure R13 | Expression pattern of *xfSi306* and *xfSi307* carrying transgenes expressing GFP*. A, C. Schematic illustrations of the assembled transgenes *xfSi306* and *xfSi307*. B, D. Wide-field micrographs of single optical sections of adult gonads expressing GFP under the control of *his-67* promoter. Scale bars = 20 µm.

RNAi-mediated depletion of TOST-1 differentially affects GFP::H4 transgene expression

Given that PETISCO binds to RD histone mRNAs in embryos and plays a role in regulating these transcripts, we hypothesized that PETISCO might also influence histone protein expression in the germline and embryos. To test this, we performed RNAi using the transgenic strains that we generated with various dsDNA sequences to induce gene silencing of different targets. As a negative control for RNAi, we used an empty vector and therefore no targeted-gene silencing was induced. However, due to the unique regulatory mechanism that governs histones and the

unknowns around how our transgenes might be regulated, we used multiple transgenic lines to capture potential regulatory differences.

tost-1 knockdown shows mild effects on spliced GFP::H4 transgenes

We started by analysing the expression of the spliced *gfp::his67* transgenes: *xfSi254[gfp::his-67]* and *xfSi255[gfp::his-67::tbb-2 3'UTR]* under *tost-1* RNAi conditions and compared to control RNAi conditions (**Figure R14**). In normal conditions, without any RNAi treatment, animals carrying the transgenes *xfSi254* and *xfSi255,* which express spliced GFP::H4, showed GFP::H4 expression throughout the germline and in embryos (**Figure R11**). Given that *tost-1* mutant animals display a significant reduction in histone mRNA levels in gravid adults, we expected similar effects on transgene expression upon *tost-1* knockdown. Using two distinct *tost-1* RNAi clones, *tost-1* (JA) and *tost-1* (JP), we observed no significant decrease of GFP::H4 signal intensity in either the gonad or embryos following *tost-1* depletion when compared with the control (**Figure R14.A-D**). Intriguingly, we noted a possible increase in GFP::H4 expression, particularly in the oocytes (**Figure R14.A, C**); however, this effect was not quantified. In both *tost-1* RNAi-treated animals, we observed mitotic defects, such as chromatin bridges (**Figure R14.D** arrows) and embryonic arrest, indicating that the RNAi treatment was effective. Both phenotypes had been previously observed using RNAi targeting *tost-1* or other PETISCO components (Cordeiro Rodrigues et al., 2019).

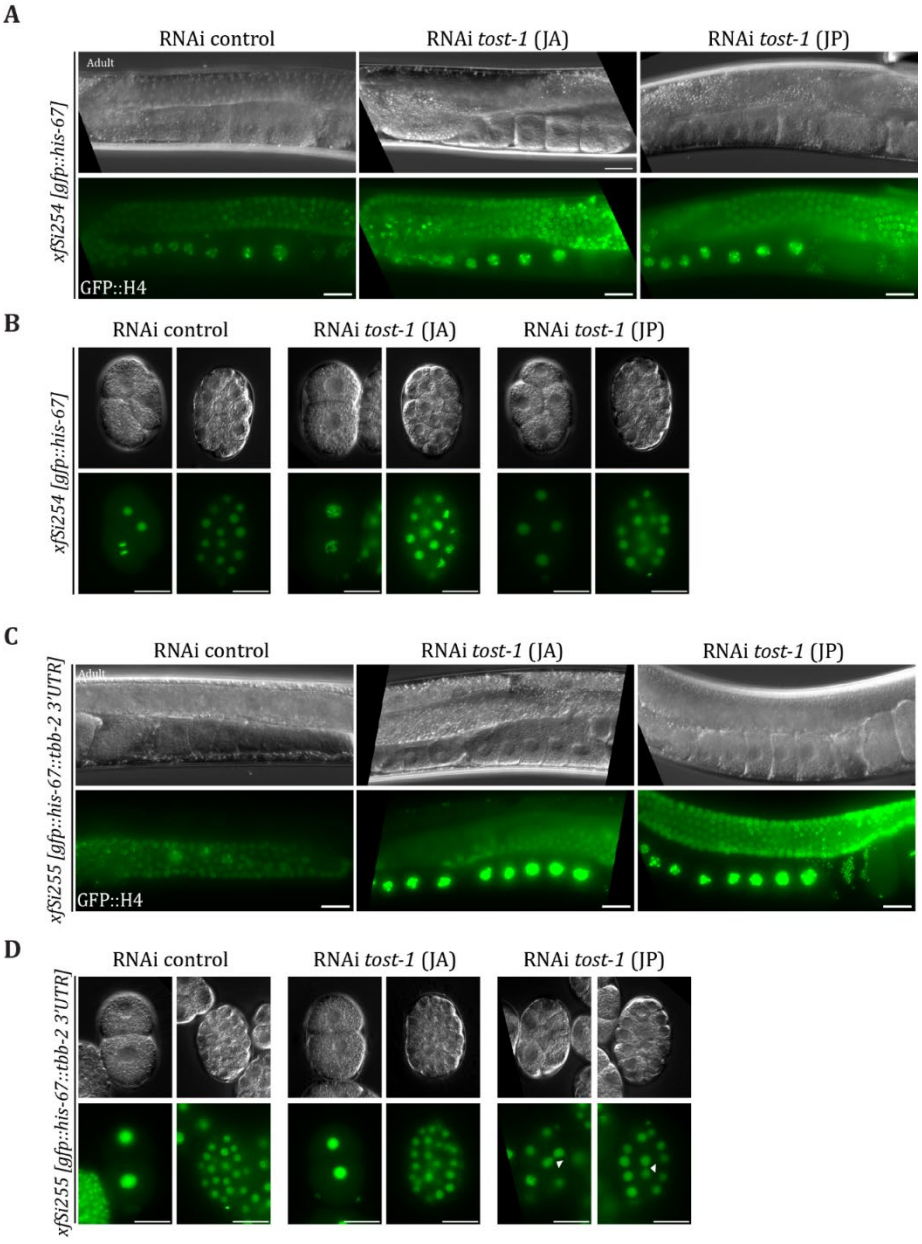

Figure R14 | Effect of *tost-1* RNAi in spliced GFP::H4 transgenes. A-D. Wide-field micrographs showing maximum projections of adult gonads (A, C) and single optical sections of dissected embryos (B, D) from animals carrying the *xfSi254* (A, B) and *xfSi255* (C, D) transgenes expressing GFP::H4. A-D. Worms were subjected to *tost-1* RNAi via feeding (JA and JP represent different clones, see methods) from the L1 larval stage to adulthood. Scale bars =20 μm.

tost-1 knockdown enhances expression of zygotically expressed intronless GFP*::H4 transgenes

Secondly, we analysed the effect of *tost-1* depletion in the intronless GFP*::H4-expressing transgenic lines carrying the alleles *xfSi268* and *xfSi269* (**Figure R15, R16**). Transcriptomic data

indicates that *his-67* is expressed in both the adult germline and early embryos (Boeck et al., 2016), and our previous experiment show that GFP*::H4 is only expressed later in embryogenesis (**Figure R12**). Based on the expression profiles in wild-type animals, these transgenes serve as reporters of zygotic expression rather than of specific histone expression aspects. Alongside *tost-1* RNAi (JA and JP clones), we knocked down *tofu*-6, a core component of PETISCO, and *cde-1,* an RNAi-defective gene serving as a control for the RNAi function (van Wolfswinkel et al., 2009). However, later findings implicated CDE-1 in histone mRNA regulation, indicating that it is not an appropriate control for these experiments. As a negative RNAi control, we used an empty vector, which does not induce gene silencing.

In animals carrying the *xfSi268[gfp*::his-67]* transgene, we observed no changes in GFP*::H4 expression in the germline following *tost-1, tofu-6* or *cde-1* depletion when compared to the RNAi control (**Figure R15.A**). Across all conditions, the transgene remained silenced in the germline, with expression only beginning at later embryonic stages following the ZGA. However, closer examination of embryonic expression revealed that GFP*::H4 appeared to be expressed earlier and more robustly during early embryogenesis upon *tost-1* depletion compared to controls (**Figure R15.B**). This enhancement in early embryonic expression was specific to *tost-1* depletion, as it was not observed with *tofu-6* or *cde-1* knockdown*.* Given the lack of difference between the two *tost-1* RNAi clones, subsequent experiments continued with only *tost-1* (JA) RNAi. Interestingly, mitotic defects, such as chromatin bridges, were apparent in *tost-1* RNAi embryos. This effect was absent in *tofu-6* RNAi-treated embryos, contrary to previous findings that *tofu-6* RNAi causes mitotic defects in embryos (Minasaki & Streit, 2007). Potentially, the RNAi *tofu-6* was insufficiently induced in this experiment, which could explain the no phenotype in the transgenes expression observed in *tofu-6*-depleted animals.

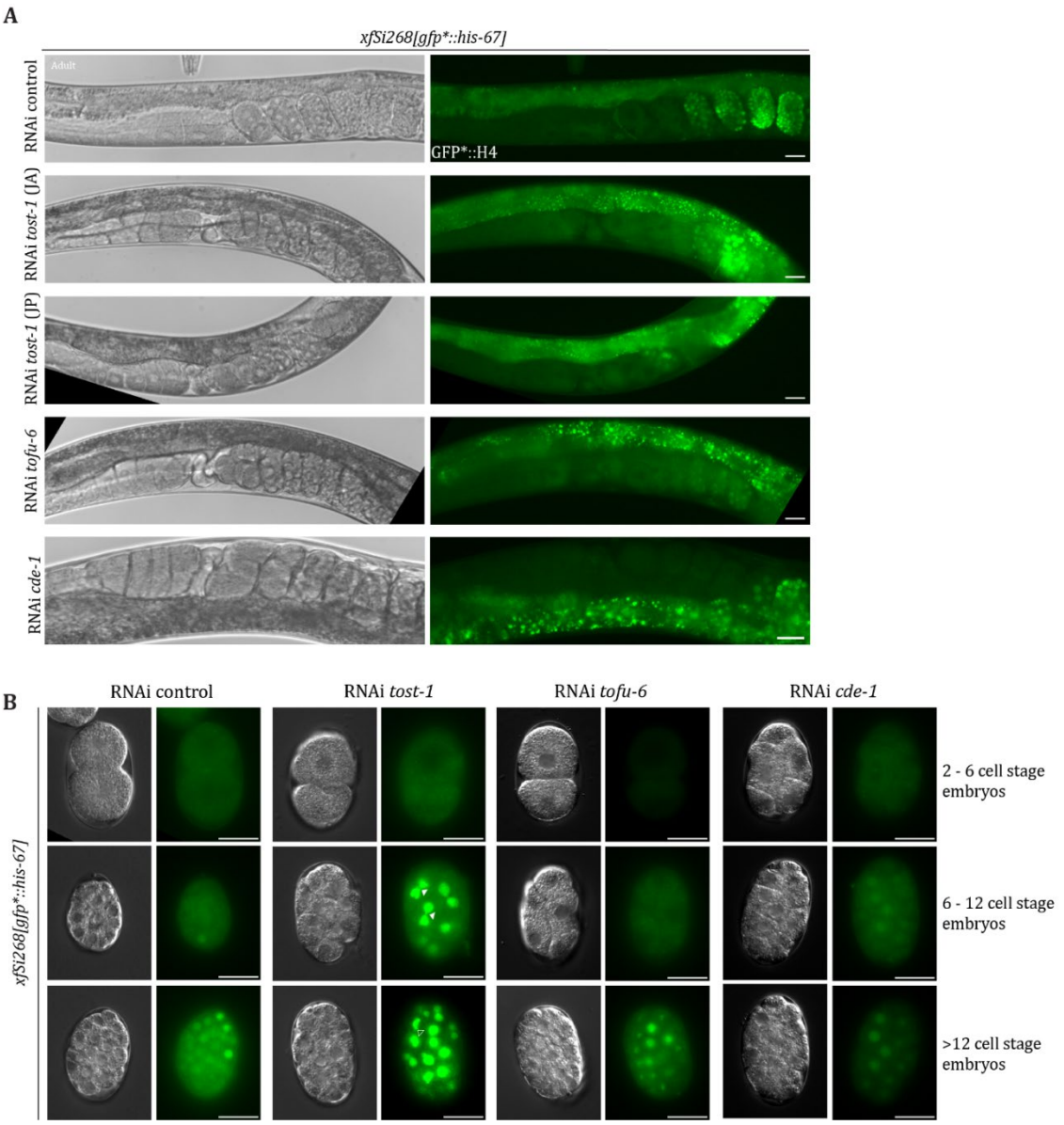

Figure R15 | Effect of *tost-1* RNAi in intronless GFP*::H4 transgenes carrying *xfSi268*. A, B. Wide-field micrographs of single optical sections of adult gonads (A) and dissected embryos (B) of animals carrying *xfSi268* transgene expressing GFP*::H4. Embryos are displayed in a development order, based on cell number counted in using the bright-field channel. Worms were subjected to RNAi via feeding (targets represented in the figure) from L1 larval stage to adulthood. Scale bars = 20 μm.

Similar results were observed in the *xfSi269[gfp*::his-67::tbb-2 3' UTR]* transgene-containing strain (**Figure R16**): expression of GFP*::H4 was silenced in the adult germline and initiated only at later embryonic stages (**Figure R16.A**). As seen in *xfSi268* animals, *tost-1* RNAi led to enhanced GFP*::H4 expression in embryos compared to RNAi control, *tofu-6* or *cde-1* depletion (**Figure R16.B**). Notably, embryos depleted of *tofu-6* or *cde-1* exhibited lower transgene expression

levels. However, additional embryos would need to be analysed to draw more definitive conclusions regarding these observations.

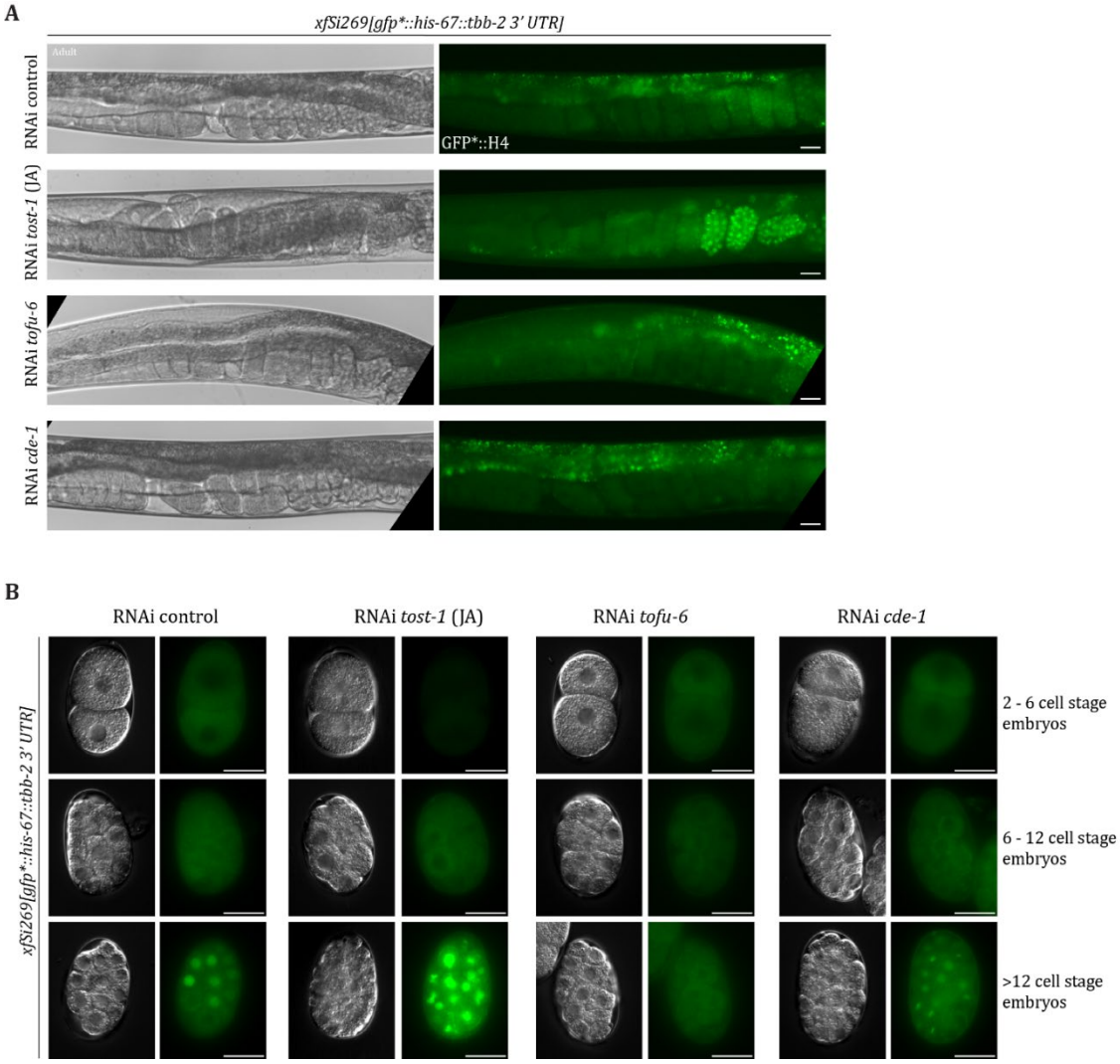

Figure R16 | Effect of *tost-1* RNAi in intronless GFP*::H4 transgenes carrying *xfSi269*. A, B. Wide-field micrographs of single optical sections of adult gonads (A) and dissected embryos (B) of animals carrying *xfSi269* transgene expressing GFP*::H4. Embryos are displayed in a development order, based on cell number counted in using the bright field channel. Worms were subjected to RNAi via feeding (targets represented in the figure) from L1 larval stage to adulthood. Scale bars = 20 μm.

In conclusion, *tost-1* affected the intronless transgenes (*xfSi268* and *xfSi269*) in that they became expressed earlier during embryogenesis, while the intro-containing transgenes (*xfSi254* and *xfSi255*) were not affected. These effects are likely not related to histone homeostasis, but indicative of zygotic genome activation effects.

Effect of *tost-1* mutation on GFP::H4 transgenes expression

To more precisely examine the impact of *tost-1* depletion in *C. elegans*, we analysed the expression of both GFP::H4 transgenes, spliced and non-spliced, in *tost-1* hypomorphic mutants (*xf196 ts)* in embryos at both permissive (15°C) and restrictive (25°C) temperatures. At 15°C, *tost-1(xf196 ts)* are viable, while at 25°C, they arrest, allowing us to investigate the differences between milder and stronger phenotypes.

Spliced GFP::H4 expression in *tost-1* mutant embryos remains unchanged

We divided embryos into four developmental stages (Stage 1-4) based on cell number to account for gene expression variation during early development: stage 1 (1-4 cells), stage 2 (5-12 cells), stage 3 (13-20 cells), and stage 4 (>20 cells). This staging approach controls for variability in cell number, allowing a clearer assessment of expression dynamics and nuclear size across developmental stages. In *C. elegans*, cell divisions occur without increasing the overall embryo size, resulting in decreased cell and nuclear sizes in later stages (Cohen-Fix & Askjaer, 2016). After staging the embryos, we randomly selected three nuclei in focus and at a similar mitotic phase within each embryo to serve as proxies for nuclear GFP::H4 expression. Alongside measuring the GFP mean intensity, we also measured the nuclear area of the same nuclei. This approach helped validate the staging, as nuclear areas should cluster within each stage and progressively decrease as cell division advances. Nonetheless, variability in nuclear size may still occur due to differences in cell cycle stages.

After confirming that the embryos clustered based on their nuclear size, in both *xfSi254* and *xfSi254;tost-1(xf196 ts)* strains (**Figure R17.A**), we quantified the GFP signal. At 15°C, there was no difference in GFP::H4 intensity between *wild-type* and *tost-1(xf196 ts)* embryos (**Figure R17.B-E)**, consistent with observations from *tost-1* RNAi-treated embryos (**Figure R14.B**). At 25°C, *tost-1(xf196 ts)* mutant embryos exhibited severe mitotic defects, particularly evident in stages 3 and 4 (**Figure R17.E**), which likely contribute to the observed embryonic arrest. However, no differences in the GFP::H4 expression were detected between *wild-type* and *tost-1(xf196 ts)* embryos under these conditions.

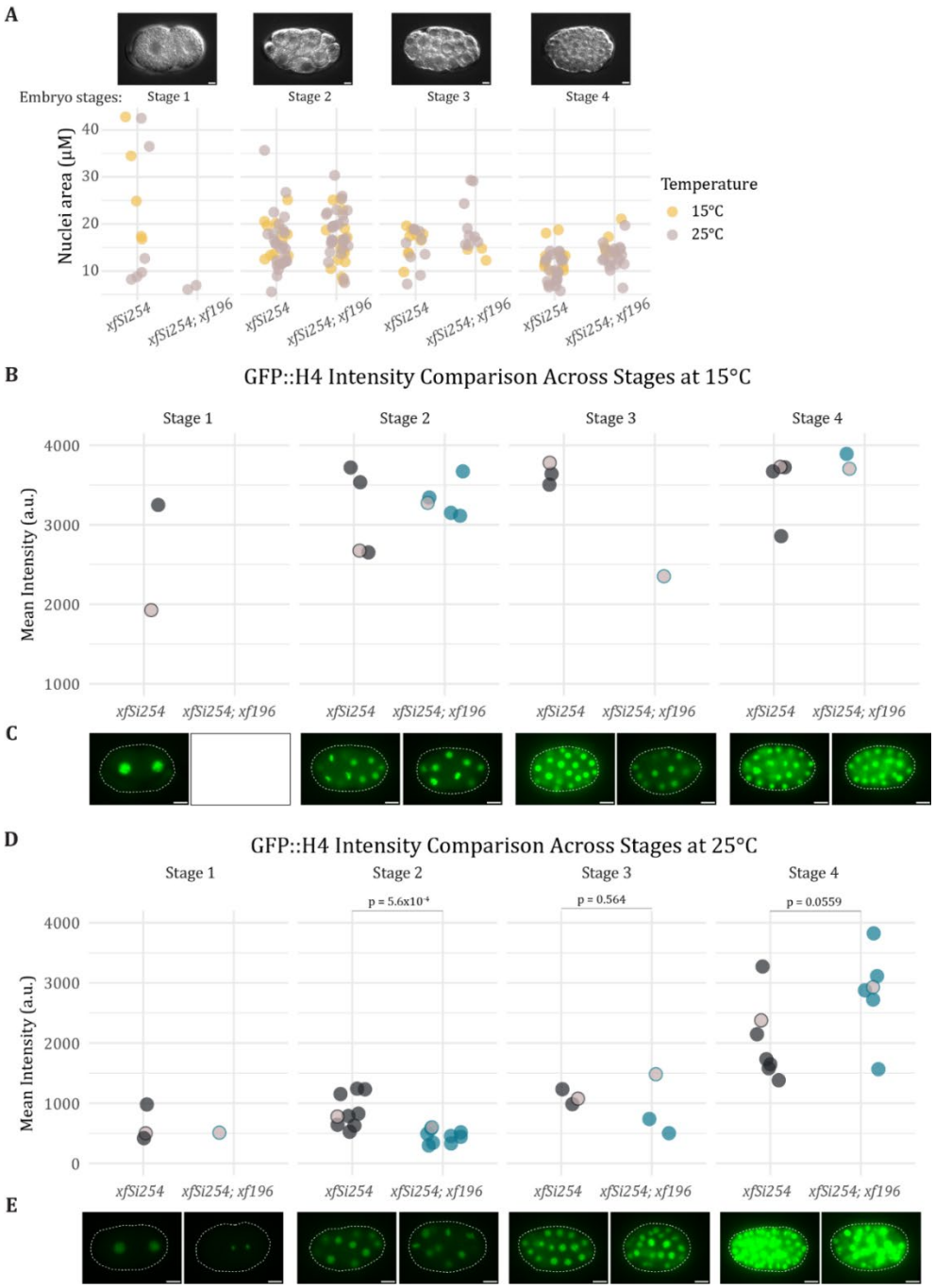

Figure R17 | GFP::H4 expression in *tost-1* mutants across different embryonic stages and different temperatures. A. Nuclei area of each nucleus used for quantification in B and D from dissected embryos of *xfSi254* transgenic worms and *xfSi254; tost-1(xf196)* mutants. Embryos were divided into stages based on cell number (stage 1: 2 to 4 cells; stage 2: 5 to 12 cells; stage 3: 13 to 20 cells; stage 4: more than 20 cells), determined from bright-field images. B, D. Quantification of the average mean intensity of GFP::H4 expression in 2 to 3 nuclei per embryo, analysed at 15°C (B) and 25°C (D) for the different strains. Each dot represents an individual embryo. C, E. Representative images showing GFP::H4 expression of the indicated embryos, with pink circle outlined with strain colour. Blue and black colours indicate different strain genotypes. Dashed lines outline the embryo based on bright-field images (not shown). P-values were calculated using an independent t-test, after testing for normality with Shapiro-Wilk test and for homogeneity of variance with the Levene test. Scale bars = 20 µm.

Enhanced expression of the intronless GFP*::H4 transgene in *tost-1* mutant embryos

We previously observed that *tost-1* depletion via RNAi led to heightened expression of the transgenes *xfSi268[gfp*::his-67]* and *xfSi269[gfp*::his-67::tbb-2 3'UTR]* compared to RNAi control embryos (**Figure R15, R16**). To obtain more robust results, we analysed the expression of the same non-spliced transgenes in a hypomorphic *tost-1* mutant background and quantified the nuclear GFP expression as described above. Consistent with the RNAi treatment results, we found that *tost-1(xf196 ts)* mutant embryos exhibited similarly elevated expression levels of GFP*::H4, indicating that *tost-1* depletion enhances the expression of these transgenes (**Figure R18, R19**). At 15°C, the upregulation of GFP*::H4 expression in *xfSi268* transgenic embryos in comparison to wild type was particularly evident in later stages of development, specifically stage 4 (embryos with more than 20 cells, **Figure R18.B**). At 25°C, the increase in GFP*::H4 expression was pronounced as early as stage 3 (13-20 cells, **Figure R18.D**). This shift suggests a temperature-dependent amplification of the transgene expression, which is likely due to the reduced functionality of TOST-1 at the restrictive temperature. It is important to note that stage 4 encompasses a range of embryos with over 20 cells, resulting in a considerable variability in mean GFP intensities within this group.

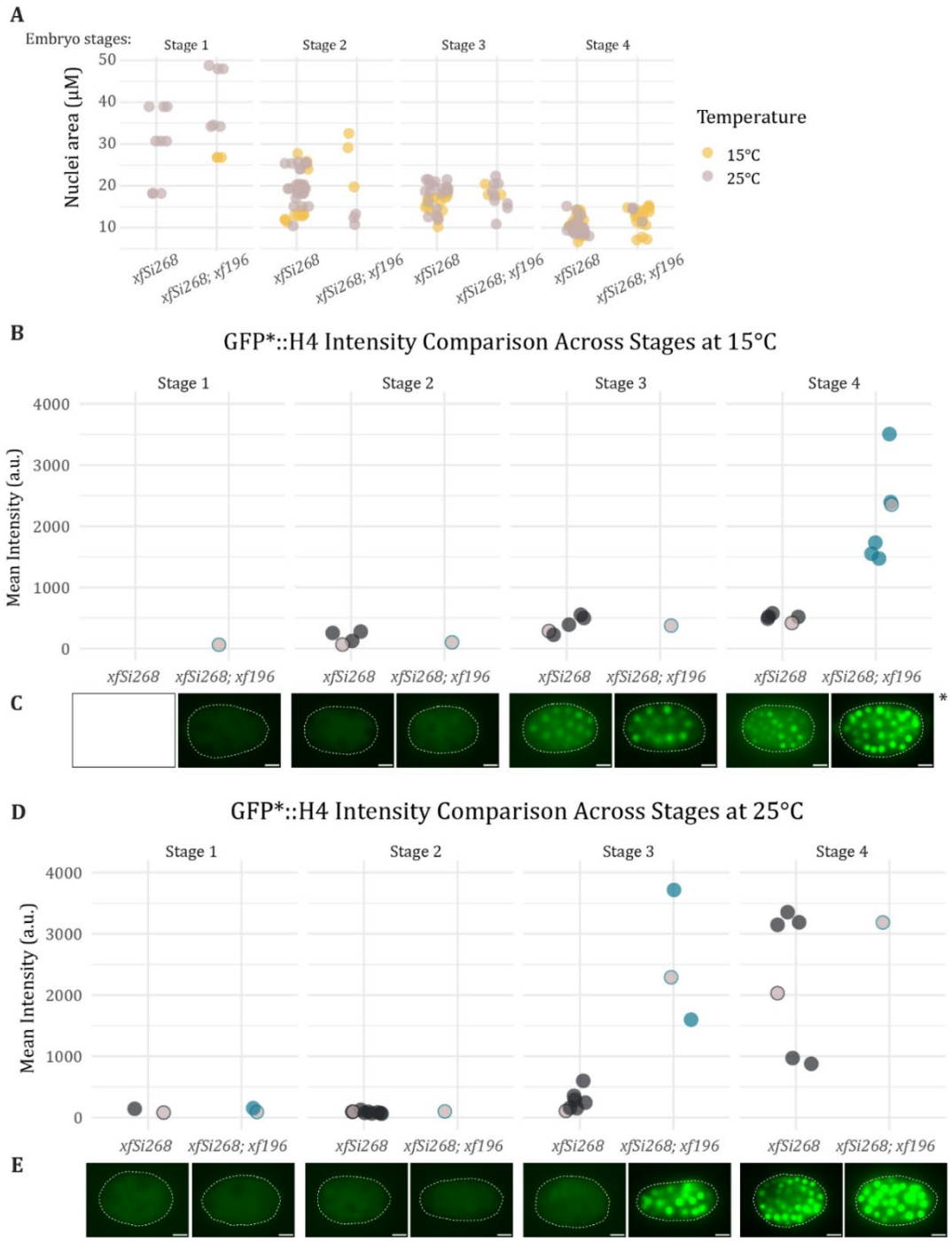

Figure R18 | GFP*::H4 expression in *tost-1* mutants across different embryonic stages and different temperatures. A. Nuclei area of each nucleus used for quantification in B and D from dissected embryos of *xfSi268* transgenic worms and *xfSi268; tost-1(xf196)* mutants. Embryos were divided in stages based on their cell number. B, D. Quantification of the average mean intensity of GFP*::H4 expression in 2 to 3 nuclei per embryo, analysed at 15°C (B) and 25°C (D) for the different strains. Each dot represents one embryo. C, E. Representative images showing GFP*::H4 expression of the indicated embryos with pink circle outlined with strain colour. Blue and black colours indicate different strain genotypes. Dashed lines outline the embryo based on bright-field images (not shown). Asterisk * indicates different brightness and contrast during image processing to avoid over-exposition during visualization. Scale bars = 20 µm.

Regarding the *xfSi269* transgene, the effect of *tost-1* mutation on GFP*::H4 expression was less pronounced compared to *xfSi268,* which differs only in the 3' UTR (**Figure R19**). However, at 25°C, *tost-1(xf196 ts)* embryos displayed a significant increase in GFP*::H4 expression but only in stage 4 (**Figure R19.D**). These findings indicate that the impaired activity of TOST-1 at the restrictive temperature consistently enhances GFP*::H4 expression across both transgenes, with stronger and earlier effects observable at 25°C.

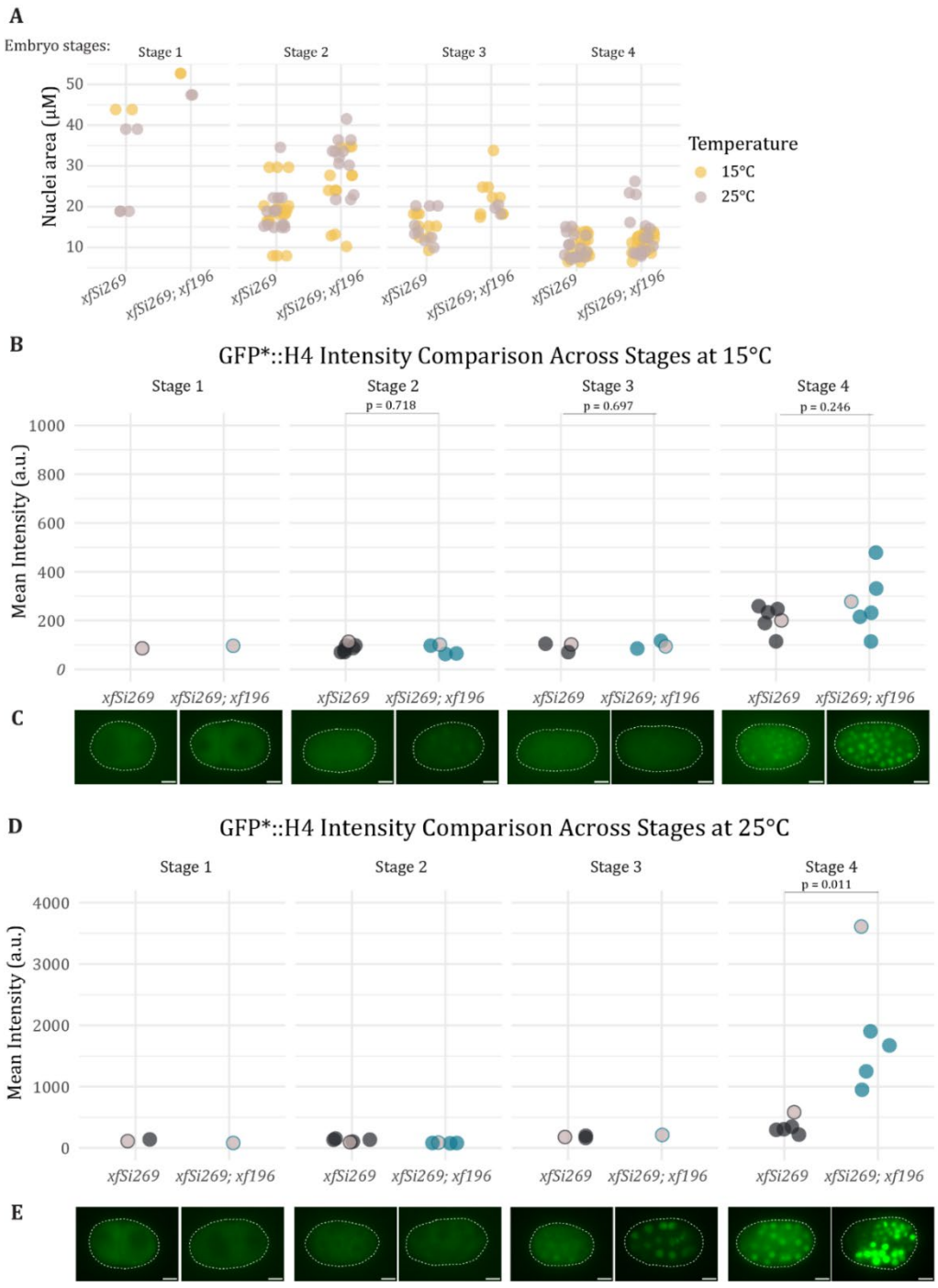

Figure R19 | GFP*::H4 expression in *tost-1* mutants across different embryonic stages and different temperatures. A. Nuclei area of each nucleus used for quantification in B and D from dissected embryos of *xfSi269* transgenic worms and *xfSi269; tost-1(xf196)* mutants. Embryos were divided in stages based on their cell number. B, D. Quantification of the average mean intensity of GFP*::H4 expression in 2 to 3 nuclei per embryo, analysed at 15°C (B) and 25°C (D) for the different strains. Each dot represents one embryo. C, E. Representative images of the GFP*::H4 expression of the indicated embryos with pink circle outlined with strain colour. Blue and black colours indicate different strain genotypes. Dashed lines outline the embryo based on bright-field images (not shown). P-values were calculated using an independent t-test, after testing for normality with Shapiro-Wilk test and for homogeneity of variance with Levene test. Scale bars = 20 µm.

Endogenously tagged H2A expression mirrors transgenic GFP::H4 patterns

In the time of this study, another group generated two strains with *his-61*, coding for H2A, fused with GFP. In one allele *gfp* includes introns (*ne4946*), while the other is intronless (*ne4847*) (Makeyeva et al., 2021). Similar to the transgenic lines with the alleles *xfSi254* and *xfSi255*, which contain intron-containing *gfp*, the strain with *ne4846(gfp::his-61)* is expressed throughout the entire germline and across all embryonic stages (Makeyeva et al., 2021) (**Figure R20**). In *tost-1(xf196 ts)* mutants, spliced GFP::H2A expression remains comparable to that in *tost-1* wild type animals (**Figure R20.B, C**). At 25°C, a significant increase in GFP expression is observed in stage 4, however, this may be attributed to the variability in cell number at this stage (**Figure R20.D**).

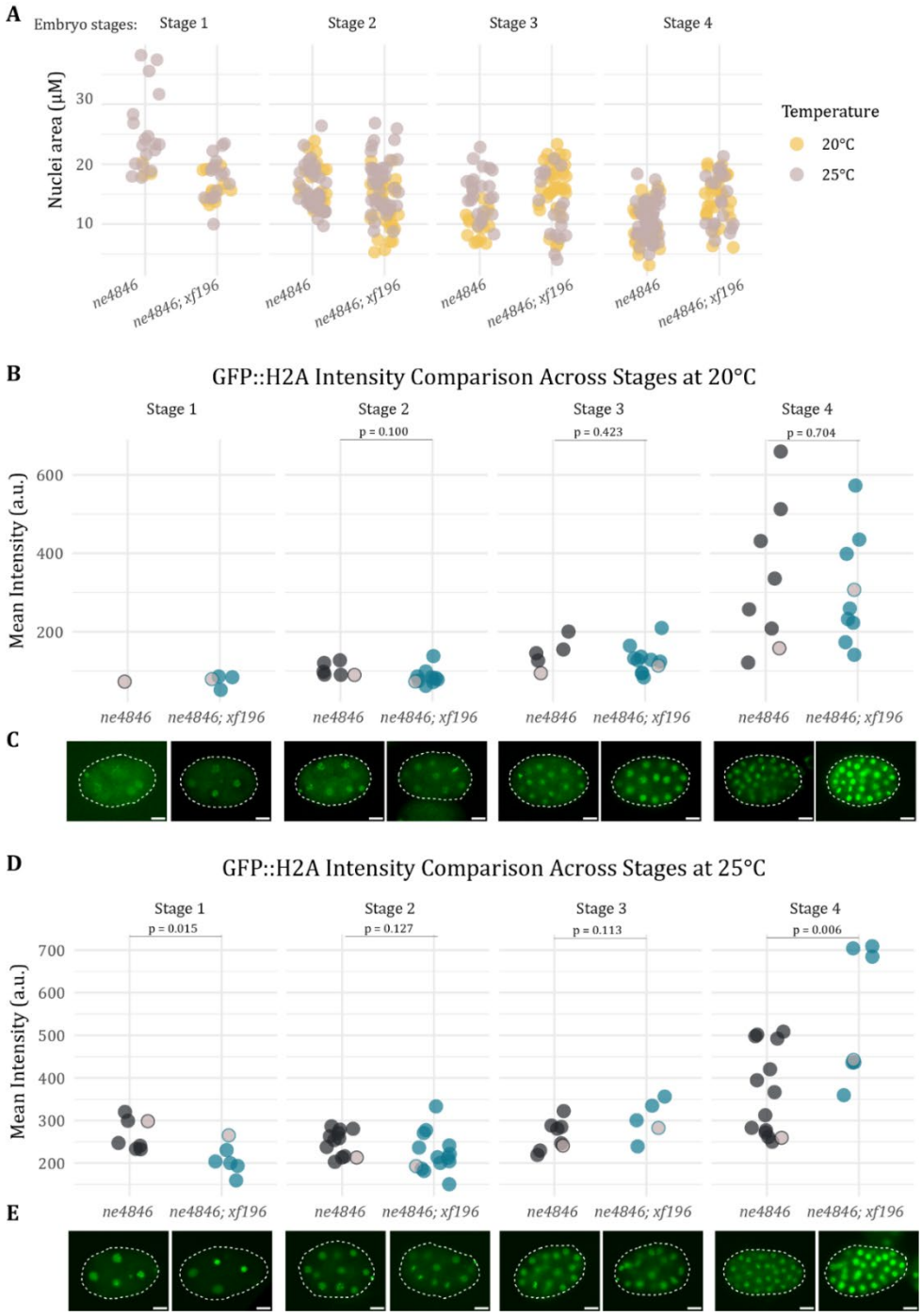

Figure R20 | GFP::H2A expression in *tost-1* mutants across different embryonic stages and different temperatures. A. Nuclei area of each nucleus used for quantification in B and D from dissected embryos of *ne4846* worms and *ne4846; tost-1(xf196)* mutants. The embryos were divided in stages based on their cell number. B, D. Quantification of the average mean intensity of GFP::H2A expression in the 2 to 3 nuclei per embryo, analysed at 20°C (B) and 25°C (D) for the different strains. Each dot represents one embryo. C, E. Representative images of the GFP::H2A expression of the indicated embryos with pink circle outlined with strain colour. Blue and black colours indicate different strain genotypes. Dashed lines outline the embryo based on the bright-field images (not shown). P-values were calculated using an independent t-test, after testing for normality with Shapiro-Wilk test and for homogeneity of variance with Levene test. Scale bars = 20 µm.

Interestingly, similar to the non-spliced *xfSi268* and *xfSi269* transgenes expression, the intronless *ne4847(gfp*::his-61)* allele is silenced in the germline and only begins expression later in embryogenesis (Makeyeva et al., 2021) (**Figure R21**). At 20°C, there is significant increase in GFP*::H2A expression in *tost-1(xf196 ts)* mutants embryos at stage 4 (**Figure R21.B**), but at 25°C, the difference in expression in stage 4 is not significant (**Figure R21.D**). However, at stage 3, *tost-1(xf196 ts)* mutant embryos show higher expression of GFP*::H2A, although the number of replicates is too low for robust conclusions. Overall, these experiments suggest that TOST-1 impairment at the restrictive temperature may enhance GFP expression in both transgenic and endogenously tagged histone proteins. This effect appears to be independent of the locus and the specific histone protein tagged.

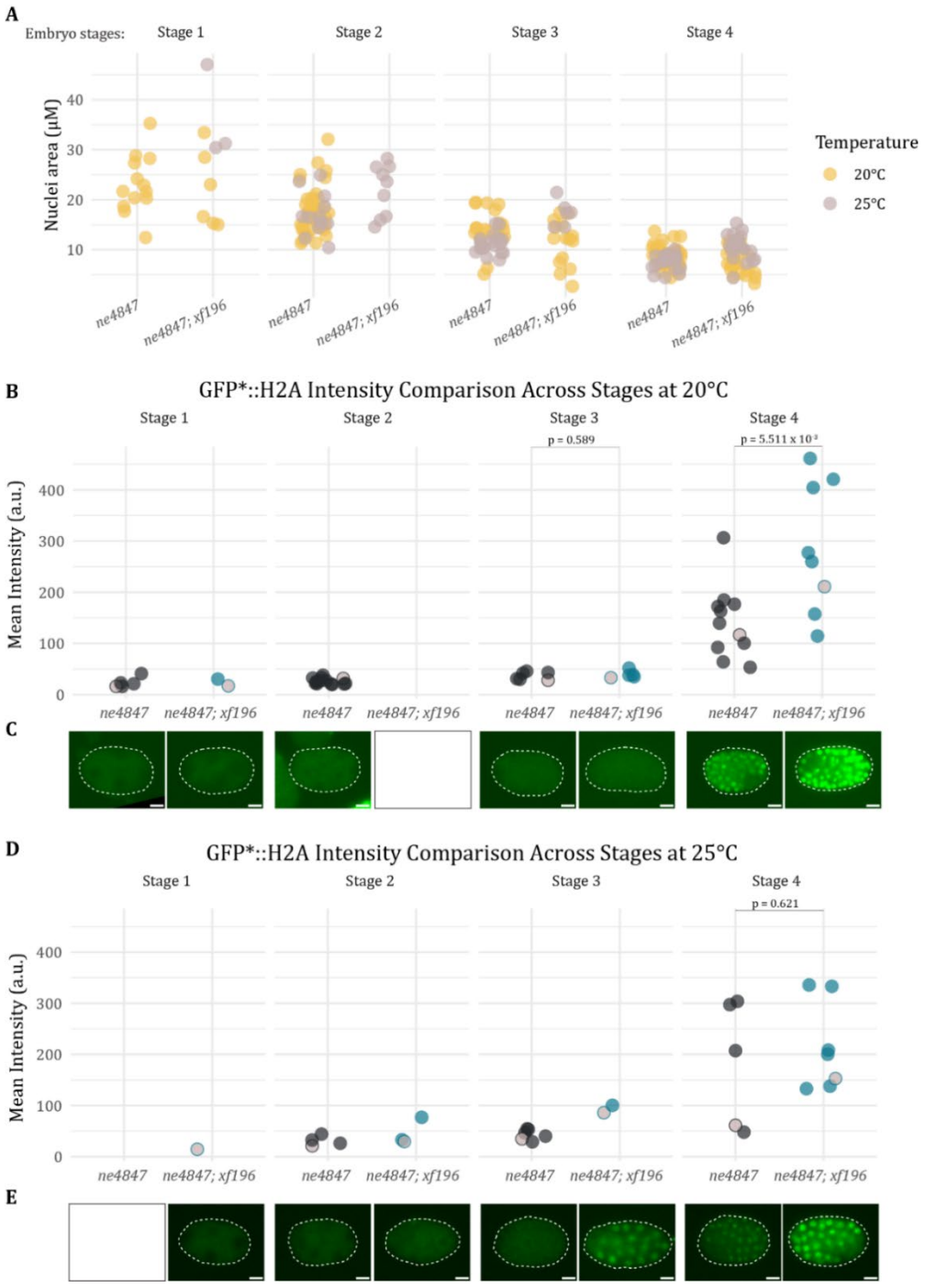

Figure R21 | GFP*::H2A expression in *tost-1* mutants across different embryonic stages and different temperatures. A. Nuclei area of each nucleus used for quantification in B and D from dissected embryos of *ne4847* worms and *ne4847; tost-1(xf196)* mutants. Embryos were divided into stages based on their cell. B, D. Quantification of the average of the mean intensity of GFP*::H2A expression in the 2 to 3 nuclei per embryo, analysed at 20°C (B) and 25°C (D) for the different strains. Each dot represents one embryo. C, E. Representative images of the GFP*::H2A expression of the indicated embryos with pink circle outlined with strain colour. Blue and black colours indicate different strain genotypes. Dashed line outlines the embryo based on the brightfield images (not shown). P-values were calculated using an independent t-test, after testing for normality with Shapiro-Wilk test and for homogeneity of variance with Levene test. Scale bars = 20 µm.

TOST-1 is essential for proper gene expression

Non-spliced GFP*::H4 transgene is expressed earlier in PETISCO mutants

Experiments on animals carrying the *xfSi268[gfp*::his-67]* transgene suggested altered zygotic expression timing in *tost-1* RNAi-depleted animals and mutants (**Figure R15, R18**). To investigate this further and determine the specific developmental stages affected, we quantified GFP*::H4 expression, using the same *xfSi268* transgene, in the whole embryo over time under RNAi depletion of *tofu-6*, *tost-1*, *his-65* and *his-66* (**Figure R22, R23**). This allowed us to monitor the onset of transgene expression under various RNAi conditions. By depleting *his-65* (coding H2A) and *his-66* (coding H2B), we could compare the phenotypes of PETISCO-depleted embryos with those of histone-depleted embryos, as we hypothesize that the phenotypes observed in PETISCO and TOST-1 mutants are due to histone depletion in both the germline and embryos.

RNAi against *tofu-6, tost-1,* and the histone genes *his-65* and *his-66* were induced to assess the effects of PETISCO and histone transcripts depletion on GFP intensity in embryos over time (**Figure R22**). As a control for RNAi, we used an empty dsDNA sequence. Embryos were staged according to cell number: t1 corresponds to the 4-cell stage, t5 to the 6-cell stage, t9 to the 8-cell stage, and t12 to the 10-cell stage, with each time point separated by 3 minutes. In *tost-1*, *tofu-6,* and *his-65* RNAi-treated embryos, we observed an earlier and faster increase in GFP mean intensity across the embryo relative to control RNAi, indicating an earlier onset of transgenes expression (**Figure R22.A**). In contrast, *his-66* RNAi did not show an increase in GFP mean intensity, but the high variability in expression among *his-66* RNAi treated embryos suggests asynchronous transgene activation across embryos compared to the control (**Figure R22.A**).

To further pinpoint the cell stages at which GFP*::H4 expression initiates across different RNAi conditions, we calculated the standard deviation (SD) of GFP intensity across the embryo at each time point (**Figure R22.B-F**). Since GFP*::H4 is localised to the nuclei and does not begin to be expressed in every nucleus simultaneously, the intensity variance across the embryo increases. The nuclear signal is much stronger than the cytoplasmic signal, which causes an increase in the SD of the GFP intensity across the embryo. As SD increases, it becomes easier to detect changes in GFP expression. Small changes in the intensity of GFP in individual nuclei will have a larger effect on the SD than on the mean intensity, which allows for more sensitive detection of the onset of GFP expression. The mean intensity remains relatively stable, while the SD becomes more sensitive to variations, making it easier to detect subtle changes in expression levels.

In control embryos, GFP*::H4 expression typically began around time point 16 across replicates (**Figure R22.B**). In contrast, in *his-65* RNAi-treated embryos showed an earlier onset of expression at time points 10 and 13 (**Figure R22.C**). The *his-66* RNAi-treated embryos exhibited notable variability, with expression onset at time point 10 in some embryos and time point 15 in others (**Figure R22.D**). In TOFU-6 depleted embryos, expression was initiated even earlier, around time point 8 (**Figure R22.E**), while TOST-1 depletion led to expression onset at time point 12 (**Figure R22.F**). Since GFP*::H4 expression in *tofu-6* and *tost-1* depleted embryos occurs 8 and 4 time points earlier, respectively (with 3 minutes between each time point), we conclude that expression in these embryos is prematurely activated by at least one cell cycle, given that the average cell cycle length during the first embryonic cleavages is 15 minutes (Bao et al., 2008).

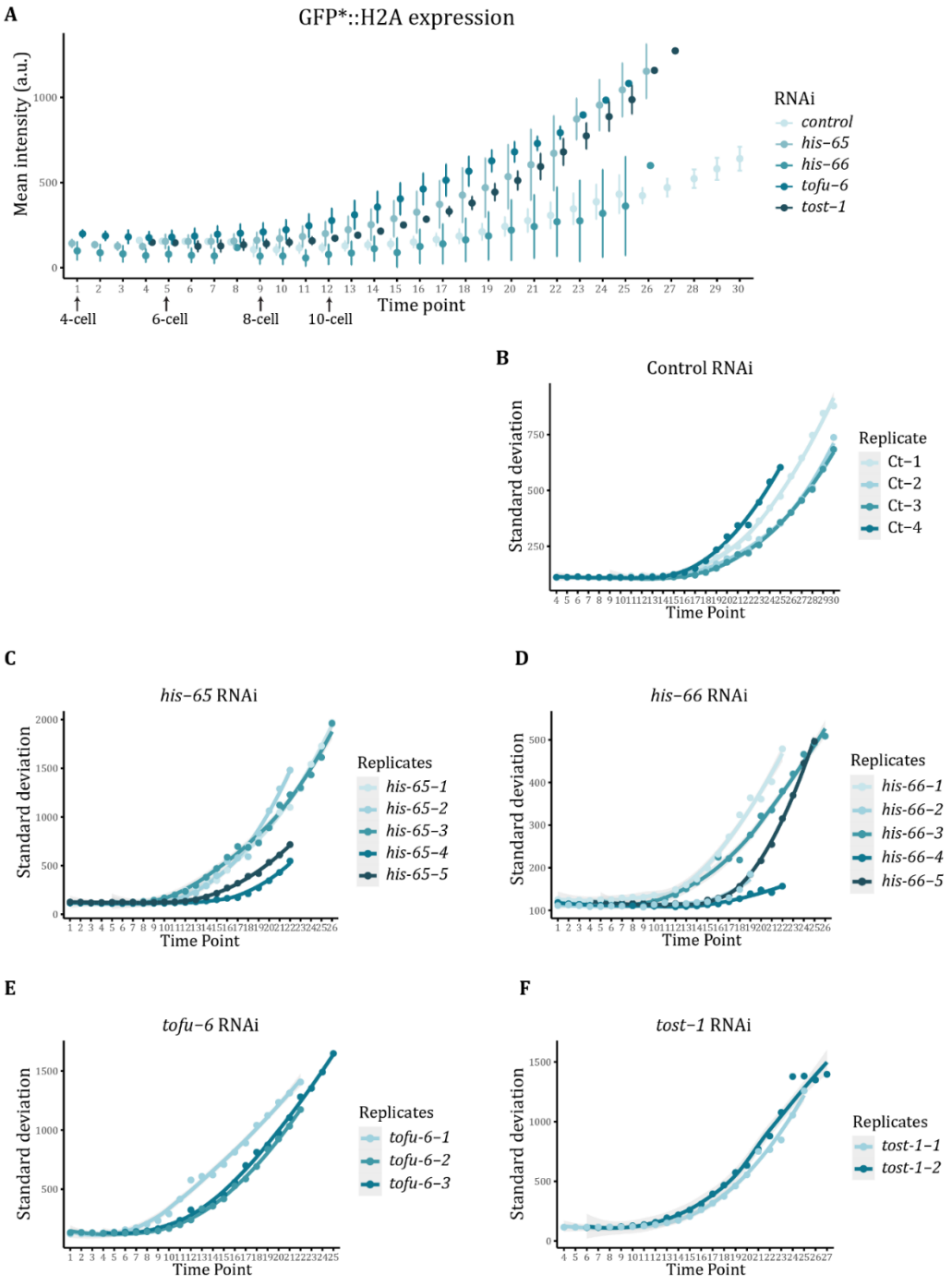

Figure R22 | Histone depletion induced by RNAi results in altered beginning of GFP*::H4 expression in early embryos. A. Average mean intensity of GFP*::H2A expression during a time lapse with 3-minute intervals. Embryos were dissected from adult worms fed with RNAi for the indicated targets. GFP mean intensity was measured in the whole embryo. The embryos were normalised by cell number and the time points were adjusted as follows: time point 1 is 4-cell embryo, time point 5 is 6-cell embryo, time point 9 is 8-cell embryo and time point 12 is 10-cell embryos. Error bars represent standard deviation across biological replicates. B-F. Standard deviation of the mean intensity of GFP*::H2A in the whole embryo across time points. Each line represents the trend of the GFP*::H2A signal quantification for one embryo over time.

To determine if GFP*::H4 expression intensity increased over time, contributing to higher nuclear H4 levels, we quantified only the nuclear GFP mean intensity at specific time points (4, 10, 16, and 22) (**Figure R23.A**), following the same approach used in the previous experiments. While the overall embryo GFP intensities, calculated in the previous quantification, could have provided sufficient information, we opted to focus on nuclear intensity. This allowed us to normalise the number of analysed nuclei and ensure a quantification that was not dependent on mitotic stages or the nuclei in focus in each image. Since the imaged embryos had slightly different cell numbers at the start of imaging, we aimed to normalise cell numbers per time point. As a result, not all embryos were present at every time point. One embryo per RNAi condition, present in all time points, was chosen for representative images and indicated with a lighter colour in the graph.

At time point 4 (5-cell stage), no GFP*::H4 expression was observed. However, by time point 10, most RNAi-treated embryos had begun expressing GFP in some nuclei, with *tofu-6* depleted embryos showing the most pronounced early expression. Eighteen minutes later, at time point 16, GFP*::H4 expression was widespread across all embryos, with stronger expression persisting in RNAi-treated groups through the final time point measured. However, the increase in the particular case of *his-66* RNAi-treated embryos is not significant.

Additionally, differences in cell cycle progression were evident: *his-65* and *tofu-6* RNAi-treated embryos showed lower cell numbers than control embryos at time points 16 and 22, indicating a delay in cell division (**Figure R23.B**). This slower cell cycle progression aligns with previous findings that histone depletion can result in lengthened cell cycles and premature onset of ZGA (Amodeo et al., 2015; Chari et al., 2019; Joseph et al., 2017). These findings suggest a direct relationship between TOST-1 function and ZGA timing, likely mediated by its role in stabilizing maternal histone mRNA levels. Without functional TOST-1, the reduced maternal histone mRNA levels mirror the effects of histone RNAi, leading to premature zygotic genome activation and altered cell cycle progression.

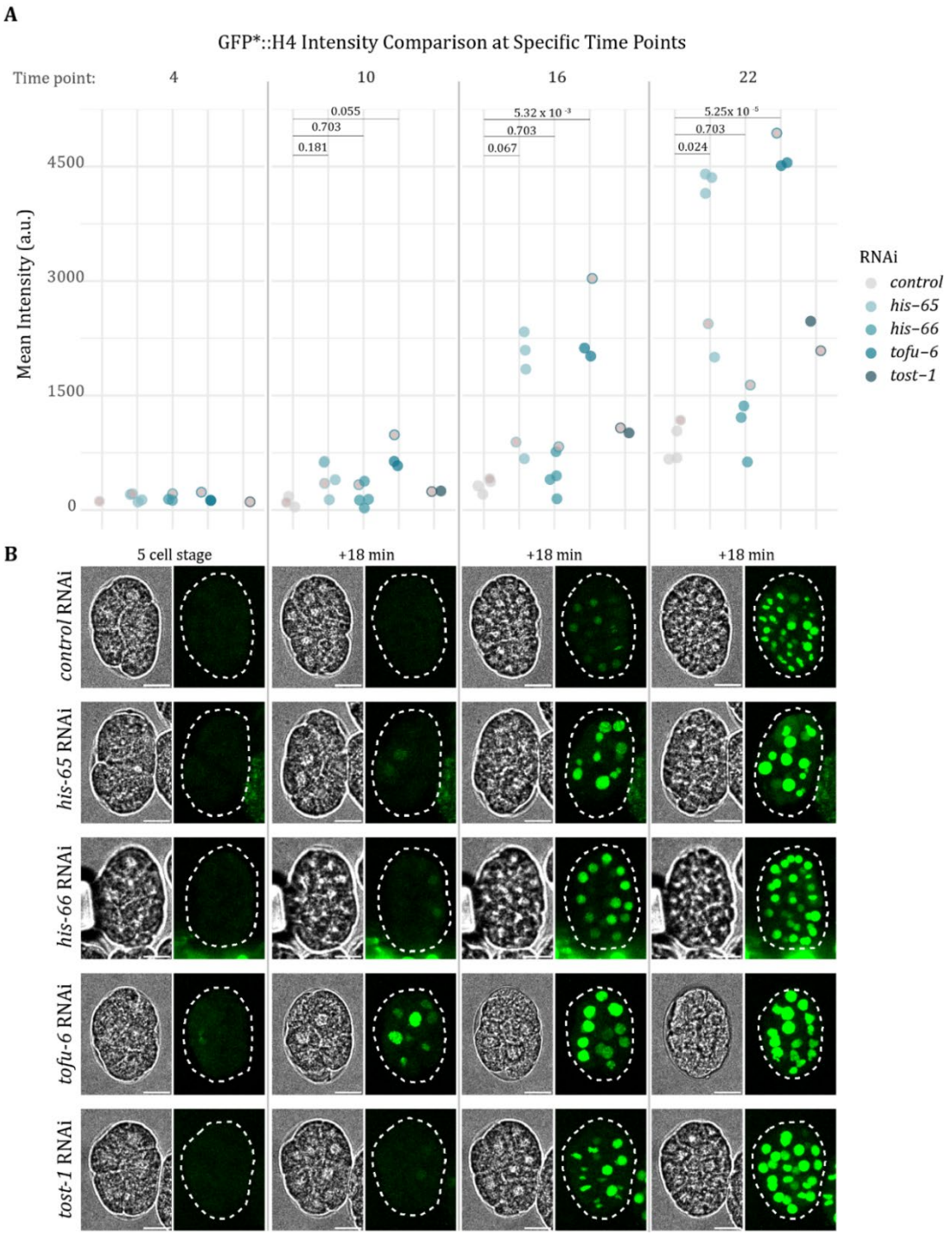

Figure R23 | Concentration of histone mRNAs affects the onset of GFP*::H4 expression in early embryos. A. Quantification of GFP*::H4 mean intensity in 3 nuclei per embryo at specific time points (4, 10, 16, and 22) under different RNAi conditions, represented by different colours (*control, his-65, his-66, tofu-6* and *tost-1*). Each dot represents the average mean intensity from the three measured nuclei. P-values were calculated using an independent t-test, adjusted with Holm–Bonferroni method to correct for multiple comparisons, after testing for normality with Shapiro-Wilk test and for homogeneity of variance with the Levene test. B. Representative images of the indicated embryos, highlighted in pink, under each condition and at the specified time points. Dashed lines outline the embryos based on the bright-field images (not shown). Scale bars = 20 µm.

tost-1 mutant embryos exhibit altered gene expression

To investigate gene expression profiles in *tost-1(xf196 ts)* hypomorphic mutants, we performed RNA-seq on early embryos from both *tost-1* mutant and wild-type animals at permissive (15°C) and restrictive (25°C) temperatures. We conducted differential expression analysis across four conditions using pairwise comparisons to identify genes with significant upregulation or downregulation, applying a fold change threshold of >1 and a corrected p-value<0.01 as criteria for significance (**Figure R24**).

In wild-type embryos, we identified 3784 upregulated genes and 4083 downregulated genes at 25°C compared with 15°C (**Figure R24.A**). In *tost-1(xf196 ts)* mutants, 2857 were upregulated and 3657 were downregulated when comparing the 25°C to 15°C conditions (**Figure R24.B**). Additionally, when comparing *tost-1* mutants to wild-type embryos at each temperature individually, 2043 genes were upregulated and 2388 downregulated in *tost-1* mutants at 15°C (**Figure R24.C**). At 25°C, we observed 2499 upregulated genes and 2457 downregulated genes in *tost-1* mutants relative to wild-type embryos (**Figure R24.D**).

Interestingly, although the number of upregulated and downregulated genes is similar across comparisons, increasing the fold change threshold to a minimum of 2 reveals a larger number of upregulated genes than downregulated, such as in *tost-1* mutant vs wt, and *tost-1* mutant at 25°C vs 15°C. With this higher threshold, we observed 1529 upregulated and 718 downregulates genes in *tost-1(xf196 ts)* at 25°C vs 15°C, 1615 upregulated and 493 downregulated genes in *tost-1(xf196 ts)* vs *wt* at 25°C, and 407 upregulated and 213 downregulated genes in *tost-1(xf196 ts)* vs *wt* at 15°C. These results suggest that a subset of upregulated genes in these conditions undergo more pronounced differential expression, potentially due to chromatin alterations in the embryos that reduce transcriptional restrictions and enable higher transcription rates.

An unexpected finding in our RNA-seq with polyA+ selection was the presence of RD histone mRNAs. RD histone mRNAs are typically non-polyadenylated, but under certain conditions such as depletion of SLBP, viral infections, terminal differentiation, environmental stress, or slow transcription elongation rate, some RD histone genes become polyadenylated (D. Chen et al., 2020; Guo et al., 2023; Kari et al., 2013; Lyons et al., 2016; Saldi et al., 2018). Therefore, the presence of polyadenylated (polyA+) RD histone transcripts in our dataset may indicate a misregulation or alternative regulation of these genes.

We observed a subset of polyA+ RD histone genes downregulated in wild-type samples at 25°C vs 15°C (Figure R24.A), as well as a subset in *tost-1* mutant at 25°C vs 15°C (**Figure R24.B**). This suggests that the temperature shift alone is sufficient to cause this change. This could be due to

increased instability of histone mRNAs at 25°C, or upregulation of mRNA degradation pathways, leading to reduced levels of polyA+ RD histone transcripts. Another possibility is that the slowing of the cell cycle in later embryogenesis could result in the downregulation of histone transcripts, even if they are polyadenylated.

When comparing *tost-1* mutants vs *wt* at 25°C and 15°C, we observed different patterns. At 25°C, a subset of polyA+ RD histone genes were detected but mostly unchanged, with only a few showing slight statistically significant upregulation (**Figure R24.C**). In contrast, at 15°C, most polyA+ RD histone genes remained unchanged (**Figure R24.D**). It is possible that the impaired TOST-1 function at 25°C, results in slight misregulation of histone mRNA, causing a few genes to become more polyadenylated.

Interestingly, RI histone genes were upregulated in all conditions, suggesting that both temperature shifts and the *tost-1* mutation influence their expression. RI histones or histone variants are known to replace RD histone transcripts in certain cell types and developmental stages (Henikoff & Ahmad, 2005; Ibarra-Morales et al., 2021; Lyons et al., 2016; Sakai et al., 2009; Talbert & Henikoff, 2016; Whittle et al., 2008). The upregulation of RI histones mRNAs in samples with increased temperature may reflect advancement in development compared to the 15°C samples, leading to a need for these histones earlier (Begasse et al., 2015). On the other hand, the upregulation in *tost-1* mutants may be a compensatory response to the downregulation of maternal histone transcripts, a phenomenon that has been observed in mammalian cells (Jimeno-González et al., 2015; T. S. Rai et al., 2014). However, since we lack data on the expression of RD histones with the stem-loop, drawing definitive conclusions about general histone expression in these samples is difficult.

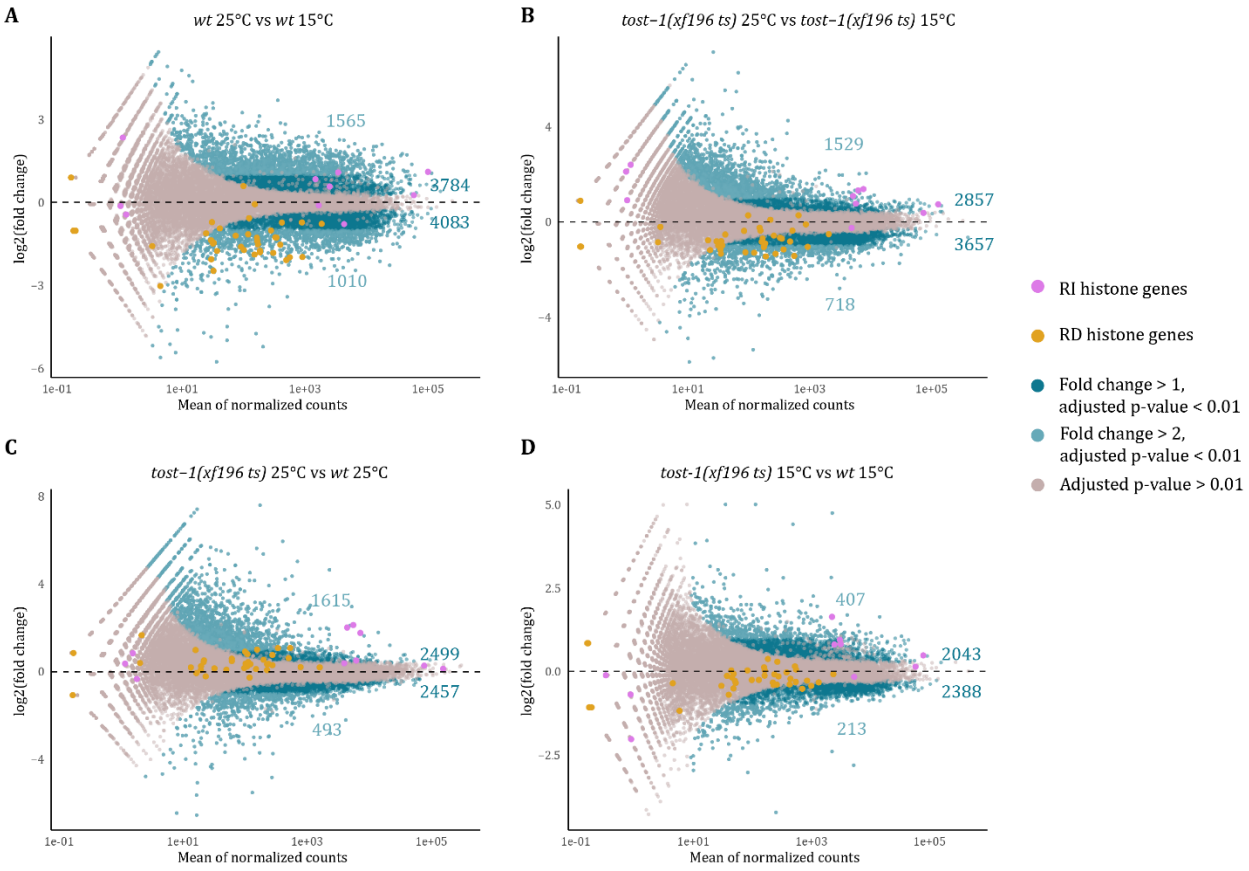

Figure R24 | RNA expression is altered in *tost-1(xf196 ts)* mutants. A-D. Pairwise differential gene expression of polyA+ RNAs from *wild-type (wt)* and *tost-1(xf196 ts)* mutants at 15°C or 25°C. A. *wt* 25°C vs *wt* 15°C; B. *tost-1(xf196 ts)* 25°C vs *tost-1(xf196 ts)* 15°C; C. *tost-1(xf196 ts)* 25°C vs *wt* 25°C; D. *tost-1(xf196 ts)* 15°C vs *wt* 15°C. Significantly differentially expressed genes are highlighted in dark blue (fold change >1) and light blue (fold change >2), with the numbers of genes indicated in each plot. Genes with no significant difference (adjusted p-value > 0.01) are shown in pink. Replication–dependent (RD) histones are indicated in yellow and replication-independent (RI) histones are indicated in lilac. Adjusted p-values were calculated using the Benjamini and Hochberg method for FDR < 0.01.

To further dissect the gene families and pathways affected by the *tost-1* mutation at both 15°C and 25°C, we performed additional differential expression comparisons across conditions and performed gene ontology (GO) analysis on specific subsets. When comparing upregulated genes between *tost-1* mutants vs *wt* at 25°C and 15°C, we found 1996 genes uniquely upregulated in *tost-1* mutants at 25°C, 503 overlapping genes upregulated at both temperatures, and 1540 uniquely upregulated at 15°C (**Figure R25.A**). Given that TOST-1 function is more severely impaired at 25°C, resulting in embryonic lethality, we hypothesize that the unique set of 1996 upregulated genes may either contribute to or reflect the lethality observed. GO analysis of this subset of genes revealed an enrichment in pathways related to signalling, such as endocytosis or autophagy, which could indicate apoptotic processes in embryos undergoing cell death (**Figure**

R25.D). Among the 503 overlapping genes, no specific GO terms were enriched, whereas the unique set of 1540 genes upregulated at 15°C showed significant enrichment in neurogenesis pathways (**Figure R25.A**). In the condition where TOST-1 is hypomorphic but not lethal, histone mRNA levels are already significantly downregulated. This allows us to study histone mRNA depletion effects without the confounding impact of cell death. The enrichment of neurogenesis-related pathways in this hypomorphic condition suggests a premature initiation of lineage specificity and differentiation in early embryos, potentially due to premature ZGA. This hypothesis aligns with the earlier expression of the *xfSi268* transgene observed in the previous experiment. Notably, this enrichment was absent at 25°C, likely because apoptotic pathways dominate under these conditions.

We further compared the genes upregulated in *tost-1* mutants at 25°C vs 15°C with those upregulated in *wt* at 25°C vs 15°C (**Figure R25.B**). This comparison highlights genes upregulated specifically due to the stronger loss of TOST-1 function, rather than due to temperature changes. From this, we identified 1512 genes that were upregulated independently of temperature alone. Comparing these 1512 genes with the 2499 genes upregulated in *tost-1* mutant vs *wt* at 25°C revealed 1067 overlapping genes, suggesting a robust overlap in genes affected solely by TOST-1 dysfunction (**Figure R25.C**). GO term analysis of these overlapping genes mirrored that of the *tost-1* mutant vs wt comparison at 25°C (data not shown), supporting the reproducibility of our dataset.

Similar analyses were performed on downregulated genes. We found 1669 genes uniquely downregulated in *tost-1* mutant vs *wt* at 25°C, 788 overlapping genes downregulated at both temperatures, and 1600 uniquely downregulated in *tost-1* mutant vs *wt* at 15°C (**Figure R25.F**). GO analysis of these subsets indicated that genes involved in neurogenesis and transcription were specifically downregulated in *tost-1* mutants with strong phenotypic defects at 25°C (**Figure R25.I**). In contrast, genes downregulated at 15°C, both overlapping or unique, were enriched in pathways related to RNA metabolism and cell cycle regulation (**Figure R25.J, K**). These findings align with our observations of disrupted cell cycle progression in PETISCO mutants, where the cell number seemed to be lower compared to control conditions (**Figure 23.B**), and support the hypothesized role of TOST-1 in maternal RD histone mRNA metabolism.

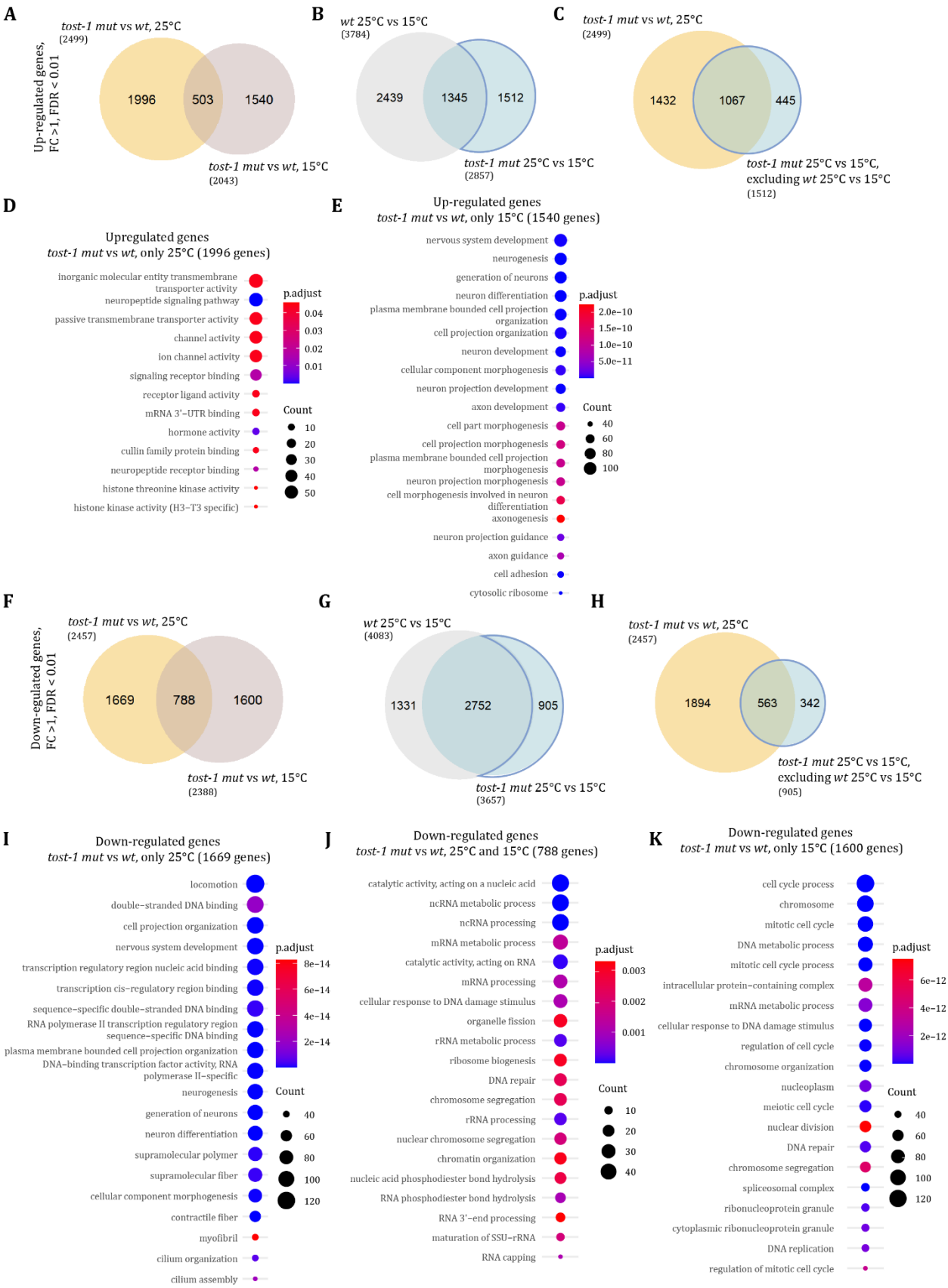
A
tost-1 mut vs wt, 25°C
(2499)
Up-regulated genes,
FC >1, FDR < 0.01
1996
503
1540
tost-1 mut vs wt, 15°C
(2043)
B
wt 25°C vs 15°C
(3784)
2439
1345
1512
tost-1 mut 25°C vs 15°C
(2857)
C
tost-1 mut vs wt, 25°C
(2499)
1432
1067
445
tost-1 mut 25°C vs 15°C,
excluding wt 25°C vs 15°C
(1512)
D
Upregulated genes
tost-1 mut vs wt, only 25°C (1996 genes)
inorganic molecular entity transmembrane transporter activity
neuropeptide signaling pathway
passive transmembrane transporter activity
channel activity
ion channel activity
signaling receptor binding
receptor ligand activity
mRNA 3'-UTR binding
hormone activity
cullin family protein binding
neuropeptide receptor binding
histone threonine kinase activity
histone kinase activity (H3-T3 specific)
p.adjust
0.04
0.03
0.02
0.01
Count
10
20
30
40
50
E
Up-regulated genes
tost-1 mut vs wt, only 15°C (1540 genes)
nervous system development
neurogenesis
generation of neurons
neuron differentiation
plasma membrane bounded cell projection organization
cell projection organization
neuron development
cellular component morphogenesis
neuron projection development
axon development
cell part morphogenesis
cell projection morphogenesis
plasma membrane bounded cell projection morphogenesis
neuron projection morphogenesis
cell morphogenesis involved in neuron differentiation
axonogenesis
neuron projection guidance
axon guidance
cell adhesion
cytosolic ribosome
p.adjust
2.0e-10
1.5e-10
1.0e-10
5.0e-11
Count
40
60
80
100
F
tost-1 mut vs wt, 25°C
(2457)
Down-regulated genes,
FC >1, FDR < 0.01
1669
788
1600
tost-1 mut vs wt, 15°C
(2388)
G
wt 25°C vs 15°C
(4083)
1331
2752
905
tost-1 mut 25°C vs 15°C
(3657)
H
tost-1 mut vs wt, 25°C
(2457)
1894
563
342
tost-1 mut 25°C vs 15°C,
excluding wt 25°C vs 15°C
(905)
I
Down-regulated genes
tost-1 mut vs wt, only 25°C (1669 genes)
locomotion
double-stranded DNA binding
cell projection organization
nervous system development
transcription regulatory region nucleic acid binding
transcription cis-regulatory region binding
sequence-specific double-stranded DNA binding
RNA polymerase II transcription regulatory region sequence-specific DNA binding
plasma membrane bounded cell projection organization
DNA-binding transcription factor activity, RNA polymerase II-specific
neurogenesis
generation of neurons
neuron differentiation
supramolecular polymer
supramolecular fiber
cellular component morphogenesis
contractile fiber
myofibril
cilium organization
cilium assembly
p.adjust
8e-14
6e-14
4e-14
2e-14
Count
40
60
80
100
120
J
Down-regulated genes
tost-1 mut vs wt, 25°C and 15°C (788 genes)
catalytic activity, acting on a nucleic acid
ncRNA metabolic process
ncRNA processing
mRNA metabolic process
catalytic activity, acting on RNA
mRNA processing
cellular response to DNA damage stimulus
organelle fission
rRNA metabolic process
ribosome biogenesis
DNA repair
chromosome segregation
rRNA processing
nuclear chromosome segregation
chromatin organization
nucleic acid phosphodiester bond hydrolysis
RNA phosphodiester bond hydrolysis
RNA 3'-end processing
maturation of SSU-rRNA
RNA capping
p.adjust
0.003
0.002
0.001
Count
10
20
30
40
K
Down-regulated genes
tost-1 mut vs wt, only 15°C (1600 genes)
cell cycle process
chromosome
mitotic cell cycle
DNA metabolic process
mitotic cell cycle process
intracellular protein-containing complex
mRNA metabolic process
cellular response to DNA damage stimulus
regulation of cell cycle
chromosome organization
nucleoplasm
meiotic cell cycle
nuclear division
DNA repair
chromosome segregation
spliceosomal complex
ribonucleoprotein granule
cytoplasmic ribonucleoprotein granule
DNA replication
regulation of mitotic cell cycle
p.adjust
6e-12
4e-12
2e-12
Count
40
60
80
100
120

Figure R25 | Differentially expressed genes in *tost-1* mutants are involved in neurogenesis and in cell cycle regulation. A-C. Venn diagrams showing the overlap of the upregulated genes: (A) *tost-1(xf196 ts)* 25°C vs *wt* 25°C (Figure r24.C) *and tost-1(xf196 ts)* 15°C vs *wt* 15°C (Figure R24.D); (B) *wt* 25°C vs 15°C (Figure R24.A) and *tost-1(xf196 ts)* 25°C vs 15°C (Figure R24.B); (C) *tost-1(xf196 ts)* 25°C vs *wt* 25°C (Figure R24.C) and *tost-1(xf196 ts)* 25°C vs 15°C, excluding *wt* 25°C vs 15°C (Figure R25.B). D,E. Gene ontology (GO) analysis of (D) genes uniquely upregulated in *tost-1(xf196 ts)* 25°C vs *wt* 25°C (Figure R25.A) and (E) genes uniquely upregulated in *tost-1(xf196 ts)* 15°C vs *wt* 15°C (Figure R25.A). F-H. Venn diagrams showing the overlap of the downregulated genes: (A) *tost-1(xf196 ts)* 25°C vs wt 25°C (Figure R24.C) and *tost-1(xf196 ts)* 15°C vs *wt* 15°C (Figure R24.D); (B) *wt* 25°C vs 15°C (Figure R24.A) and *tost-1(xf196 ts)* 25°C vs 15°C (Figure R24.B); (C) *tost-1(xf196 ts)* 25°C vs *wt* 25°C (Figure R24.C) and *tost-1(xf196 ts)* 25°C vs 15°C, excluding *wt* 25°C vs 15°C (Figure R25.B). I-K. GO analysis of: (I) genes uniquely downregulated in *tost-1(xf196 ts)* 25°C vs *wt* 25°C (Figure R25.F), (J) overlapping genes down regulated in *tost-1(xf196 ts)* 25°C vs *wt* 25°C and *tost-1(xf196 ts)* 15°C vs *wt* 15°C (Figure R25.F), and (K) genes uniquely downregulated in *tost-1(xf196 ts)* 15°C vs *wt* 15°C (Figure R25.F). D,E,I-K. All GO terms are displayed for biological processes, molecular function and cellular components.

In conclusion, our findings demonstrate that *tost-1* mutant embryos exhibit disrupted gene expression at both 25°C and 15°C. The pathways involving the genes affected at each temperature differ evidently, aligning with the distinct phenotypes observed at each temperature. At 25°C, the differential expression likely reflects the lethality observed in these embryos, whereas at 15°C, it appears more directly influenced by the downregulation of histone mRNAs due to TOST-1 dysfunction.

Premature expression of zygotic transcripts in *tost-1* mutants

Analysing the 25% of the most highly expressed genes, as well as the upregulated and downregulated genes in *tost-1* mutants vs *wt* at 15°C (**Figure R24.D**), we compared these findings with available data on *C. elegans* maternal and embryonic transcript expression (Boeck et al., 2016)(**Figure R26.A**). We observed that the most highly expressed genes in *tost*-1 mutants corresponded to maternally-provided and early zygotic transcripts, characteristic of early embryonic stages, confirming that our dataset represents early embryos. In contrast, the upregulated genes in this dataset were enriched for transcripts typically expressed later in embryogenesis, while downregulated genes were enriched for maternal and early zygotic transcripts (**Figure R26.B**). This pattern suggests transcriptional dysregulation in *tost-1* mutants that may prematurely activate ZGA. This conclusion is consistent with the altered timing of transgene expression observed in *tost-1* mutants, as illustrated by earlier activation of the GFP*::H4 transgene in PETISCO- and histone-depleted embryos (**Figures R22, R23**). Similar findings have been reported in histone-depleted *Drosophila* embryos, where premature ZGA was characterized by upregulated zygotic transcripts and reduced maternal transcript levels (Chari et al., 2019).

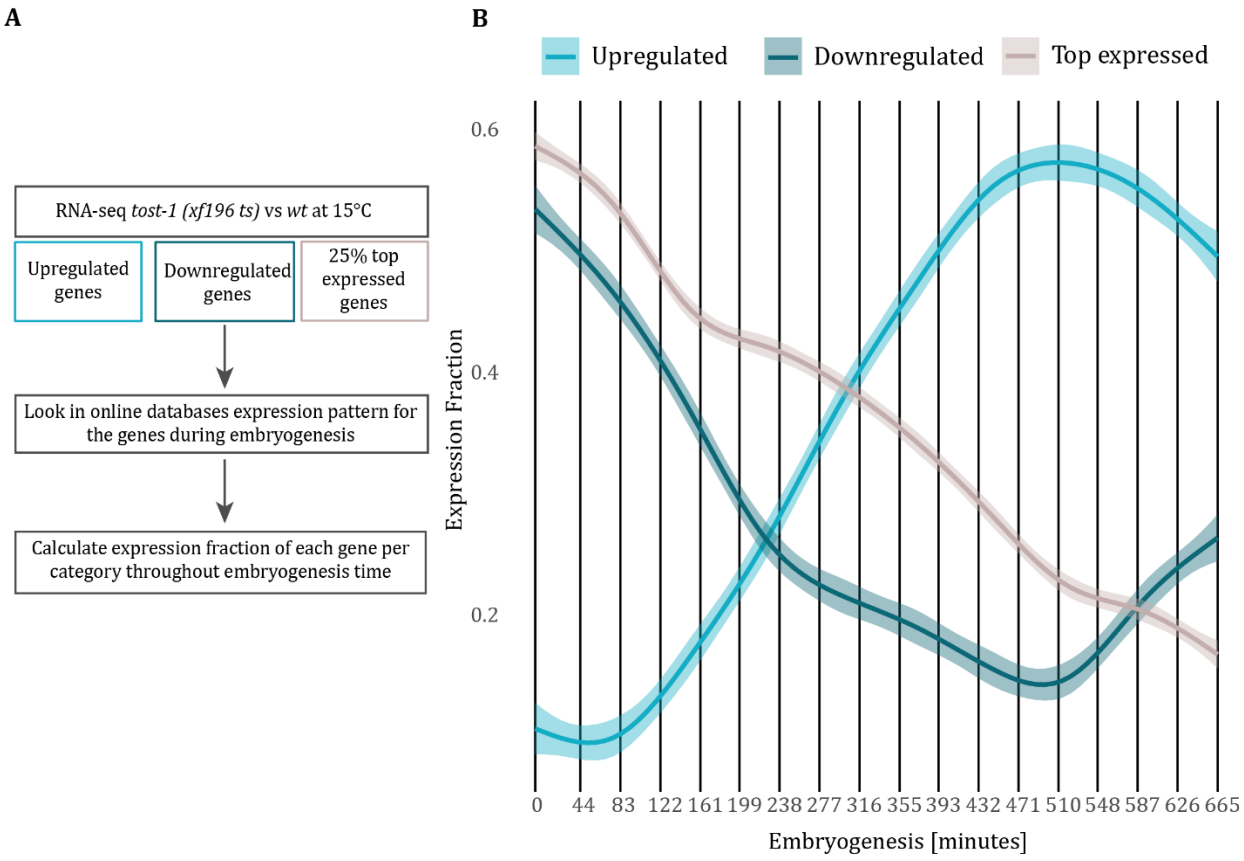

Figure R26 | *tost-1(xf196 ts)* mutants express prematurely zygotic transcripts at 15°C. A. Schematic representation explaining the data shown in B. B. Fraction of gene expression contributed by the top 25% most highly expressed genes, upregulated genes, and downregulated genes during embryogenesis in *tost-1(xf196 ts)* mutants vs *wt* at 15°C. Expression fractions are plotted across embryonic development, with time on the x-axis representing embryogenesis stages and the fraction of gene expression on the y-axis. The three curves represent the distribution of expression for each gene group during different stages of embryogenesis.

In conclusion, our findings suggest that the absence of PETISCO disrupts transcriptional regulation during early embryogenesis. PETISCO depletion results in phenotypes that mirror those of histone depletion, supporting the hypothesis that histone availability influences the timing and regulation of ZGA in *C. elegans* and that PETISCO regulates maternal histone mRNA levels. The transcriptional changes we observe in *tost-1* mutants likely arise from reduced histone maternal mRNA concentration in early embryos, leading to premature activation of zygotic genes and consequent developmental dysregulation.

Histone concentration regulates embryonic development

Our results indicate that PETISCO mutants have downregulated RD histone mRNAs, leading to arrested embryonic development in the progeny. We hypothesize that this impairment in development arises from the depletion of maternal histone mRNAs in the zygote, a resource essential for early embryonic divisions.

Genetic depletion of histones exacerbates the *tost-1 ts* phenotype

To investigate the effects of histone depletion further, we explored the impact of genetic reduction of histone mRNA abundance on *tost-1(xf196 ts)* mutant phenotype. Under standard conditions, the hypomorphic *tost-1(xf196 ts)* allele yields healthy and fertile animals at 15°C and 20°C, despite reduced RD histone mRNA levels. However, at 25°C, *tost-1(xf196 ts)* embryos display further reduced histone expression and experience embryonic arrest due to decreased functionality of TOST-1, ultimately leading to embryonic arrest.

To explore the dependency on maternal histone mRNA levels in embryonic development, we crossed the *tost-1(xf196 ts)* strain with a strain with the allele *ugeDf12*, which contains a large deletion on chromosome II encompassing 13 histone genes (*his-16, his-15, his-14, his-13, his-12, his-11, his-10, his-9, his-25, his-26, his-44, his-43, his-42*), and we evaluated their embryonic viability (**Figure R27**). While *ugeDf12* animals alone are fully fertile, the resulting double mutants *tost-1(xf196 ts);ugeDf12* exhibit a Mel phenotype at *tost-1(xf196 ts)* permissive temperatures (**Figure 27B**). This result suggests that a threshold of histone mRNA must be maintained in adults to support successful embryonic development. However, the expression of histone mRNAs was not quantified in these animals.

These findings collectively suggest that histone mRNA concentration plays a critical role in the progression of embryonic development in *C. elegans.*

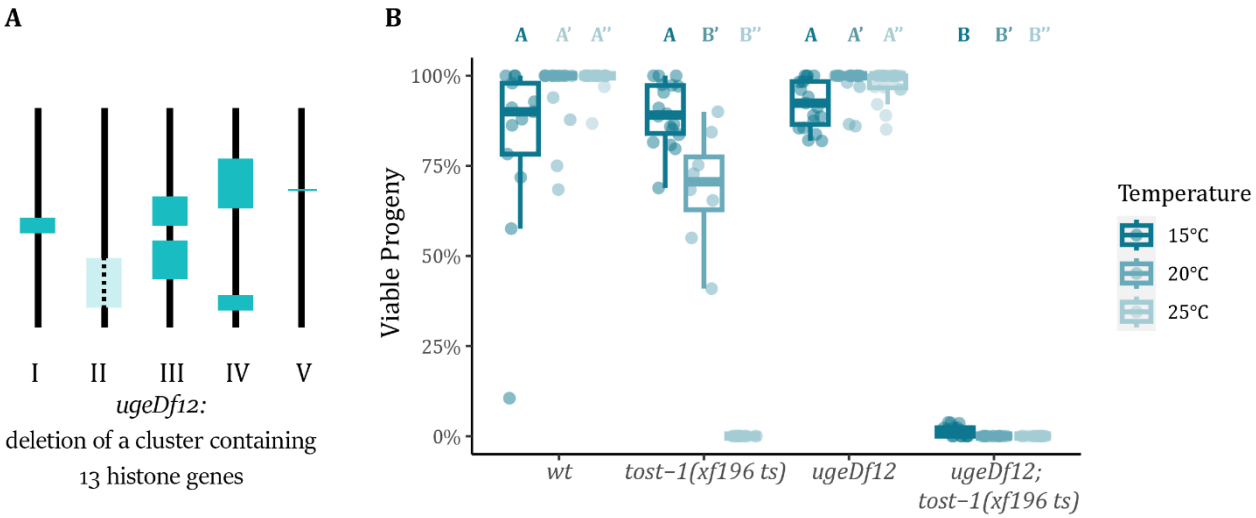

Figure R27 | Histone cluster deletion sensitizes *tost-1(xf196 ts)* embryos. A. Schematic illustration of histone gene clusters in the *C. elegans* genome and the *ugeDf12* deletion. B. Percentage of viable progeny from animals with the indicated genotype. Each data point represents an individual worm. P-values were calculated using the pairwise Dunn test (within each temperature condition) and adjusted with Holm–Bonferroni method, after failing the Shapiro-Wilk normality test. Different letters indicate p-value < 0.05.

Components of the histone mRNA degradation pathway are necessary for the PETISCO-related Mel phenotype

To further test if PETISCO-mediated stabilization of maternal histone mRNAs is critical for embryonic development, we investigated whether impairing histone mRNA degradation could alleviate the Mel phenotype in *tost-1* and other PETISCO mutants (**Figure R28**). We utilized mutant alleles for *cde-1*, *smg-2* and *eri-1* (Barstead et al., 2012; Page et al., 1999; Parry et al., 2007), which are homologs of key components of the histone mRNA degradation pathway in other species. Specifically, CDE-1 is the *C. elegans* homolog of human TUT7, which uridylates the stem-loop of RD histone mRNAs to mark them for degradation at the end of DNA replication (Lackey et al., 2016; van Wolfswinkel et al., 2009). SMG-2 is homologous to human UPF1, a factor that interacts with SLBP and recruits additional histone degradation machinery (Brooks et al., 2015; Kaygun & Marzluff, 2005; Page et al., 1999), while ERI-1 is the homolog of 3'hExo/ERI1, an exonuclease that cleaves the stem loop structure before degradation (Hoefig et al., 2012). Notably, while these proteins are well-characterized in other organisms, their roles in *C. elegans* histone mRNA regulation have not been previously established.

Our results indicate that loss of CDE-1 and SMG-2 rescues the embryonic development of *tost-1(xf196 ts)* mutants at the restrictive temperature of 25°C (**Figure R28.A**). To validate these findings, we generated new deletion alleles of *cde-1* and *smg-2* using CRISPR/Cas9-mediated

genome editing. Consistent with our initial observations, deletion of *smg-2* in the *tost-1(xf196 ts)* hypomorphic background allowed complete embryonic development, and deletion of *cde-1* rescued the Mel phenotype in the *tost-1(xf194)* null mutant background (**Figure R28.B**), supporting the idea that histone mRNA stabilization may rescue the PETISCO-related Mel phenotype. In contrast, *eri-1; tost-1(xf196 ts)* double mutants did not produce viable progeny at 25°C, and *smg-2* mutants did not rescue the *tost-1(xf194)* null Mel phenotype (data not quantified). Possibly, other exonucleases may initiate histone mRNA degradation, as previously suggested (Holmquist et al., 2022), and SMG-2 may play a relatively minor role in RD histone mRNA degradation. Furthermore, depletion of PUP-2, other poly(U) polymerase present in *C. elegans*, also did not rescue the *tost-1 ts* Mel phenotype at 25°C (data not quantified), suggesting a specificity for CDE-1/PUP-1 uridylation.

Furthermore, we found that *cde-1* deletion rescues embryonic development across other PETISCO mutants as well (**Figure R28.C**). However, this rescue effect is transient: the second generation of strains containing *cde-1* and PETISCO double mutations exhibit reduced viability in the case of *pid-3,* and *erh-2* mutants become again fully Mel in the second generation (**Figure R28.C**). This variability in rescue strength across different PETISCO mutants might suggest differential importance of PETISCO subunits in histone mRNA stabilization or reveal secondary effects related to PETISCO disruption. The relatively weaker rescue in *erh-2; cde-1* double mutants is particularly interesting, as ERH-2 is the most conserved PETISCO protein across eukaryotes. This suggests that ERH-2 is critically required for PETICO functions, whereas in other PETISCO mutants, some functionalities may remain intact, or ERH-2 has additional roles beyond PETISCO-related activities. However, alternative functions for ERH-2 in *C. elegans* have yet to be identified.

An additional consideration is that PETISCO mutants are defective in piRNA processing, which leads to failure in piRNA activity (Cordeiro Rodrigues et al., 2019; Zeng et al., 2019). Recent findings have shown that, in the absence of piRNAs, histone mRNAs can become targets of endo-siRNA/22G RNA, leading to their silence through a cumulative generational effect (Barucci et al., 2020; Reed et al., 2019). To test if endo-siRNAs accumulation was contributing to the gradual loss of viability in *cde-1;* PETISCO double mutants, we crossed *mut-7* mutant animals with *cde-1; tofu-6* double mutants and scored embryonic viability. However, we did not observe an improvement in viability (**Figure R28.D**), indicating that 22G RNAs targeting histones are not responsible for the weakened rescue effect over generations.

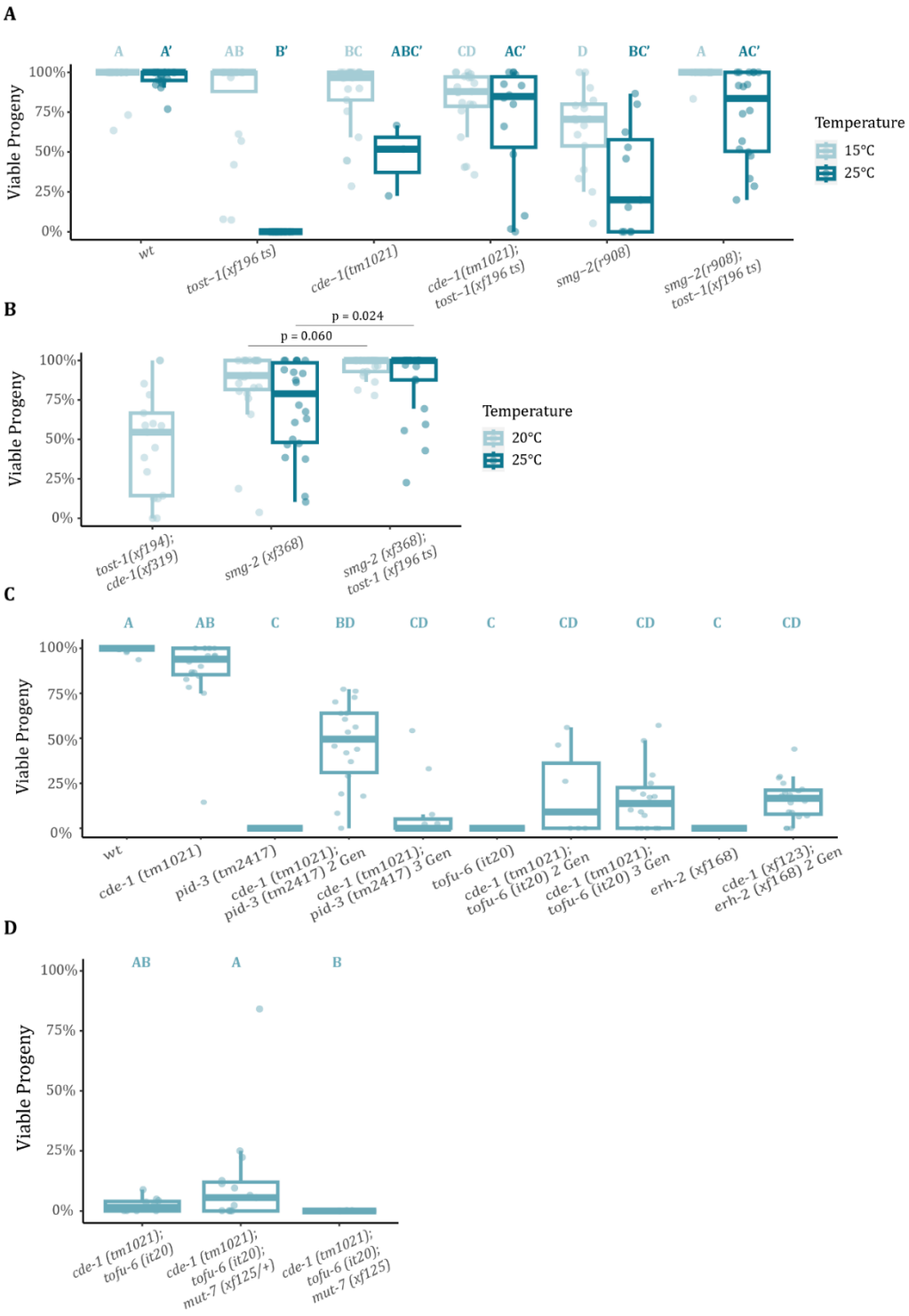

Figure R28 | Loss of CDE-1 and SMG-2 rescue *tost-1* mutant Mel phenotype. A-D. Percentage of viable progeny from animals with the indicated genotype. Strains were synchronized and cultured at the indicated temperature. Each data point represents an individual worm Pair wise comparisons are done only within each temperature. A,C,D. Pairwise comparisons were conducted only within each temperature group. P-values were calculated using the pairwise Dunn test and adjusted with Holm–Bonferroni method. Different letter indicate p-value < 0.05. B. P-values were calculated using the Wilcoxon test after testing for normality with Shapiro-Wilk test.

TOST-1 is required for histone mRNA expression in the adult germline but not in mixed embryos

To investigate whether loss of CDE-1 and SMG-2 rescues embryonic viability by preventing degradation of RD histone mRNA, we performed RT-qPCR to measure the relative expression of histone genes *his-65* and *his-66* in *tost-1(xf196 ts)* hypomorphic mutant and wild-type gravid adults (**Figure R29**). This analysis was conducted with animals grown at both permissive temperature (15°C), where *tost-1(xf196 ts)* mutant progeny remains viable despite RD histone mRNA depletion, and the restrictive temperature (25°C), where histone mRNA levels are more reduced (**Figure R7.B**), resulting in arrested embryogenesis. In this experiment, the depletion of *his-66* in *tost-1* mutant at 25°C is not more pronounced than at 15°C, as observed in previous experiments. This discrepancy may be attributed to technical issues, as wild-type samples, to which the other samples are normalized, exhibit high variation (**Figure R29**). Interestingly, we found that histone expression in *cde-1* mutants was reduced to similar levels as *tost-1(xf196 ts)* mutants at 15°C, with even greater reduction at 25°C. In *cde-1(tm1021);tost-1(xf196 ts)* double mutants, histone expression was not restored at 25°C. At 15°C, the biological replicates showed considerable variation, preventing any definitive conclusions.

In contrast *smg-2(r908);tost-1(xf196 ts)* double mutant showed a slight increase in histone expression, although it remains unclear if this increase is biologically significant or sufficient to explain the partial rescue of embryonic arrest. Furthermore, it is important to note that histone mRNAs in gravid adults represent a mix of maternal transcripts present in the germline and embryonic transcripts from developing embryos within the worm. Additionally, *cde-1* mutants are known to have germline defects and are sterile at 25°C (Y. Li & Maine, 2018), which may explain reduced histone expression in *cde-1* mutants since there are no embryos undergoing cell division.

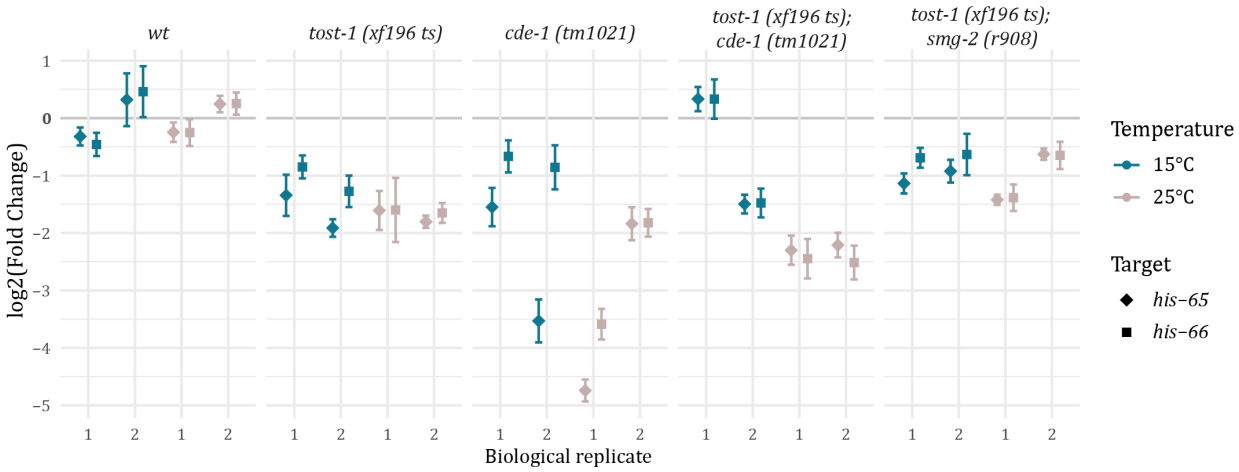

Figure R29 | Expression of histone mRNAs in gravid adults upon loss of CDE-1 and SMG-2. Quantitative RT-PCR of *his-65* (H2A) and *his-66 (*H2B) expression in *wild type* (*wt*), *tost-1(xf196 ts)*, *cde-1(tm1021), tost-1(xf196 ts); cde-1(tm1021),* and *tost-1(xf196 ts);smg-2(r908)* gravid adults cultured at 15°C or 25°C. The reference gene *pmp-3* was used for normalisation. Each sample represents a biological replicate, with three technical replicates per sample, and standard deviation was calculated from these replicates. Fold change was calculated relative to the average of the two biological replicates of the *wt* strain at the respective temperature.

To distinguish maternal histone mRNAs from zygotic expression, we analysed histone mRNA levels in young adults and embryos separately. Young adults, which have completed gametogenesis without yet fertilizing oocytes, were used to approximate maternal mRNA levels. We analysed histone expression at 15°C, 20°C, and 25°C across both *tost-1* mutants, *cde-1* mutants, and *tost-1; cde-1* double mutants, and additionally in *tost-1; pid-1* double mutants (**Figure R30, R31**).

In young adults at 15°C, *tost-1(xf196 ts)* mutant displayed histone mRNA depletion with a fold change reduction of 2 to 4, which was further amplified to a 4- to 16-fold reduction at 25°C (**Figure R30**), consistent with the previous results in gravid adults (**Figure R7**). Similarly, *tost-1(xf194)* null mutant showed reduced histones expression in young adults (**Figure R30.B**). In *cde-1* mutants, histone expression was unaffected at 15°C (**Figure R30.A**) but showed progressive reduction at elevated temperatures (**Figure R30.B, C**), likely due to germline defects in these animals. For the same reason, histone expression in *tost-1(xf196 ts);cde-1(tm1021)* and *tost-1(xf194);cde-1(xf319)* double mutants was reduced to levels similar to the single *tost-1* mutants (**Figure R30.B, C**). Interestingly, at 15°C, where *cde-1* mutants have fewer germline defects and remain fertile, *tost-1(xf196 ts); cde-1(tm1021)* double mutants appeared to restore histone expression to wild-type levels (**Figure R31.A**). However, similar experiment in *smg-2* mutants, which do not exhibit severe fertility defects like *cde-1* mutants, are needed to confirm

that reestablishment of maternal histone mRNA levels are associated with rescue of the viability of *tost-1* mutant embryos.

Additionally, we examined histone expression in *tost-1(xf196 ts); pid-1(xf35)* double mutants due to a slight increase in progeny viability observed in these animals (**Figure R6**). We observed as increase of histone expression in young adults across 15°C, 20°C and 25°C in *tost-1(xf196 ts); pid-1(xf35)* double mutants (**Figure R30**). However, the expression levels at 20°C and 25°C did not reach wild-type values, which aligns with the modest improvement progeny viability (**Figure R6**). We hypothesize that, in the presence of a hypomorphic TOST-1, the loss of PID-1 allows more free PETISCO to compensate for the partially functional TOST-1.

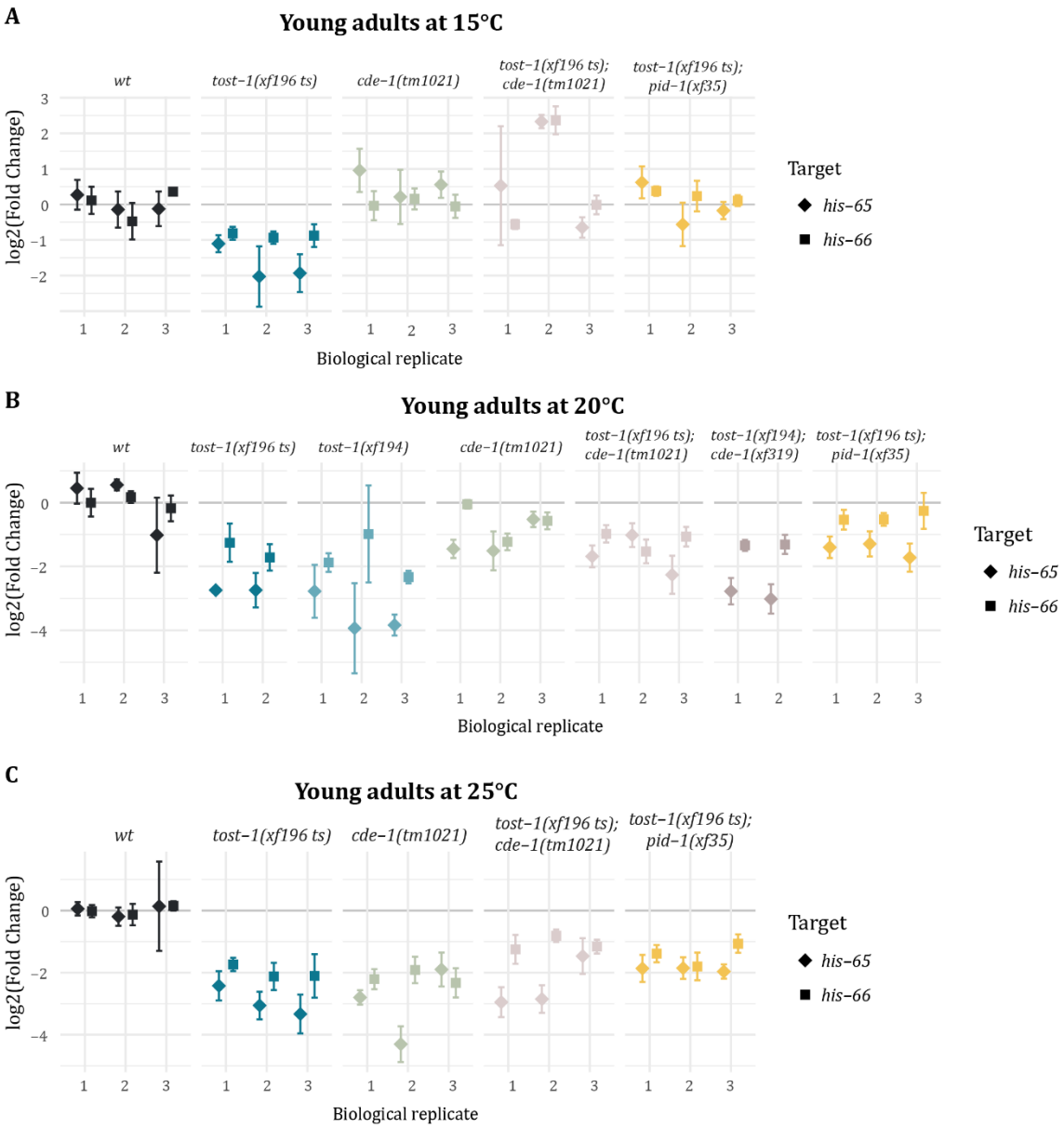

Figure R30 | Expression of histone mRNAs in embryos upon loss of CDE-1. A-C. Quantitative RT-PCR of *his-65* (H2A) and *his-66* (H2B) expression in *wild-type (wt), tost-1(xf196 ts), tost-1(xf194), cde-1(tm1021), tost-1(xf196 ts);cde-1(tm1021),* and *tost-1(xf196 ts); pid-1(xf35)* embryos obtained from adults cultured at 15°C (A), 20°C (B) and 25°C (D). The reference gene *pmp-3* was used for normalisation. Each sample represents a biological replicate, with three technical replicates per sample, and standard deviation was calculated from these replicates. Fold change was calculated relative to the average of the three biological replicates of the *wt* strain.

By examining the expression levels of histone mRNAs in embryos, we found that they differed notably from those in young adults. It is important to note that the embryo samples include both pre- and post- ZGA embryos. Interestingly, histone expression in *tost-1* mutant embryos was near wild-type levels at 15°C and 20°C in the hypomorphic mutant, *tost-1(xf196 ts)*, and only slightly

reduced in the null mutant, *tost-1(xf194)* (**Figure R31.A, B**). At 25°C, histone mRNA expression was reduced 2- to 4-fold in *tost-1* mutant embryos, compared to 4- to 16-fold in young adults (**Figure R30.C, R31.C**). This discrepancy suggests that zygotically transcribed histones mRNAs in embryos may partially compensate for maternally depleted histones levels, further supporting our hypothesis that PETISCO predominantly functions in stabilizing maternal histone mRNAs.

Notably, histone mRNAs were upregulated in *cde-1* mutant embryos, potentially due to impaired degradation of histone mRNAs (**Figure R31.A, B**). At 25°C, *cde-1* mutant adults were sterile, so we could not assess histone expression in the embryos at this temperature. Furthermore, in *cde-1;tost-1* double mutant embryos, both hypomorphic, *(xf196 ts),* and null, *(xf194),* backgrounds, histone expression approached wild-type levels, indicating that both CDE-1 and TOST-1 contribute to balanced histone expression in embryos. Conversely, the *tost-1* mutation rescues the sterility of *cde-1* mutants at 25°C, potentially by reducing the excess of histone mRNAs that may exist in cde-1 mutants.

Lastly, histone mRNA expression in *pid-1;tost-1* double mutant embryos were variable across temperatures, with a slight upregulation at 15°C that may be due to increased PETISCO availability, but stronger depletion that *tost-1* single mutants at 20°C and 25°C (**Figure R31**). This surprising result may suggest a potential role for piRNAs in regulating zygotic histone mRNAs. Alternatively, it could reflect a general alteration in gene expression in the germline caused by piRNA defects, which might influence the reference gene used in the experiment.

In conclusion, our findings suggest that TOST-1 is required to stabilize histone mRNAs in the adult gonad, allowing sufficient maternal histone mRNA deposition for early embryogenesis. By contrast, its function in the embryo itself, particularly regarding zygotically expressed histone mRNAs, appears to be less significant. However, further experiments focusing on embryos prior to ZGA are needed to substantiate these findings.

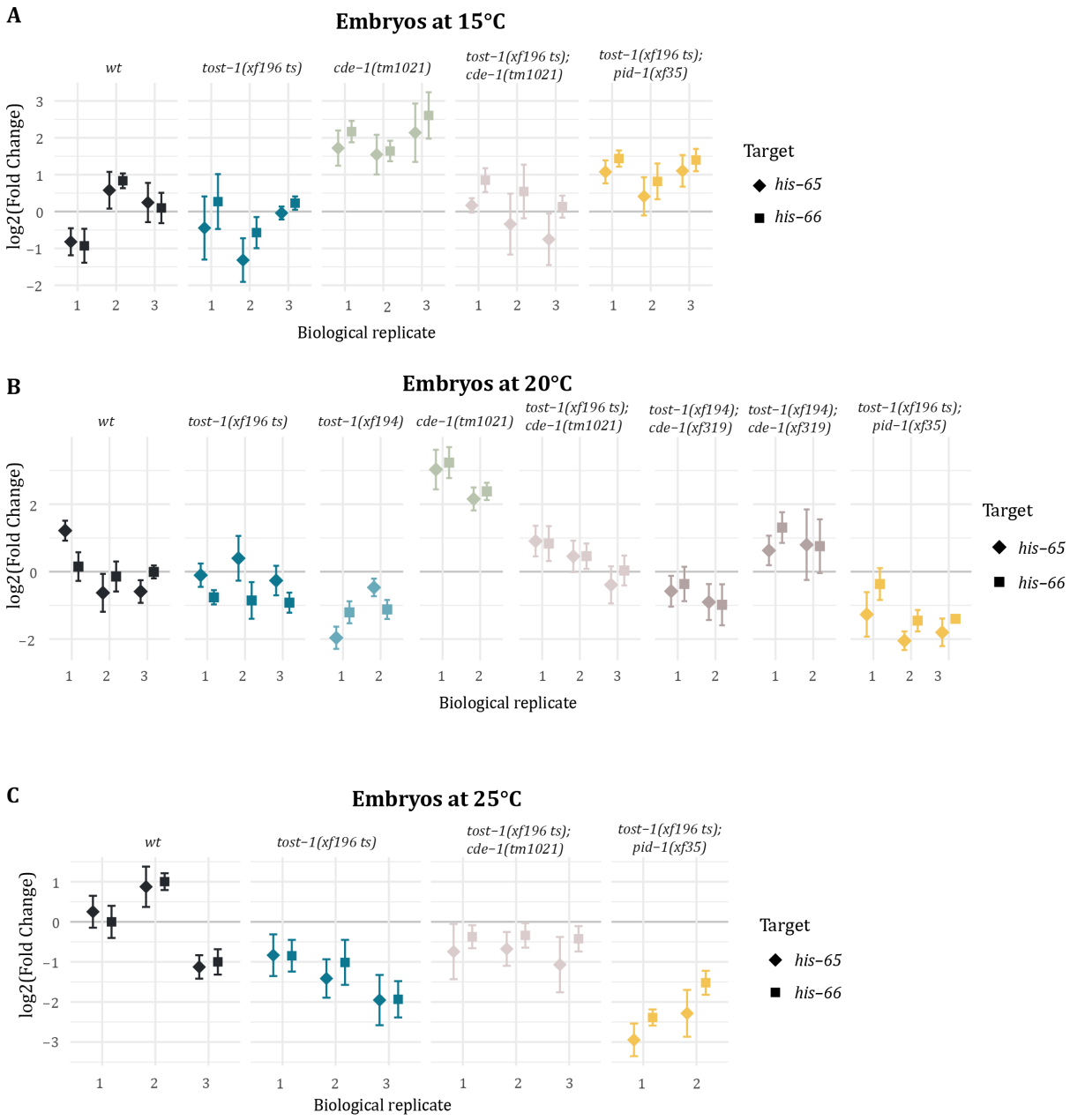

Figure R31 | Expression of histone mRNAs in young adults upon loss of CDE-1. A-C. Quantitative RT-PCR of *his-65* (H2A) and *his-66* (H2B) expression in *wild-type (wt), tost-1(xf196 ts), tost-1(xf194), cde-1(tm1021), tost-1(xf196 ts);cde-1(tm1021),* and *tost-1(xf196 ts); pid-1(xf35)* young adults cultured at 15°C (A), 20°C (B) and 25°C (D). The gene *pmp-3* was used as reference gene. Each sample represents a biological replicate and each one was used in three technical replicates and used for standard deviation. The fold change was done using the average of the three biological replicates of the wt strain.

Loss of CDE-1 does not rescue the premature expression of *xfSi268*

To determine whether removing CDE-1 could restore transgene *xfSi268* expression to wild-type levels in the *tost-1* mutant background, we examined GFP*::H4 expression in embryos (**Figure R32**). As described previously, embryos were categorized into four stages based on cell number, and we measured their nuclear areas to confirm accurate staging (**Figure R32.A**). We quantified the mean GFP intensity in three nuclei per embryo across *cde-1* and *tost-1* mutant strains and found that, at both 15°C and 20°C, GFP*::H4 was silenced during in the first stage withi all strains. However from stage 3 (13 to 20 cells), the GFP*::H4 expression was stronger in *cde-1* mutants, similarly to *tost-1* mutants (**Figure R32.B-E**). Given that histone mRNA levels are higher in *cde-1* mutants (**Figure R29**), this elevated mRNA likely contributes to the stronger GFP*::H4 expression observed in these embryos. Conversely, in *tost-1(xf196 ts)* mutants, the depletion of maternal histone mRNAs may induce premature ZGA, leading to earlier and stronger GFP*::H4 expression in these mutants compared to wild-type embryos at equivalent stages.

These two effects, resulting from *cde-1* or *tost-1* depletion, are likely additive at 20°C, in stage 3, where *cde-1; tost-1; xfSi268* embryos show the highest GFP*::H4 expression (**Figure R32.D, E**). Although this additive effect may seem counterintuitive given the rescue of histone mRNA levels in *cde-1* and *tost-1* mutants, we interpret these results as indicating that both proteins influence histone mRNA regulation through distinct mechanisms. These effects likely impact transgene expression by modulating ZGA timing and cell cycle progression.

Interpretation of results at stage 4 is challenging, as this stage includes embryos with no upper cell number limit, potentially introducing variability from later-stage embryos across different strains.

In conclusion, the loss of CDE-1 does not restore GFP*::H4 expression to wild-type levels in *tost-1* mutants. Instead, it has an additive effect, likely due to the lack of degradation of the transgenic histone mRNA.

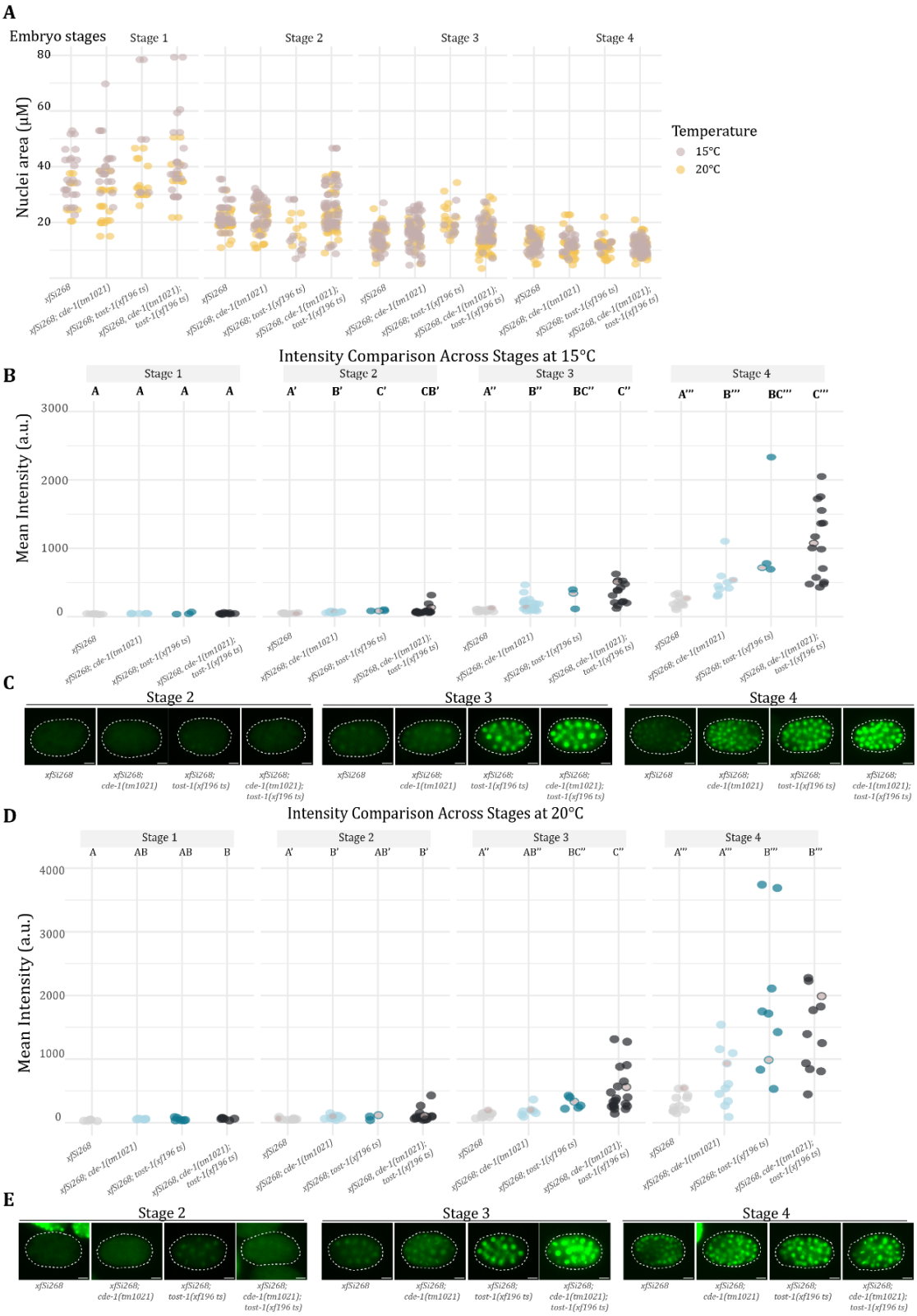

Figure R32 | GFP*::H2A expression in *tost-1* mutants upon CDE-1 depletion across different embryonic stages and different temperatures. A. Nuclei area of each nucleus used for quantification in B and D of dissected embryos from the indicated genotypes. Embryos were divided into stages based on their cell number. B, D. Quantification of the average

mean intensity of GFP*::H2A expression in the 2 to 3 nuclei analysed per embryo for the different strains at 15°C (B) and 20°C (D). Each dot represents one embryo. C, E. Representative images showing GFP*::H2A expression of the indicated embryos. Dashed lines outline the embryo based on the brightfield images (not shown). Pairwise comparisons are performed only within each stage. P-values were calculated using pairwise Dunn test, with Holm–Bonferroni correction. Different letters indicate p-value < 0.05. Scale bars = 20 μm.

A forward-genetic screen identifies new suppressors of *tost-1* mutants' lethality

To identify novel candidates involved in the embryonic arrest of offspring of *tost-1* mutants, we performed a forward genetic screening using ethyl methanesulfonate (EMS) mutagenesis (**Figure R33**). We mutagenized L4 larvae of the *tost-1 (xf196 ts)* mutant strain and collected 1100 F1 individuals from 40 plates with the mutagenized P0 worms. These F1 individuals were allowed to produce F2 progeny, which were subsequently tested for mutations that could revert the Mel phenotype of *tost-1(xf196 ts)* hypomorphic mutants at the restrictive temperature of 25°C. To screen for viable progeny at this temperature, we assessed the fertility of F2 individuals by selecting those that produced healthy F3 offspring. This viability was confirmed for an additional generation at 25°C to ensure stable suppression of the Mel phenotype. From the initial 852 plates with F3 progeny, 93 plates yielded viable F4 offspring, which were again confirmed to be viable at 25°C. Among these, only 26 clonal populations had viable offspring at 25°C and were selected for further analysis of the suppressors.

To confirm retention of the *tost-1(xf196 ts)* mutant allele in these new mutants, we performed Sanger-sequencing of the *tost-1* gene. Each new mutant strain was subsequently backcrossed twice with the original *tost-1* hypomorphic mutant strain to partially eliminate non-contributory mutations. The F2 individuals were assessed for viability at 25°C, and this phenotype was confirmed in an additional generation at the same temperature to minimize the possibility of false positives. Ultimately, we obtained 21 mutant alleles that consistently rescued the *tost-1(xf196 ts)* Mel phenotype at 25°C (**Figure R33**).

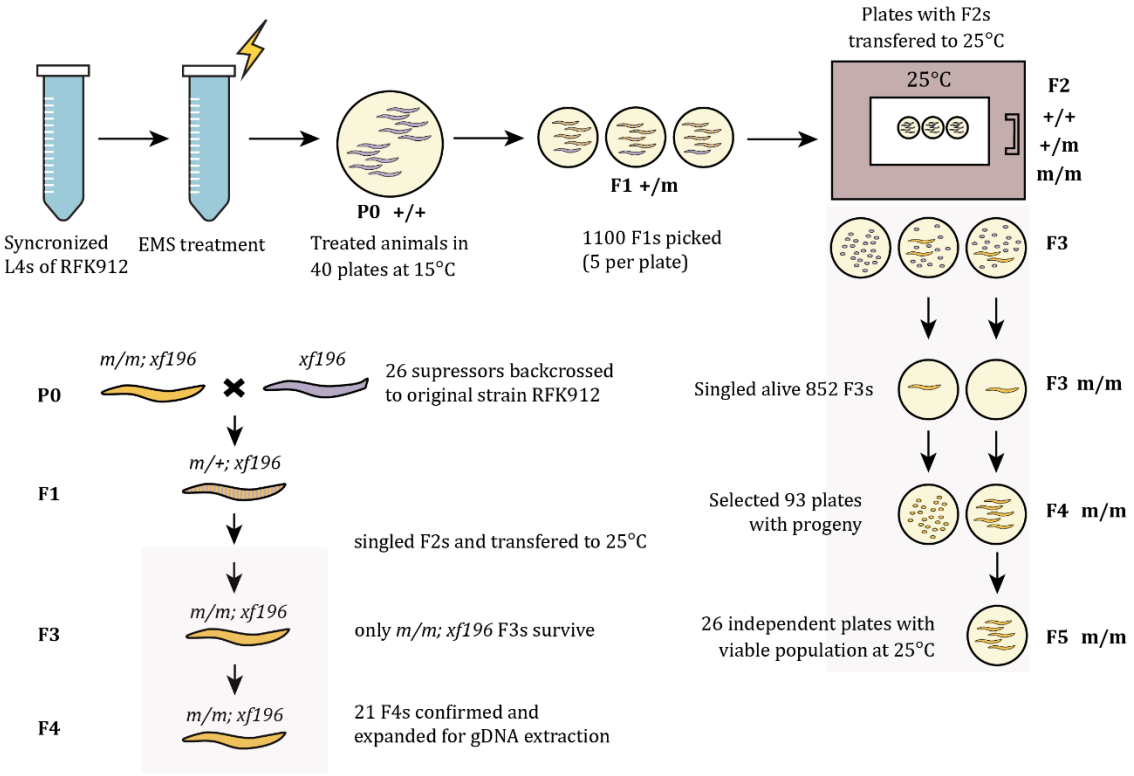

Figure R33 | EMS mutagenesis schematic illustration. Synchronized L4s of RFK912 *tost-1(xf196 ts)* were treated with EMS at a final concentration of 47mM at 20°C for four hours. Following EMS treatment, the worms were plated onto 40 NGM plates and incubated at 15°C. After five days, 1100 F1s larvae at the L4 stage were picked, five larvae placed on each plate and transferred to 25°C. After five additional days, the plates were screened for F3 survivors (homozygous for the suppressing mutation, m/m). A total of 852 F3 individuals were singled and maintained at 25°C for two subsequent generations, selecting the survival worms each generation. From this, 26 final suppressor strains with viable progeny at 25°C were identified and backcrossed with the original RFK912 strain. Worms were phenotyped for survival at 25°C, and after confirmation, 21 strains were expanded and sent for whole genome sequencing.

Identification of novel suppressors

The 21 suppressor strains were sequenced, with the initial mutagenized strain *tost-1(xf196 ts)* used as the reference genome. Variants identified in the sequenced strains were quantified and mapped, revealing that single nucleotide polymorphisms (SNPs) are the predominant variant type across the different strains (**Figure R34.A**). The mutagenic agent EMS introduces mutations by modifying guanine to O^6-ethylguanine, which then pairs with thymine instead of cytosine, producing a characteristic G/C-to-A/T transition bias in the induced mutations (Greene et al., 2003). Consistent with this mechanism, the majority of SNP transitions we identified were C-to-T (**Figure R34.B**).

To locate the chromosome carrying the suppressor mutation responsible for the phenotype, we analysed the distribution of all expected SNPs across the six chromosomes (**Figure**

R34.C). In some strains, such as strain 1, 11, and 16, a high number of SNPs were detected, complicating the identification of the chromosome containing the suppressor mutation.

Further analysis of variant overlap across strains identified different mutations in recurrent genes potentially involved in RD histone mRNA regulation. We identified three different variants in the *smg-1* gene, four variants in *C14C10.5,* and a 96-nt deletion in *smg-3* (**Figure R34.D**).

SMG-1 is a phosphatidylinositol kinase-related protein kinase essential for SMG-2 phosphorylation in the NMD pathway (Grimson et al., 2004). SMG-3 (*C. elegans* orthologue of Upf2) contains a MIF4G domain and together with SMG-4 (Upf3 orthologue), is required for SMG-1-dependent SMG-2 phosphorylation (Page et al., 1999). These proteins function in the NMD pathway, marking mRNAs with premature termination codons for decay (Johns et al., 2007). Although Upf2 and Upf3 are not associated with RD histone mRNA degradation (a process involving Upf1/SMG-2 in metazoans) (Choe et al., 2014), recent studies in *Aspergillus nidulans*, suggest their involvement in histone mRNA regulation (Mossanen-Parsi et al., 2021). In fungi, histone mRNAs are cell-cycle regulated and are modified by uridylation upon DNA replication inhibition, similar to processes in metazoans (Mossanen-Parsi et al., 2021), although fungal histone transcripts are adenylated rather than containing the stem-loop structure.

The other identified suppressor gene, *C14C10.5*, is the ortholog of the human *Psme4* gene, which codes for the Proteasome activator complex subunit 4 (PA200 in humans, Blm10 in yeast). PA200 specifically recognizes acetylated histones, facilitating ubiquitin-independent degradation of core histones during spermatogenesis and in response to DNA damage (Qian et al., 2013). This result suggests that the Mel phenotype of *tost-1* mutants can be rescued by modulating histones at the protein level.

A

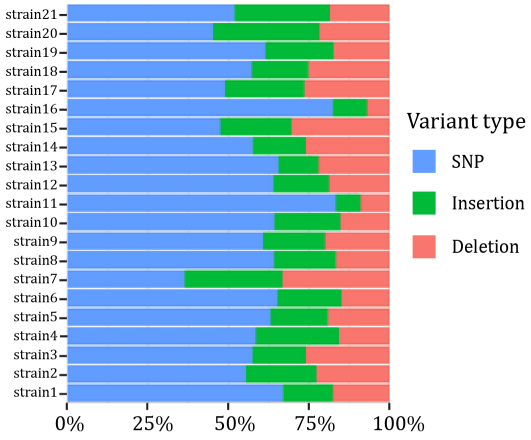

B

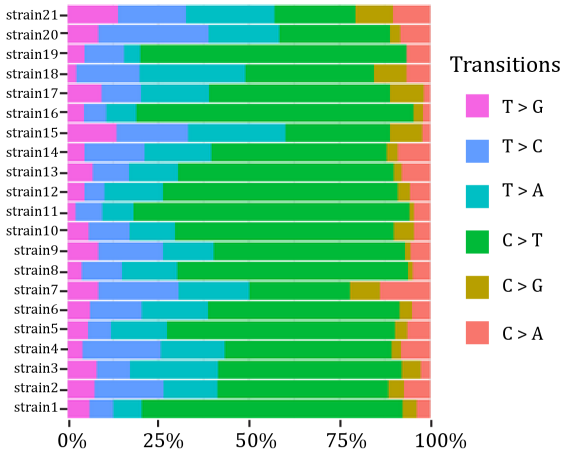

C

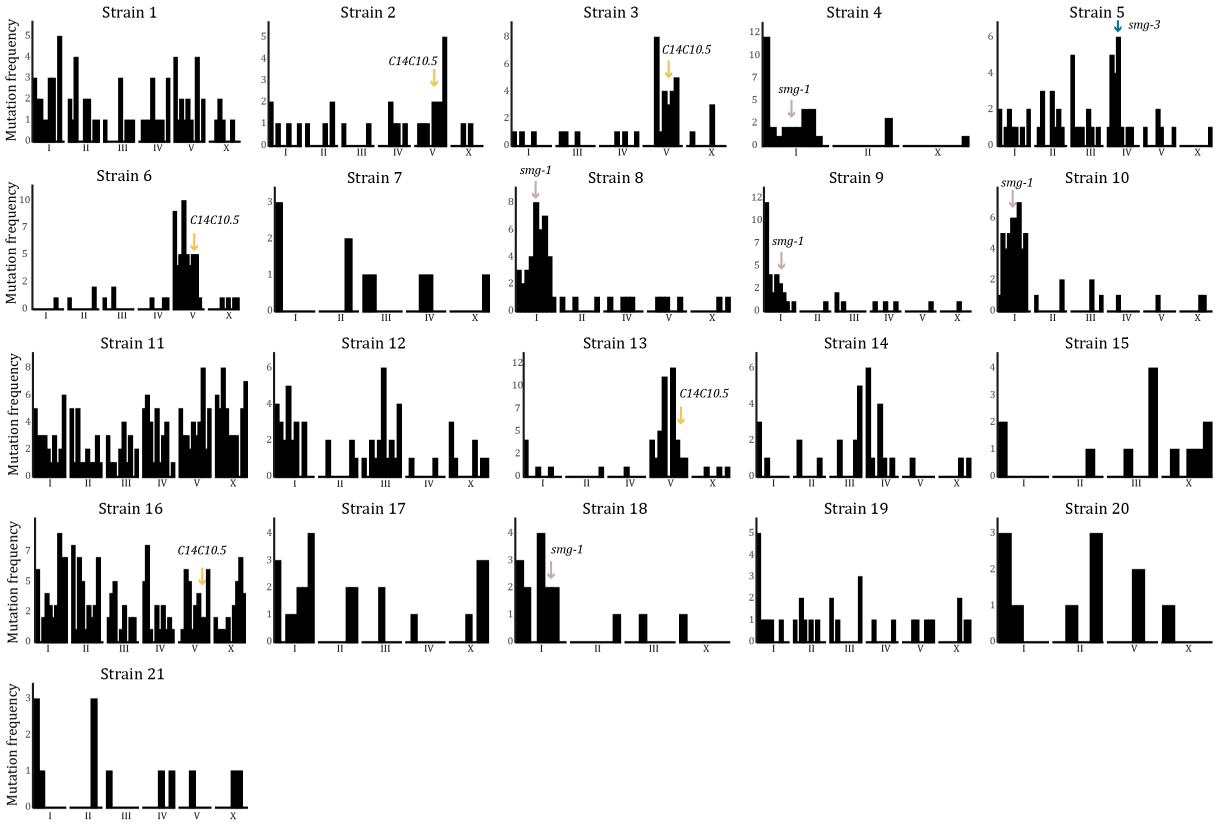

D

Gene	LG	Position	Mutation	Variant	Strain
smg-1	I	6908080	splicing	2891C>T	4
smg-1	I	6905781	missense	E1491K	8, 9, 10
smg-1	I	6902942	missense	G2017E	18
C14C10.5	V	12604120	nonsense	Q1038*	2, 3
C14C10.5	V	12602905	nonsense	Q799*	13
C14C10.5	V	12600666	missense	P84S	16
C14C10.5	V	12601030	missense	G205E	6
smg-3	IV	6365644	deletion	Q1049_E1081del	5

Figure R34 | EMS sequencing results. A. Distribution of variant types, including single nucleotide polymorphisms (SNPs), insertions, and deletions, after filtering for the original strain. B. Distribution of single nucleotide variant transitions. C. Expected SNPs (G/C-to-A/T) distribution across chromosomes in each sequenced strain. Chromosomes were divided into 10 bins. Candidate suppressors are identified in the respective graphs. D. Summary of candidate suppressor genes based on the identification of multiple alleles in independent strains and known protein interactors.

Verification of EMS hits by CRISPR/Cas9-mediated genome editing

In *smg-1*, we identified a SNP in the 5'splice acceptor of the exon 18, likely resulting in a frameshift or truncated protein. Additionally, we found two SNPs within the protein domains: one in the FAT domain and another in the PI3K catalytic domain (**Figure R34.D and R35.A**), both of which may impair the catalytic activity of SMG-1. For *C14C10.5*, we identified two SNPs introducing premature stop codons and two SNPs causing missense mutations in exon 2, corresponding to uncharacterized region of the protein (**Figure R34.D and R35.B**). Lastly, a variant in *smg-3* was predicted to truncate the protein just before its disordered C-terminal region (**Figure R34.D and R35.C**).

To confirm that these mutations in *smg-1, smg-3,* and *C14C10.5* were responsible for suppressing the *tost-1(xf196 ts)* Mel phenotype, we generated targeted deletions of these genes using CRISPR/Cas9-genome editing and performed viability assays in *tost-1(xf196 ts)* mutant background at 25°C. Loss of SMG-1 (alleles *xf369* and *xf370*) and SMG-3 (allele *xf391*) restored progeny viability of *tost-1* mutants at 25°C (**Figure R35.D**). In contrast, a deletion in the first exon of *C14C10.5* (allele *xf371*) did not rescue the embryonic lethality at 25°C (**Figure R35.D**). We then generated additional *C14C10.5* deletions: one strain was generated directly in *tost-1(xf196 ts)* mutant background, and another in a wild-type background that was later crossed with *tost-1(xf196 ts)* strain. In both cases, progeny viability was restored (**Figure R35.E**).

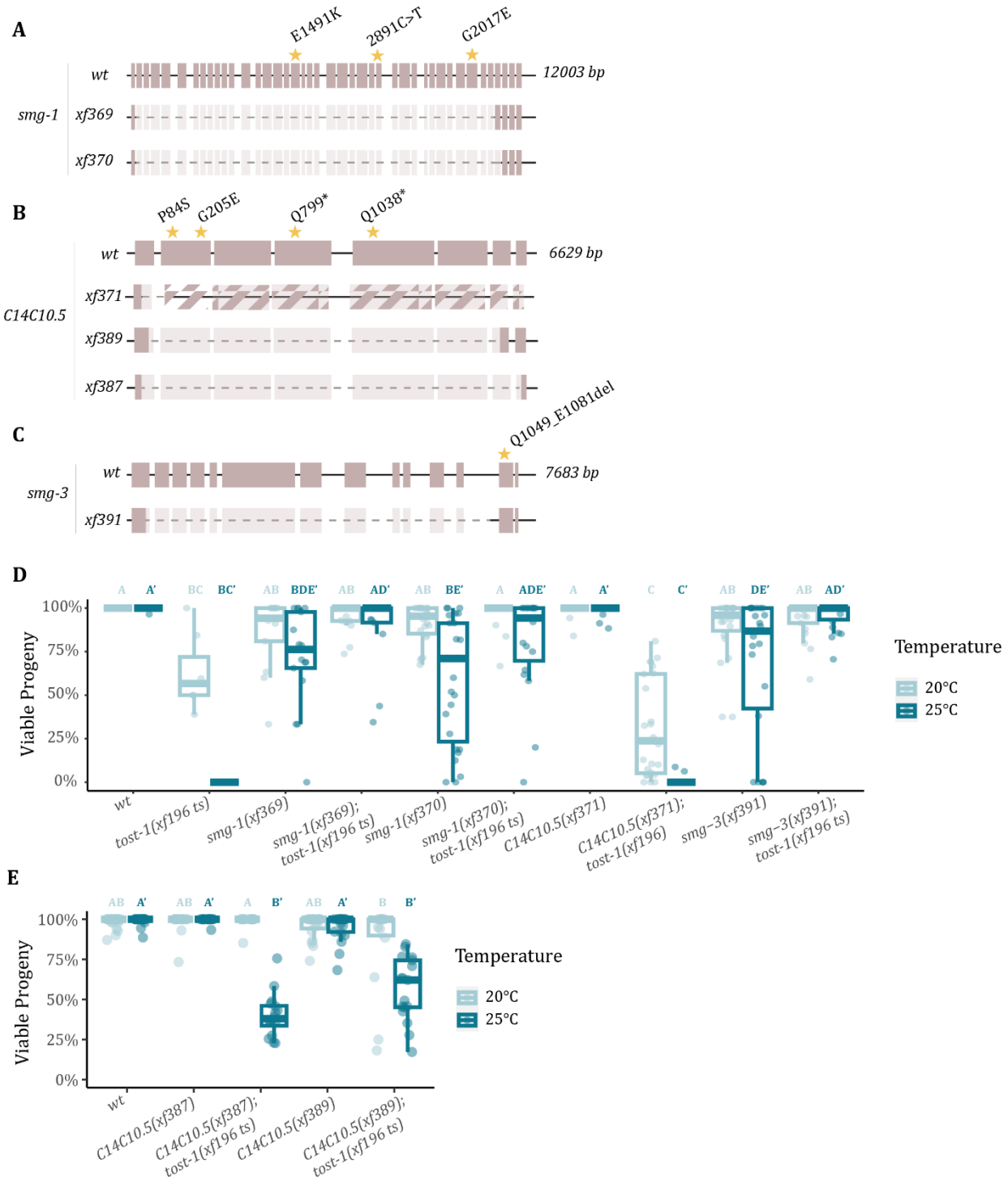

Figure R35 | Depletion of SMG-1, SMG-3 and C14C10.5 rescue *tost-1* Mel phenotype. A-C. Schematic representation of gene deletions for (A) *smg-1*, (B) *C14C10.5,* and (C) *smg-3,* generated by CRISPR/Cas9-mediated genome editing. Stars indicate point mutations identified in the EMS screen. Light pink highlights the deleted sequences, and patterned pink indicates potential frameshift mutations in the protein. D, E. Percentage of viable progeny from animals with the indicated genotype. Strains were synchronized and cultured at the indicated temperature. Pairwise comparisons were performed within each temperature. P-values were calculated using the pairwise Dunn test, with Holm–Bonferroni adjustment for multiple comparisons. Different letters indicate p-values < 0.05.

These findings indicate that components of the NMD pathway, such as SMG-1 and SMG-3, may play a role in histone mRNA degradation in *C. elegans*, differing from what is known in mammals. Additionally, these results suggest that precise regulation of both histones mRNA, via SMG-1 and SMG-3, and protein levels, via C14C10, is essential for embryonic development in *C. elegans*. This evidence supports our hypothesis that PETISCO is required in the regulatory pathway governing histone levels in early embryos.

Identification of potential novel interactors of TOST-1

TOST-1 is currently known to interact only with other PETISCO components. To better understand how PETISCO and TOST-1 selectively bind and regulate histone mRNAs, we aimed to identify additional proteins that may interact with TOST-1 that might help elucidate its role in histone mRNA regulation.

Quantitative proteomics of TOST-1 reveals transcription and translation regulators

To uncover novel interactors, we performed immunoprecipitation 2xFLAG::TOST-1 from embryo extracts, followed by label-free quantitative mass spectrometry. This approach identified 73 co-enriched proteins, with PETISCO components being the most highly enriched as expected. Additionally, we identified several proteins involved in transcription and translation (**Figure R36.A**). Among transcription-related interactors, we detected components of the Integrator complex, specifically INTS-3, INTS-6, INTS-2, INTS-7, and INTS-1, as well as Integrator-interacting proteins SPT-4 and NABP-1 (Pfleiderer & Galej, 2021). The Integrator complex, composed of 15 subunits (13 identified in *C. elegans)*, associates with paused RNA Pol II at the promoter-proximal sites, preventing productive elongation. In this process, the transcription factor complex DSIF, comprising SPT4 and SPT5, also plays a role, as DSIF phosphorylation is required for RNA Pol II to enter productive elongation (Decker, 2021). Integrator-PP2A phosphatase activity, on the other hand, prevents pause release and promotes transcription termination (Huang et al., 2020). NABP-1, a member of the SOSS complex involved in DNA damage repair, is also known to interact with Integrator subunits INTS3 and INTS6 in other organisms (Gromak, 2023).

We also observed enrichment of eukaryotic translation initiation factors (eIFs) involved in the 43S pre-initiation complex (PIC), including eIF2 subunits α/β/γ and eIF3c. The PIC associates with mRNA via the eIF4F complex to initiate translation (Hinnebusch, 2017). Notably, certain

eIF3 subunits have been reported to bind a stem-loop structure within histone H4 mRNA, potentially linking TOST-1 to specific translation initiation steps for histone mRNAs (Hayek et al., 2021).

Additionally, several proteins involved in ribosome biogenesis within the nucleolus were enriched, including MRPS-5, NUCL-1, NOLA-3, NOL-56/58 and F53F4.11. Other interactors included transcription-related factors, such as the Mediator subunit MDT-10; splicing factors, such as CYN-10 and SNU-66; transcription termination factors, including FIPP-1, NRD-1 and CPSF-4; 3' end processing regulators, such as SUP-46 and TAG-153; and SMG-4, a component of the NMD pathway, required for the function of SMG-2. Lastly, proteins involved in DNA repair (MSH-6), and molecular transport (NRF-5 and GLB-1) were identified.

Based on these findings, we hypothesized that TOST-1 may function within the nucleus and participate in various aspects of histone mRNA regulation, potentially influencing transcription, translation, and mRNA decay.

TOST-1 does not co-precipitate with INTS-6

In metazoans, the Integrator complex is essential for transcription termination of snRNA genes, and recent studies have identified its role in terminating piRNA transcripts in *C. elegans*. Given the parallels between piRNA precursors and histone mRNAs and their relationship with PETISCO, we hypothesized that PETISCO, via TOST-1, might also facilitate histone mRNA transcription termination through the Integrator complex.

To validate the potential interaction suggested by our mass spectrometry data, we conducted immunoprecipitation (IP) experiments in embryos expressing INTS-6::GFP::FLAG to test if 2xFLAG::TOST-1 would co-precipitate with INTS-6::GFP::FLAG (**Figure R36.B**). For this pull-down, we used two sets of GFP-coupled beads (A and B). Although INTS-6::GFP::FLAG was successfully detected in the IP by western-blot, we did not detect co-enrichment of 2XFLAG::TOST-1 using an anti-FLAG antibody. Instead, TOST-1 was found in the flow-through, indicating it did not associate with INTS-6 in this experimental setup. Notably, the GFP-coupled beads B showed higher levels of nonspecific binding, which may have affected specificity.

One possible explanation for the absence of TOST-1 in the INTS-6 IP is that while INTS-6, as part of the Integrator complex, binds broadly to mRNAs during transcription, TOST-1 is relatively low-abundance protein predominantly located in the cytoplasm. To address this, a future experiment could involve performing the IP with TOST-1 from nuclear extracts instead of the whole embryo

lysates, potentially increasing specificity and allowing for the detection of TOST-1 in nuclear contexts where it may interact with transcriptional regulators.

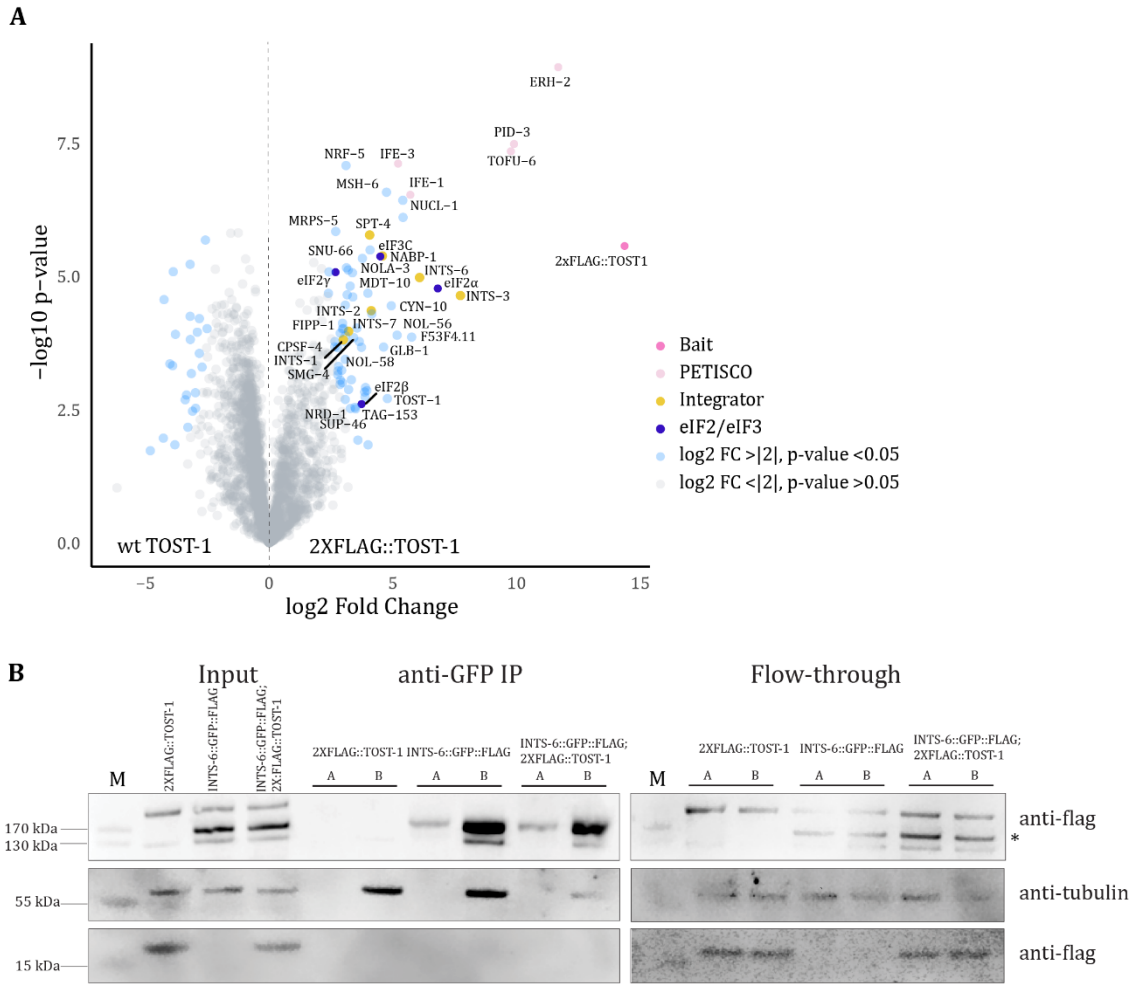

Figure R36 | Identification of potential TOST-1 interactors. A. Volcano plot representing label-free proteomic quantification of 2xFLAG::TOST-1 immunoprecipitation experiments from embryo extracts. The X-axis indicates the mean fold enrichment of individual proteins in the control (wild-type TOST-1) versus the genome-edited strain (2xFLAG::TOST-1). The Y-axis represents −log10(p-value) of observed enrichments. Dashed lines show thresholds at P = 0.05 and twofold enrichment. Coloured data points represent proteins that meet both the threshold for statistical significance (t.sam = 1.4) and twofold enrichment. Proteins of interest are highlighted: 2xFLAG::TOST-1 (bait) in pink, PETISCO components in light pink, Integrator and associated proteins in yellow, and eIF2 and eIF3 subunits in dark blue. B. Co-immunoprecipitation (Co-IP) experiments using embryo extracts. Input and immunoprecipitation (IP) samples were separated via SDS-PAGE, followed by Western transfer and chemiluminescence detection of 2xFLAG::TOST-1, INTS-6::GFP::FLAG and TUBULIN. The asterisk indicates the predicted full-length INTS-6::GFP::FLAG fusion-protein. A and B represent two different bead preparations used for the IP. M represents the protein marker.

PETISCO and Integrator interaction via yeast two-hybrid

To explore potential direct interactions between PETISCO and Integrator complexes, we employed the yeast two-hybrid (Y2H) system. This method allows for the assessment of protein-protein interactions by exposing pairs of proteins in the auxotrophic strain of Saccharomyces cerevisiae, where interactions are scored based on the proliferation of the yeast.

We tested all PETISCO subunits (TOFU-6, PID-3, ERH-2, IFE-3, PID-1 and TOST-1) and ERH-1 against several Integrator-associated proteins, including INTS-3, INTS-6, SPT-4, SPT-5 and NABP-1. Notably, INTS-3 and NABP-1 exist in multiple isoforms, and we included all of them in our assays. The cDNAs for these proteins were fused to either the Gal4 transcription factor binding or activation domain, allowing us to assess positive interactions through the expression of genes that compensate for the yeast's auxotrophy in histidine and adenine.

However, we did not identify any direct interaction between the PETISCO subunits and the Integrator-associated proteins tested (**Figure R37**). It is possible that if interactions do occur in *C. elegans*, they may be dependent on PTM or the presence of specific RNA molecules, factors that were not included in our Y2H assay.

In conclusion, our follow-up studies thus far did not validate the potential interactions between PETISCO and Integrator as suggested by the immunoprecipitation and mass spectrometry experiment.

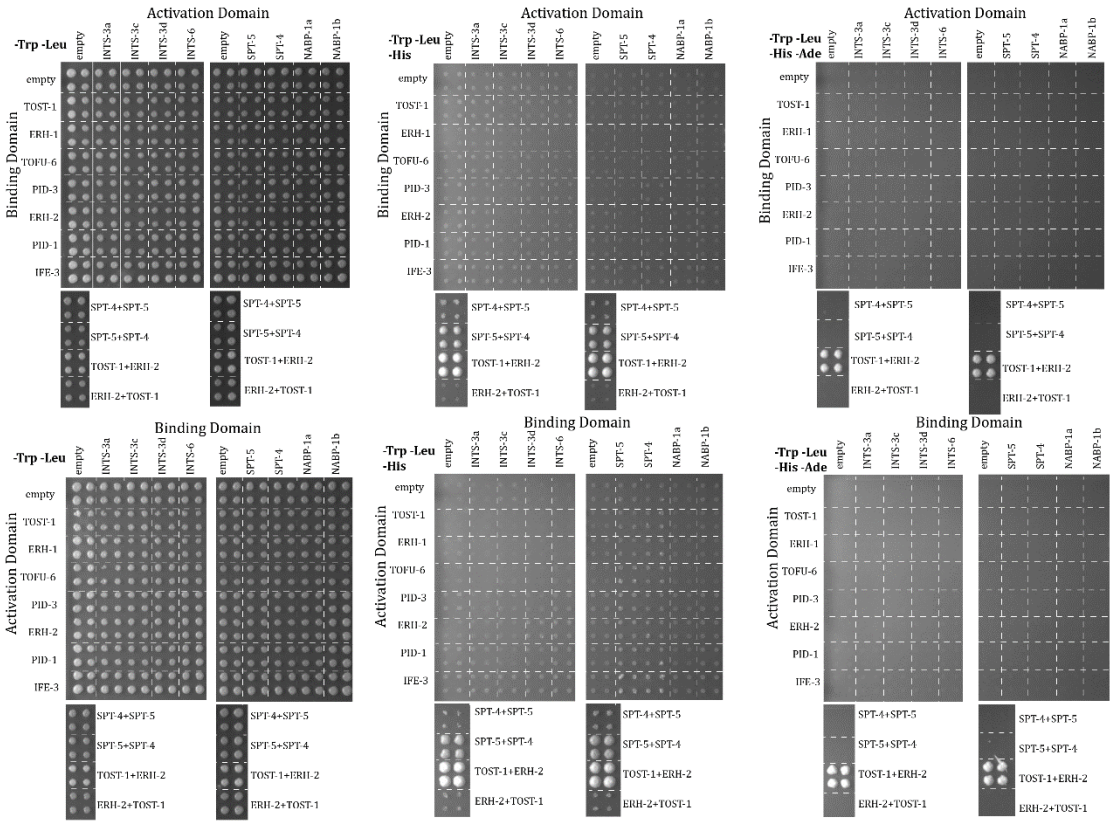

Figure R37 | PETISCO and Integrator interaction. Yeast two-hybrid (Y2H) analysis of PETISCO subunits with Integrator and associated proteins enriched in the IP-MS experiment (Figure 35): INTS-3, INTS-6, SPT-5, SPT-4 and NABP-1. Three media conditions were used: control (-Trp-Leu), low stringency (-Trp-Leu-His) and high stringency (-Trp-Leu-His-Ade), in both Y2H orientations. The orientation and selection media are indicated in the individual panel

DISCUSSION

Transcripts in a cell are subjected to many different processes. Being relatively unstable, RNA in general is turned over rather quickly if not stabilised in some manner. Being bound to proteins in so-called Ribonucleoproteins (RNPs, RNA-Protein complexes) is one way of increasing RNA stability. Short and non-adenylated transcripts are particularly unstable, as they are often considered the result of non-productive transcription and targeted to dedicated RNA breakdown machinery. This poses a challenge for piRNA biogenesis in *C. elegans*, which depends on short non-adenylated transcripts. PETISCO is a protein complex that was identified as required for piRNA/21U-RNA biogenesis in the *C. elegans* germline (Cordeiro Rodrigues et al., 2019; Zeng et al., 2019). Its binding to 21U-RNA precursors is essential for their stabilization and accumulation, which are important for further processing (Cordeiro Rodrigues et al., 2019; Podvalnaya et al., 2023; X. Wang et al., 2021). This function is mediated by PID-1, which interacts with PETISCO through ERH-2. However, ERH-2 can also bind TOST-1, effectively switching PETISCO functions. Loss of TOST-1 does not affect the stabilization of 21U-RNAs precursors but instead affects embryonic development.

In this work, we demonstrate that PETISCO in embryos binds specifically to replication-dependent (RD) histone mRNAs. This interaction is crucial for their stabilization, particularly for the maternal histone mRNAs, which ensure proper early embryonic development. We hypothesize that PETISCO protects histone mRNAs from degradation maintaining their concentration and ensuring adequate histone protein levels at the beginning of embryonic development. Furthermore, we observe the enrichment of Integrator proteins in association with TOST-1. This finding suggests that PETISCO may have additional regulatory functions in the context of this transcription termination complex, potentially in histone mRNA transcription.

In this section, I will discuss various aspects and hypotheses related to our findings, ending with an evolutionary perspective of PETISCO adaptation for piRNA/21U RNA precursors and histone mRNAs from existent machinery.

PETISCO binds histones in the stem-loop region

We found that TOFU-6 binds RD histone mRNA, with enrichment at the 3'-end of the transcripts near their conserved stem-loop structure (**Figure R2 and R3**). This interaction appears to depend on the presence of both the stem-loop and an upstream consensus sequence, which marks the peak of crosslinking events (**Figure R3**). This finding highlights a question of this project: *What confers specificity to PETISCO in recognizing its RNA targets?* In case of RD histone mRNAs, two major differences set them apart from canonical transcripts: the lack of splicing and

the presence of a stem-loop structure. Our results suggest that the stem-loop and its associated consensus sequence may be determinants of binding specificity. To understand if splicing is also an important factor for PETISCO recognition, we analysed the binding to different histone transcripts. One histone gene in *C. elegans*, lacks both introns and the stem-loop structure. However, this gene is not expressed in the embryos, preventing definitive conclusions. We also observed enrichment, though below the significance threshold, for *his-69,* which encodes the histone variant H3.3. This gene lacks introns but has a stem-loop and the consensus sequence, where we also observed crosslinking events. This observation suggests that independently of the type of histone protein, canonical or variant, PETISCO binding is dependent on the mRNA structure. This supports the hypothesis that the stem-loop is a primary regulatory region for PETISCO binding, but it does not exclude the possibility of the lack of introns also have an important regulatory function. It would be interesting to assess the binding capacity of PETISCO in histone transcripts that have only one of the two features: lack of splicing or the stem-loop. However, the fact that other non-spliced mRNAs, for example, genes from the S-phase kinase-associated protein 1 family (*skr-10, -13, -15*) or from the SKN-dependent zygotic transcript (*sdz-30, -36, -37*) families that are expressed in embryos and are intronless, are not enriched in our iCLIP. This supports a model where stem-loop specificity is the main driver of RD histone transcript binding to PETISCO.

PETISCO or CDL-1: both stem-loop binding factors in *C. elegans*?

The stem-loop is known to be bound by SLBP (CDL-1 in *C. elegans*), which plays a central role in histone mRNA metabolism. In mammals, specific nucleotides in the conserved stem-loop and flanking regions are required for SLBP binding (Battle & Doudna, 2001) (**Figure D1**, light blue). Interestingly, in contrast to other metazoans, *C. elegans* has a cytidine at position 1 of the loop instead of a conserved uracil (Michel et al., 2000), and has a conserved sequence of 12 nt just upstream the stem-loop. This cytidine is essential for CDL-1 binding, while the conserved 12 nt flanking sequence is not required. Additionally, the mammalian SLBP-binding motif includes two adenines (**Figure D1**, light blue), but it remains unclear whether these are necessary for CDL-1 binding in *C. elegans*.

Our results indicate that TOFU-6 binds the stem-loop region approximately 9 nt apart from where CDL-1 is expected to bind. However, no interactions between the two proteins have been detected in pull-down experiments, even though RD histone transcripts bind very well. This suggests two possible scenarios: first, PETISCO might bind histone mRNA, potentially via the

stem-loop, even in the absence of CDL-1. This would represent a unique mechanism in metazoans, as SLBP has thus far always been observed on RD histone transcripts. Alternatively, there could be an indirect interaction mediated by other proteins, which may remain undetected due to technical limitations.

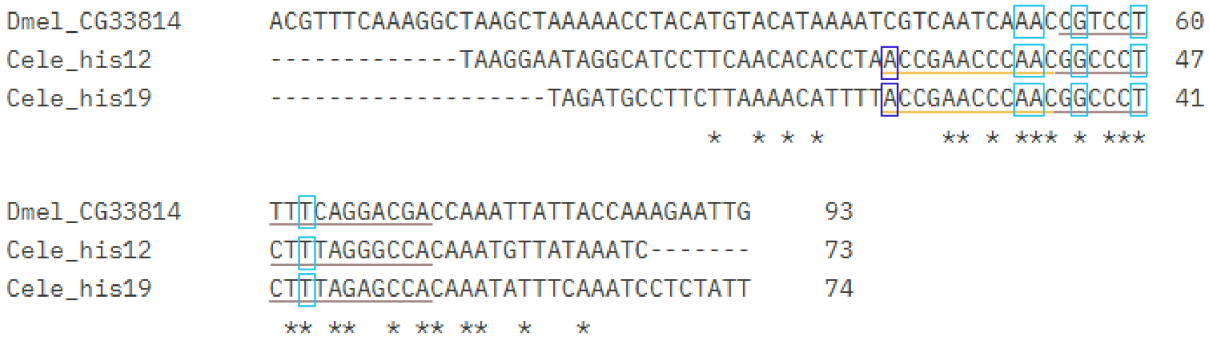

Figure D1 | Alignment of the 3' UTR of the histone genes *CG33814* in *D. melanogaster*, *his-12* and *his-19* in *C. elegans*, coding for H2A. Yellow underline represents the consensus sequence found only in *C. elegans*. Grey underline indicated the stem-loop sequence. Light blue squares indicate essential nucleotides for human SLBP binding. Dark blue square indicates the main crosslinking event with TOFU-6, obtained in the iCLIP experiment from this study.

CDL-1 and SLBP of *Drosophila* share 30.5% similarity (EMBOSS Needle, (Madeira et al., 2024)), with only the RNA-binding domain conserved between *C. elegans* and other species, like *Drosophila* or humans (Kodama et al., 2002). This domain is essential for processing and translation of RD histone mRNA. In *Drosophila,* however, a basic region in the N-terminal domain is required for maternal histone mRNA deposition in the embryo (Potter-Birriel et al., 2021). In *C. elegans,* the N-terminal region of CDL-1 differs significantly from that found in *Drosophila* SLBP, suggesting that CDL-1 might not be required for maternal stabilization. It is possible that PETISCO has adopted this function instead.

AlphaFold3 predictions support the hypothesis that PETISCO might directly bind to the stem-loop structure. PETISCO in the presence of the structured region of TOST-1 (Y7 - A53) accommodates the RD histone 3' UTR better than in the presence of structured region of PID-1 (H9 – K74), where PETISCO loses its expected conformation (**Figure D2.A, B**). The predicted structure of the 3' UTR of the RD histone gene *his-7* shows higher confidence in the presence of the structured part of TOST-1, compared to the structured part of PID-1 (**Figure D2.C, D**). Changes to the upstream sequence of the stem-loop affect TOST-1 binding, suggesting that these elements influence PETISCO's structural stability (**Figure D2.E**). These predictions imply that PID-1 and TOST-1 influence PETISCO's interaction with the stem-loop differently, supporting the

model that these two PETISCO ligands may have a direct effect on its RNA-substrate binding. However, the mechanisms behind this regulation are still unclear.

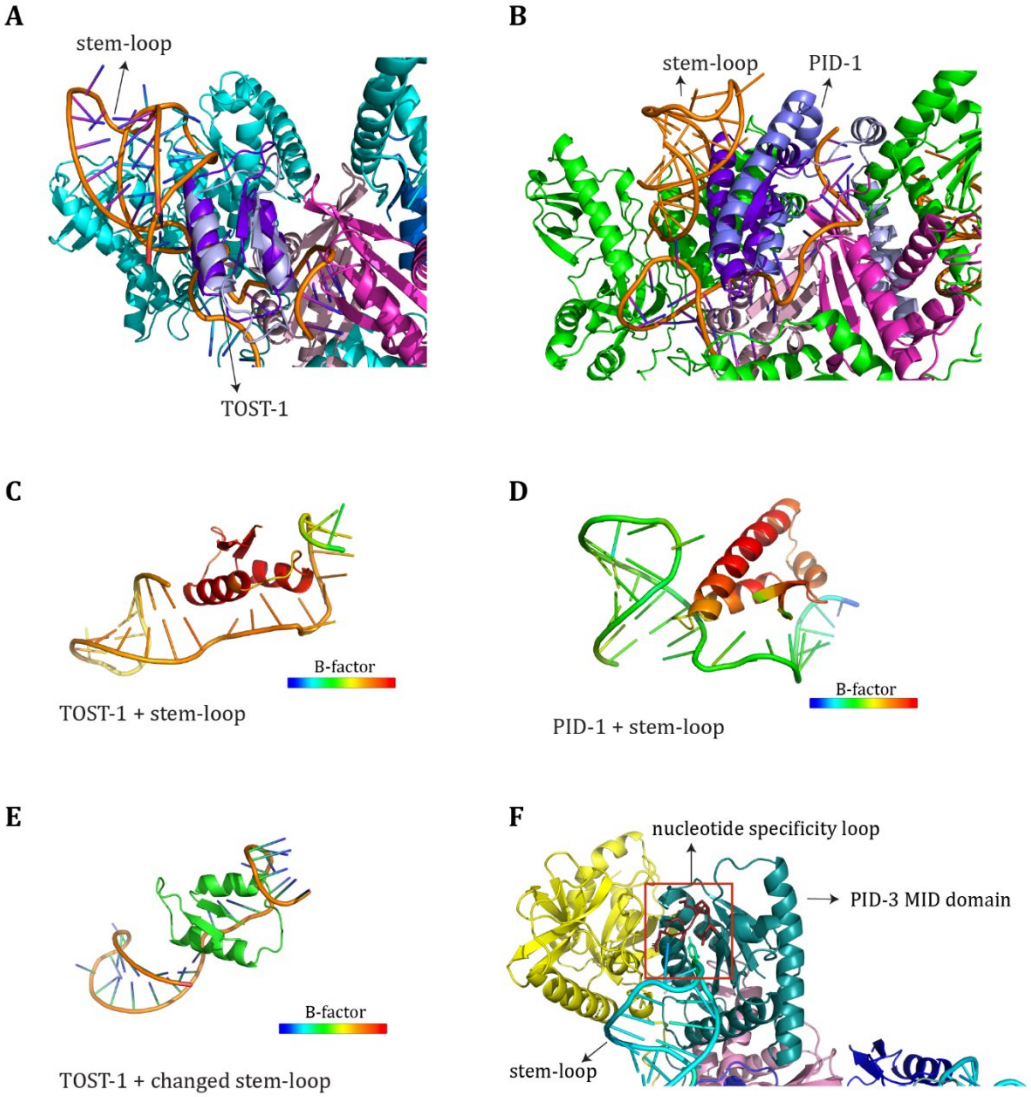

Figure D2 | AlphaFold3 predictions of intercations between PETISCO components and the stem-loop of *his-7*. A. Overlapping predicted structure of PETISCO with TOST-1 and free TOST-1 with the stem-loop sequence, including 10 bp upstream. B. Overlapping predicted structure of PETISCO with PID-1 and free PID-1 with the stem-loop sequence, including 12 bp upstream. C. Predicted interaction of the structured region of TOST-1 (Y7 - A53) with the stem-loop. D. Predicted interaction of the structured region of PID-1 (H9 – K74) with the stem-loop. E. Predicted interaction of the structured region of TOST-1 with the stem-loop, with the upstream sequenced modified. F. Predicted interaction of the MID domain of PID-3 with the stem-loop, highlighting a stronger predicted interaction between the uracil in the loop and the nucleotide specificity loop of the MID domain (Boland et al., 2010; Frank et al., 2010).

RNA-binding options of PETISCO

The specific parts of PETISCO that bind transcripts remain an open question. Both PID-3 and TOFU-6 have RNA-binding domains, with PID-3 having an RRM domain and a MID domain, and TOFU-6 containing an RRM domain and a TUDOR domain (Cordeiro Rodrigues et al., 2019; Perez-Borrajero et al., 2021; X. Wang et al., 2021; Zeng et al., 2019). The RRM domain of PID-3, which facilitates its homodimerization, is occupied by ERH-2 interaction (Perez-Borrajero et al., 2021), whereas the RRM domain of TOFU-6 is more accessible for RNA binding. The MID domain in PID-3 may also contribute to RNA binding, as MID domains in Argonaute proteins preferentially bind 5' uridine or adenosine of small RNAs (Boland et al., 2010; Frank et al., 2010). This could be relevant to PID-3's role in binding 21U RNA precursors, where the third base uracil, is a necessity for their 5' end processing (Podvalnaya et al., 2023). In the case of RD histone mRNAs, PID-3 may help stabilize the U-rich stem-loop. Notably, AlphaFold3 predictions show the proximity of a uracil to PID-3's MID domain (**Figure D2.F**) (Boland et al., 2010; Frank et al., 2010). These hypotheses on binding specificity could be tested using both *in vitro* and *in vivo* approaches. *In vitro* binding assays such as Electrophoretic Mobility Shift Assay (EMSA) could be employed to directly test the interaction between the 3' UTR of the RD histone mRNA and the RNA-binding domains of TOFU-6 and PID-3. To determine the contribution of specific nucleotides or motifs, such as the uracils in the loop or the consensus sequence upstream of the stem-loop, mutations in these regions could be introduced. *In vivo* interaction experiments could also be use: iCLIP using a PID-3-specific antibody would allow precise mapping of the binding sites on the histone transcripts.

Another potential interaction between PETISCO and RD histone mRNAs involves IFE-3 and its binding capacity to the m7GpppN cap of histone mRNAs (**Figure D3)**. As mentioned above, germline-specific IFE-3 is part of the eIF4F protein complex (Amiri et al., 2001). During translation, eIF4F associates with the mRNA cap and interacts with the 43S PIC via eIF3 to commit to translation (Hinnebusch & Lorsch, 2012). In *C. elegans*, IFE-3 represses translation in the germline and associates with RD histone mRNAs (Gajjar et al., 2024). If PETISCO binds to RD histone mRNAs in the germline and stabilizes them for early embryonic use, it may prevent premature degradation or translation. PETISCO could achieve this by impeding SLBP/CDL-1 interactions with other effectors required for downstream functions. This could occur through structural conformation changes or by directly preventing CDL-1 binding.

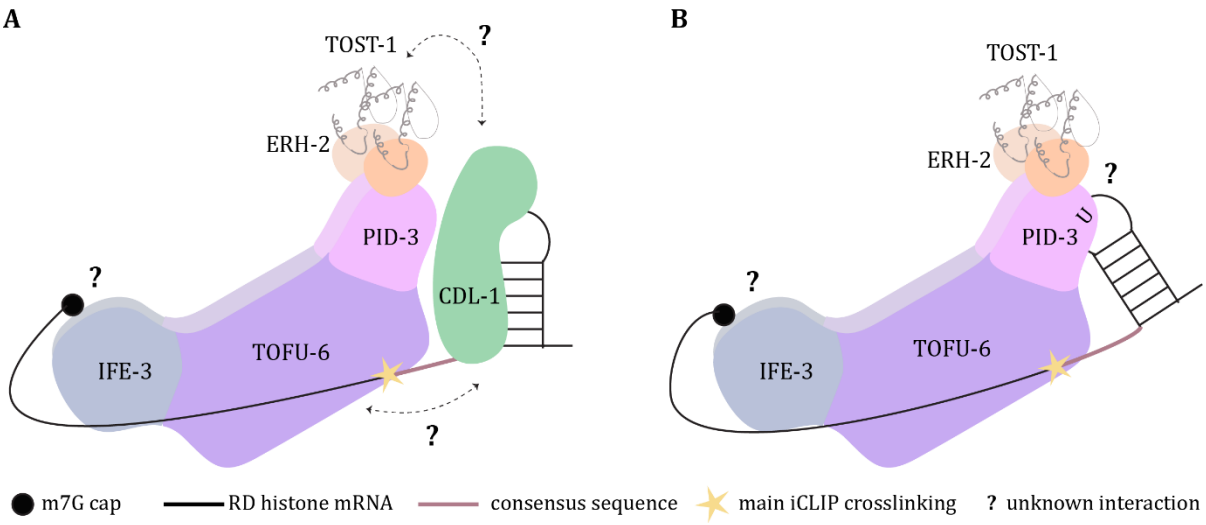

Figure D3 | Models for PETISCO binding to RD histone transcripts. A. PETISCO binds primarily via the conserved consensus sequence in the 3' UTR of the transcript upstream of the stem-loop, where the main iCLIP crosslinking event was identified (indicated by a star). PETISCO may share this region with CDL-1, although interactions between CDL-1 and PETISCO remain unknown. B. PETISCO binds to the transcripts in the absence of CDL-1, potentially via the nucleotide specificity loop of the MID domain of PID-3. The binding of IFE-3 to the m7G cap of histone transcripts is also currently unknown.

PETISCO and stabilization mechanisms for maternal histone mRNAs

In *C. elegans* adult gonads, many mRNAs are transcribed in the mitotic region and early pachytene stages but are destined for translation only in the embryo. To achieve this, these mRNAs must be maintained in a translationally silenced state to prevent premature translation, which would interfere with oocyte development (Evans & Hunter, 2005). Several mechanisms have evolved to stabilize maternal mRNAs and repress their translation until needed during embryogenesis (Evans & Hunter, 2005; G. Yang et al., 2024). One main mechanism involves regulating the poly(A) tail length, with deadenylases and polyadenylases playing a central role (Barckmann & Simonelig, 2013). In many species, short poly(A) tails in germ cells correlate with low translation rates and storage and stability of mRNAs (Lorenzo-Orts & Pauli, 2024).

However, RD histone mRNAs do not have poly(A) tails, raising the question of how they are stabilized in the germ cells. Our results show that the loss of TOST-1 causes RD histone depletion in young and gravid adults, yet has minimal effect on their expression in embryos (**Figures R7, R29, R30**). This suggests that PETISCO, with TOST-1, primarily stabilizes maternal histone mRNAs, possibly by repressing their translation and preventing degradation during oogenesis. In contrast, zygotic histone transcripts, which are regulated by the cell cycle, depend less on

PETISCO, leading to no phenotype upon PETISCO loss. It would be interesting to further investigate the functions of PETISCO in embryos to better understand the contrasting phenotypes observed in adults - where RD histone mRNAs are downregulated - and in embryos, where PETISCO binds to RD histone mRNAs but their expression does not seem to be affected according to our qRT-PCR results. A limitation of our analysis is the inability to assess histone mRNA levels specifically in early embryos, where we think that PETISCO is more crucial, as our data represents a bulk population of mixed embryos, where maternal and zygotic transcripts cannot be differentiated.

Interestingly, in zebrafish, a germline-specific paralog of eiF4E known as eIF4E1b binds the cap of mRNAs with short poly(A) tails but also RD histone transcripts to prevent their translation. This occurs because eIF4E1b does not interact with eIF4G, a key factor in translation initiation (Lorenzo-Orts et al., 2024). In mammals, SLBP interacts with eIF4G1 during translation (Dankert et al., 2016) and eIF4G1 is a component of the eIF4F multi-subunit complex that also includes eIF4E. In *C. elegans*, IFE-3, which is an eIF4E homolog, is also involved in translation repression, it is tempting to speculate that IFE-3 may perform a similar role for maternal histone mRNAs in the context of PETISCO (**Figure D4**). IFE-3 may stabilize histone transcripts by preventing premature translation. In the embryo, the transcripts could be bound instead to IFE-1, an eIF4E ortholog that supports active translation (Gajjar et al., 2024). This model aligns with the observed enrichment of IFE-1 with TOFU-6 and the enrichment of translational factors eIF2 and eIF3, in a TOST-1 pull-down experiment in embryos (**Figure R36**). During such a transition from a stabilized by translationally inactive RD histone transcript to a translated transcript, CDL-1 may interact with IFE-1 to promote histone mRNA translation, similarly to what was explained above on the interaction between SLBP and eiF4G in mammals. Testing whether CDL-1 interacts with IFE-1 in early embryos and whether this interaction is disrupted in PETISCO mutants, due to loss of maternal histone mRNAs, could clarify this relationship.

Other proteins, such as Y-box proteins, have been implicated in the stabilization of maternal mRNAs in frogs, zebrafish and mice, through mechanisms dependent on RNA modifications (Bouvet & Wolffe, 1994; Medvedev et al., 2011; Sun et al., 2018). In *C. elegans* Y-box proteins, known as CEY proteins, have not been directly implicated in maternal mRNA dormancy or storage, but they are known interactors of DEAD-box helicase CGH-1, which is critical for both for translation repression and the stability of stored maternal mRNAs (Boag et al., 2005b; Rajyaguru & Parker, 2009). This is particularly interesting because some CEY proteins, as well as CGH-1, have been shown to interact with PETISCO subunits such as IFE-3 and TOFU-6 (A. Arnold et al.,

2014; Cordeiro Rodrigues et al., 2019; Zeng et al., 2019). Although direct evidence is lacking, these interactions could suggest that CEY proteins and CGH-1 may cooperate with PETISCO to stabilize maternal histone mRNAs.

Another mechanism used for maternal mRNA stabilization involved their sequestration in specific RNA granules, where translation components and mRNA decay factors are absent. This storage mechanism is observed in various organisms during oogenesis (Boag et al., 2008; Cassani & Seydoux, 2022; Ivanov et al., 2019; Lin et al., 2008; R. Parker & Sheth, 2007). PETISCO could stabilize histone mRNAs in the germline by keeping them in P granules, already known to be implicated in translation repression and maternal mRNA storage (D. M. Parker et al., 2020; Putnam et al., 2023).

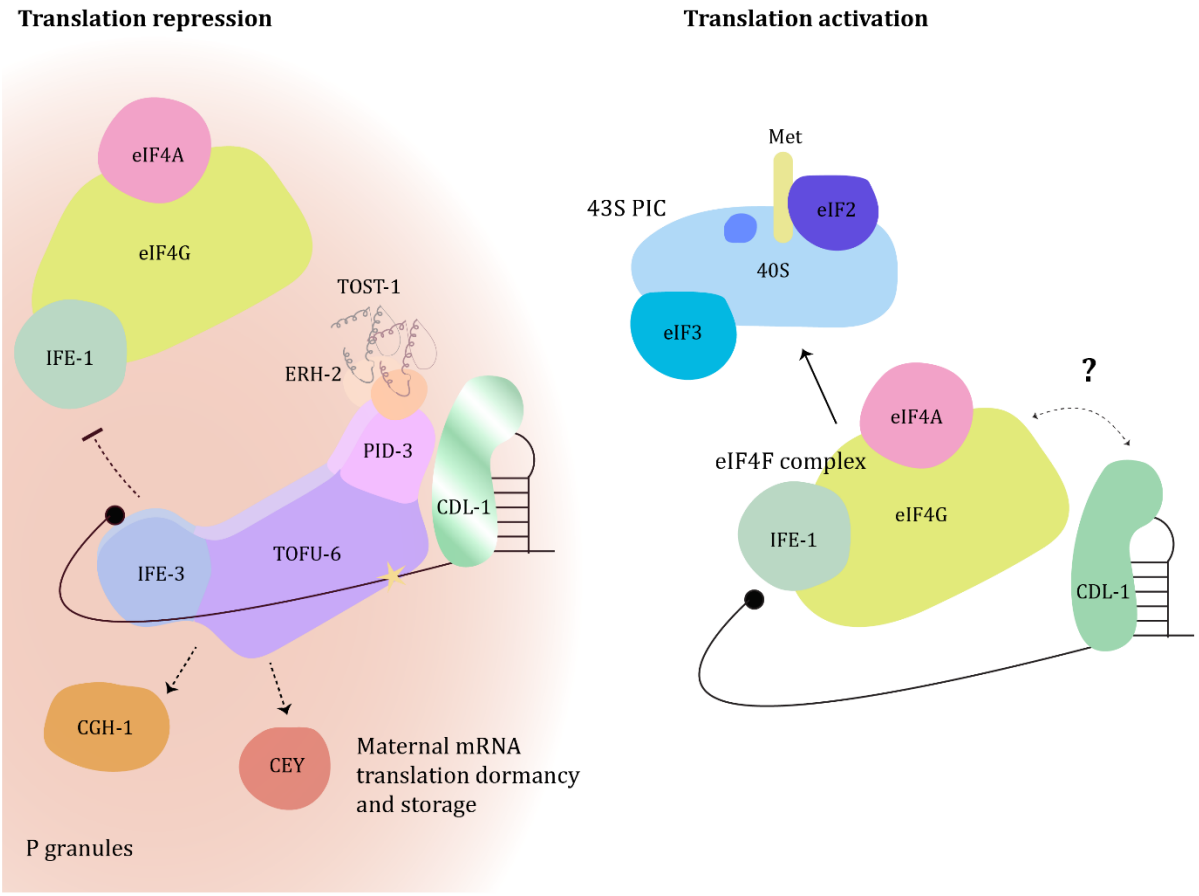

Figure D4 | Model for the interplay between IFE-3 and IFE-1 in the repression and activation of RD histone translation. In P granules, where PETISCO is predominantly localised, its binding to histone transcripts may repress translation, by preventing IFE-1 from binding to the cap, thereby blocking the recruitment of the other components of the eIF4F complex. Translation repression may also involve known proteins associated with maternal transcripts stabilization, such as CGH-1 and Y-box proteins (CEYs), both of which were found to be enriched in PETISCO pull-down assays. The presence of CDL-1 at this stage remains unknown. During translation activation, PETISCO is replaced by IFE-1 and the

remaining components of the eIF4F complex, facilitating recruitment of the pre-initiation complex (PIC) for translation initiation. An interaction between CDL-1 and eIF4G during this process is possible, although it has not been detected at the time of this study.

The only well-characterized mechanism for stabilizing maternal histone mRNAs in oocytes in other species involves SLBP. In zebrafish, flies, mice and frogs, SLBP is required for the accumulation of histone mRNAs in oocytes (D. R. Arnold et al., 2008; He et al., 2018; Lanzotti et al., 2002; Z.-F. Wang et al., 1999). In mice, SLBP is produced in growing oocytes and is essential for accumulating H3 and H4-coding genes in oocytes (D. R. Arnold et al., 2008). Similarly, in *Drosophila*, a small region in SLBP has been identified as critical for the accumulation of histone mRNAs in the ovaries (Potter-Birriel et al., 2021). As described above, this region is not present in CDL-1 (*C. elegans* SLBP), and PETISCO could play a role as possible replacement.

Our experiments suggest that PETISCO is also required for the accumulation and deposit maternal histone mRNAs in *C. elegans*. We observed transcript depletion in *tost-1* mutants using smFISH with *gfp::his-61* in early embryos (**Figure R9**). However, this result must be interpreted cautiously as the presence of the *gfp* sequence may alter the expression and regulation of histone genes, as noted in a personal communication. To conclusively determine whether PETISCO stabilizes maternal histone transcripts, quantifying wild-type endogenous histone transcripts, using smFISH during oogenesis and in early embryos will be crucial.

Embryonic defects in PETISCO mutants

When PETISCO was identified as a component of the piRNA biogenesis pathway in *C. elegans*, it was surprising to observe such severe embryonic defects in PETISCO mutants, given that piRNAs are not required during early embryogenesis (Cordeiro Rodrigues et al., 2019; Zeng et al., 2019). TOFU-6, previously identified as MEL-47, was found to exhibit fully penetrant maternal-effect lethality, with early embryos arresting at variable stages, containing between 50 and 80 cells (Minasaki & Streit, 2007). Despite these observations, defects in nuclear shape were already evident at the 2-cell stage, and embryos exhibited delays in reaching the 4-cell stage. Interestingly, early cell polarity and the distributions of different proteins were unaffected. However, after the 4-cell stage, defects in the synchrony of cell divisions became evident, with some blastomeres ceasing to divide at various time points. Additional mitotic defects, such as chromosome segregation errors and chromatin bridges, were also observed. These phenotypes

were consistent across mutants of other PETISCO components and *tost-1* depleted embryos, as observed in this study (Cordeiro Rodrigues et al., 2019; Zeng et al., 2019) (**Figure R14**).

Chromatin bridges and delays in cell cycle progression are hallmark features of DNA replication mutants (Brauchle et al., 2003; Encalada et al., 2000). Notably, knockdown of DNA replication checkpoint components partially suppresses these delays (Brauchle et al., 2003). Activation of DNA replication checkpoint, dependent on Chk1, is influenced by the nuclear-to-cytoplasmic (N/C) ratio and has been shown to affect MZT (Shindo & Amodeo, 2021). RD histone expression is tightly linked to DNA replication. Misregulation of RD histones during embryogenesis leads to defects in cell cycle progression and chromosome segregation (Chari et al., 2019; Günesdogan et al., 2014; E. Sullivan et al., 2001). In *Drosophila*, SLBP mutants exhibit chromosome segregation defects, though these defects do not manifest in the earliest cell divisions (E. Sullivan et al., 2001). In *C. elegans*, RNAi depletion of *cdl-1* also causes chromatin bridges in embryos starting at the 2-cell stage, and similar phenotypes are observed with RNAi targeting H2B genes (Kodama et al., 2002). These observations led us to hypothesize that PETISCO mitotic defects in embryos are likely due to insufficient RD histone mRNAs (**Figure D5**). However, it remains unclear whether these phenotypes result solely from the depletion of maternal histone transcripts or if zygotic histone transcripts also play a role.

The link between histone mRNA levels and embryonic development was further supported by observations of stronger phenotypes in *tost-1* hypomorphic mutant and embryonic arrest independently of the temperature when a histone gene cluster was deleted (**Figure R27**). Although we did not quantify histone expression in these mutants, the results suggest that *tost-1* mutant adults, already depleted of histone mRNAs, become more depleted in combination with the histone cluster deletion. We hypothesize that this would lead to a mild histone mRNA downregulation in embryos and more pronounced downregulation in the adult gonad and very early embryos. These effects could be confirmed through quantitative RT-qPCR, as performed for the other mutants.

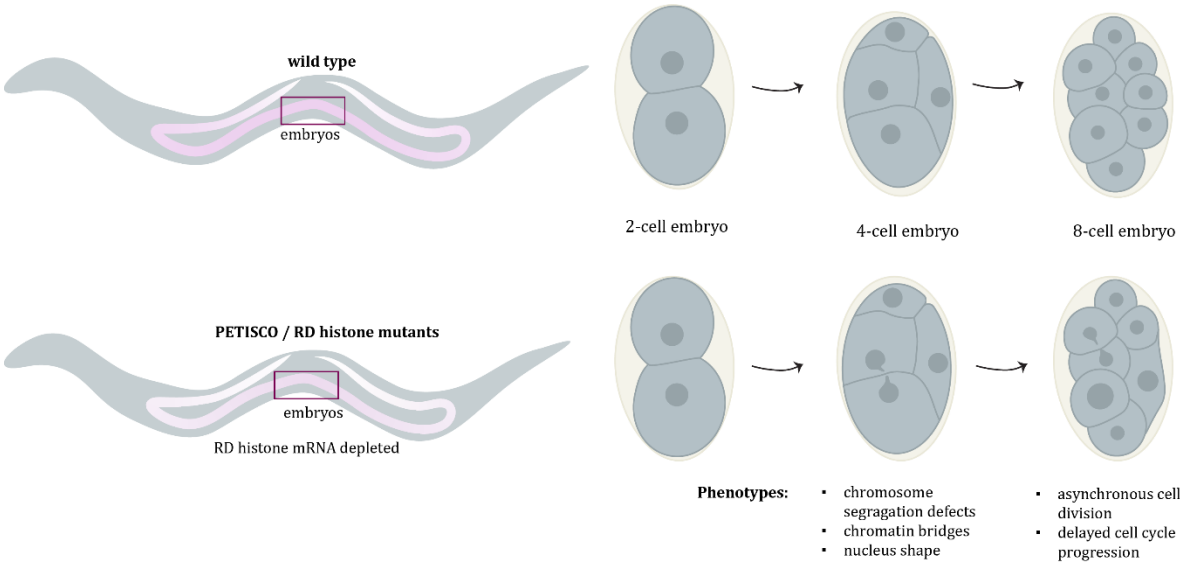

Figure D5 | Embryonic defects observed in PETISCO- and histone-depleted embryos compared to *wild-type* embryos. In *wild-type* adults, RD histones are expressed in the germline and require stabilization before being deposited into embryos. In adults where PETISCO is depleted or RD histones are targeted by RNAi, histone expression is reduced, resulting in lower amounts being deposited into embryos. We hypothesize that the reduced concentration of maternal histones in embryos leads to the embryonic defects observed in these mutants. Pink gradients represent the histone mRNA concentration in ther germline.

Gene expression dysregulation in *tost-1* hypomorphic mutants

During this study, we found that gene expression is significantly altered in *tost-1* hypomorphic mutants at both 15°C and 25°C. Notably, we observed a higher number of upregulated genes (Fold change >2) than downregulated genes (**Figure R24**). This imbalance suggests that chromatin accessibility may be affected, leading to widespread changes in gene regulation. To explore whether these differentially expressed genes are localized in specific genomic regions susceptible to chromatin structure changes, ATAC-seq could be used to analyse genome-wide chromatin accessibility in *tost-1* mutant embryos. Studies across species, from yeast to mammals, have shown that histone depletion causes genetic instability and alterations in chromatin structure, often leading to cell cycle arrest, particularly in the S-phase (Ghule, Xie, Medina, Colby, Jones, Lian, Stein, Wijnen, et al., 2014; Jimeno-González et al., 2015; Prado et al., 2017; Saunders et al., 1990; Wyrick et al., 1999). However, nucleosome occupancy does not decrease uniformly across the genome (Gossett & Lieb, 2012), which may explain the variability in fold changes in gene expression observed in our samples.

The ZGA process is tightly regulated by multiple mechanisms, including chromatin accessibility (Eckersley-Maslin et al., 2018). Regions of more open chromatin are generally expressed earlier. In our experiments with *tost-1* mutant embryos, we observed that genes typically expressed in later stages of embryogenesis were upregulated prematurely, indicating altered expression (**Figure R26**). This premature gene expression could result from accelerated ZGA due to increased chromatin accessibility. Supporting this hypothesis, earlier expression of the *xfSi268* transgene was observed upon depletion of *tost-1*, *tofu-6* and *his-65* (**Figure R22, R23**). The phenotypic similarities between *his-65* RNAi and PETISCO depletion in cell cycle progression and gene expression suggest that PETISCO's effects are primarily due to histone mRNA depletion. Interestingly, *his-66* depletion did not consistently result in earlier transgene activation, though variability across embryos was increased. This inconsistency could stem from incomplete RNAi effects, potentially because fewer histone mRNAs are targeted by the dsRNA. In *Drosophila,* depleting maternal SLBP reduces histones concentration, accelerating ZGA and altering gene expression and cell cycle timing (Chari et al., 2019; Günesdogan et al., 2014). These findings support the model that histone concentration regulates transcriptional activation in embryos, which may be an explanation for the altered gene expression in PETISCO mutants.

Temperature-specific gene expression changes in *tost-1* mutants

The hypomorphic and temperature-dependent nature of the *tost*-1 mutant function, provides a unique context to study and distinguish the effects of gene expression based on histone depletion in viable embryos, at 15°C, and histone depletion in arrested embryos, at 25°C. At 15°C, upregulated genes in *tost-1* mutants compared to *wild-type* are enriched for processes related to neurogenesis and neuronal differentiation (**Figure R25.E**). This could indicate premature cell differentiation, or maybe more accurate (since the embryos are viable) premature gene expression. Interestingly, genes involved in neurogenesis are also upregulated in *wild-type* embryos at 25°C compared to 15°C (data not shown), consistent with the fact that higher temperatures accelerate the *C. elegans* lifecycle and developmental processes (Gómez-Orte et al., 2017). Which is in accordance with our hypothesis that in *tost-1* mutant gene expression is also happening prematurely. For instance, the neuronal transcription factors *lin-11* and *lin-32* are upregulated in *wild type* at 25°C compared to 15°C (Log2 FC = 1.66, p-value = 1,01554E-40; Log2 FC = 2.79, p-value = 2,79487E-17 respectively). Similarly, these genes are also upregulated in *tost-1* mutants vs *wild-type* at 15°C (Log2 FC = 1.01, p-value = 8,47579E-13; Log2 FC = 0,47, p-value = 9,73447E-05). *lin-11* encodes a transcription factor with a LIM homeobox domain critical

for cell type specification and neuronal differentiation (Hobert et al., 1998; Sarafi-Reinach et al., 2001), while *lin-32* is necessary for neuronal lineage development (Portman & Emmons, 2000; C. Zhao & Emmons, 1995). These observations align with the hypothesis of premature neuronal differentiation in *tost-1* mutants, due to accelerated ZGA.

At 25°C, the upregulated genes in *tost-1* mutants compared to *wild-type* differ from those at 15°C, with enrichment in processes such as neuropeptide and insulin signalling (**Figure 25.D**). This could reflect accelerated neural development or a stress response due to mitotic defects and eventual embryonic arrest. Interestingly, proteins from the cullin family, which are involved in protein degradation of cell cycle regulators and transcription factors, were enriched and may contribute to this stress response (Deshaies, 1999; Tyers & Jorgensen, 2000).

Conversely, genes downregulated at 25°C in *tost-1* mutants compared to *wild-type* include those involved in neurogenesis, muscle development, and locomotion (**Figure R25.I**). These results suggest that differentiation pathways might be disrupted due to accelerated neural development or embryonic arrest in the mutants. Transcription-related genes were also downregulated, consistent with cell cycle arrest observed in these embryos.

Interestingly, genes downregulated genes at both 25°C and 15°C, when comparing *tost-1* mutant with *wild-type* embryos were enriched for RNA metabolism and processing, including ncRNA, rRNA and mRNA (**Figure R25.J**). This could reflect the depletion of RD histone mRNAs and a broader role of PETISCO together with TOST-1, in RNA metabolism. Supporting this, PETISCO and TOST-1 might be involved in SL snRNA processing (Cordeiro Rodrigues et al., 2019). Additionally, our IP-MS experiment identified potential interactors between TOST-1 and Integrator subunits (**Figure R36**), a complex involved in transcription termination of small RNAs, which could also explain these downregulated genes. Enriched proteins related to ribosome biogenesis were also identified in the IP-MS that together with the downregulation of RNA processing pathways in *tost*-1 mutants might suggest a broader role for TOST-1 in RNA processing, though further investigation is needed to understand.

Lastly, at 15°C, upregulated genes in *tost-1* mutant compared to *wild-type*, were enriched for processes related to cell cycle progression, nuclear division and chromosome segregation (**Figure R25.K**). Although this appears counterintuitive given the apparent premature ZGA, it may reflect a breakdown of the tightly coordinated balance between cell cycle and transcription regulation. In accordance with these results, we observed that embryos depleted of *tost-1, tofu-6* and *his-65* by RNAi displayed fewer nuclear divisions compared to *wild-type* embryos (**Figure R23**). Additionally, *tost-1* hypomorphic mutants developed more slowly, taking longer to reach

the same developmental stage as *wild-type* worms, at 15°C or 20°C. However, this observation is solely based on the handling of the animals and average times during larval development were not quantified in these mutants.

These differences in gene expression between 15°C and 25°C likely contribute to the observed phenotypically variability in embryonic development in *tost-1* hypomorphic mutants at both temperatures. This suggests that histone mRNA concentration may influence embryonic development in these mutants. However, the direct link between maternal histone mRNA stability mediated by PETISCO and the observed gene expression alterations remains to be fully confirmed.

Rescuing embryonic development by affecting histone degradation pathways

Genetically depleting *cde-1* and *smg-2* from embryos was sufficient to rescue the Mel phenotype of *tost-1* hypomorphic mutants at 25°C (**Figure R27**). Both proteins are known to participate in histone mRNA degradation in other species (Choe et al., 2014; Kaygun & Marzluff, 2005; Lackey et al., 2016; Lim et al., 2014). Although their role in histone mRNA degradation has not been confirmed in *C. elegans*, it is plausible that their functions are conserved, and that histone mRNA degradation is impaired in the absence of these proteins. This hypothesis could be tested by detecting RD histone degradation intermediates of different lengths in *cde-1* and *smg-2* mutants. We did find that embryos depleted of *cde-1* had elevated levels of histone mRNAs, suggesting a role in their degradation (**Figure R31**).

Interestingly, depletion of *cde-1* was the only experiment that could rescue the Mel phenotype in *tost-1* null mutants and mutants of other PETISCO components (**Figure R28**). In contrast, *smg-1*, *smg-2 and smg-3* mutants, as well as *C14C10.5* mutants (**Figure R35**), were unable to rescue the *tost-1* null Mel phenotype.

Determining whether the loss of these proteins impairs RD histone mRNA degradation and whether this contributes to the rescue of *tost-1* mutants' embryonic development is essential. If so, the inability of *smg-1, -2* and *-3* mutants to rescue the *tost-1* null phenotype, in contrast to *cde-1,* would require further explanation. One hypothesis is that CDE-1 plays a more critical role in marking RD histone mRNAs for degradation, which becomes irreplaceable in the complete absence of PETISCO. We can hypothesize several reasons to explain the differences in the rescue

of the SMG mutants in the various *tost-1* alleles. The most direct explanation is that SMG-2, and potentially SMG-1 and SMG-3, are involved in histone mRNA degradation. However, their role may not be essential, as degradation can still occur through alternative mRNA decay pathways. It is well-established that when RD histone transcripts are oligouridylated at their 3' ends, these sequences create a platform for loading the LSM1-7 complex, which triggers decapping followed by 5′-to-3′ degradation (Rissland & Norbury, 2009). Both SMG-1 and SMG-3 are components of the NMD pathway, in which they are required for the activity of SMG-2 (Kishor et al., 2019). However, only SMG-2 homolog (UPF1), and once reported also SMG1, have been implicated in RD histone mRNA degradation in other eukaryotes, typically in a cell-cycle dependent manner or upon inhibition of DNA replication (Choe et al., 2014; Kaygun & Marzluff, 2005; Meaux et al., 2018). Moreover, the involvement of the NMD pathway may also be indirect and not related to histone degradation pathway. SMG-1, SMG-2 and SMG-3 might influence embryonic development through broader impacts on gene regulation, unrelated to histone mRNA degradation (explained below).

Additionally, the loss of ERI-1 (*C. elegans* homolog of 3'hExo), a known histone mRNA degradation factor in other species (Hoefig et al., 2012), does not rescue embryonic viability in *tost-1* mutants, whether in the hypomorphic or null mutant background. This could be because other 3'-5' exonucleases might compensate for the absence of ERI-1, or potentially serve as the primary exonucleases involved in degrading the stem-loop in *C. elegans*. One candidate is DISL-2*,* which is known to interact with CDE-1 and is involved in the uridylation and degradation of rRNAs (Y. Wang et al., 2020). Another possibility already mentioned above, is that the rescue is not dependent on histone mRNA degradation pathways.

CDE-1's role in histone mRNA regulation is supported by qRT-PCR results showing upregulation of RD histone transcripts in embryos lacking CDE-1 (**Figure R31**). This suggests that CDE-1 polyuridylation is both sufficient and necessary to mark RD histone transcripts for degradation. When CDE-1 is lost, histone mRNA degradation is prevented, increasing enough transcript availability even in *tost*-1 null mutants or other PETISCO-depleted embryos. This aligns with the idea of a finely tuned maternal histone concentration required for early embryonic development (**Figure D6**). Supporting this, the genetic depletion of 13 histone genes within a cluster leads to synthetic lethality in *tost-1* hypomorphic mutants. Similarly, mutations in *C14C10.5*, predicted to be involved in acetylated histone protein degradation, rescue the *tost-1* hypomorphic phenotype reinforcing the importance of sufficient histone levels. However, further experiments are needed

to confirm whether loss of *C14C10.5* directly affects histone protein levels during oogenesis and/or early embryogenesis.

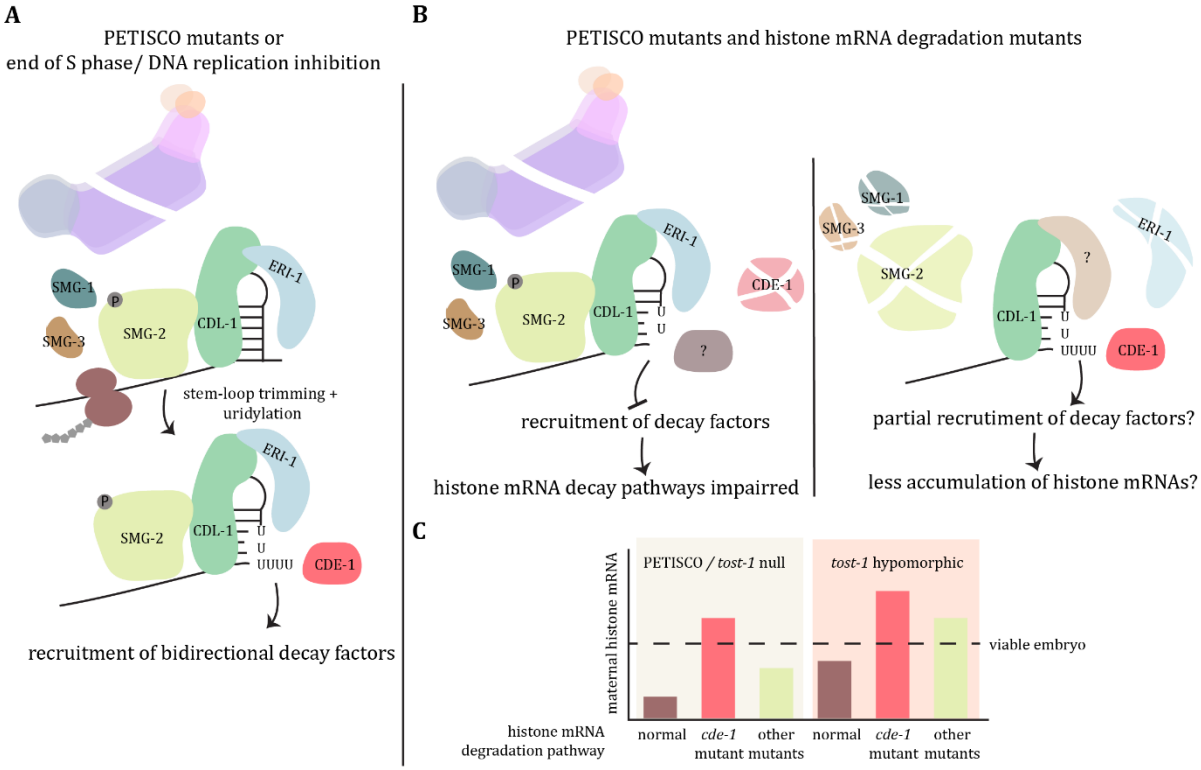

Figure D6 | Consequences of depletion of histone mRNA degradation components in PETISCO mutants. A. Model of histone mRNA degradation at the end of the S phase or upon DNA replication inhibition based on mechanisms known in other organisms. We hypothesize that, in the absence of PETISCO, maternal histone mRNAs undergo a similar degradation pathway. This involves trimming and polyuridylation of the stem-loop, followed by recruitment of the Lsm1-7 complex, which facilitates mRNA decay via decapping and 5'-3' exonuclease activity, as well as degradation by the exosome in the 3'-5' direction. B. Proposed models illustrating the effects of different mutants on histone transcript regulation in the PETISCO mutant background. Left: Loss of CDE-1 results in inefficient urydilation of the stem-loop. Some uridylation may still occur via other poly-U polymerases, but this is insufficient to recruit the Lsm1-7 complex for stem-loop degradation and bidirectional decay. Right. Loss of ERI-1 is compensated by other 3'-5' exonucleases, which can still trim the stem-loop, allowing urydilation by CDE-1. Loss of SMG-1, -2, -3 partially prevents the recruitment of decay factors but less efficiently than in *cde-1* mutants. C. Schematic representation of a threshold model for maternal histone mRNA levels in embryos required for full embryonic development. The graph shows how different mutants in the histone mRNA degradation pathway affect these levels in different tost-1 mutant alleles.

Alternative mechanisms for developmental rescue independent of histone mRNA degradation

Additional pathways may also contribute to the observed rescues. Loss of SMG-1 and SMG-3 could impair the NMD pathway, indirectly influencing gene expression in early embryos, due to the role of this pathway in mRNA regulation including normally-transcribed mRNAs (Kim &

Maquat, 2019; Muir et al., 2018). Another hypothesis, to the involved of NMD pathway could be related to the increase of polyadenylated RD histone mRNAs in *tost-1* mutants, observed in our RNA-seq experiments (**Figure R24**). Polyadenylated RD histone mRNAs are not cell-cycle regulated, which impacts the chromatin landscape and can be a source of genomic instability and alter gene expression (D. Chen et al., 2020; Harada et al., 2015). Impairment of the NMD pathway could alleviate developmental defects by adjusting transcriptional dynamics in a compensatory manner (Isken & Maquat, 2008).

CDE-1's role as a strong suppressor may extend beyond histone mRNA regulation. CDE-1 uridylates siRNAs bound by CSR-1 (van Wolfswinkel et al., 2009). CSR-1 pathway ensures proper transcriptional reprogramming during MZT, with its absence leading to premature embryonic transcription in developing oocytes (Fassnacht et al., 2018). CSR-1 is also implicated with fine-tuning germline transcripts levels in embryos, correlating with the abundance of CSR-1-bound 22G RNAs (Gerson-Gurwitz et al., 2016). CDE-1's activity in uridylating CSR-1-bound siRNAs might modulate CSR-1 activity during MZT, enhancing transcriptional tuning to counteract the effects of histone mRNA depletion. These ideas could explain why CDE-1 depletion alone is sufficient to rescue embryonic development in *tost-1* null mutants, while other suppressors show limited or no effect.

PETISCO possible connection with transcription termination

PETISCO binds RD histone mRNAs very specifically in the embryos and it is required for their stabilization in both the adult germline and early embryos. Surprisingly, when we immunoprecipitated TOST-1 to identify potential interactors, several proteins involved in transcription were found, including subunits of the Integrator complex (**Figure R36**). The Integrator complex, composed of 15 proteins (13 identified in *C. elegans*), has been recently suggested to play a role in transcription elongation regulation for most mRNAs and as quality control mechanism for short mRNAs (Garland & Jensen, 2024; Welsh & Gardini, 2022). Its most well-known function, however, is in the termination of snRNAs (Baillat et al., 2005). More recently, Integrator has also been implicated in the transcription termination of piRNAs/21U RNAs in *C. elegans* (Beltran et al., 2020).

In our experiment, we also found NABP1 (human SSB1), which along with INST3, NABP2 (human SSB2) and INIP, forms the SOSS complex involved in DNA damage response in human cells (Ren et al., 2014). Both NABP2 and INIP interact with INTS3, coordinating the activities of the SOSS

and Integrator complexes during transcription termination (Ren et al., 2014; Xu et al., 2023). While *C. elegans* lacks NABP2 and INIP, AlphaFold3 predictions suggest a potential interaction between ERH-2 and INTS-3, which could compensate for the absence of INIP in *C. elegans* (data not shown, acquired by João Marques). If this interaction is indeed real, it is likely to be transcript-specific, happening only with piRNAs and perhaps histone mRNAs, as ERH-2 was not previously found to enrich transcription-related proteins in other IP-MS experiments (Cordeiro Rodrigues et al., 2019; Zeng et al., 2019). ERH-2 is part of the highly conserved enhancer of rudimentary (ERH) family, comprised by proteins known to interact with various RNA metabolism proteins (Kozlowski, 2023). Interestingly, ERH in humans was detected using an affinity purification followed by mass spectrometry (AP-MS) method of SPT5 as well as other affinity assays with other proteins involved in transcription (Kozlowski, 2023; Y. T. Kwak et al., 2003). This is interesting because SPT5, like Integrator, acts in the promotor-proximal pausing by RNA Pol II before committing for productive elongation (Decker, 2021). ERH-2 involvement in Integrator and PETISCO interaction remains a potential area of further exploration

Interestingly, Integrator has recently been found to be required for the transcription termination of piRNA/21U RNAs in *C. elegans,* similar to the role of Integrator in snRNAs termination in other species (Beltran et al., 2020; Berkyurek, Furlan et al., 2021). While it remains unclear when and how PETISCO binds 21U RNA precursors, it is possible that this binding occurs after transcription termination, positioning PETISCO and Integrator close in both time and space. Since PETISCO binds both 21U RNAs and RD histone mRNAs, and Integrator is enriched in TOST-1 pull-down experiments, it is tempting to speculate that Integrator might also play a role in histone mRNA transcription in *C. elegans*. However, this involvement has only been reported once, in mammalian cells (Skaar et al., 2015). In that study, INTS3 and NABP2 were found to bind RD histone transcripts, and depletion of INTS3 affected the processing of their 3'UTR, leading to an increase in unprocessed histone transcripts and polyadenylated histones (Skaar et al., 2015). This might be explained because the transcription termination of RD histone mRNAs is tightly coupled with 3'-end processing. For example, disruption of the processing machinery, such as through U7 snRNA gene mutations, results in polyadenylation of RD histone mRNAs (Godfrey et al., 2006), due to extended transcription. Another possibility is that failure in transcription termination would result in RNA Pol II readthrough, causing transcription to proceed into downstream regions (Crisp et al., 2018; Miki et al., 2017). However, the precise mechanisms connecting these processes remains unclear.

Furthermore, *C. elegans* lacks U7 snRNP and the LSm associated proteins involved in histone 3' end processing (López & Samuelsson, 2008), raising the question of how this processing occurs in *C. elegans*. One possibility is that CSR-1 in involved in this mechanism (Avgousti et al., 2012). However, another option is that PETISCO plays a role. PETISCO has been shown to bind SL1 snRNAs, which could potentially target histone mRNAs for processing (Cordeiro Rodrigues et al., 2019). Interestingly, these snRNAs accumulate in mutants of *tofu-6*, *erh-2* and *tost-1*, suggesting a potential role in their processing. However, we do not think this function is directly related to Integrator's role in snRNAs biogenesis.

An alternative hypothesis for the role of PETISCO is that PETISCO does not directly affect RD histone mRNA transcription or processing but instead stabilizes these transcripts during germline development in the adult gonad, as suggested in the above sections. In this model, PETISCO could help transport the transcripts from the transcription site in the nucleus to the cytoplasm or be loaded in the P granules with the nascent transcripts. One option for how this could work would be via dissociation of the SOSS complex from the Integrator and RNA Pol II. Indeed, it was recently suggested that SOSS can dissociate from the core Integrator complex at the transcription site (Fianu et al., 2024; Xu et al., 2023). To address this hypothesis, it will be crucial to examine the precise localization of these proteins. PETISCO is primarily localised in P granules, but under certain genetic conditions, some of its components can be shuttled to the nucleus (Zeng et al., 2019). Although these observations were made using a transgene rather than endogenously tagged proteins, they suggest that PETISCO may enter the nucleus where it could bind to its substrates transcripts, or they could be brought to PETISCO in the P granules.

Lastly, we were unable to confirm direct interactions between PETISCO proteins and INTS-3, INTS-6, NABP-1, SPT-4 and SPT-5 using the Y2H system, nor between TOST-1 and INTS-6 through co-IP experiments (**Figure R36, R37**). These negative results could be due to the absence of direct interactions, the need for specific biological conditions in Y2H, or weak/transient interactions in co-IP. Further experiments, testing different experimental conditions and protein domains, are necessary to better understand these interactions. However, we must also consider the possibility that these connections may not be biologically relevant.

PETISCO: one complex, two flavours

PETISCO components were initially identified as interactors of PID-1, assembling into a complex required for the stabilization of 21U RNAs precursors, along with PID-1(Cordeiro Rodrigues et

al., 2019; de Albuquerque et al., 2014; Zeng et al., 2019). TOST-1 was also found to interact with PETISCO components, but in a mutually exclusive matter with PID-1 (Perez-Borrajero et al., 2021). In this study, we have shown that PETISCO with TOST-1 binds RD histone mRNAs and it is needed for their stabilization in the gonad and early embryos, similar to its function with piRNA/21U RNA precursors. Despite these insights, several questions remain, particularly regarding the dual functions and substrates of PETISCO. Specifically, the factors that determine PETISCO's RNA-binding specificity, as explored in the sections above, but also the precise roles of PID-1 and TOST-1, are still unclear.

One hypothesis is that differential expression patterns of PID-1 and TOST-1 influence PETISCO's functions in a temporally regulated manner. PID-1 is expressed predominantly in the distal gonad and pachytene region of the adult, while TOST-1 is more strongly expressed in the diplotene and diakinesis stages but also in embryos (Cordeiro Rodrigues et al., 2019; X. Wang et al., 2021; Zeng et al., 2019). piRNAs are expressed in the germline from L3 and are mostly localized to the distal and pachytene regions of the adult gonad, overlapping with PID-1 expression (Weick et al., 2014). Similarly, RD histone mRNAs are predominantly expressed in the pachytene region (personal communication Geraldine Seydoux). However, while piRNA/21U RNA precursors are processed and handed to PRG-1 in the same region of transcription and processing (based on PRG-1 expression), most RD histone mRNAs need to be preserved for deposition into the embryo, which aligns with PETISCO and TOST-1 localisation. More detailed microscopic analysis is required to assess the precise expression pattern of PID-1 and TOST-1, but it is possible that they overlap in the pachytene region (**Figure D7**). This raises the question of how substrates are selected, especially since neither PID-1 nor TOST-1 appears to possess RNA-binding domains that would directly confer selectivity. Based on experiments already discussed in this study, we suggest that the RD histone mRNA stem-loop can confer this specificity.

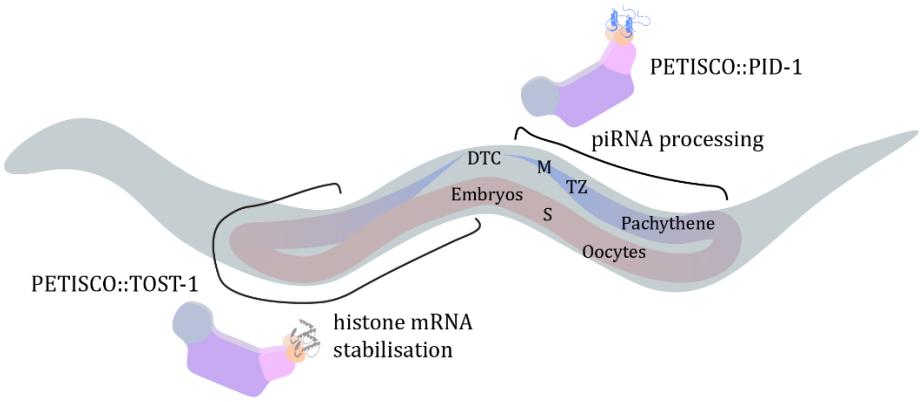

Figure D7 | Schematic representation of PETISCO::PID-1 and PETISCO::TOST-1 localisation in the adult germline. The gradient in the germline illustrates the suggested levels of the two PETISCO versions, corresponding to their respective functions. Blue represents PETISCO::PID-1, and brown PETISCO::TOST-1. In the pachythene region, both versions are proposed to be present. DTC, distal tip cell; M, mitotic region; TZ, transition zone; S, spermatheca.

Another interesting observation is the competition between the two versions of PETISCO. This can be observed when either PID-1 or TOST-1 is depleted. In *tost-1* hypomorphic mutants, adults depleted of PID-1 exhibit a slight increase in progeny viability (**Figure R6**) and a small increase in histone mRNA expression (**Figure R30, R31**). However, the phenotypes in *tost-1* null mutants remain unchanged. We propose that in the *tost-1* hypomorphic mutant, in the presence of wild-type PID-1, PETISCO is normally dedicated to stabilizing 21U RNA precursors, reducing its availability for TOST-1-related functions. When PID-1 is depleted, more "free" PETISCO is available to bind the hypomorphic TOST-1 mutant that is still able to provide partial functionality. The additional available PETISCO may thus allow increased TOST-1 functionality, resulting in some rescue of the phenotype. Furthermore, since PID-1 depletion does not rescue the *tost-1* null phenotype, it suggests that PETISCO alone cannot fully carry out its functions without TOST-1 binding. Interestingly, in *tost-1* mutants, an increase in 21U RNA levels has been reported (Cordeiro Rodrigues et al., 2019; Zeng et al., 2019). This suggests that during certain stages of development, PID-1 and TOST-1 are expressed concurrently and can bind to PETISCO, further supporting the idea that PETISCO functions require substrate specificity and it is not only based on the overall expression of its substrates and ligand proteins.

What is the ancestral function of PETISCO?

An intriguing question arising from the study of PETISCO is its evolutionary origin and how its functions diversified. TOST-1 is evolutionary more conserved than PID-1, though both are

exclusively found in nematodes (Cordeiro Rodrigues et al., 2019). TOST-1 is present in Clade III nematodes along with TOFU-6, PID-3, IFE-3, and ERH-1, whereas PID-1 and ERH-2 appear only from Clade V, coinciding with the emergence of PRDE-1 and PRG-1 (Cordeiro Rodrigues et al., 2019). IFE-3 and the ERH protein family, however, are conserved across all eukaryotes, suggesting that PETISCO, together with PID-1, represents a specialization of pre-existing molecular machinery for the 21U RNA pathway. Biochemical evidence indicates that TOST-1 can outcompete PID-1 for PETISCO binding when expressed in excess (Perez-Borrajero et al., 2021). Collectively, these observations suggest that PETISCO and TOST-1 functions are more ancestral than those involving PID-1. However, the precise point at which PETISCO acquired its essential role in embryonic development remains unknown.

Evidence from multiple lines of research supports the idea that existing cellular machinery, particularly related to snRNA pathways, was adapted and specialized for piRNA biogenesis (Beltran et al., 2019; Kasper et al., 2014; Weng et al., 2019). For instance, the USTC, a complex involved in piRNA biogenesis, incorporates SNPC-4, a transcription factor previously identified as part of an ancient complex for snRNA transcription (Jawdekar & Henry, 2008; Kasper et al., 2014; Weng et al., 2019). Similarly, the transcription termination of piRNAs and snRNAs is regulated by the Integrator complex, highlighting the shared evolutionary roots of these pathways (Baillat et al., 2005; Beltran et al., 2020).

Interestingly, snRNAs and histone mRNAs share several features, including tightly coupled termination and 3’-end processing. Both types of transcripts are processed by mechanisms distinct from canonical mRNA termination pathways. Their precursors require trimming to produce mature transcripts, and both are insensitive to the common termination components used for other mRNAs (Rodríguez-Molina et al., 2023). These shared features suggest a possible ancestral connection between the processing pathways of RD histone mRNAs and snRNAs, with PETISCO potentially acting as a common factor. PETISCO's ability to bind both histone mRNAs and SL snRNAs, and its more recent role in piRNA/21U RNA precursor stabilization, may reflect a gradual evolutionary adaptation.

An additional level of commonality may lie in the regulation of transcript termination by transcript length. Both snRNAs and RD histone mRNAs rely on NELF activity for transcriptional termination regulation (Narita et al., 2007; Yamamoto et al., 2014). In the case of snRNAs, this process also depends on the Integrator complex (Yamamoto et al., 2014). While Integrator's involvement in RD histone transcription termination has been suggested (Skaar et al., 2015), more evidence is needed. If true, factors such as the transcript length and promoter regions may

play a decisive role in transcription termination regulation (Dasilva et al., 2021; Lykke-Andersen et al., 2021; Sabath et al., 2024). This can also be seen in the regulation of snRNA transcription termination (Ramamurthy et al., 1996). However, since PETISCO does not bind other small transcripts, these factors may not be in the origin of the ancestral PETISCO functions.

A final interesting evolutionary aspect that might lead to a better understanding of the ancestral functions of PETISCO is related to the conservation of RD histone mRNA 3' end regulation. Initially thought to be exclusive to metazoans, the stem-loop structure of RD histone transcripts has been identified in some protozoa, including *Trichomonas* and *Euglenozoa* genera (López & Samuelsson, 2008). Most of these species also express SLBP and possess conserved nucleotides in the stem-loop structures required for the SLBP recognition, such as those found in metazoans (Battle & Doudna, 2001; López & Samuelsson, 2008). However, other components, such as the U7 snRNP and the U7-specific Lsm10 or Lsm11 proteins are restricted to metazoans, with exceptions in *Caenorhabditis*, some insects and sea anemonas (López & Samuelsson, 2008). This suggests that histone mRNA termination and processing mechanisms in these organisms have adapted from other pathways, possibly those involved in snRNA transcription. Interestingly, PETISCO and TOST-1 have been shown to bind SL1 snRNAs and participate in their processing. This supports the idea that PETISCO has the capacity to process diverse transcript types, including histone mRNAs, snRNAs, and more recently, piRNA/21U RNA precursors. Understanding how PETISCO evolved to handle these distinct functions will be key to uncovering its ancestral role and its specialization in nematode development.

Limitations of the study

In this study, we have confidently demonstrated that PETISCO binds RD histone mRNAs in embryos and that the loss of PETISCO or TOST-1 profoundly disrupts histone mRNAs expression in the adult gonad, potentially being the cause for embryonic lethality. However, certain limitations remain, primarily due to technical challenges.

One key limitation is our inability to conclusively determine the effect of PETISCO on maternal RD histone mRNAs in early embryos. This is largely due to the difficulty in isolating sufficient early embryos, prior to ZGA, for omics-level analyses and the unique regulatory mechanism of RD histone genes, which render tagged versions of these genes unreliable. A critical experiment to address this limitation would involve quantifying wild-type RD histone transcript levels

specifically in early embryos. Such data would clarify the impact of PETISCO on maternal histone mRNA stability.

Additionally, the distinct mechanisms governing RD histone mRNA 3' end processing and the influence of the splicing in gene expression regulation, make it challenging to conclude which, if any, assembled histone transgenes best replicate endogenous regulation and expression. This limitation affects our ability to test different mutants or knockdowns with confidence.

Another limitation is the reliance on CDE-1 as an effector in RD histone mRNA degradation pathway. While CDE-1's role in regulating RD histone mRNAs expression is evident, its involvement in the RNAi pathway of CSR-1 and its essential role in germline development, complicate interpretations. To address this, other proteins implicated in RD histone mRNA degradation should be explored, particularly to validate their involvement in regulating histone mRNA expression and stability.

Concluding remarks

PETISCO, initially found as part of the *C. elegans* piRNAs biogenesis pathway, plays an essential role in embryonic development through a piRNA-independent manner. In this study, we identified RD-histone transcripts as substrates for PETISCO, which likely stabilizes them in the germline of adult worms. This stabilization enables the deposition into the embryo, where RD histones are utilized during the first embryonic divisions before the zygotic transcripts start to be expressed. RD histone genes are known to be cell-cycle regulated; however, little is understood about how these transcripts are stabilized in the maternal germline, where their regulation is no longer cell-cycle dependent.

We propose a model in which maternal RD histone mRNA stabilization occurs through the prevention of premature translation and/or degradation, through their interaction with PETISCO (**Figure D8**). Furthermore, our findings provide insights into the cause of embryonic arrest in PETISCO mutants, which is possibly a secondary effect of maternal RD histone misregulation. We also hypothesize that PETISCO's role in RD histone homeostasis represents its ancient function in nematodes, with its subsequent adaptation for the piRNA pathway, which was also already suggested to be from the snRNA regulation intervenients.

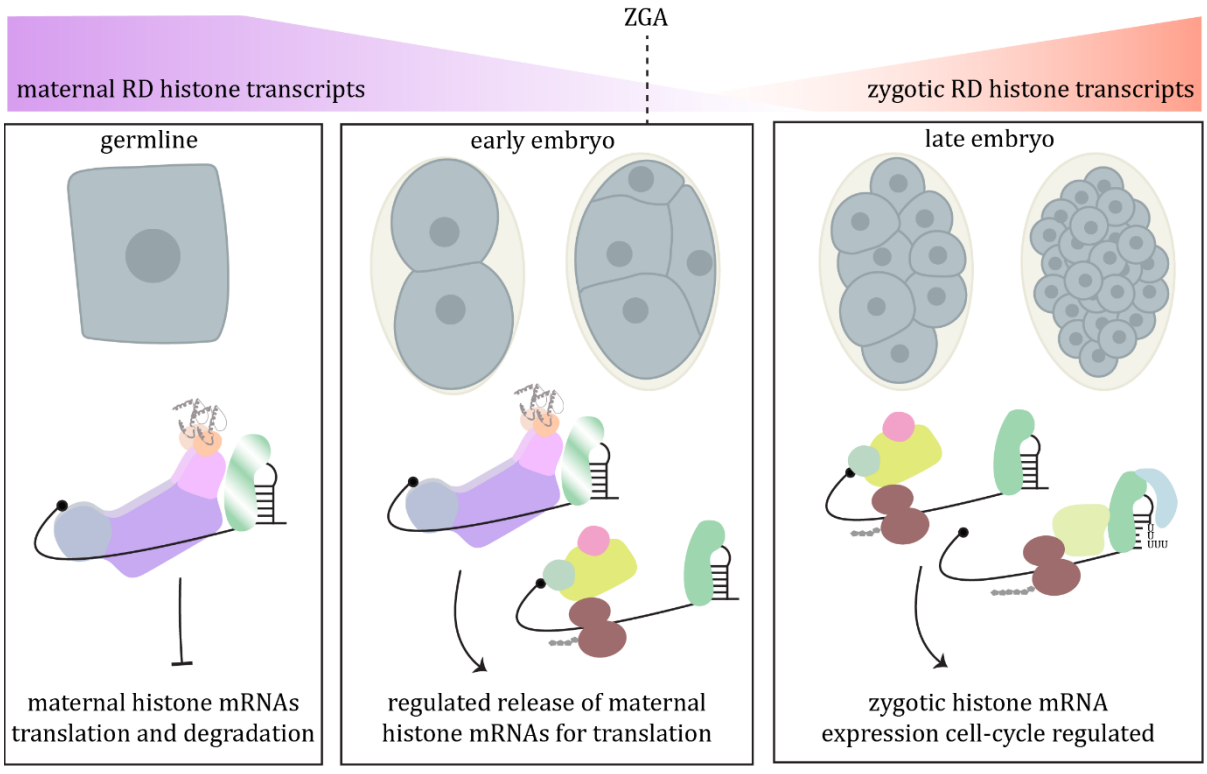

Figure D8 | Proposed model for the function of PETISCO::TOST-1 in the regulation of maternal RD histone mRNAs. In the germline, where histone mRNAs are expressed for subsequent deposition into the embryo and are not cell-cycle

regulated, PETISCO stabilizes these transcripts by preventing their premature translation or degradation. Upon fertilization and during the initial embryonic divisions, the maternal histone transcripts are released for translation to incoorporrate the newly synthetized DNA replication. After zygotic genome activation, newly transcribed RD histone mRNAs become cell-cycle regulated and no longer require PETISCO stabilization.

Despite these advances, many questions remain to be answered, particularly regarding PETISCO's interaction with histone transcripts and the functional duality of PETISCO with either TOST-1 or PID-1. Key questions include: What determines PETISCO's specificity for binding piRNA precursors versus RD histone transcripts? How do the two PETISCO complexes are regulated and function in the germline? What mechanisms underlie PETISCO's loading and release of transcripts? Does PETISCO also play a role in zygotic RD histone regulation?

Although this story is far from being complete, it offers novel insights into the regulation of maternal RD histone mRNAs in *C. elegans.* It highlights PETISCO as a specialized RNA-binding complex that stabilizes unstable transcripts in the germline, advancing our understanding of RNA regulation during early embryogenesis.

List of References

Aanes, H., Østrup, O., Andersen, I. S., Moen, L. F., Mathavan, S., Collas, P., & Alestrom, P. (2013). Differential transcript isoform usage pre- and post-zygotic genome activation in zebrafish. *BMC Genomics*, *14*(1), 1–15.

Aanes, H., Winata, C. L., Lin, C. H., Chen, J. P., Srinivasan, K. G., Lee, S. G. P., Lim, A. Y. M., Hajan, H. S., Collas, P., Bourque, G., Gong, Z., Korzh, V., Aleström, P., & Mathavan, S. (2011). Zebrafish mRNA sequencing deciphers novelties in transcriptome dynamics during maternal to zygotic transition. *Genome Research*, *21*(8), 1328–1338.

Adams, M. D., Celniker, S. E., Holt, R. A., Evans, C. A., Gocayne, J. D., Amanatides, P. G., Scherer, S. E., Li, P. W., Hoskins, R. A., Galle, R. F., George, R. A., Lewis, S. E., Richards, S., Ashburner, M., Henderson, S. N., Sutton, G. G., Wortman, J. R., Yandell, M. D., Zhang, Q., … Craig Venter, J. (2000). The genome sequence of Drosophila melanogaster. *Science (New York, N.Y.)*, *287*(5461), 2185–2195.

Adamson, E. D., & Woodland, H. R. (1977). Changes in the rate of histone synthesis during oocyte maturation and very early development of Xenopus laevis. *Developmental Biology*, *57*(1), 136–149.

Adelman, K., & Lis, J. T. (2012). Promoter-proximal pausing of RNA polymerase II: emerging roles in metazoans. *Nature Reviews Genetics 2012 13:10*, *13*(10), 720–731.

Akay, A., Di Domenico, T., Suen, K. M., Nabih, A., Parada, G. E., Larance, M., Medhi, R., Berkyurek, A. C., Zhang, X., Wedeles, C. J., Rudolph, K. L. M., Engelhardt, J., Hemberg, M., Ma, P., Lamond, A. I., Claycomb, J. M., & Miska, E. A. (2017). The Helicase Aquarius/EMB-4 Is Required to Overcome Intronic Barriers to Allow Nuclear RNAi Pathways to Heritably Silence Transcription. *Developmental Cell*, *42*(3), 241-255.e6.

Akkouche, A., Mugat, B., Barckmann, B., Varela-Chavez, C., Li, B., Raffel, R., Pélisson, A., & Chambeyron, S. (2017). Piwi Is Required during Drosophila Embryogenesis to License Dual-Strand piRNA Clusters for Transposon Repression in Adult Ovaries. *Molecular Cell*, *66*(3), 411-419.e4.

Albig, W., Kioschis, P., Poustka, A., Meergans, K., & Doenecke, D. (1997). Human histone gene organization: nonregular arrangement within a large cluster. *Genomics*, *40*(2), 314–322.

Alcazar, R. M., Lin, R., & Fire, A. Z. (2008). Transmission Dynamics of Heritable Silencing Induced by Double-Stranded RNA in Caenorhabditis elegans. *Genetics*, *180*(3), 1275–1288.

Aljohani, M. D., El Mouridi, S., Priyadarshini, M., Vargas-Velazquez, A. M., & Frøkjær-Jensen, C. (2020). Engineering rules that minimize germline silencing of transgenes in simple extrachromosomal arrays in C. elegans. *Nature Communications*, *11*(1), 1–14.

Allan, C., Burel, J. M., Moore, J., Blackburn, C., Linkert, M., Loynton, S., MacDonald, D., Moore, W. J., Neves, C., Patterson, A., Porter, M., Tarkowska, A., Loranger, B., Avondo, J., Lagerstedt, I., Lianas, L., Leo, S., Hands, K., Hay, R. T., … Swedlow, J. R. (2012). OMERO: flexible, model-driven data management for experimental biology. *Nature Methods 2012 9:3*, *9*(3), 245–253.

Allard, P., Yang, Q., Marzluff, W. F., & Clarke, H. J. (2005). The stem-loop binding protein regulates translation of histone mRNA during mammalian oogenesis. *Developmental Biology*, *286*(1), 195–206.

Allen, M. A., Hillier, L. D. W., Waterston, R. H., & Blumenthal, T. (2011). A global analysis of C. elegans trans-splicing. *Genome Research*, *21*(2), 255–264.

Almeida, M. V., Andrade-Navarro, M. A., & Ketting, R. F. (2019). Function and evolution of nematode RNAi pathways. In *Non-coding RNA* (Vol. 5, Issue 1).

Ameres, S. L., Horwich, M. D., Hung, J. H., Xu, J., Ghildiyal, M., Weng, Z., & Zamore, P. D. (2010). Target RNA-directed trimming and tailing of small silencing RNAs. *Science*, *328*(5985), 1534–1539.

Amiri, A., Keiper, B. D., Kawasaki, I., Fan, Y., Kohara, Y., Rhoads, R. E., & Strome, S. (2001). An isoform of eIF4E is a component of germ granules and is required for spermatogenesis in C. elegans. *Development (Cambridge, England)*, *128*(20), 3899–3912.

Amodeo, A. A., Jukam, D., Straight, A. F., & Skotheim, J. M. (2015). Histone titration against the genome sets the DNA-to-cytoplasm threshold for the Xenopus midblastula transition. *Proceedings of the National Academy of Sciences of the United States of America*, *112*(10), E1086–E1095.

Anamika, K., Gyenis, À., Poidevin, L., Poch, O., & Tora, L. (2012). RNA Polymerase II Pausing Downstream of Core Histone Genes Is Different from Genes Producing Polyadenylated Transcripts. *PLOS ONE*, *7*(6), e38769.

Anantharaman, V., Koonin, E. V., & Aravind, L. (2002). Comparative genomics and evolution of proteins involved in RNA metabolism. *Nucleic Acids Research*, *30*(7), 1427.

Anderson, K. V., & Lengyel, J. A. (1980). Changing rates of histone mRNA synthesis and turnover in Drosophila embryos. *Cell*, *21*(3), 717–727.

Armstrong, C., Passanisi, V. J., Ashraf, H. M., & Spencer, S. L. (2023). Cyclin E/CDK2 and feedback from soluble histone protein regulate the S phase burst of histone biosynthesis. *Cell Reports*, *42*(7).

Arnold, A., Rahman, M. M., Lee, M. C., Muehlhaeusser, S., Katic, I., Gaidatzis, D., Hess, D., Scheckel, C., Wright, J. E., Stetak, A., Boag, P. R., & Ciosk, R. (2014). Functional characterization of C. elegans Y-box-binding proteins reveals tissue-specific functions and a critical role in the formation of polysomes. *Nucleic Acids Research*, *42*(21), 13353–13369.

Arnold, D. R., Françon, P., Zhang, J., Martin, K., & Clarke, H. J. (2008). Stem–loop binding protein expressed in growing oocytes is required for accumulation of mRNAs encoding histones H3 and H4 and for early embryonic development in the mouse. *Developmental Biology*, *313*(1), 347–358.

Arribere, J. A., Bell, R. T., Fu, B. X. H., Artiles, K. L., Hartman, P. S., & Fire, A. Z. (2014). Efficient marker-free recovery of custom genetic modifications with CRISPR/Cas9 in Caenorhabditis elegans. *Genetics*, *198*(3), 837–846.

Arribere, J. A., & Fire, A. Z. (2018). Nonsense mRNA suppression via nonstop decay. *ELife*, *7*.

Arribere, J. A., Kuroyanagi, H., & Hundley, H. A. (2020). mRNA Editing, Processing and Quality Control in Caenorhabditis elegans. *Genetics*, *215*(3), 531–568.

Ashe, A., Sapetschnig, A., Weick, E.-M., Mitchell, J., Bagijn, M. P., Cording, A. C., Doebley, A.-L., Goldstein, L. D., Lehrbach, N. J., Le Pen, J., Pintacuda, G., Sakaguchi, A., Sarkies, P., Ahmed, S., & Miska, E. A. (2012). piRNAs can trigger a multigenerational epigenetic memory in the germline of C. elegans. *Cell*, *150*(1), 88–99.

Avgousti, D. C., Palani, S., Sherman, Y., & Grishok, A. (2012). CSR-1 RNAi pathway positively regulates histone expression in C. elegans. *EMBO Journal*, *31*(19), 3821–3832.

Baillat, D., Hakimi, M. A., Näär, A. M., Shilatifard, A., Cooch, N., & Shiekhattar, R. (2005). Integrator, a Multiprotein Mediator of Small Nuclear RNA Processing, Associates with the C-Terminal Repeat of RNA Polymerase II. *Cell*, *123*(2), 265–276.

Bao, Z., Zhao, Z., Boyle, T. J., Murray, J. I., & Waterston, R. H. (2008). Control of Cell Cycle Timing during C. elegans Embryogenesis. *Developmental Biology*, *318*(1), 65.

Barcaroli, D., Bongiorno-Borbone, L., Terrinoni, A., Hofmann, T. G., Rossi, M., Knight, R. A., Matera, A. G., Melino, G., & De Laurenzi, V. (2006). FLASH is required for histone transcription and S-phase progression. *Proceedings of the National Academy of Sciences of the United States of America*, *103*(40), 14808–14812.

Barckmann, B., Pierson, S., Dufourt, J., Papin, C., Armenise, C., Port, F., Grentzinger, T., Chambeyron, S., Baronian, G., Desvignes, J. P., Curk, T., & Simonelig, M. (2015). Aubergine iCLIP Reveals piRNA-Dependent Decay of mRNAs Involved in Germ Cell Development in the Early Embryo. *Cell Reports*, *12*(7), 1205–1216.

Barckmann, B., & Simonelig, M. (2013). Control of maternal mRNA stability in germ cells and early embryos. *Biochimica et Biophysica Acta*, *1829*(6–7), 714–724.

Barstead, R., Moulder, G., Cobb, B., Frazee, S., Henthorn, D., Holmes, J., Jerebie, D., Landsdale, M., Osborn, J., Pritchett, C., Robertson, J., Rummage, J., Stokes, E., Vishwanathan, M., Mitani, S., Gengyo-Ando, K., Funatsu, O., Hori, S., Imae, R., … Zapf, R. (2012). Large-scale screening for targeted knockouts in the caenorhabditis elegans genome. *G3: Genes, Genomes, Genetics*, *2*(11), 1415–1425.

Bartel, D. P. (2018). Metazoan MicroRNAs. *Cell*, *173*(1), 20–51.

Barucci, G., Cornes, E., Singh, M., Li, B., Ugolini, M., Samolygo, A., Didier, C., Dingli, F., Loew, D., Quarato, P., & Cecere, G. (2020). Small RNA-mediated transgenerational silencing of histone genes impairs fertility in piRNA mutants. *Nature Cell Biology*.

Batchelder, C., Dunn, M. A., Choy, B., Suh, Y., Cassie, C., Shim, E. Y., Shin, T. H., Mello, C., Seydoux, G., & Blackwell, T. K. (1999). Transcriptional repression by the Caenorhabditis elegans germ-line protein PIE-1. *Genes & Development*, *13*(2), 202–212.

Bateman, A. (2019). UniProt: a worldwide hub of protein knowledge. *Nucleic Acids Research*, *47*(D1), D506–D515.

Batista, P. J., Ruby, J. G., Claycomb, J. M., Chiang, R., Fahlgren, N., Kasschau, K. D., Chaves, D. A., Gu, W., Vasale, J. J., Duan, S., Conte, D., Luo, S., Schroth, G. P., Carrington, J. C., Bartel, D. P., & Mello, C. C. (2008). PRG-1 and 21U-RNAs Interact to Form the piRNA Complex Required for Fertility in C. elegans. *Molecular Cell*, *31*(1), 67–78.

Battle, D. J., & Doudna, J. A. (2001). The stem-loop binding protein forms a highly stable and specific complex with the 3' stem-loop of histone mRNAs. *RNA (New York, N.Y.)*, *7*(1), 123–132.

Baugh, L. R., Hill, A. A., Slonim, D. K., Brown, E. L., & Hunter, C. P. (2003). Composition and dynamics of the Caenorhabditis elegans early embryonic transcriptome. *Development*, *130*(5), 889–900.

Begasse, M. L., Leaver, M., Vazquez, F., Grill, S. W., & Hyman, A. A. (2015). Temperature Dependence of Cell Division Timing Accounts for a Shift in the Thermal Limits of C. elegans and C. briggsae. *Cell Reports*, *10*(5), 647–653.

Beltran, T., Barroso, C., Birkle, T. Y., Stevens, L., Schwartz, H. T., Sternberg, P. W., Fradin, H., Gunsalus, K., Piano, F., Sharma, G., Cerrato, C., Ahringer, J., Martínez-Pérez, E., Blaxter, M., & Sarkies, P. (2019). Comparative Epigenomics Reveals that RNA Polymerase II Pausing and Chromatin Domain Organization Control Nematode piRNA Biogenesis. *Developmental Cell*, *48*(6), 793-810.e6.

Beltran, T., Pahita, E., Ghosh, S., Lenhard, B., & Sarkies, P. (2020). Integrator is recruited to promoter-proximally paused RNA Pol II to generate Caenorhabditis elegans piRNA precursors. *The EMBO Journal*.

Berkyurek, A. C., Furlan, G., Lampersberger, L., Beltran, T., Weick, E.-M., Nischwitz, E., Navarro, I. C., Braukmann, F., Akay, A., Price, J., Butter, F., Sarkies, P., & Miska, E. A. (2021). The RNA polymerase II subunit RPB-9 recruits the integrator complex to terminate Caenorhabditis elegans piRNA transcription. *The EMBO Journal*, *40*(5), e105565.

Bernard, F., Dargère, D., Rechavi, O., & Dupuy, D. (2023). Quantitative analysis of C. elegans transcripts by Nanopore direct-cDNA sequencing reveals terminal hairpins in non trans-spliced mRNAs. *Nature Communications 2023 14:1*, *14*(1), 1–11.

Bilinski, S. M., Kloc, M., & Tworzydlo, W. (2017). Selection of mitochondria in female germline cells: is Balbiani body implicated in this process? *Journal of Assisted Reproduction and Genetics*, *34*(11), 1405.

Billi, A. C., Alessi, A. F., Khivansara, V., Han, T., Freeberg, M., Mitani, S., & Kim, J. K. (2012). The Caenorhabditis elegans HEN1 Ortholog, HENN-1, Methylates and Stabilizes Select Subclasses of Germline Small RNAs. *PLoS Genetics*, *8*(4), e1002617.

Blackwell, T. K., & Walker, A. K. (2006). Transcription mechanisms. *WormBook : The Online Review of C. Elegans Biology*, 1–16.

Blumenthal, T. (2005). Trans-splicing and operons. *WormBook : The Online Review of C. Elegans Biology*, 1–9.

Blumenthal, T., Evans, D., Link, C. D., Guffanti, A., Lawson, D., Thierry-Mieg, J., Thierry-Mieg, D., Chiu, W. L., Duke, K., Kiraly, M., & Kim, S. K. (2002). A global analysis of Caenorhabditis elegans operons. *Nature 2002 417:6891*, *417*(6891), 851–854.

Boag, P. R., Atalay, A., Robida, S., Reinke, V., & Blackwell, T. K. (2008). Protection of specific maternal messenger RNAs by the P body protein CGH-1 (Dhh1/RCK) during Caenorhabditis elegans oogenesis. *The Journal of Cell Biology*, *182*(3), 543–557.

Boag, P. R., Nakamura, A., & Blackwell, T. K. (2005). A conserved RNA-protein complex component involved in physiological germline apoptosis regulation in C. elegans. *Development*, *132*(22), 4975–4986.

Boeck, M. E., Huynh, C., Gevirtzman, L., Thompson, O. A., Wang, G., Kasper, D. M., Reinke, V., Hillier, L. W., & Waterston, R. H. (2016). The time-resolved transcriptome of C. Elegans. *Genome Research*, *26*(10), 1441–1450.

Boland, A., Tritschler, F., Heimstädt, S., Izaurralde, E., & Weichenrieder, O. (2010). Crystal structure and ligand binding of the MID domain of a eukaryotic Argonaute protein. *EMBO Reports*, *11*(7), 522–527.

Borchers, C. H., Thapar, R., Petrotchenko, E. V., Torres, M. P., Speir, J. P., Easterling, M., Dominski, Z., & Marzluff, W. F. (2006). Combined top-down and bottom-up proteomics identifies a phosphorylation site in stem-loop-binding proteins that contributes to high-affinity RNA binding. *Proceedings of the National Academy of Sciences of the United States of America*, *103*(9), 3094–3099.

Bouvet, P., & Wolffe, A. (1994). A role for transcription and FRGY2 in masking maternal mRNA within Xenopus oocytes. *Cell*, *77*(6), 931–941.

Bowman, E. A., & Kelly, W. G. (2014). RNA Polymerase II transcription elongation and Pol II CTD Ser2 phosphorylation. *Nucleus*, *5*(3), 224–236.

Brauchle, M., Baumer, K., & Gönczy, P. (2003). Differential activation of the DNA replication checkpoint contributes to asynchrony of cell division in C. elegans embryos. *Current Biology*, *13*(10), 819–827.

Brennecke, J., Malone, C. D., Aravin, A. A., Sachidanandam, R., Stark, A., & Hannon, G. J. (2008). An epigenetic role for maternally inherited piRNAs in transposon silencing. *Science (New York, N.Y.)*, *322*(5906), 1387–1392.

Brenner, S. (1974). The genetics of Caenorhabditis elegans. *Genetics*, *77*(1), 71–94.

Brooks, L., Lyons, S. M., Mahoney, J. M., Welch, J. D., Liu, Z., Marzluff, W. F., & Whitfield, M. L. (2015). A multiprotein occupancy map of the mRNP on the 3' end of histone mRNAs. *RNA (New York, N.Y.)*, *21*(11), 1943–1965.

Buchbender, A., Mutter, H., Sutandy, F. X. R., Körtel, N., Hänel, H., Busch, A., Ebersberger, S., & König, J. (2020). Improved library preparation with the new iCLIP2 protocol. *Methods (San Diego, Calif.)*, *178*, 33–48.

Bulchand, S., Menon, S. D., George, S. E., & Chia, W. (2010). Muscle wasted: a novel component of the Drosophila histone locus body required for muscle integrity. *Journal of Cell Science*, *123*(16), 2697–2707.

Busch, A., Brüggemann, M., Ebersberger, S., & Zarnack, K. (2020). iCLIP data analysis: A complete pipeline from sequencing reads to RBP binding sites. *Methods*, *178*, 49–62.

Bushati, N., Stark, A., Brennecke, J., & Cohen, S. M. (2008). Temporal Reciprocity of miRNAs and Their Targets during the Maternal-to-Zygotic Transition in Drosophila. *Current Biology*, *18*(7), 501–506.

Cakmakci, N. G., Lerner, R. S., Wagner, E. J., Zheng, L., & Marzluff, W. F. (2008). SLIP1, a Factor Required for Activation of Histone mRNA Translation by the Stem-Loop Binding Protein. *Molecular and Cellular Biology*, *28*(3), 1182.

Camacho, C., Coulouris, G., Avagyan, V., Ma, N., Papadopoulos, J., Bealer, K., & Madden, T. L. (2009). BLAST+: Architecture and applications. *BMC Bioinformatics*, *10*(1), 1–9.

Campbell, A. C., & Updike, D. L. (2015). CSR-1 and P granules suppress sperm-specific transcription in the C. elegans germline. *Development (Cambridge)*, *142*(10), 1745–1755.

Campos, E. I., & Reinberg, D. (2009). Histones: Annotating chromatin. *Annual Review of Genetics*, *43*(Volume 43, 2009), 559–599.

Carthew, R. W., & Sontheimer, E. J. (2009). Origins and Mechanisms of miRNAs and siRNAs. *Cell*, *136*(4), 642.

Cassani, M., & Seydoux, G. (2022). Specialized germline P-bodies are required to specify germ cell fate in Caenorhabditis elegans embryos. *Development (Cambridge)*, *149*(21).

Chang, H., Yeo, J., Kim, J. gyun, Kim, H., Lim, J., Lee, M., Kim, H. H., Ohk, J., Jeon, H. Y., Lee, H., Jung, H., Kim, K. W., & Kim, V. N. (2018). Terminal Uridylyltransferases Execute Programmed Clearance of Maternal Transcriptome in Vertebrate Embryos. *Molecular Cell*, *70*(1), 72-82.e7.

Chari, S., Wilky, H., Govindan, J., & Amodeo, A. A. (2019a). Histone concentration regulates the cell cycle and transcription in early development. *Development (Cambridge)*, *146*(19).

Chari, S., Wilky, H., Govindan, J., & Amodeo, A. A. (2019b). Histone concentration regulates the cell cycle and transcription in early development. *Development (Cambridge)*, *146*(19).

Charlesworth, A. G., Seroussi, U., Lehrbach, N. J., Renaud, M. S., Sundby, A. E., Molnar, R. I., Lao, R. X., Willis, A. R., Woock, J. R., Aber, M. J., Diao, A. J., Reinke, A. W., Ruvkun, G., & Claycomb, J. M. (2021). Two isoforms of the essential C. elegans Argonaute CSR-1 differentially regulate sperm and oocyte fertility. *Nucleic Acids Research*, *49*(15), 8836–8865.

Chen, B., Gilbert, L. A., Cimini, B. A., Schnitzbauer, J., Zhang, W., Li, G. W., Park, J., Blackburn, E. H., Weissman, J. S., Qi, L. S., & Huang, B. (2013). Dynamic imaging of genomic loci in living human cells by an optimized CRISPR/Cas system. *Cell*, *155*(7), 1479–1491.

Chen, D., Chen, Q. Y., Wang, Z., Zhu, Y., Kluz, T., Tan, W., Li, J., Wu, F., Fang, L., Zhang, X., He, R., Shen, S., Sun, H., Zang, C., Jin, C., & Costa, M. (2020a). Polyadenylation of Histone H3.1 mRNA Promotes Cell Transformation by Displacing H3.3 from Gene Regulatory Elements. *IScience*, *23*(9).

Chen, D., Chen, Q. Y., Wang, Z., Zhu, Y., Kluz, T., Tan, W., Li, J., Wu, F., Fang, L., Zhang, X., He, R., Shen, S., Sun, H., Zang, C., Jin, C., & Costa, M. (2020b). Polyadenylation of Histone H3.1 mRNA Promotes Cell Transformation by Displacing H3.3 from Gene Regulatory Elements. *IScience*, *23*(9).

Chen, J., Ezzeddine, N., Waltenspiel, B., Albrecht, T. R., Warren, W. D., Marzluff, W. F., & Wagner, E. J. (2012). An RNAi screen identifies additional members of the Drosophila Integrator complex and a requirement for cyclin C/Cdk8 in snRNA 3'-end formation. *RNA*, *18*(12), 2148–2156.

Chen, Q., Zhang, X., Shi, J., Yan, M., & Zhou, T. (2021). Origins and evolving functionalities of tRNA-derived small RNAs. *Trends in Biochemical Sciences*, *46*(10), 790–804. https://doi.org/10.1016/J.TIBS.2021.05.001

Chiu, J., March, P. E., Lee, R., & Tillett, D. (2004). Site-directed, Ligase-Independent Mutagenesis (SLIM): a single-tube methodology approaching 100% efficiency in 4 h. *Nucleic Acids Research*, *32*(21).

Chiu, J., Tillett, D., Dawes, I. W., & March, P. E. (2008). Site-directed, Ligase-Independent Mutagenesis (SLIM) for highly efficient mutagenesis of plasmids greater than 8kb. *Journal of Microbiological Methods*, *73*(2), 195–198.

Chivu, A. G., Abuhashem, A., Barshad, G., Rice, E. J., Leger, M. M., Vill, A. C., Wong, W., Brady, R., Smith, J. J., Wikramanayake, A. H., Arenas-Mena, C., Brito, I. L., Ruiz-Trillo, I., Hadjantonakis, A.-K., Lis, J. T., Lewis, J. J., & Danko, C. G. (2023). Evolution of promoter-proximal pausing enabled a new layer of transcription control. *Research Square*.

Chodchoy, N., Pandey, N. B., & Marzluff, W. F. (1991). An intact histone 3'-processing site is required for transcription termination in a mouse histone H2a gene. *Molecular and Cellular Biology*, *11*(1), 497.

Choe, J., Ahn, S. H., & Kim, Y. K. (2014a). The mRNP remodeling mediated by UPF1 promotes rapid degradation of replication-dependent histone mRNA. *Nucleic Acids Research*, *42*(14), 9334–9349.

Choe, J., Ahn, S. H., & Kim, Y. K. (2014b). The mRNP remodeling mediated by UPF1 promotes rapid degradation of replication-dependent histone mRNA. *Nucleic Acids Research*, *42*(14), 9334–9349.

Cho, E. J., Takagi, T., Moore, C. R., & Buratowski, S. (1997). mRNA capping enzyme is recruited to the transcription complex by phosphorylation of the RNA polymerase II carboxy-terminal domain. *Genes & Development*, *11*(24), 3319–3326.

Chul Kwon, S., Jang, H., Shen, S., Baek, S. C., Kim, K., Yang, J., Kim, J., Kim, J. S., Wang, S., Shi, Y., Li, F., & Narry Kim, V. (2020). ERH facilitates microRNA maturation through the interaction with the N-terminus of

DGCR8. *Nucleic Acids Research*, *48*(19), 11097–11112.

Chuma, S., Hosokawa, M., Tanaka, T., & Nakatsuji, N. (2009). Ultrastructural characterization of spermatogenesis and its evolutionary conservation in the germline: Germinal granules in mammals. *Molecular and Cellular Endocrinology*, *306*(1–2), 17–23.

Claycomb, J. M., Batista, P. J., Pang, K. M., Gu, W., Vasale, J. J., van Wolfswinkel, J. C., Chaves, D. A., Shirayama, M., Mitani, S., Ketting, R. F., Conte, D., & Mello, C. C. (2009). The Argonaute CSR-1 and its 22G-RNA cofactors are required for holocentric chromosome segregation. *Cell*, *139*(1), 123–134.

Cohen-Fix, O., & Askjaer, P. (2016). Cell Biology of the Caenorhabditis elegans Nucleus. *Genetics*, *205*(1), 25.

Collart, C., Allen, G. E., Bradshaw, C. R., Smith, J. C., & Zegerman, P. (2013). Titration of four replication factors is essential for the Xenopus laevis midblastula transition. *Science*, *341*(6148), 893–896.

Concordet, J. P., & Haeussler, M. (2018). CRISPOR: intuitive guide selection for CRISPR/Cas9 genome editing experiments and screens. *Nucleic Acids Research*, *46*(W1), W242–W245.

Cordeiro Rodrigues, R. J. (2019). *Searching and characterizing novel 21U RNA biogenesis factors in Caenorhabditis elegans*. Johannes Gutenberg-Universität Mainz Ricardo.

Cordeiro Rodrigues, R. J., de Jesus Domingues, A. M., Hellmann, S., Dietz, S., de Albuquerque, B. F. M., Renz, C., Ulrich, H. D., Sarkies, P., Butter, F., & Ketting, R. F. (2019). PETISCO is a novel protein complex required for 21U RNA biogenesis and embryonic viability. *Genes & Development*, *33*(13–14), 857–870.

Core, L., & Adelman, K. (2019). Promoter-proximal pausing of RNA polymerase II: a nexus of gene regulation. *Genes & Development*, *33*(15–16), 960–982.

Corsi, A. K., Wightman, B., & Chalfie, M. (2015). A Transparent Window into Biology: A Primer on Caenorhabditis elegans. *Genetics*, *200*(2), 387.

Cox, J., Hein, M. Y., Luber, C. A., Paron, I., Nagaraj, N., & Mann, M. (2014). Accurate proteome-wide label-free quantification by delayed normalization and maximal peptide ratio extraction, termed MaxLFQ. *Molecular & Cellular Proteomics : MCP*, *13*(9), 2513–2526.

Cox, J., & Mann, M. (2008). MaxQuant enables high peptide identification rates, individualized p.p.b.-range mass accuracies and proteome-wide protein quantification. *Nature Biotechnology*, *26*(12), 1367–1372.

Cox, J., Neuhauser, N., Michalski, A., Scheltema, R. A., Olsen, J. V., & Mann, M. (2011). Andromeda: a peptide search engine integrated into the MaxQuant environment. *Journal of Proteome Research*, *10*(4), 1794–1805.

Cox, R. T., & Spradling, A. C. (2003). A Balbiani body and the fusome mediate mitochondrial inheritance during Drosophila oogenesis. *Development*, *130*(8), 1579–1590.

Crisp, P. A., Smith, A. B., Ganguly, D. R., Murray, K. D., Eichten, S. R., Millar, A. A., & Pogson, B. J. (2018). RNA Polymerase II Read-Through Promotes Expression of Neighboring Genes in SAL1-PAP-XRN Retrograde Signaling. *Plant Physiology*, *178*(4), 1614.

Czech, B., & Hannon, G. J. (2010). Small RNA sorting: matchmaking for Argonautes. *Nature Reviews Genetics 2011 12:1*, *12*(1), 19–31.

Danecek, P., Auton, A., Abecasis, G., Albers, C. A., Banks, E., DePristo, M. A., Handsaker, R. E., Lunter, G., Marth, G. T., Sherry, S. T., McVean, G., & Durbin, R. (2011). The variant call format and VCFtools. *Bioinformatics*, *27*(15), 2156.

Danecek, P., Bonfield, J. K., Liddle, J., Marshall, J., Ohan, V., Pollard, M. O., Whitwham, A., Keane, T., McCarthy, S. A., & Davies, R. M. (2021). Twelve years of SAMtools and

Dankert, J. F., Pagan, J. K., Starostina, N. G., Kipreos, E. T., & Pagano, M. (2017). FEM1 proteins are ancient regulators of SLBP degradation. *Cell Cycle (Georgetown, Tex.)*, *16*(6), 556–564.

Dasilva, L. F., Blumenthal, E., Beckedorff, F., Cingaram, P. R., Santos, H. G. Dos, Edupuganti, R. R., Zhang, A., Dokaneheifard, S., Aoi, Y., Yue, J., Kirstein, N., Tayari, M. M., Shilatifard, A., & Shiekhattar, R. (2021). Integrator enforces the fidelity of transcriptional termination at protein-coding genes. *Science Advances*, *7*(45), 3393.

Das, P. P., Bagijn, M. P., Goldstein, L. D., Woolford, J. R., Lehrbach, N. J., Sapetschnig, A., Buhecha, H. R., Gilchrist, M. J., Howe, K. L., Stark, R., Matthews, N.,

Berezikov, E., Ketting, R. F., Tavaré, S., & Miska, E. A. (2008). Piwi and piRNAs Act Upstream of an Endogenous siRNA Pathway to Suppress Tc3 Transposon Mobility in the Caenorhabditis elegans Germline. *Molecular Cell*, *31*(1), 79–90.

de Albuquerque, B. F. M., Luteijn, M. J., Cordeiro Rodrigues, R. J., van Bergeijk, P., Waaijers, S., Kaaij, L. J. T., Klein, H., Boxem, M., & Ketting, R. F. (2014). PID-1 is a novel factor that operates during 21U-RNA biogenesis in Caenorhabditis elegans. *Genes and Development*, *28*(7), 683–688.

de Albuquerque, B. F. M., Placentino, M., & Ketting, R. F. (2015). Maternal piRNAs Are Essential for Germline Development following De Novo Establishment of Endo-siRNAs in Caenorhabditis elegans. *Developmental Cell*, *34*(4), 448–456.

Decker, T. M. (2021). Mechanisms of Transcription Elongation Factor DSIF (Spt4–Spt5). *Journal of Molecular Biology*, *433*(14), 166657.

DeLisle, A. J., Graves, R. A., Marzluff, W. F., & Johnson, L. F. (1983). Regulation of Histone mRNA Production and Stability in Serum-Stimulated Mouse 3T6 Fibroblasts. *Molecular and Cellular Biology*, *3*(11), 1920–1929.

Deng, M., Wang, X., Xiong, Z., & Tang, P. (2023). Control of RNA degradation in cell fate decision. *Frontiers in Cell and Developmental Biology*, *11*.

De Renzis, S., Elemento, O., Tavazoie, S., & Wieschaus, E. F. (2007). Unmasking Activation of the Zygotic Genome Using Chromosomal Deletions in the Drosophila Embryo. *PLOS Biology*, *5*(5), e117.

Deshaies, R. J. (1999). SCF and cullin/RING H2-based ubiquitin ligases. *Annual Review of Cell and Developmental Biology*, *15*(Volume 15, 1999), 435–467.

Despic, V., & Neugebauer, K. M. (2018). RNA tales - how embryos read and discard messages from mom. *Journal of Cell Science*, *131*(5).

Diao, A. J., Su, B. G., & Vos, S. M. (2024). Pause Patrol: Negative Elongation Factor's Role in Promoter-Proximal Pausing and Beyond. *Journal of Molecular Biology*, 168779.

Dickinson, D. J., Ward, J. D., Reiner, D. J., & Goldstein, B. (2013). Engineering the Caenorhabditis elegans genome using Cas9-triggered homologous recombination. *Nature Methods*, *10*(10), 1028–1034.

Djakbarova, U., Marzluff, W. F., & Köseoğlu, M. M. (2014). Translation Regulation and Proteasome Mediated Degradation Cooperate to Keep Stem-Loop Binding Protein Low in G1-Phase. *Journal of Cellular Biochemistry*, *115*(3), 523–530.

Dobin, A., Davis, C. A., Schlesinger, F., Drenkow, J., Zaleski, C., Jha, S., Batut, P., Chaisson, M., & Gingeras, T. R. (2013). STAR: ultrafast universal RNA-seq aligner. *Bioinformatics*, *29*(1), 15–21.

Dominski, Z., Yang, X. C., & Marzluff, W. F. (2005). The polyadenylation factor CPSF-73 is involved in histone-pre-mRNA processing. *Cell*, *123*(1), 37–48.

Dominski, Z., Yang, X. C., Purdy, M., & Marzluff, W. F. (2005). Differences and similarities between Drosophila and mammalian 3' end processing of histone pre-mRNAs. *RNA (New York, N.Y.)*, *11*(12), 1835–1847.

Dominski, Z., Yang, X., Purdy, M., Wagner, E. J., & Marzluff, W. F. (2005). A CPSF-73 homologue is required for cell cycle progression but not cell growth and interacts with a protein having features of CPSF-100. *Molecular and Cellular Biology*, *25*(4), 1489–1500.

Duronio, R. J., & Marzluff, W. F. (2017). Coordinating cell cycle-regulated histone gene expression through assembly and function of the Histone Locus Body. *RNA Biology*, *14*(6), 726–738.

Eberle, A. B., Lykke-Andersen, S., Mühlemann, O., & Jensen, T. H. (2008). SMG6 promotes endonucleolytic cleavage of nonsense mRNA in human cells. *Nature Structural & Molecular Biology 2008 16:1*, *16*(1), 49–55.

Eckersley-Maslin, M. A., Alda-Catalinas, C., & Reik, W. (2018). Dynamics of the epigenetic landscape during the maternal-to-zygotic transition. *Nature Reviews Molecular Cell Biology*, *19*(7), 436–450.

Eckner, R., Ellmeier, W., & Birnstiel, M. L. (1991). Mature mRNA 3' end formation stimulates RNA export from the nucleus. *The EMBO Journal*, *10*(11), 3513.

Edgar, B. A., Kiehle, C. P., & Schubiger, G. (1986). Cell cycle control by the nucleo-cytoplasmic ratio in early Drosophila development. *Cell*, *44*(2), 365–372.

Elrod, N. D., Henriques, T., Huang, K. L., Tatomer, D. C., Wilusz, J. E., Wagner, E. J., & Adelman, K. (2019). The Integrator Complex Attenuates Promoter-Proximal Transcription at Protein-Coding Genes. *Molecular Cell*, *76*(5), 738-752.e7.

Encalada, S. E., Martin, P. R., Phillips, J. B., Lyczak, R., Hamill, D. R., Swan, K. A., & Bowerman, B. (2000). DNA Replication Defects Delay Cell Division and Disrupt Cell Polarity in Early Caenorhabditis elegans Embryos. *Developmental Biology*, *228*(2), 225–238.

Evans, T. C., & Hunter, C. P. (2005). Translational control of maternal RNAs. *WormBook : The Online Review of C. Elegans Biology*, 1–11.

Ezzeddine, N., Chen, J., Waltenspiel, B., Burch, B., Albrecht, T., Zhuo, M., Warren, W. D., Marzluff, W. F., & Wagner, E. J. (2011). A subset of Drosophila integrator proteins is essential for efficient U7 snRNA and spliceosomal snRNA 3'-end formation. *Molecular and Cellular Biology*, *31*(2), 328–341.

Fabry, M. H., Falconio, F. A., Joud, F., Lythgoe, E. K., Czech, B., & Hannon, G. J. (2021). Maternally inherited piRNAs direct transient heterochromatin formation at active transposons during early Drosophila embryogenesis. *ELife*, *10*.

Faehnle, C. R., Elkayam, E., Haase, A. D., Hannon, G. J., & Joshua-Tor, L. (2013). The making of a slicer: activation of human Argonaute-1. *Cell Reports*, *3*(6), 1901–1909.

Fang, W., & Bartel, D. P. (2020). MicroRNA Clustering Assists Processing of Suboptimal MicroRNA Hairpins through the Action of the ERH Protein. *Molecular Cell*, *78*(2), 289-302.e6.

Farrell, J. A., & O'Farrell, P. H. (2013). Mechanism and Regulation of Cdc25/Twine Protein Destruction in Embryonic Cell-Cycle Remodeling. *Current Biology*, *23*(2), 118–126.

Fassnacht, C., Tocchini, C., Kumari, P., Gaidatzis, D., Stadler, M. B., & Ciosk, R. (2018). The CSR-1 endogenous RNAi pathway ensures accurate transcriptional reprogramming during the oocyte-to-embryo transition in Caenorhabditis elegans. *PLoS Genetics*, *14*(3), e1007252.

Feng, Q., Zhao, D., Lin, Z., Li, M., Xiang, A. P., Ye, C., & Yao, C. (2024). U4 snRNP inhibits premature cleavage and polyadenylation of pre-mRNAs. *Proceedings of the National Academy of Sciences of the United States of America*, *121*(27).

Fianu, I., Ochmann, M., Walshe, J. L., Dybkov, O., Cruz, J. N., Urlaub, H., & Cramer, P. (2024). Structural basis of Integrator-dependent RNA polymerase II termination. *Nature*.

Fire, A., Xu, S., Montgomery, M. K., Kostas, S. A., Driver, S. E., & Mello, C. C. (1998). Potent and specific genetic interference by double-stranded RNA in Caenorhabditis elegans. *Nature 1998 391:6669*, *391*(6669), 806–811.

Frank, F., Sonenberg, N., & Nagar, B. (2010). Structural basis for 5'-nucleotide base-specific recognition of guide RNA by human AGO2. *Nature*, *465*(7299), 818–822.

Frøkjær-Jensen, C. (2019). A balance between silencing foreign DNA and protecting self in Caenorhabditis elegans. *Current Opinion in Systems Biology*, *13*, 37–43.

Frøkjær-Jensen, C., Davis, M. W., Ailion, M., & Jorgensen, E. M. (2012). Improved Mos1-mediated transgenesis in C. elegans. *Nature Methods*, *9*(2), 117.

Frøkjær-Jensen, C., Wayne Davis, M., Hopkins, C. E., Newman, B. J., Thummel, J. M., Olesen, S. P., Grunnet, M., & Jorgensen, E. M. (2008). Single-copy insertion of transgenes in Caenorhabditis elegans. *Nature Genetics*, *40*(11), 1375–1383.

Frolows, N., & Ashe, A. (2021). Small RNAs and chromatin in the multigenerational epigenetic landscape of Caenorhabditis elegans. In *Philosophical Transactions of the Royal Society B: Biological Sciences* (Vol. 376, Issue 1826). Royal Society Publishing.

Fuda, N. J., Ardehali, M. B., & Lis, J. T. (2009). Defining mechanisms that regulate RNA polymerase II transcription in vivo. *Nature 2009 461:7261*, *461*(7261), 186–192.

Fu, G., Ghadam, P., Sirotkin, A., Khochbin, S., Skoultchi, A. I., & Clarke, H. J. (2003). Mouse oocytes and early embryos express multiple histone H1 subtypes. *Biology of Reproduction*, *68*(5), 1569–1576.

Fujiwara, R., Zhai, S.-N., Liang, D., Tracey, M., Ma, X.-K., Shah, A. P., Fields, C. J., Saraí Mendoza-Figueroa, M., Meline, M. C., Tatomer, D. C., Yang, L., Wilusz, J. E., & McLean, M. (2023). *IntS6 and the Integrator phosphatase module tune the efficiency of select premature transcription termination events*. 1–16.

Gajjar, G., Huggins, H. P., Kim, E. S., Huang, W., Bonnet, F. X., Updike, D. L., & Keiper, B. D. (2024). Two germ granule eIF4E isoforms reside in different mRNPs to hand off C elegans mRNAs from translational repression to activation. *BioRxiv*, 2024.05.24.595216.

Garland, W., & Jensen, T. H. (2024). Nuclear sorting of short RNA polymerase II transcripts. *Molecular Cell*, *84*(19), 3644–3655.

Gatfield, D., & Izaurralde, E. (2004). Nonsense-mediated messenger RNA decay is initiated by endonucleolytic cleavage in Drosophila. *Nature 2004 429:6991*, *429*(6991), 575–578.

Geisler, M. S., Kemp, J. P., & Duronio, R. J. (2023). Histone locus bodies: a paradigm for how nuclear biomolecular condensates control cell cycle regulated gene expression. *Nucleus*, *14*(1), 2293604.

Gerson-Gurwitz, A., Wang, S., Sathe, S., Green, R., Yeo, G. W., Oegema, K., & Desai, A. (2016). A Small RNA-Catalytic Argonaute Pathway Tunes Germline Transcript Levels to Ensure Embryonic Divisions. *Cell*, *165*(2), 396–409.

Gerstberger, S., Hafner, M., & Tuschl, T. (2014). A census of human RNA-binding proteins. *Nature Reviews Genetics 2014 15:12*, *15*(12), 829–845.

Ghosh, D., & Seydoux, G. (2008). Inhibition of Transcription by the Caenorhabditis elegans Germline Protein PIE-1: Genetic Evidence for Distinct Mechanisms Targeting Initiation and Elongation. *Genetics*, *178*(1), 235–243.

Ghule, P. N., Xie, R. L., Colby, J. L., Rivera-Pérez, J. A., Jones, S. N., Lian, J. B., Stein, J. L., van Wijnen, A. J., & Stein, G. S. (2016). Maternal expression and early induction of histone gene transcription factor Hinfp sustains development in pre-implantation embryos. *Developmental Biology*, *419*(2), 311.

Ghule, P. N., Xie, R.-L., Medina, R., Colby, J. L., Jones, S. N., Lian, J. B., Stein, J. L., van Wijnen, A. J., & Stein, G. S. (2014). Fidelity of histone gene regulation is obligatory for genome replication and stability. *Molecular and Cellular Biology*, *34*(14), 2650–2659.

Ghule, P. N., Xie, R.-L., Medina, R., Colby, J. L., Jones, S. N., Lian, J. B., Stein, J. L., Wijnen, A. J. van, & Stein, G. S. (2014). Fidelity of Histone Gene Regulation Is Obligatory for Genome Replication and Stability. *Molecular and Cellular Biology*, *34*(14), 2650–2659.

Giraldez, A. J. (2010). microRNAs, the cell's Nepenthe: clearing the past during the maternal-to-zygotic transition and cellular reprogramming. *Current Opinion in Genetics & Development*, *20*(4), 369–375.

Glavan, F., Behm-Ansmant, I., Izaurralde, E., & Conti, E. (2006). Structures of the PIN domains of SMG6 and SMG5 reveal a nuclease within the mRNA surveillance complex. *EMBO Journal*, *25*(21), 5117–5125.

Gleason, R. J., Guo, Y., Semancik, C. S., Ow, C., Lakshminarayanan, G., & Chen, X. (2023). Developmentally programmed histone H3 expression regulates cellular plasticity at the parental-to-early embryo transition. *Science Advances*, *9*(14).

Godfrey, A. C., Kupsco, J. M., Burch, B. D., Zimmerman, R. M., Dominski, Z., Marzluff, W. F., & Duronio, R. J. (2006). U7 snRNA mutations in Drosophila block histone pre-mRNA processing and disrupt oogenesis. *RNA (New York, N.Y.)*, *12*(3), 396–409.

Goh, W. S. S., Seah, J. W. E., Harrison, E. J., Chen, C., Hammell, C. M., & Hannon, G. J. (2014). A genome-wide RNAi screen identifies factors required for distinct stages of C. elegans piRNA biogenesis. *Genes and Development*, *28*(7), 797–807.

Gómez-Orte, E., Cornes, E., Zheleva, A., Sáenz-Narciso, B., de Toro, M., Iñiguez, M., López, R., San-Juan, J. F., Ezcurra, B., Sacristán, B., Sánchez-Blanco, A., Cerón, J., & Cabello, J. (2017). Effect of the diet type and temperature on the C. elegans transcriptome. *Oncotarget*, *9*(11), 9556.

Gómez-Orte, E., Sáenz-Narciso, B., Zheleva, A., Ezcurra, B., de Toro, M., López, R., Gastaca, I., Nilsen, H., Sacristán, M. P., Schnabel, R., & Cabello, J. (2019). Disruption of the Caenorhabditis elegans Integrator complex triggers a non-conventional transcriptional mechanism beyond snRNA genes. *PLOS Genetics*, *15*(2), e1007981.

Gossett, A. J., & Lieb, J. D. (2012). In vivo effects of histone H3 depletion on nucleosome occupancy and position in Saccharomyces cerevisiae. *PLoS Genetics*, *8*(6).

Greene, E. A., Codomo, C. A., Taylor, N. E., Henikoff, J. G., Till, B. J., Reynolds, S. H., Enns, L. C., Burtner, C., Johnson, J. E., Odden, A. R., Comai, L., & Henikoff, S. (2003). Spectrum of Chemically Induced Mutations From a Large-Scale Reverse-Genetic Screen in Arabidopsis. *Genetics*, *164*(2), 731–740.

Green, R. A., Khaliullin, R. N., Zhao, Z., Ochoa, S. D., Hendel, J. M., Chow, T. L., Moon, H. K., Biggs, R. J., Desai, A., & Oegema, K. (2024). Automated profiling of gene function during embryonic development. *Cell*, *187*(12), 3141-3160.e23.

Grimson, A., O'Connor, S., Newman, C. L., & Anderson, P. (2004). SMG-1 is a phosphatidylinositol kinase-related protein kinase required for nonsense-

mediated mRNA Decay in Caenorhabditis elegans. *Molecular and Cellular Biology*, *24*(17), 7483–7490.

Gromak, N. (2023). SOSS-INTAC: a new gatekeeper of genomic integrity at the interface of transcription and R-loops. *Molecular Cell*, *83*(20), 3593–3595.

Guidi, R., Wedeles, C., Xu, D., Kolmus, K., Headland, S. E., Teng, G., Guillory, J., Zeng, Y. J., Cheung, T. K., Chaudhuri, S., Modrusan, Z., Liang, Y., Horswell, S., Haley, B., Rutz, S., Rose, C., Franke, Y., Kirkpatrick, D. S., Hackney, J. A., & Wilson, M. S. (2023). Argonaute3-SF3B3 complex controls pre-mRNA splicing to restrain type 2 immunity. *Cell Reports*, *42*(12).

Günesdogan, U., Jäckle, H., & Herzig, A. (2014). Histone supply regulates S phase timing and cell cycle progression. *ELife*, *3*, e02443.

Gunjan, A., & Verreault, A. (2003). A Rad53 Kinase-Dependent Surveillance Mechanism that Regulates Histone Protein Levels in S. cerevisiae. *Cell*, *115*(5), 537–549.

Guo, M., Zhu, J., Hu, Z., Wang, Q., Songyang, Z., & Xiong, Y. (2023). Histone mRNA polyadenylation-mediated inflammation underlies various virus infections and cancers. *Journal of Medical Virology*, *95*(6).

Guven-Ozkan, T., Nishi, Y., Robertson, S. M., & Lin, R. (2008). Global Transcriptional Repression in C. elegans Germline Precursors by Regulated Sequestration of TAF-4. *Cell*, *135*(1), 149–160.

Gu, W., Lee, H. C., Chaves, D., Youngman, E. M., Pazour, G. J., Conte, D., & Mello, C. C. (2012). CapSeq and CIP-TAP identify pol ii start sites and reveal capped small RNAs as C. elegans piRNA precursors. *Cell*, *151*(7), 1488–1500.

Haeussler, M., Schönig, K., Eckert, H., Eschstruth, A., Mianné, J., Renaud, J. B., Schneider-Maunoury, S., Shkumatava, A., Teboul, L., Kent, J., Joly, J. S., & Concordet, J. P. (2016). Evaluation of off-target and on-target scoring algorithms and integration into the guide RNA selection tool CRISPOR. *Genome Biology*, *17*(1), 1–12.

Hannon, G. J., Maroney, P. A., & Nilsen, T. W. (1991). U small nuclear ribonucleoprotein requirements for nematode cis- and trans-splicing in vitro. *Journal of Biological Chemistry*, *266*(34), 22792–22795.

Harada, A., Maehara, K., Sato, Y., Konno, D., Tachibana, T., Kimura, H., & Ohkawa, Y. (2015). Incorporation of histone H3.1 suppresses the lineage potential of skeletal muscle. *Nucleic Acids Research*, *43*(2), 775–786.

Harrison, P. W., Amode, M. R., Austine-Orimoloye, O., Azov, A. G., Barba, M., Barnes, I., Becker, A., Bennett, R., Berry, A., Bhai, J., Bhurji, S. K., Boddu, S., Lins, P. R. B., Brooks, L., Ramaraju, S. B., Campbell, L. I., Martinez, M. C., Charkhchi, M., Chougule, K., … Yates, A. D. (2024). Ensembl 2024. *Nucleic Acids Research*, *52*(D1), D891–D899.

Harvey, S. A., Sealy, I., Kettleborough, R., Fenyes, F., White, R., Stemple, D., & Smith, J. C. (2013). Identification of the zebrafish maternal and paternal transcriptomes. *Development*, *140*(13), 2703–2710.

Hashimoto, Y., Takahashi, M., Sakota, E., & Nakamura, Y. (2017). Nonstop-mRNA decay machinery is involved in the clearance of mRNA 5′-fragments produced by RNAi and NMD in Drosophila melanogaster cells. *Biochemical and Biophysical Research Communications*, *484*(1), 1–7.

Hauptmann, J., Dueck, A., Harlander, S., Pfaff, J., Merkl, R., & Meister, G. (2013). Turning catalytically inactive human Argonaute proteins into active slicer enzymes. *Nature Structural & Molecular Biology*, *20*(7), 814–817.

Hauptmann, J., Kater, L., Löffler, P., Merkl, R., & Meister, G. (2014). Generation of catalytic human Ago4 identifies structural elements important for RNA cleavage. *RNA (New York, N.Y.)*, *20*(10), 1532–1538.

Hayek, H., Gross, L., Janvier, A., Schaeffer, L., Martin, F., Eriani, G., & Allmang, C. (2021). eIF3 interacts with histone H4 messenger RNA to regulate its translation. *The Journal of Biological Chemistry*, *296*.

Henikoff, S., & Ahmad, K. (2005). Assembly of variant histones into chromatin. *Annual Review of Cell and Developmental Biology*, *21*, 133–153.

Hentze, M. W., Castello, A., Schwarzl, T., & Preiss, T. (2018). A brave new world of RNA-binding proteins. *Nature Reviews Molecular Cell Biology 2018 19:5*, *19*(5), 327–341.

He, W. X., Wu, M., Liu, Z., Li, Z., Wang, Y., Zhou, J., Yu, P., Zhang, X. J., Zhou, L., & Gui, J. F. (2018). Oocyte-specific maternal Slbp2 is required for replication-dependent histone storage and early nuclear cleavage in zebrafish oogenesis and embryogenesis. *RNA*, *24*(12), 1738–1748.

Heyn, P., Kircher, M., Dahl, A., Kelso, J., Tomancak, P., Kalinka, A. T., & Neugebauer, K. M. (2014). The

Earliest Transcribed Zygotic Genes Are Short, Newly Evolved, and Different across Species. *Cell Reports*, *6*(2), 285–292.

Hinnebusch, A. G. (2017). Structural Insights into the Mechanism of Scanning and Start Codon Recognition in Eukaryotic Translation Initiation. *Trends in Biochemical Sciences*, *42*(8), 589–611.

Hinnebusch, A. G., & Lorsch, J. R. (2012). The Mechanism of Eukaryotic Translation Initiation: New Insights and Challenges. *Cold Spring Harbor Perspectives in Biology*, *4*(10).

Hobert, O., D'Alberti, T., Liu, Y., & Ruvkun, G. (1998). Control of neural development and function in a thermoregulatory network by the LIM homeobox gene lin-11. *The Journal of Neuroscience : The Official Journal of the Society for Neuroscience*, *18*(6), 2084–2096.

Ho, C. K., & Shuman, S. (1999). Distinct roles for CTD Ser-2 and Ser-5 phosphorylation in the recruitment and allosteric activation of mammalian mRNA capping enzyme. *Molecular Cell*, *3*(3), 405–411.

Hoefig, K. P., Rath, N., Heinz, G. A., Wolf, C., Dameris, J., Schepers, A., Kremmer, E., Ansel, K. M., & Heissmeyer, V. (2012). Eri1 degrades the stem-loop of oligouridylated histone mRNAs to induce replication-dependent decay. *Nature Structural & Molecular Biology 2012 20:1*, *20*(1), 73–81.

Holmquist, C. E., He, W., Meganck, R. M., & Marzluff, W. F. (2022). Knockouts of TUT7 and 3'hExo show that they cooperate in histone mRNA maintenance and degradation. *RNA*, *28*(11), 1519–1533.

Hoogewijs, D., Houthoofd, K., Matthijssens, F., Vandesompele, J., & Vanfleteren, J. R. (2008). Selection and validation of a set of reliable reference genes for quantitative sod gene expression analysis in C. elegans. *BMC Molecular Biology*, *9*, 9.

Huang, K. L., Jee, D., Stein, C. B., Elrod, N. D., Henriques, T., Mascibroda, L. G., Baillat, D., Russell, W. K., Adelman, K., & Wagner, E. J. (2020). Integrator Recruits Protein Phosphatase 2A to Prevent Pause Release and Facilitate Transcription Termination. *Molecular Cell*, *80*(2), 345-358.e9.

Hubbard, E. J. A., & Greenstein, D. (2005). Introduction to the germ line. *WormBook : The Online Review of C. Elegans Biology*, 1–4.

Huber, W., Carey, V. J., Gentleman, R., Anders, S., Carlson, M., Carvalho, B. S., Bravo, H. C., Davis, S., Gatto, L., Girke, T., Gottardo, R., Hahne, F., Hansen, K. D., Irizarry, R. A., Lawrence, M., Love, M. I., MaCdonald, J., Obenchain, V., Oleš, A. K., … Morgan, M. (2015). Orchestrating high-throughput genomic analysis with Bioconductor. *Nature Methods 2015 12:2*, *12*(2), 115–121.

Huggins, H. P., Subash, J. S., Stoffel, H., Henderson, M. A., Hoffman, J. L., Buckner, D. S., Sengupta, M. S., Boag, P. R., Lee, M. H., & Keiper, B. D. (2020). Distinct roles of two eIF4E isoforms in the germline of Caenorhabditis elegans. *Journal of Cell Science*, *133*(6).

Hughes, C. S., Moggridge, S., Müller, T., Sorensen, P. H., Morin, G. B., & Krijgsveld, J. (2019). Single-pot, solid-phase-enhanced sample preparation for proteomics experiments. *Nature Protocols*, *14*(1), 68–85.

Huntzinger, E., Kashima, I., Fauser, M., Saulière, J., & Izaurralde, E. (2008). SMG6 is the catalytic endonuclease that cleaves mRNAs containing nonsense codons in metazoan. *RNA*, *14*(12), 2609–2617.

Hu, S., Peng, L., Song, A., Ji, Y. X., Cheng, J., Wang, M., & Chen, F. X. (2023). INTAC endonuclease and phosphatase modules differentially regulate transcription by RNA polymerase II. *Molecular Cell*, *83*(10), 1588-1604.e5.

Ibarra-Morales, D., Rauer, M., Quarato, P., Rabbani, L., Zenk, F., Schulte-Sasse, M., Cardamone, F., Gomez-Auli, A., Cecere, G., & Iovino, N. (2021). Histone variant H2A.Z regulates zygotic genome activation. *Nature Communications 2021 12:1*, *12*(1), 1–14.

Isken, O., & Maquat, L. E. (2008). The multiple lives of NMD factors: balancing roles in gene and genome regulation. *Nature Reviews Genetics 2008 9:9*, *9*(9), 699–712.

Ivanov, P., Kedersha, N., & Anderson, P. (2019). Stress Granules and Processing Bodies in Translational Control. *Cold Spring Harbor Perspectives in Biology*, *11*(5), a032813.

Iwakawa, H. oki, & Tomari, Y. (2022). Life of RISC: Formation, action, and degradation of RNA-induced silencing complex. *Molecular Cell*, *82*(1), 30–43.

James, P., Halladay, J., & Craig, E. A. (1996). Genomic libraries and a host strain designed for highly efficient two-hybrid selection in yeast. *Genetics*, *144*(4), 1425–1436.

Jamieson-Lucy, A., & Mullins, M. C. (2019). The vertebrate Balbiani body, germ plasm, and oocyte polarity. *Current Topics in Developmental Biology*, *135*, 1–34.

Jankowska-Anyszka, M., Lamphear, B. J., Aamodt, E. J., Harrington, T., Darzynkiewicz, E., Stolarski, R., & Rhoads, R. E. (1998). Multiple Isoforms of Eukaryotic Protein Synthesis Initiation Factor 4E in Caenorhabditis elegans Can Distinguish between Mono- and Trimethylated mRNA Cap Structures. *Journal of Biological Chemistry*, *273*(17), 10538–10542.

Jawdekar, G. W., & Henry, R. W. (2008). Transcriptional regulation of human small nuclear RNA genes. *Biochimica et Biophysica Acta*, *1779*(5), 295–305.

Jedrusik, M. A., & Schulze, E. (2001). A single histone H1 isoform (H1.1) is essential for chromatin silencing and germline development in Caenorhabditis elegans. *Development (Cambridge, England)*, *128*(7), 1069–1080.

Jimeno-González, S., Payán-Bravo, L., Muñoz-Cabello, A. M., Guijo, M., Gutierrez, G., Prado, F., & Reyes, J. C. (2015). Defective histone supply causes changes in RNA polymerase II elongation rate and cotranscriptional pre-mRNA splicing. *Proceedings of the National Academy of Sciences of the United States of America*, *112*(48), 14840–14845.

Johns, L., Grimson, A., Kuchma, S. L., Newman, C. L., & Anderson, P. (2007). Caenorhabditis elegans SMG-2 Selectively Marks mRNAs Containing Premature Translation Termination Codons. *Molecular and Cellular Biology*, *27*(16), 5630–5638.

Jonkers, I., Kwak, H., & Lis, J. T. (2014). Genome-wide dynamics of Pol II elongation and its interplay with promoter proximal pausing, chromatin, and exons. *ELife*, *2014*(3).

Jorgensen, E. M., & Mango, S. E. (2002). The art and design of genetic screens: Caenorhabditis elegans. In *Nature Reviews Genetics* (Vol. 3, Issue 5, pp. 356–369).

Joseph, S. R., Pálfy, M., Hilbert, L., Kumar, M., Karschau, J., Zaburdaev, V., Shevchenko, A., & Vastenhouw, N. L. (2017). Competition between histone and transcription factor binding regulates the onset of transcription in zebrafish embryos. *ELife*, *6*.

Kamath, R. S., & Ahringer, J. (2003). Genome-wide RNAi screening in Caenorhabditis elegans. *Methods*, *30*(4), 313–321.

Kamath, R. S., Fraser, A. G., Dong, Y., Poulin, G., Durbin, R., Gotta, M., Kanapin, A., Le Bot, N., Moreno, S., Sohrmann, M., Welchman, D. P., Zipperien, P., & Ahringer, J. (2003). Systematic functional analysis of the Caenorhabditis elegans genome using RNAi. *Nature*, *421*(6920), 231–237.

Kamminga, L. M., van Wolfswinkel, J. C., Luteijn, M. J., Kaaij, L. J. T., Bagijn, M. P., Sapetschnig, A., Miska, E. A., Berezikov, E., & Ketting, R. F. (2012). Differential Impact of the HEN1 Homolog HENN-1 on 21U and 26G RNAs in the Germline of Caenorhabditis elegans. *PLoS Genetics*, *8*(7), e1002702.

Kari, V., Karpiuk, O., Tieg, B., Kriegs, M., Dikomey, E., Krebber, H., Begus-Nahrmann, Y., & Johnsen, S. A. (2013). A Subset of Histone H2B Genes Produces Polyadenylated mRNAs under a Variety of Cellular Conditions. *PLoS ONE*, *8*(5).

Kasper, D. M., Wang, G., Gardner, K. E., Johnstone, T. G., & Reinke, V. (2014). The C.elegans SNAPc component SNPC-4 coats piRNA domains and is globally required for piRNA abundance. *Developmental Cell*, *31*(2), 145–158.

Katznelson, A., Hernandez, B., Fahning, H., Zhang, J., Burton, A., Torres-Padilla, M.-E., Plachta, N., Zaret, K. S., & McCarthy, R. L. (2024). Heterochromatin protein ERH represses alternative cell fates during early mammalian differentiation. *BioRxiv : The Preprint Server for Biology*.

Kaygun, H., & Marzluff, W. F. (2005). Regulated degradation of replication-dependent histone mRNAs requires both ATR and Upf1. *Nature Structural & Molecular Biology*, *12*(9), 794–800.

Keall, R., Whitelaw, S., Pettitt, J., & Müller, B. (2007). Histone gene expression and histone mRNA 3' end structure in Caenorhabditis elegans. *BMC Molecular Biology*, *8*(1), 51.

Keiper, B. D., Lamphear, B. J., Deshpande, A. M., Jankowska-Anyszka, M., Aamodt, E. J., Blumenthal, T., & Rhoads, R. E. (2000). Functional Characterization of Five eIF4E Isoforms inCaenorhabditis elegans. *Journal of Biological Chemistry*, *275*(14), 10590–10596.

Kelley, L. H., Caldas, I. V, Sullenberger, M. T., Yongblah, K. E., Niazi, A. M., Iyer, A., Li, Y., Tran, P. M., Valen, E., Ahmed-Braimah, Y. H., & Maine, E. M. (2024). Poly(U) polymerase activity in Caenorhabditis elegans regulates abundance and tailing of sRNA and mRNA. *Genetics*.

Kent, W. J., Zweig, A. S., Barber, G., Hinrichs, A. S., & Karolchik, D. (2010). BigWig and BigBed: enabling browsing of large distributed datasets. *Bioinformatics (Oxford, England)*, *26*(17), 2204–2207.

Kerner, P., Degnan, S. M., Marchand, L., Degnan, B. M., & Vervoort, M. (2011). Evolution of RNA-Binding Proteins in Animals: Insights from Genome-Wide Analysis in the Sponge Amphimedon queenslandica. *Molecular Biology and Evolution*, *28*(8), 2289–2303.

Ketting, F. R., & Cochella, L. (2020). Concepts and functions of small RNA pathways in C. elegans. *Current Topics in Developmental Biology*, 1–45.

Ketting, R. F. (2011). The many faces of RNAi. *Developmental Cell*, *20*(2), 148–161.

Ketting, R. F., Haverkamp, T. H. A., Van Luenen, H. G. A. M., & Plasterk, R. H. A. (1999). mut-7 of C. elegans, Required for Transposon Silencing and RNA Interference, Is a Homolog of Werner Syndrome Helicase and RNaseD. *Cell*, *99*(2), 133–141.

Kilchert, C., Wittmann, S., & Vasiljeva, L. (2016). The regulation and functions of the nuclear RNA exosome complex. *Nature Reviews Molecular Cell Biology 2016 17:4*, *17*(4), 227–239.

Kim, Y. K. I., & Maquat, L. E. (2019). UPFront and center in RNA decay: UPF1 in nonsense-mediated mRNA decay and beyond. *RNA*, *25*(4), 407.

Kishor, A., Fritz, S. E., & Hogg, J. R. (2019). Nonsense-mediated mRNA decay: The challenge of telling right from wrong in a complex transcriptome. *Wiley Interdisciplinary Reviews. RNA*, *10*(6).

Kodama, Y., Rothman, J. H., Sugimoto, A., & Yamamoto, M. (2002). The stem-loop binding protein CDL-1 is required for chromosome condensation, progression of cell death and morphogenesis in Caenorhabditis elegans. *Development (Cambridge, England)*, *129*(1), 187–196.

Köhn, M., Ihling, C., Sinz, A., Krohn, K., & Hüttelmaier, S. (2015). The Y3** ncRNA promotes the 3′ end processing of histone mRNAs. *Genes & Development*, *29*(19), 1998–2003.

Kolev, N. G., & Steitz, J. A. (2005). Symplekin and multiple other polyadenylation factors participate in 3′-end maturation of histone mRNAs. *Genes & Development*, *19*(21), 2583–2592.

König, J., Zarnack, K., Rot, G., Curk, T., Kayikci, M., Zupan, B., Turner, D. J., Luscombe, N. M., & Ule, J. (2010). ICLIP reveals the function of hnRNP particles in splicing at individual nucleotide resolution. *Nature Structural and Molecular Biology*, *17*(7), 909–915.

Koseoglu, M. M., Graves, L. M., & Marzluff, W. F. (2008). Phosphorylation of Threonine 61 by Cyclin A/Cdk1 Triggers Degradation of Stem-Loop Binding Protein at the End of S Phase. *Molecular and Cellular Biology*, *28*(14), 4469–4479.

Kowalski, M. P., Baylis, H. A., & Krude, T. (2015). Non-coding stem-bulge RNAs are required for cell proliferation and embryonic development in C. elegans. *Journal of Cell Science*, *128*(11), 2118–2129.

Kozlowski, P. (2023). Thirty Years with ERH: An mRNA Splicing and Mitosis Factor Only or Rather a Novel Genome Integrity Protector? *Cells 2023, Vol. 12, Page 2449*, *12*(20), 2449.

Krishnan, N., Lam, T. T., Fritz, A., Rempinski, D., O'Loughlin, K., Minderman, H., Berezney, R., Marzluff, W. F., & Thapar, R. (2012). The Prolyl Isomerase Pin1 Targets Stem-Loop Binding Protein (SLBP) To Dissociate the SLBP-Histone mRNA Complex Linking Histone mRNA Decay with SLBP Ubiquitination. *Molecular and Cellular Biology*, *32*(21), 4306.

Kruesi, W. S., Core, L. J., Waters, C. T., Lis, J. T., & Meyer, B. J. (2013). Condensin controls recruitment of RNA polymerase ii to achieve nematode X-chromosome dosage compensation. *ELife*, *2013*(2).

Kumar, A., Clerici, M., Muckenfuss, L. M., Passmore, L. A., & Jinek, M. (2019). Mechanistic insights into mRNA 3′-end processing. *Current Opinion in Structural Biology*, *59*, 143–150.

Kwak, H., & Lis, J. T. (2013). Control of transcriptional elongation. *Annual Review of Genetics*, *47*(Volume 47, 2013), 483–508.

Kwak, Y. T., Guo, J., Prajapati, S., Park, K. J., Surabhi, R. M., Miller, B., Gehrig, P., & Gaynor, R. B. (2003). Methylation of SPT5 Regulates Its Interaction with RNA Polymerase II and Transcriptional Elongation Properties. *Molecular Cell*, *11*(4), 1055–1066.

Kwasnieski, J. C., Orr-Weaver, T. L., & Bartel, D. P. (2019). Early genome activation in Drosophila is extensive with an initial tendency for aborted transcripts and retained introns. *Genome Research*, *29*(7), 1188–1197.

Lackey, P. E., Welch, J. D., & Marzluff, W. F. (2016). TUT7 catalyzes the uridylation of the 3′ end for rapid

degradation of histone mRNA. *RNA*, *22*(11), 1673–1688.

Lanzotti, D. J., Kaygun, H., Yang, X., Duronio, R. J., & Marzluff, W. F. (2002). Developmental control of histone mRNA and dSLBP synthesis during Drosophila embryogenesis and the role of dSLBP in histone mRNA 3' end processing in vivo. *Molecular and Cellular Biology*, *22*(7), 2267–2282.

Lawrence, M., Gentleman, R., & Carey, V. (2009). rtracklayer: an R package for interfacing with genome browsers. *Bioinformatics (Oxford, England)*, *25*(14), 1841–1842.

Lawrence, M., Huber, W., Pagès, H., Aboyoun, P., Carlson, M., Gentleman, R., Morgan, M. T., & Carey, V. J. (2013). Software for Computing and Annotating Genomic Ranges. *PLOS Computational Biology*, *9*(8), e1003118.

Lee, C.-Y. S., Putnam, A., Lu, T., He, S., Ouyang, J. P. T., & Seydoux, G. (2020). Recruitment of mRNAs to P granules by condensation with intrinsically-disordered proteins. *ELife*, *9*.

Lee, D. R., Lee, J. E., Yoon, H. S., Roh, S. Il, & Kim, M. K. (2001). Compaction in preimplantation mouse embryos is regulated by a cytoplasmic regulatory factor that alters between 1- and 2-cell stages in a concentration-dependent manner. *Journal of Experimental Zoology*, *290*(1), 61–71.

Lee, H. C., Gu, W., Shirayama, M., Youngman, E., Conte, D., & Mello, C. C. (2012). C. elegans piRNAs mediate the genome-wide surveillance of germline transcripts. *Cell*, *150*(1), 78–87.

Lee, M. T., Bonneau, A. R., Takacs, C. M., Bazzini, A. A., Divito, K. R., Fleming, E. S., & Giraldez, A. J. (2013). Nanog, Pou5f1 and SoxB1 activate zygotic gene expression during the maternal-to-zygotic transition. *Nature 2013 503:7476*, *503*(7476), 360–364.

Lee, S. R., & Lykke-Andersen, J. (2013). Emerging roles for ribonucleoprotein modification and remodeling in controlling RNA fate. *Trends in Cell Biology*, *23*(10), 504–510.

Lei, Q., Li, C., Zuo, Z., Huang, C., Cheng, H., & Zhou, R. (2016). Evolutionary Insights into RNA trans-Splicing in Vertebrates. *Genome Biology and Evolution*, *8*(3), 562–577.

Le Pen, J., Jiang, H., Di Domenico, T., Kneuss, E., Kosałka, J., Leung, C., Morgan, M., Much, C., Rudolph, K. L. M., Enright, A. J., O'Carroll, D., Wang, D., & Miska, E. A. (2018). Terminal uridylyltransferases target RNA viruses as part of the innate immune system. *Nature Structural & Molecular Biology 2018 25:9*, *25*(9), 778–786.

Lesch, B. J., & Page, D. C. (2012). Genetics of germ cell development. In *Nature Reviews Genetics* (Vol. 13, Issue 11, pp. 781–794).

Liao, Y., Smyth, G. K., & Shi, W. (2014). featureCounts: an efficient general purpose program for assigning sequence reads to genomic features. *Bioinformatics*, *30*(7), 923–930.

Li, H. (2013). *Aligning sequence reads, clone sequences and assembly contigs with BWA-MEM*.

Lim, J., Ha, M., Chang, H., Kwon, S. C., Simanshu, D. K., Patel, D. J., & Kim, V. N. (2014). Uridylation by TUT4 and TUT7 Marks mRNA for Degradation. *Cell*, *159*(6), 1365–1376.

Lim, J., Kim, D., Lee, Y. S., Ha, M., Lee, M., Yeo, J., Chang, H., Song, J., Ahn, K., & Kim, V. N. (2018). Mixed tailing by TENT4A and TENT4B shields mRNA from rapid deadenylation. *Science (New York, N.Y.)*, *361*(6403), 701–704.

Lin, M. Der, Jiao, X., Grima, D., Newbury, S. F., Kiledjian, M., & Chou, T. Bin. (2008). Drosophila processing bodies in oogenesis. *Developmental Biology*, *322*(2), 276–288.

Liudkovska, V., & Dziembowski, A. (2021). Functions and mechanisms of RNA tailing by metazoan terminal nucleotidyltransferases. *Wiley Interdisciplinary Reviews: RNA*, *12*(2), e1622.

Li, Y., & Maine, E. M. (2018). The balance of poly(U) polymerase activity ensures germline identity, survival and development in Caenorhabditis elegans. *Development (Cambridge, England)*, *145*(19).

López, M. D., & Samuelsson, T. (2008). Early evolution of histone mRNA 3' end processing. *RNA*, *14*(1), 1.

Lorenzo-Orts, L., & Pauli, A. (2024). The molecular mechanisms underpinning maternal mRNA dormancy. *Biochemical Society Transactions*, *52*(2), 861–871.

Lorenzo-Orts, L., Strobl, M., Steinmetz, B., Leesch, F., Pribitzer, C., Roehsner, J., Schutzbier, M., Dürnberger, G., & Pauli, A. (2024). eIF4E1b is a non-canonical eIF4E protecting maternal dormant mRNAs. *EMBO Reports*, *25*(1), 404–427.

Love, M. I., Huber, W., & Anders, S. (2014). Moderated estimation of fold change and dispersion for RNA-seq data with DESeq2. *Genome Biology*, *15*(12), 1–21.

Lu, F., Park, B. J., Fujiwara, R., Wilusz, J. E., Gilmour, D. S., Lehmann, R., & Lionnet, T. (2024). Integrator-mediated clustering of poised RNA polymerase II synchronizes histone transcription. *BioRxiv : The Preprint Server for Biology*.

Luteijn, M. J., Van Bergeijk, P., Kaaij, L. J. T., Almeida, M. V., Roovers, E. F., Berezikov, E., & Ketting, R. F. (2012). Extremely stable Piwi-induced gene silencing in Caenorhabditis elegans. *The EMBO Journal*, *31*(16), 3422.

Lu, X., Li, J. M., Elemento, O., Tavazoie, S., & Wieschaus, E. F. (2009). Coupling of zygotic transcription to mitotic control at the Drosophila mid-blastula transition. *Development (Cambridge, England)*, *136*(12), 2101–2110.

Lykke-Andersen, S., Žumer, K., Molska, E. Š., Rouvière, J. O., Wu, G., Demel, C., Schwalb, B., Schmid, M., Cramer, P., & Jensen, T. H. (2021). Integrator is a genome-wide attenuator of non-productive transcription. *Molecular Cell*, *81*(3), 514-529.e6.

Lyons, S. M., Cunningham, C. H., Welch, J. D., Groh, B., Guo, A. Y., Wei, B., Whitfield, M. L., Xiong, Y., & Marzluff, W. F. (2016). A subset of replication-dependent histone mRNAs are expressed as polyadenylated RNAs in terminally differentiated tissues. *Nucleic Acids Research*, *44*(19), 9190–9205.

Lyons, S. M., Ricciardi, A. S., Guo, A. Y., Kambach, C., & Marzluff, W. F. (2014). The C-terminal extension of Lsm4 interacts directly with the 3′ end of the histone mRNP and is required for efficient histone mRNA degradation. *RNA*, *20*(1), 88–102.

Lyssenko, N. N., Hanna-Rose, W., & Schlegel, R. A. (2007). Cognate putative nuclear localization signal effects strong nuclear localization of a GFP reporter and facilitates gene expression studies in Caenorhabditis elegans. *BioTechniques*, *43*(5), 596–600.

Madeira, F., Madhusoodanan, N., Lee, J., Eusebi, A., Niewielska, A., Tivey, A. R. N., Lopez, R., & Butcher, S. (2024). The EMBL-EBI Job Dispatcher sequence analysis tools framework in 2024. *Nucleic Acids Research*, *52*(W1), W521–W525.

Madeira, F., Park, Y. M., Lee, J., Buso, N., Gur, T., Madhusoodanan, N., Basutkar, P., Tivey, A. R. N., Potter, S. C., Finn, R. D., & Lopez, R. (2019). The EMBL-EBI search and sequence analysis tools APIs in 2019. *Nucleic Acids Research*, *47*(W1), W636–W641.

Ma, J. B., Yuan, Y. R., Meister, G., Pei, Y., Tuschl, T., & Patel, D. J. (2005). Structural basis for 5′-end-specific recognition of guide RNA by the A. fulgidus Piwi protein. *Nature 2005 434:7033*, *434*(7033), 666–670.

Makeyeva, Y. V., Shirayama, M., & Mello, C. C. (2021). Cues from mRNA splicing prevent default Argonaute silencing in C. elegans. *Developmental Cell*, *56*(18), 2636-2648.e4.

Malik, H. S., & Henikoff, S. (2003). Phylogenomics of the nucleosome. *Nature Structural Biology*, *10*(11), 882–891.

Mangone, M., Manoharan, A. P., Thierry-Mieg, D., Thierry-Mieg, J., Han, T., Mackowiak, S. D., Mis, E., Zegar, C., Gutwein, M. R., Khivansara, V., Attie, O., Chen, K., Salehi-Ashtiani, K., Vidal, M., Harkins, T. T., Bouffard, P., Suzuki, Y., Sugano, S., Kohara, Y., … Kim, J. K. (2010). The landscape of C. elegans 3′UTRs. *Science*, *329*(5990), 432–435.

Martin, F., Schaller, A., Eglite, S., Schümperli, D., & Müller, B. (1997). The gene for histone RNA hairpin binding protein is located on human chromosome 4 and encodes a novel type of RNA binding protein. *The EMBO Journal*, *16*(4), 769–778.

Martin, M. (2011). Cutadapt removes adapter sequences from high-throughput sequencing reads. *EMBnet.Journal*, *17*(1), 10–12.

Marzluff, W. F., & Koreski, K. P. (2017). Birth and Death of Histone mRNAs. In *Trends in Genetics* (Vol. 33, Issue 10, pp. 745–759). Elsevier Ltd.

Marzluff, W. F., Wagner, E. J., & Duronio, R. J. (2008). Metabolism and regulation of canonical histone mRNAs: life without a poly(A) tail. *Nature Reviews. Genetics*, *9*(11), 843–854.

Matera, A. G., & Wang, Z. (2014). A day in the life of the spliceosome. *Nature Reviews Molecular Cell Biology 2014 15:2*, *15*(2), 108–121.

Ma, T., Van Tine, B. A., Wei, Y., Garrett, M. D., Nelson, D., Adams, P. D., Wang, J., Qin, J., Chow, L. T., & Harper, J. W. (2000). Cell cycle–regulated phosphorylation of p220NPAT by cyclin E/Cdk2 in Cajal bodies promotes histone gene transcription. *Genes & Development*, *14*(18), 2298.

Mayakonda, A., Lin, D. C., Assenov, Y., Plass, C., & Koeffler, H. P. (2018). Maftools: efficient and comprehensive

analysis of somatic variants in cancer. *Genome Research*, *28*(11), 1747–1756.

Mayr, F., & Heinemann, U. (2013). Mechanisms of Lin28-Mediated miRNA and mRNA Regulation—A Structural and Functional Perspective. *International Journal of Molecular Sciences 2013, Vol. 14, Pages 16532-16553*, *14*(8), 16532–16553.

McCarthy, R. L., Kaeding, K. E., Keller, S. H., Zhong, Y., Xu, L., Hsieh, A., Hou, Y., Donahue, G., Becker, J. S., Alberto, O., Lim, B., & Zaret, K. S. (2021). Diverse heterochromatin-associated proteins repress distinct classes of genes and repetitive elements. *Nature Cell Biology*, *23*(8), 905–914.

McLaren, W., Gil, L., Hunt, S. E., Riat, H. S., Ritchie, G. R. S., Thormann, A., Flicek, P., & Cunningham, F. (2016). The Ensembl Variant Effect Predictor. *Genome Biology*, *17*(1), 1–14.

Meaux, S. A., Holmquist, C. E., & Marzluff, W. F. (2018). Role of oligouridylation in normal metabolism and regulated degradation of mammalian histone mRNAs. *Philosophical Transactions of the Royal Society B: Biological Sciences*, *373*(1762).

Medvedev, S., Pan, H., & Schultz, R. M. (2011). Absence of MSY2 in Mouse Oocytes Perturbs Oocyte Growth and Maturation, RNA Stability, and the Transcriptome. *Biology of Reproduction*, *85*(3), 575–583.

Mendell, J. T., Sharifi, N. A., Meyers, J. L., Martinez-Murillo, F., & Dietz, H. C. (2004). Nonsense surveillance regulates expression of diverse classes of mammalian transcripts and mutes genomic noise. *Nature Genetics 2004 36:10*, *36*(10), 1073–1078.

Mendoza-Figueroa, M. S., Tatomer, D. C., & Wilusz, J. E. (2020). The Integrator Complex in Transcription and Development. *Trends in Biochemical Sciences*, *45*(11), 923–934.

Meng, Y., Ma, X., Li, J., Ito, H., Oracz, K., Cai, J., & Shao, C. (2022). The novel activity of Argonautes in intron splicing: A transcriptome-wide survey in plants. *Journal of Plant Physiology*, *270*, 153632.

Merritt, C., Rasoloson, D., Ko, D., & Seydoux, G. (2008). 3′ UTRs Are the Primary Regulators of Gene Expression in the C. elegans Germline. *Current Biology*, *18*(19), 1476–1482.

Metzstein, M. M., & Krasnow, M. A. (2006). Functions of the Nonsense-Mediated mRNA Decay Pathway in Drosophila Development. *PLOS Genetics*, *2*(12), e180.

Michel, F., Schümperli, D., & Müller, B. (2000). Specificities of Caenorhabditis elegans and human hairpin binding proteins for the first nucleotide in the histone mRNA hairpin loop. *RNA (New York, N.Y.)*, *6*(11), 1539–1550.

Miki, T. S., Carl, S. H., & Großhans, H. (2017). Two distinct transcription termination modes dictated by promoters. *Genes and Development*, *31*(18), 1870–1879.

Minasaki, R., & Streit, A. (2007). MEL-47, a novel protein required for early cell divisions in the nematode Caenorhabditis elegans. *Molecular Genetics and Genomics*, *277*(3), 315–328.

Miyoshi, H., Dwyer, D. S., Keiper, B. D., Jankowska-Anyszka, M., Darzynkiewicz, E., & Rhoads, R. E. (2002). Discrimination between mono- and trimethylated cap structures by two isoforms of Caenorhabditis elegans eIF4E. *The EMBO Journal*, *21*(17), 4680.

Montemayor, E. J., Virta, J. M., Hayes, S. M., Nomura, Y., Brow, D. A., & Butcher, S. E. (2020). Molecular basis for the distinct cellular functions of the Lsm1-7 and Lsm2-8 complexes. *RNA*, *26*(10), 1400–1413.

Montgomery, B. E., Vijayasarathy, T., Marks, T. N., Cialek, C. A., Reed, K. J., & Montgomery, T. A. (2021). Dual roles for piRNAs in promoting and preventing gene silencing in C. elegans. *Cell Reports*, *37*(10), 110101.

Montgomery, T. A., Rim, Y.-S., Zhang, C., Dowen, R. H., Phillips, C. M., Fischer, S. E. J., & Ruvkun, G. (2012). PIWI Associated siRNAs and piRNAs Specifically Require the Caenorhabditis elegans HEN1 Ortholog henn-1. *PLoS Genetics*, *8*(4), e1002616.

Mossanen-Parsi, A., Parisi, D., Browne-Marke, N., Bharudin, I., Connell, S. R., Mayans, O., Fucini, P., Morozov, I. Y., & Caddick, M. X. (2021). Histone mRNA is subject to 3′ uridylation and re-adenylation in Aspergillus nidulans. *Molecular Microbiology*, *115*(2), 238–254.

Mowry, K. L., & Steitz, J. A. (1987). Identification of the human U7 snRNP as one of several factors involved in the 3′ end maturation of histone premessenger RNA's. *Science (New York, N.Y.)*, *238*(4834), 1682–1687.

Muir, V. S., Gasch, A. P., & Anderson, P. (2018). The substrates of nonsense-mediated mRNA decay in Caenorhabditis elegans. *G3: Genes, Genomes, Genetics*, *8*(1), 195–205.

Mukherjee, N., & Mukherjee, C. (2021). Germ cell ribonucleoprotein granules in different clades of life: From insects to mammals. *Wiley Interdisciplinary Reviews: RNA*.

Mullen, T. E., & Marzluff, W. F. (2008). Degradation of histone mRNA requires oligouridylation followed by decapping and simultaneous degradation of the mRNA both 5′ to 3′ and 3′ to 5′. *Genes & Development*, *22*(1), 50–65.

Müller, K., & Wickham, H. (2024). Tibble: Simple data frames. In *https://github.com/tidyverse/tibble*.

Murphy, P. J., Wu, S. F., James, C. R., Wike, C. L., & Cairns, B. R. (2018). Placeholder Nucleosomes Underlie Germline-to-Embryo DNA Methylation Reprogramming. *Cell*, *172*(5), 993-1006.e13.

Nakanishi, K., Ascano, M., Gogakos, T., Ishibe-Murakami, S., Serganov, A. A., Briskin, D., Morozov, P., Tuschl, T., & Patel, D. J. (2013). Eukaryote-specific insertion elements control human ARGONAUTE slicer activity. *Cell Reports*, *3*(6), 1893–1900.

Narita, T., Yamaguchi, Y., Yano, K., Sugimoto, S., Chanarat, S., Wada, T., Kim, D., Hasegawa, J., Omori, M., Inukai, N., Endoh, M., Yamada, T., & Handa, H. (2003). Human transcription elongation factor NELF: identification of novel subunits and reconstitution of the functionally active complex. *Molecular and Cellular Biology*, *23*(6), 1863–1873.

Narita, T., Yung, T. M. C., Yamamoto, J., Tsuboi, Y., Tanabe, H., Tanaka, K., Yamaguchi, Y., & Handa, H. (2007). NELF Interacts with CBC and Participates in 3′ End Processing of Replication-Dependent Histone mRNAs. *Molecular Cell*, *26*(3), 349–365.

Nazer, E., Gómez Acuña, L., & Kornblihtt, A. R. (2022). Seeking the truth behind the myth: Argonaute tales from “nuclearland”. *Molecular Cell*, *82*(3), 503–513.

Newman, M. A., Ji, F., Fischer, S. E. J., Anselmo, A., Sadreyev, R. I., & Ruvkun, G. (2018). The surveillance of pre-mRNA splicing is an early step in C. elegans RNAi of endogenous genes. *Genes & Development*, *32*(9–10), 670–681.

Newport, J., & Kirschner, M. (1982). A major developmental transition in early xenopus embryos: I. characterization and timing of cellular changes at the midblastula stage. *Cell*, *30*(3), 675–686.

Obenchain, V., Lawrence, M., Carey, V., Gogarten, S., Shannon, P., & Morgan, M. (2014). VariantAnnotation : a Bioconductor package for exploration and annotation of genetic variants. *Bioinformatics*, *30*(14), 2076–2078.

Olina, A. V., Kulbachinskiy, A. V., Aravin, A. A., & Esyunina, D. M. (2018). Argonaute Proteins and Mechanisms of RNA Interference in Eukaryotes and Prokaryotes. *Biochemistry (Moscow) 2018 83:5*, *83*(5), 483–497.

Ozata, D. M., Gainetdinov, I., Zoch, A., O’Carroll, D., & Zamore, P. D. (2019). PIWI-interacting RNAs: small RNAs with big functions. In *Nature Reviews Genetics* (Vol. 20, Issue 2).

Page, M. F., Carr, B., Anders, K. R., Grimson, A., & Anderson, P. (1999). SMG-2 Is a Phosphorylated Protein Required for mRNA Surveillance in Caenorhabditis elegans and Related to Upf1p of Yeast. *Molecular and Cellular Biology*, *19*(9), 5943–5951.

Pagès, H. (2022). Software infrastructure for efficient representation of full genomes and their SNPs. In *https://bioconductor.org/packages/BSgenome*.

Pagès, H., Aboyoun, P., Gentleman, R., & DebRoy, S. (2022). Biostrings: Efficient manipulation of biological strings. In *https://bioconductor.org/packages/Biostrings*.

Pandey, N. B., Chodchoy, N., Liu, T. J., & Marzluff, W. F. (1990). Introns in histone genes alter the distribution of 3′ ends. *Nucleic Acids Research*, *18*(11), 3161.

Pardue, M. L., Kedes, L. H., Weinberg, E. S., & Birnstiel, M. L. (1977). Localization of sequences coding for histone messenger RNA in the chromosomes of Drosophila melanogaster. *Chromosoma*, *63*(2), 135–151.

Parker, D. M., Winkenbach, L. P., Boyson, S., Saxton, M. N., Daidone, C., Al-Mazaydeh, Z. A., Nishimura, M. T., Mueller, F., & Nishimura, E. O. (2020). mRNA localization is linked to translation regulation in the Caenorhabditis elegans germ lineage. *Development (Cambridge, England)*, *147*(13).

Parker, J. S., Roe, S. M., & Barford, D. (2004). Crystal structure of a PIWI protein suggests mechanisms for siRNA recognition and slicer activity. *EMBO Journal*, *23*(24), 4727–4737.

Parker, J. S., Roe, S. M., & Barford, D. (2005). Structural insights into mRNA recognition from a PIWI domain–siRNA guide complex. *Nature 2005 434:7033*, *434*(7033), 663–666.

Parker, R., & Sheth, U. (2007). P bodies and the control of mRNA translation and degradation. *Molecular Cell*, *25*(5), 635–646.

Parry, D. H., Xu, J., & Ruvkun, G. (2007). A whole-genome RNAi screen for C. elegans miRNA pathway genes. *Current Biology : CB*, *17*(23), 2013.

Passmore, L. A., & Coller, J. (2021). Roles of mRNA poly(A) tails in regulation of eukaryotic gene expression. *Nature Reviews Molecular Cell Biology 2021 23:2*, *23*(2), 93–106.

Pastore, B., Hertz, H. L., Price, I. F., & Tang, W. (2021). pre-piRNA trimming and 2'-O-methylation protect piRNAs from 3' tailing and degradation in C. elegans. *Cell Reports*, *36*(9).

Pastore, B., Hertz, H. L., & Tang, W. (2024). Pre-piRNA trimming safeguards piRNAs against erroneous targeting by RNA-dependent RNA polymerase. *Cell Reports*, *43*(2).

Peng, F., Nordgren, C. E., & Murray, J. I. (2024). A spatiotemporally resolved atlas of mRNA decay in the C. elegans embryo reveals differential regulation of mRNA stability across stages and cell types. *Genome Research*, *34*(8).

Perez-Borrajero, C., Podvalnaya, N., Holleis, K., Lichtenberger, R., Karaulanov, E., Simon, B., Basquin, J., Hennig, J., Ketting, R. F., & Falk, S. (2021). Structural basis of PETISCO complex assembly during piRNA biogenesis in C. elegans. *Genes and Development*, *35*(17–18), 1304–1323.

Pérez-Montero, S., Carbonell, A., Morán, T., Vaquero, A., & Azorín, F. (2013). The embryonic linker histone H1 variant of Drosophila, dBigH1, regulates zygotic genome activation. *Developmental Cell*, *26*(6), 578–590.

Pettitt, J., Crombie, C., Schümperli, D., & Müller, B. (2002). The Caenorhabditis elegans histone hairpin-binding protein is required for core histone gene expression and is essential for embryonic and postembryonic cell division. *Journal of Cell Science*, *115*(4).

Pfleiderer, M. M., & Galej, W. P. (2021). Emerging insights into the function and structure of the Integrator complex. *Transcription*, *12*(5), 251–265.

Phatnani, H. P., & Greenleaf, A. L. (2006). Phosphorylation and functions of the RNA polymerase II CTD. *Genes & Development*, *20*(21), 2922–2936.

Philippe, L., Pandarakalam, G. C., Fasimoye, R., Harrison, N., Connolly, B., Pettitt, J., & Müller, B. (2017). An in vivo genetic screen for genes involved in spliced leader trans-splicing indicates a crucial role for continuous de novo spliced leader RNP assembly. *Nucleic Acids Research*, *45*(14), 8474–8483.

Phillips, C. M., & Updike, D. L. (2022). Germ granules and gene regulation in the Caenorhabditis elegans germline. *Genetics*, *220*(3).

Picard toolkit. (2019). In *Broad Institute, GitHub repository*.

Pillai, R. S., Grimmler, M., Meister, G., Will, C. L., Lührmann, R., Fischer, U., & Schümperli, D. (2003). Unique Sm core structure of U7 snRNPs: assembly by a specialized SMN complex and the role of a new component, Lsm11, in histone RNA processing. *Genes & Development*, *17*(18), 2321.

Pillai, R. S., Will, C. L., Lührmann, R., Schümperli, D., & Müller, B. (2001). Purified U7 snRNPs lack the Sm proteins D1 and D2 but contain Lsm10, a new 14 kDa Sm D1-like protein. *The EMBO Journal*, *20*(19), 5470.

Placentino, M., de Jesus Domingues, A. M., Schreier, J., Dietz, S., Hellmann, S., de Albuquerque, B. F., Butter, F., & Ketting, R. F. (2021). Intrinsically disordered protein PID-2 modulates Z granules and is required for heritable piRNA-induced silencing in the Caenorhabditis elegans embryo . *The EMBO Journal*, *40*(3).

Podvalnaya, N. (2023). *Identification and characterization of the 21U RNA processing enzyme in Caenorhabditis elegans*. Johannes Gutenberg-Universität Mainz.

Podvalnaya, N., Bronkhorst, A. W., Lichtenberger, R., Hellmann, S., Nischwitz, E., Falk, T., Karaulanov, E., Butter, F., Falk, S., & Ketting, R. F. (2023). piRNA processing by a trimeric Schlafen-domain nuclease. *Nature 2023 622:7982*, *622*(7982), 402–409.

Poplin, R., Ruano-Rubio, V., DePristo, M. A., Fennell, T. J., Carneiro, M. O., Auwera, G. A. Van der, Kling, D. E., Gauthier, L. D., Levy-Moonshine, A., Roazen, D., Shakir, K., Thibault, J., Chandran, S., Whelan, C., Lek, M., Gabriel, S., Daly, M. J., Neale, B., MacArthur, D. G., & Banks, E. (2018). Scaling accurate genetic variant discovery to tens of thousands of samples. *BioRxiv*, 201178.

Portman, D. S., & Emmons, S. W. (2000). The basic helix-loop-helix transcription factors LIN-32 and HLH-2 function together in multiple steps of a C. elegans neuronal sublineage. *Development (Cambridge, England)*, *127*(24), 5415–5426.

Potter-Birriel, J. M., Gonsalvez, G. B., & Marzluff, W. F. (2021). A region of SLBP outside the mRNA-processing domain is essential for deposition of

histone mRNA into the Drosophila egg. *Journal of Cell Science*, *134*(3).

Powell-Coffman, J. A., Knight, J., & Wood, W. B. (1996). Onset ofC. elegansGastrulation Is Blocked by Inhibition of Embryonic Transcription with an RNA Polymerase Antisense RNA. *Developmental Biology*, *178*(2), 472–483.

Prado, F., & Aguilera, A. (2005). Partial depletion of histone H4 increases homologous recombination-mediated genetic instability. *Molecular and Cellular Biology*, *25*(4), 1526–1536.

Prado, F., Jimeno-González, S., & Reyes, J. C. (2017a). Histone availability as a strategy to control gene expression. *RNA Biology*, *14*(3), 281–286.

Prado, F., Jimeno-González, S., & Reyes, J. C. (2017b). Histone availability as a strategy to control gene expression. *RNA Biology*, *14*(3), 281–286.

Presnyak, V., Alhusaini, N., Chen, Y. H., Martin, S., Morris, N., Kline, N., Olson, S., Weinberg, D., Baker, K. E., Graveley, B. R., & Coller, J. (2015). Codon optimality is a major determinant of mRNA stability. *Cell*, *160*(6), 1111–1124.

Prioleau, M. N., Huet, J., Sentenac, A., & Méchali, M. (1994). Competition between chromatin and transcription complex assembly regulates gene expression during early development. *Cell*, *77*(3), 439–449.

Pulak, R., & Anderson, P. (1993). mRNA surveillance by the Caenorhabditis elegans smg genes. *Genes & Development*, *7*(10), 1885–1897.

Pule, M. N., Glover, M. L., Fire, A. Z., & Arribere, J. A. (2019). Ribosome clearance during RNA interference. *RNA*, *25*(8), 963–974.

Putnam, A., Thomas, L., & Seydoux, G. (2023). RNA granules: functional compartments or incidental condensates? *Genes & Development*, *37*(9–10), 354–376.

Qian, M. X., Pang, Y., Liu, C. H., Haratake, K., Du, B. Y., Ji, D. Y., Wang, G. F., Zhu, Q. Q., Song, W., Yu, Y., Zhang, X. X., Huang, H. T., Miao, S., Chen, L. Bin, Zhang, Z. H., Liang, Y. N., Liu, S., Cha, H., Yang, D., … Qiu, X. B. (2013). Acetylation-mediated proteasomal degradation of core histones during DNA repair and spermatogenesis. *Cell*, *153*(5), 1012.

Quarato, P., Singh, M., Bourdon, L., & Cecere, G. (2022). Inheritance and maintenance of small RNA-mediated epigenetic effects. *BioEssays*, 2100284.

Quarato, P., Singh, M., Cornes, E., Li, B., Bourdon, L., Mueller, F., Didier, C., & Cecere, G. (2021). Germline inherited small RNAs facilitate the clearance of untranslated maternal mRNAs in C. elegans embryos. *Nature Communications 2021 12:1*, *12*(1), 1–14.

Quinlan, A. R., & Hall, I. M. (2010). BEDTools: a flexible suite of utilities for comparing genomic features. *Bioinformatics*, *26*(6), 841–842.

Quintas, A., Harvey, R. F., Horvilleur, E., Garland, G. D., Schmidt, T., Kalmar, L., Dezi, V., Marini, A., Fulton, A. M., Pöyry, T. A. A., Cole, C. H., Turner, M., Sawarkar, R., Chapman, M. A., Bushell, M., & Willis, A. E. (2013). Eukaryotic initiation factor 4B is a multi-functional RNA binding protein that regulates histone mRNAs. *Nucleic Acids Research*, *1*(1256879), 13–14.

Rai, A. K., Chen, J. X., Selbach, M., & Pelkmans, L. (2018). Kinase-controlled phase transition of membraneless organelles in mitosis. *Nature*, *559*(7713), 211–216.

Rai, T. S., Cole, J. J., Nelson, D. M., Dikovskaya, D., Faller, W. J., Vizioli, M. G., Hewitt, R. N., Anannya, O., McBryan, T., Manoharan, I., Van Tuyn, J., Morrice, N., Pchelintsev, N. A., Ivanov, A., Brock, C., Drotar, M. E., Nixon, C., Clark, W., Sansom, O. J., … Adams, P. D. (2014). HIRA orchestrates a dynamic chromatin landscape in senescence and is required for suppression of neoplasia. *Genes & Development*, *28*(24), 2712–2725.

Rajyaguru, P., & Parker, R. (2009). CGH-1 and the control of maternal mRNAs. *Trends in Cell Biology*, *19*(1), 24–28.

Ramakrishnan, V. (2014). The Ribosome Emerges from a Black Box. *Cell*, *159*(5), 979–984.

Ramamurthy, L., Ingledue, T. C., Pilch, D. R., Kay, B. K., & Marzluff, W. F. (1996). Increasing the Distance Between the snRNA Promoter and the 3′ Box Decreases the Efficiency of snRNA 3-End Formation. *Nucleic Acids Research*, *24*(22), 4525–4534.

Ramanathan, A., Robb, G. B., & Chan, S. H. (2016). mRNA capping: biological functions and applications. *Nucleic Acids Research*, *44*(16), 7511–7526.

Ramírez, F., Ryan, D. P., Grüning, B., Bhardwaj, V., Kilpert, F., Richter, A. S., Heyne, S., Dündar, F., & Manke, T. (2016). deepTools2: a next generation web server for deep-sequencing data analysis. *Nucleic Acids Research*, *44*(W1), W160–W165.

Rappsilber, J., Ishihama, Y., & Mann, M. (2003). Stop and go extraction tips for matrix-assisted laser desorption/ionization, nanoelectrospray, and LC/MS sample pretreatment in proteomics. *Analytical Chemistry*, *75*(3), 663–670.

Rashid, U. J., Paterok, D., Koglin, A., Gohlke, H., Piehler, J., & Chen, J. C. H. (2007). Structure of Aquifex aeolicus Argonaute Highlights Conformational Flexibility of the PAZ Domain as a Potential Regulator of RNA-induced Silencing Complex Function. *Journal of Biological Chemistry*, *282*(18), 13824–13832.

R Core Team. (2019). *R: A language and environment for statistical computing*. R Foundation for Statistical Computing. https://www.r-project.org/search.html

Reed, K. J., Svendsen, J. M., Brown, K. C., Montgomery, B. E., Marks, T. N., Vijayasarathy, T., Parker, D. M., Nishimura, E. O., Updike, D. L., & Montgomery, T. A. (2019). Widespread roles for piRNAs and WAGO-class siRNAs in shaping the germline transcriptome of Caenorhabditis elegans. *Nucleic Acids Research*.

Reinke, V., Krause, M., & Okkema, P. (2013). Transcriptional regulation of gene expression in C. elegans. *WormBook : The Online Review of C. Elegans Biology*, 1–34.

Ren, W., Chen, H., Sun, Q., Tang, X., Lim, S. C., Huang, J., & Song, H. (2014). Structural Basis of SOSS1 Complex Assembly and Recognition of ssDNA. *Cell Reports*, *6*(6), 982–991.

Ripin, N., & Parker, R. (2023). Formation, function, and pathology of RNP granules. *Cell*, *186*(22), 4737–4756.

Rissland, O. S., & Norbury, C. J. (2009). Decapping is preceded by 3′ uridylation in a novel pathway of bulk mRNA turnover. *Nature Structural & Molecular Biology*, *16*(6), 616–623.

Robertson, S., & Lin, R. (2015). The Maternal-to-Zygotic Transition in C. elegans. In *Current Topics in Developmental Biology* (1st ed., Vol. 113). Elsevier Inc.

Roberts, S. B., Emmons, S. W., & Childs, G. (1989). Nucleotide sequences of Caenorhabditis elegans core histone genes. Genes for different histone classes share common flanking sequence elements. *Journal of Molecular Biology*, *206*(4), 567–577.

Roberts, S. B., Sanicola, M., Emmons, S. W., & Childs, G. (1987). Molecular characterization of the histone gene family of Caenorhabditis elegans. *Journal of Molecular Biology*, *196*(1), 27–38.

Rodríguez-Molina, J. B., & Turtola, M. (2023). Birth of a poly(A) tail: mechanisms and control of mRNA polyadenylation. *FEBS Open Bio*, *13*(7), 1140.

Rodríguez-Molina, J. B., West, S., & Passmore, L. A. (2023). Knowing when to stop: Transcription termination on protein-coding genes by eukaryotic RNAPII. *Molecular Cell*, *83*(3), 404–415.

Roehr, J. T., Dieterich, C., & Reinert, K. (2017). Flexbar 3.0 - SIMD and multicore parallelization. *Bioinformatics (Oxford, England)*, *33*(18), 2941–2942.

Rohban, S., Rafiee, M.-R., Ule, J., & Luscombe, N. M. (2023). Human Integrator provides a quality checkpoint during elongation to facilitate RNA polymerase II processivity. *BioRxiv*, 2023.02.17.528960.

Rosa-Mercado, N. A., Zimmer, J. T., Apostolidi, M., Rinehart, J., Simon, M. D., & Steitz, J. A. (2021). Hyperosmotic stress alters the RNA polymerase II interactome and induces readthrough transcription despite widespread transcriptional repression. *Molecular Cell*, *81*(3), 502-513.e4.

Rouget, C., Papin, C., Boureux, A., Meunier, A. C., Franco, B., Robine, N., Lai, E. C., Pelisson, A., & Simonelig, M. (2010). Maternal mRNA deadenylation and decay by the piRNA pathway in the early Drosophila embryo. *Nature*, *467*(7319), 1128–1132.

Rouvière, J. O., Lykke-Andersen, S., & Jensen, T. H. (2022). Control of non-productive RNA polymerase II transcription via its early termination in metazoans. *Biochemical Society Transactions*, *50*(1), 283–295.

Ruby, J. G., Jan, C., Player, C., Axtell, M. J., Lee, W., Nusbaum, C., Ge, H., & Bartel, D. P. (2006). Large-Scale Sequencing Reveals 21U-RNAs and Additional MicroRNAs and Endogenous siRNAs in C. elegans. *Cell*, *127*(6), 1193–1207.

Ruddell, A., & Jacobs-Lorena, M. (1985). Biphasic pattern of histone gene expression during Drosophila oogenesis. *Proceedings of the National Academy of Sciences of the United States of America*, *82*(10), 3316–3319.

Sabath, K., Nabih, A., Arnold, C., Moussa, R., Domjan, D., Zaugg, J. B., & Jonas, S. (2024). Basis of gene-specific transcription regulation by the Integrator complex. *Molecular Cell*, *84*(13), 2525-2541.e12.

Sakai, A., Schwartz, B. E., Goldstein, S., & Ahmad, K. (2009). Transcriptional and Developmental Functions of the

H3.3 Histone Variant in Drosophila. *Current Biology*, *19*(21), 1816–1820.

Saldi, T., Fong, N., & Bentley, D. L. (2018). Transcription elongation rate affects nascent histone pre-mRNA folding and 3′ end processing. *Genes and Development*, *32*(3–4), 297–308.

Sànchez, R., & Marzluff, W. F. (2002). The stem-loop binding protein is required for efficient translation of histone mRNA in vivo and in vitro. *Molecular and Cellular Biology*, *22*(20), 7093–7104.

Sánchez, R., & Marzluff, W. F. (2004). The oligo(A) tail on histone mRNA plays an active role in translational silencing of histone mRNA during Xenopus oogenesis. *Molecular and Cellular Biology*, *24*(6), 2513–2525.

Santilli, F., & Boskovic, A. (2023). Mechanisms of transgenerational epigenetic inheritance: lessons from animal model organisms. *Current Opinion in Genetics & Development*, *79*.

Sarafi-Reinach, T. R., Melkman, T., Hobert, O., & Sengupta, P. (2001). The lin-11 LIM homeobox gene specifies olfactory and chemosensory neuron fates in C. elegans. *Development (Cambridge, England)*, *128*(17), 3269–3281.

Saunders, M. J., Yeh, E., Grunstein, M., & Bloom, K. (1990). Nucleosome Depletion Alters the Chromatin Structure of Saccharomyces cerevisiae Centromeres. *Molecular and Cellular Biology*, *10*(11), 5721–5727.

Scharl, E. C., & Steitz, J. A. (1994). The site of 3′ end formation of histone messenger RNA is a fixed distance from the downstream element recognized by the U7 snRNP. *The EMBO Journal*, *13*(10), 2432.

Schauberger, P., Walker, A., & Garbuszus, J. M. (2024). *openxlsx: Read, Write and Edit xlsx Files*. https://ycphs.github.io/openxlsx/index.html.

Schisa, J. A., Pitt, J. N., & Priess, J. R. (2001). Analysis of RNA associated with P granules in germ cells of C. elegans adults. *Development (Cambridge, England)*, *128*(8), 1287–1298.

Schmittgen, T. D., & Livak, K. J. (2008). Analyzing real-time PCR data by the comparative C(T) method. *Nature Protocols*, *3*(6), 1101–1108.

Scholl, A., Liu, Y., & Seydoux, G. (2024). Caenorhabditis elegans germ granules accumulate hundreds of low translation mRNAs with no systematic preference for germ cell fate regulators. *Development (Cambridge, England)*, *151*(13).

Schulz, K. N., & Harrison, M. M. (2019). Mechanisms regulating zygotic genome activation. *Nature Reviews Genetics*, *20*(4), 221–234.

Schweinsberg, P. J., & Grant, B. D. (2013). C. elegans gene transformation by microparticle bombardment. *WormBook : The Online Review of C. Elegans Biology*, 1–10.

Seth, M., Shirayama, M., Gu, W., Ishidate, T., Conte, D., & Mello, C. (2013). The C. elegans CSR-1 Argonaute Pathway Counteracts Epigenetic Silencing to Promote Germline Gene Expression. *Developmental Cell*, *27*(6), 656–663.

Seydoux, G. (2018). The P Granules of C. elegans: A Genetic Model for the Study of RNA–Protein Condensates. In *Journal of Molecular Biology* (Vol. 430, Issue 23, pp. 4702–4710). Academic Press.

Sharp, P., Roberts, R., & Shi, Y. (2017). Mechanistic insights into precursor messenger RNA splicing by the spliceosome. *Nature Reviews Molecular Cell Biology 2017 18:11*, *18*(11), 655–670.

Shindo, Y., & Amodeo, A. A. (2021). Excess histone H3 is a competitive Chk1 inhibitor that controls cell-cycle remodeling in the early Drosophila embryo. *Current Biology : CB*, *31*(12), 2633-2642.e6.

Shine, M., Harris, S. E., Pellegrene, K. A., Kensinger, A. H., Mihailescu, M. R., Evanseck, J. D., & Lackey, P. E. (2023). Uridylation of the histone mRNA stem-loop weakens binding interactions with SLBP while maintaining interactions with 3′hExo. *RNA Biology*, *20*(1), 469–481.

Shirayama, M., Seth, M., Lee, H. C., Gu, W., Ishidate, T., Conte, D., & Mello, C. C. (2012). piRNAs initiate an epigenetic memory of nonself RNA in the C. elegans germline. *Cell*, *150*(1), 65–77.

Shukla, A., Perales, R., & Kennedy, S. (2021). piRNAs coordinate poly(UG) tailing to prevent aberrant and perpetual gene silencing. *Current Biology : CB*, *31*(20), 4473-4485.e3.

Shukla, A., Yan, J., Pagano, D. J., Dodson, A. E., Fei, Y., Gorham, J., Seidman, J. G., Wickens, M., & Kennedy, S. (2020). poly(UG)-tailed RNAs in genome protection and epigenetic inheritance. *Nature*, 1–6.

Simon, M., Sarkies, P., Ikegami, K., Doebley, A. L., Goldstein, L. D., Mitchell, J., Sakaguchi, A., Miska, E. A., & Ahmed, S. (2014). Reduced Insulin/IGF-1 Signaling Restores Germ Cell Immortality to Caenorhabditis elegans Piwi Mutants. *Cell Reports*, *7*(3), 762–773.

Singh, R., Bassett, E., Chakravarti, A., & Parthun, M. R. (2018). Replication-dependent histone isoforms: a new source of complexity in chromatin structure and function. *Nucleic Acids Research*, *46*(17), 8665–8678.

Singh, R. K., Kabbaj, M. H. M., Paik, J., & Gunjan, A. (2009). Histone levels are regulated by phosphorylation and ubiquitylation-dependent proteolysis. *Nature Cell Biology 2009 11:8*, *11*(8), 925–933.

Skaar, J. R., Ferris, A. L., Wu, X., Saraf, A., Khanna, K. K., Florens, L., Washburn, M. P., Hughes, S. H., & Pagano, M. (2015). The Integrator complex controls the termination of transcription at diverse classes of gene targets. *Cell Research*, *25*(3), 288–305.

Skaar, J. R., Richard, D. J., Saraf, A., Toschi, A., Bolderson, E., Florens, L., Washburn, M. P., Khanna, K. K., & Pagano, M. (2009). INTS3 controls the hSSB1-mediated DNA damage response. *The Journal of Cell Biology*, *187*(1), 25–32.

Skrajna, A., Yang, X. C., Bucholc, K., Zhang, J., Hall, T. M. T., Dadlez, M., Marzluff, W. F., & Dominski, Z. (2017). U7 snRNP is recruited to histone pre-mRNA in a FLASH-dependent manner by two separate regions of the stem-loop binding protein. *RNA (New York, N.Y.)*, *23*(6), 938–951.

Skvortsova, K., Iovino, N., & Bogdanović, O. (2018). Functions and mechanisms of epigenetic inheritance in animals. In *Nature Reviews Molecular Cell Biology* (Vol. 19, Issue 12, pp. 774–790). Nature Publishing Group.

Slevin, M. K., Meaux, S., Welch, J. D., Bigler, R., Miliani de Marval, P. L., Su, W., Rhoads, R. E., Prins, J. F., & Marzluff, W. F. (2014). Deep Sequencing Shows Multiple Oligouridylations Are Required for 3′ to 5′ Degradation of Histone mRNAs on Polyribosomes. *Molecular Cell*, *53*(6), 1020–1030.

Smith, R. C., Dworkin-Rastl, E., & Dworkin, M. B. (1988). Expression of a histone H1-like protein is restricted to early Xenopus development. *Genes & Development*, *2*(10), 1284–1295.

Song, J. J., Smith, S. K., Hannon, G. J., & Joshua-Tor, L. (2004). Crystal structure of argonaute and its implications for RISC slicer activity. *Science*, *305*(5689), 1434–1437.

Spichal, M., Heestand, B., Billmyre, K. K., Frenk, S., Mello, C. C., & Ahmed, S. (2021). Germ granule dysfunction is a hallmark and mirror of Piwi mutant sterility. *Nature Communications 2021 12:1*, *12*(1), 1–15.

Spieth, J., Lawson, D., Davis, P., Williams, G., & Howe, K. (2014). Overview of gene structure in C. elegans. *WormBook : The Online Review of C. Elegans Biology*, 1–18.

Stachelska, A., Wieczorek, Z., Ruszczyńska, K., Stolarski, R., Pietrzak, M., Lamphear, B. J., Rhoads, R. E., Darzynkiewicz, E., & Jankowska-Anyszka, M. (2002). Interaction of three Caenorhabditis elegans isoforms of translation initiation factor eIF4E with mono- and trimethylated mRNA 5′ cap analogues. *Acta Biochimica Polonica*, *49*(3), 671–682.

Stoeckius, M., Grün, D., Kirchner, M., Ayoub, S., Torti, F., Piano, F., Herzog, M., Selbach, M., & Rajewsky, N. (2014). Global characterization of the oocyte-to-embryo transition in C aenorhabditis elegans uncovers a novel mRNA clearance mechanism. *The EMBO Journal*, *33*(16), 1751–1766.

Strobino, M., Wenda, J. M., Padayachy, L., & Steiner, F. A. (2020). Loss of histone H3.3 results in DNA replication defects and altered origin dynamics in C. elegans. *Genome Research*, *31*(12), 1740–1751.

Strome, S., & Wood, W. B. (1982). Immunofluorescence visualization of germ-line-specific cytoplasmic granules in embryos, larvae, and adults of Caenorhabditis elegans. *Proceedings of the National Academy of Sciences of the United States of America*, *79*(5), 1558.

Strub, K., & Birnstiel, M. L. (1986). Genetic complementation in the Xenopus oocyte: co-expression of sea urchin histone and U7 RNAs restores 3′ processing of H3 pre-mRNA in the oocyte. *The EMBO Journal*, *5*(7), 1675–1682.

Subtelny, A. O., Eichhorn, S. W., Chen, G. R., Sive, H., & Bartel, D. P. (2014). Poly(A)-tail profiling reveals an embryonic switch in translational control. *Nature 2014 508:7494*, *508*(7494), 66–71.

Sugiyama, T., Thillainadesan, G., Chalamcharla, V. R., Meng, Z., Balachandran, V., Dhakshnamoorthy, J., Zhou, M., & Grewal, S. I. S. (2016). Enhancer of Rudimentary Cooperates with Conserved RNA-Processing Factors to Promote Meiotic mRNA Decay and Facultative Heterochromatin Assembly. *Molecular Cell*, *61*(5), 747–759.

Sullivan, E., Santiago, C., Parker, E. D., Dominski, Z., Yang, X., Lanzotti, D. J., Ingledue, T. C., Marzluff, W. F., & Duronio, R. J. (2001). Drosophila stem loop binding protein coordinates accumulation of mature histone mRNA with cell cycle progression. *Genes & Development*, *15*(2), 173–187.

Sullivan, K. D., Steiniger, M., & Marzluff, W. F. (2009). A Core Complex of CPSF73, CPSF100, and Symplekin May Form Two Different Cleavage Factors for Processing of Poly(A) and Histone mRNAs. *Molecular Cell*, *34*(3), 322–332.

Sulston, J. E., Schierenberg, E., White, J. G., & Thomson, J. N. (1983). The embryonic cell lineage of the nematode Caenorhabditis elegans. *Developmental Biology*, *100*(1), 64–119.

Sun, J., Yan, L., Shen, W., & Meng, A. (2018). Maternal ybx1 safeguards zebrafish oocyte maturation and maternal-to-zygotic transition by repressing global translation. *Development (Cambridge)*, *145*(19).

Sutton, R. E., & Boothroyd, J. C. (1986). Evidence for trans splicing in trypanosomes. *Cell*, *47*(4), 527–535.

Su, W., Slepenkov, S. V., Slevin, M. K., Lyons, S. M., Ziemniak, M., Kowalska, J., Darzynkiewicz, E., Jemielity, J., Marzluff, W. F., & Rhoads, R. E. (2013). mRNAs containing the histone 3' stem-loop are degraded primarily by decapping mediated by oligouridylation of the 3' end. *RNA (New York, N.Y.)*, *19*(1), 1–16.

Svoboda, P., & Flemr, M. (2010). The role of miRNAs and endogenous siRNAs in maternal-to-zygotic reprogramming and the establishment of pluripotency. *EMBO Reports*, *11*(8), 590–597.

Swarts, D. C., Jore, M. M., Westra, E. R., Zhu, Y., Janssen, J. H., Snijders, A. P., Wang, Y., Patel, D. J., Berenguer, J., Brouns, S. J. J., & Van Der Oost, J. (2014). DNA-guided DNA interference by a prokaryotic Argonaute. *Nature 2014 507:7491*, *507*(7491), 258–261.

Swarts, D. C., Makarova, K., Wang, Y., Nakanishi, K., Ketting, R. F., Koonin, E. V., Patel, D. J., & Van Der Oost, J. (2014). The evolutionary journey of Argonaute proteins. *Nature Structural & Molecular Biology 2014 21:9*, *21*(9), 743–753.

Szenker, E., Ray-Gallet, D., & Almouzni, G. (2011). The double face of the histone variant H3.3. *Cell Research 2011 21:3*, *21*(3), 421–434.

Takahashi, H., Ranjan, A., Chen, S., Suzuki, H., Shibata, M., Hirose, T., Hirose, H., Sasaki, K., Abe, R., Chen, K., He, Y., Zhang, Y., Takigawa, I., Tsukiyama, T., Watanabe, M., Fujii, S., Iida, M., Yamamoto, J., Yamaguchi, Y., … Hatakeyama, S. (2020). The role of Mediator and Little Elongation Complex in transcription termination. *Nature Communications*, *11*(1), 1–20.

Talbert, P. B., & Henikoff, S. (2016). Histone variants on the move: substrates for chromatin dynamics. *Nature Reviews Molecular Cell Biology 2016 18:2*, *18*(2), 115–126.

Tan, D., Marzluff, W. F., Dominski, Z., & Tong, L. (2013). Structure of histone mRNA stem-loop, human stem-loop binding protein, and 3'hExo ternary complex. *Science*, *339*(6117), 318–321.

Tang, W., Tu, S., Lee, H. C., Weng, Z., & Mello, C. C. (2016). The RNase PARN-1 Trims piRNA 3' Ends to Promote Transcriptome Surveillance in C. elegans. *Cell*, *164*(5), 974–984.

Tatomer, D. C., Elrod, N. D., Liang, D., Xiao, M. S., Jiang, J. Z., Jonathan, M., Huang, K. L., Wagner, E. J., Cherry, S., & Wilusz, J. E. (2019). The Integrator complex cleaves nascent mRNAs to attenuate transcription. *Genes & Development*, *33*(21–22), 1525–1538.

Terzo, E. A., Lyons, S. M., Poulton, J. S., Temple, B. R. S., Marzluff, W. F., & Duronio, R. J. (2015). Distinct self-interaction domains promote Multi Sex Combs accumulation in and formation of the Drosophila histone locus body. *Molecular Biology of the Cell*, *26*(8), 1559.

Tharun, S., He, W., Mayes, A. E., Lennertz, P., Beggs, J. D., & Parker, R. (2000). Yeast Sm-like proteins function in mRNA decapping and decay. *Nature 2000 404:6777*, *404*(6777), 515–518.

Thomas, M. F., L'Etoile, N. D., & Ansel, K. M. (2014). Eri1: A Conserved Enzyme at the Crossroads of Multiple RNA Processing Pathways. *Trends in Genetics : TIG*, *30*(7), 298.

Thomsen, S., Anders, S., Janga, S. C., Huber, W., & Alonso, C. R. (2010). Genome-wide analysis of mRNA decay patterns during early Drosophila development. *Genome Biology*, *11*(9), 1–27.

Tian, B., & Manley, J. L. (2016). Alternative polyadenylation of mRNA precursors. *Nature Reviews Molecular Cell Biology 2016 18:1*, *18*(1), 18–30.

Timmons, L., & Fire, A. (1998). Specific interference by ingested dsRNA. *Nature*, *395*(6705), 854.

Toralova, T., Kinterova, V., Chmelikova, E., & Kanka, J. (2020). The neglected part of early embryonic development: maternal protein degradation. *Cellular and Molecular Life Sciences : CMLS*, *77*(16), 3177–3194.

Tourasse, N. J., Millet, J. R. M., & Dupuy, D. (2017). Quantitative RNA-seq meta-analysis of alternative

exon usage in C. elegans. *Genome Research*, *27*(12), 2120–2128.

Tsukamoto, T., Gearhart, M. D., Spike, C. A., Huelgas-Morales, G., Mews, M., Boag, P. R., Beilharz, T. H., & Greenstein, D. (2017). LIN-41 and OMA Ribonucleoprotein Complexes Mediate a Translational Repression-to-Activation Switch Controlling Oocyte Meiotic Maturation and the Oocyte-to-Embryo Transition in Caenorhabditis elegans. *Genetics*, *206*(4), 2007–2039.

Turner, P. C., & Woodland, H. R. (1983). Histone gene number and organisation in Xenopus: Xenopus borealis has a homogeneous major cluster. *Nucleic Acids Research*, *11*(4), 971.

Tusher, V. G., Tibshirani, R., & Chu, G. (2001). Significance analysis of microarrays applied to the ionizing radiation response. *Proceedings of the National Academy of Sciences of the United States of America*, *98*(9), 5116–5121.

Tyers, M., & Jorgensen, P. (2000). Proteolysis and the cell cycle: with this RING I do thee destroy. *Current Opinion in Genetics & Development*, *10*(1), 54–64.

Untergasser, A., Cutcutache, I., Koressaar, T., Ye, J., Faircloth, B. C., Remm, M., & Rozen, S. G. (2012). Primer3--new capabilities and interfaces. *Nucleic Acids Research*, *40*(15).

Updike, D. L., Hachey, S. J., Kreher, J., & Strome, S. (2011). P granules extend the nuclear pore complex environment in the C. elegans germ line. *The Journal of Cell Biology*, *192*(6), 939–948.

Updike, D., & Strome, S. (2010). P granule assembly and function in Caenorhabditis elegans germ cells. *Journal of Andrology*, *31*(1), 53–60.

Ushey, K. (2022). RcppRoll: Efficient Rolling / Windowed Operations. In *CRAN: Contributed Packages*. https://CRAN.R-project.org/package=RcppRoll.

Van Doren, K., & Hirsh, D. (1988). Trans-spliced leader RNA exists as small nuclear ribonucleoprotein particles in Caenorhabditis elegans. *Nature 1988 335:6190*, *335*(6190), 556–559.

van Wolfswinkel, J. C., Claycomb, J. M., Batista, P. J., Mello, C. C., Berezikov, E., & Ketting, R. F. (2009). CDE-1 affects chromosome segregation through uridylation of CSR-1-bound siRNAs. *Cell*, *139*(1), 135–148.

Vastenhouw, N. L., Brunschwig, K., Okihara, K. L., Müller, F., Tijsterman, M., & Plasterk, R. H. A. (2006). Long-term gene silencing by RNAi. *Nature 2006 442:7105*, *442*(7105), 882–882.

Vastenhouw, N. L., Cao, W. X., & Lipshitz, H. D. (2019). The maternal-to-zygotic transition revisited. *Development (Cambridge, England)*, *146*(11).

Vieux, K. F., Prothro, K. P., Kelley, L. H., Palmer, C., Maine, E. M., Veksler-Lublinsky, I., & McJunkin, K. (2021). Screening by deep sequencing reveals mediators of microRNA tailing in C. elegans. *Nucleic Acids Research*, *49*(19), 11167–11180.

Voronina, E., Seydoux, G., Sassone-Corsi, P., & Nagamori, I. (2011). RNA Granules in Germ Cells. *Cold Spring Harbor Perspectives in Biology*, *3*(12), a002774.

Waddell, B. M., & Wu, C. W. (2024). A role for the C. elegans Argonaute protein CSR-1 in small nuclear RNA 3' processing. *PLoS Genetics*, *20*(5).

Wagner, E. J., Tong, L., & Adelman, K. (2023). Integrator is a global promoter-proximal termination complex. *Molecular Cell*, *83*(3), 416–427.

Wahba, L., Hansen, L., & Fire, A. Z. (2021). An essential role for the piRNA pathway in regulating the ribosomal RNA pool in C. elegans. *Developmental Cell*, *56*(16), 2295-2312.e6.

Walker, J., & Bownes, M. (1998). The expression of histone genes during Drosophila melanogaster oogenesis. *Development Genes and Evolution*, *207*(8), 535–541.

Wang, G., & Reinke, V. (2008). A C. elegans Piwi, PRG-1, Regulates 21U-RNAs during Spermatogenesis. *Current Biology*, *18*(12), 861–867.

Wang, M., Liang, A. M., Zhou, Z. Z., Pang, T. L., Fan, Y. J., & Xu, Y. Z. (2023). Deletions of singular U1 snRNA gene significantly interfere with transcription and 3'-end mRNA formation. *PLoS Genetics*, *19*(11 NOVEMBER).

Wang, M., Ly, M., Lugowski, A., Laver, J. D., Lipshitz, H. D., Smibert, C. A., & Rissland, O. S. (2017). ME31B globally represses maternal mRNAs by two distinct mechanisms during the Drosophila maternal-to-zygotic transition. *ELife*, *6*.

Wang, Q. T., Piotrowska, K., Ciemerych, M. A., Milenkovic, L., Scott, M. P., Davis, R. W., & Zernicka-Goetz, M. (2004). A Genome-Wide Study of Gene Activity Reveals Developmental Signaling Pathways in the Preimplantation Mouse Embryo. *Developmental Cell*, *6*(1), 133–144.

Wang, X., Zeng, C., Liao, S., Zhu, Z., Zhang, J., Tu, X., Yao, X., Feng, X., Guang, S., & Xu, C. (2021). Molecular basis

for PICS-mediated piRNA biogenesis and cell division. *Nature Communications 2021 12:1*, *12*(1), 1–14.

Wang, Y., Juranek, S., Li, H., Sheng, G., Tuschl, T., & Patel, D. J. (2008). Structure of an argonaute silencing complex with a seed-containing guide DNA and target RNA duplex. *Nature 2008 456:7224*, *456*(7224), 921–926.

Wang, Y., Weng, C., Chen, X., Zhou, X., Huang, X., Yan, Y., & Zhu, C. (2020). CDE-1 suppresses the production of risiRNA by coupling polyuridylation and degradation of rRNA. *BMC Biology*, *18*(1), 1–13.

Wang, Z.-F., Ingledue, T. C., Dominski, Z., Sanchez, R., & Marzluff, W. F. (1999). Two Xenopus proteins that bind the 3' end of histone mRNA: implications for translational control of histone synthesis during oogenesis. *Molecular and Cellular Biology*, *19*(1), 835–845.

Warkocki, Z., Krawczyk, P. S., Adamska, D., Bijata, K., Garcia-Perez, J. L., & Dziembowski, A. (2018). Uridylation by TUT4/7 Restricts Retrotransposition of Human LINE-1s. *Cell*, *174*(6), 1537-1548.e29.

Wedeles, C. J., Wu, M. Z., & Claycomb, J. M. (2013). Protection of germline gene expression by the C. elegans Argonaute CSR-1. *Developmental Cell*, *27*(6), 664–671.

Weick, E. M., Sarkies, P., Silva, N., Chen, R. A., Moss, S. M. M., Cording, A. C., Ahringer, J., Martinez-Perez, E., & Miska, E. A. (2014). PRDE-1 is a nuclear factor essential for the biogenesis of Ruby motif-dependent piRNAs in C. elegans. *Genes and Development*, *28*(7), 783–796.

Welch, J. D., Slevin, M. K., Tatomer, D. C., Duronio, R. J., Prins, J. F., & Marzluff, W. F. (2015). EnD-Seq and AppEnD: sequencing 3' ends to identify nontemplated tails and degradation intermediates. *RNA*, *21*(7), 1375.

Welsh, S. A., & Gardini, A. (2022). Genomic regulation of transcription and RNA processing by the multitasking Integrator complex. *Nature Reviews Molecular Cell Biology 2022 24:3*, *24*(3), 204–220.

Weng, C., Kosalka, J., Berkyurek, A. C., Stempor, P., Feng, X., Mao, H., Zeng, C., Li, W. J., Yan, Y. H., Dong, M. Q., Morero, N. R., Zuliani, C., Barabas, O., Ahringer, J., Guang, S., & Miska, E. A. (2019). The USTC co-opts an ancient machinery to drive piRNA transcription in C. Elegans. *Genes and Development*, *33*(1–2), 90–102.

Werner, F. (2012). A Nexus for Gene Expression—Molecular Mechanisms of Spt5 and NusG in the Three Domains of Life. *Journal of Molecular Biology*, *417*(1–2), 13–27.

White, A. E., Leslie, M. E., Calvi, B. R., Marzluff, W. F., & Duronio, R. J. (2007). Developmental and Cell Cycle Regulation of the Drosophila Histone Locus Body. *Molecular Biology of the Cell*, *18*(7), 2491.

Whitfield, M. L., Kaygun, H., Erkmann, J. A., Townley-Tilson, W. H. D., Dominski, Z., & Marzluff, W. F. (2004). SLBP is associated with histone mRNA on polyribosomes as a component of the histone mRNP. *Nucleic Acids Research*, *32*(16), 4833.

Whitfield, M. L., Zheng, L.-X., Baldwin, A., Ohta, T., Hurt, M. M., & Marzluff, W. F. (2000). Stem-loop binding protein, the protein that binds the 3' end of histone mRNA, is cell cycle regulated by both translational and posttranslational mechanisms. *Molecular and Cellular Biology*, *20*(12), 4188–4198.

Whittle, C. M., McClinic, K. N., Ercan, S., Zhang, X., Green, R. D., Kelly, W. G., & Lieb, J. D. (2008). The Genomic Distribution and Function of Histone Variant HTZ-1 during C. elegans Embryogenesis. *PLOS Genetics*, *4*(9), e1000187.

Wickham, H. (2022). stringr: Simple, Consistent Wrappers for Common String Operations. In *CRAN: Contributed Packages*.

Wickham, H., François, R., Henry, L., Müller, K., & Vaughan, D. (2023). dplyr: A Grammar of Data Manipulation. In *https://dplyr.tidyverse.org*.

Wickham, H., & Henry, L. (2024). *Purrr: Functional programming tools*. https://github.com/tidyverse/purrr.

Wickham, H., Navarro, D., & Pedersen, T. (2016). *ggplot2: Elegant Graphics for Data Analysis* (3rd ed.). Springer New York. https://ggplot2-book.org/

Wickham, H., Vaughan, D., & Girlich, M. (2024). tidyr: Tidy Messy Data. In *https://tidyr.tidyverse.org*.

Wittkopp, N., Huntzinger, E., Weiler, C., Saulière, J., Schmidt, S., Sonawane, M., & Izaurralde, E. (2009). Nonsense-mediated mRNA decay effectors are essential for zebrafish embryonic development and survival. *Molecular and Cellular Biology*, *29*(13), 3517–3528.

Woodland, H. R., & Adamson, E. D. (1977). The synthesis and storage of histones during the oogenesis of

Xenopus laevis. *Developmental Biology*, *57*(1), 118–135.

Wu, J., Yang, J., Cho, W. C., & Zheng, Y. (2020). Argonaute proteins: Structural features, functions and emerging roles. *Journal of Advanced Research*, *24*, 317–324.

Wu, Q., & Bazzini, A. A. (2023). Translation and mRNA Stability Control. *Annual Review of Biochemistry*, *92*, 227–245.

Wyrick, J. J., Holstege, F. C. P., Jennings, E. G., Causton, H. C., Shore, D., Grustein, M., Lander, E. S., & Young, R. A. (1999). Chromosomal landscape of nucleosome-dependent gene expression and silencing in yeast. *Nature*, *402*(6760), 418–421.

Xing, Y., Yang, W., Liu, G., Cui, X., Meng, H., Zhao, H., Zhao, X., Li, J., Liu, Z., Zhang, M. Q., & Cai, L. (2020). Dynamic Alternative Splicing During Mouse Preimplantation Embryo Development. *Frontiers in Bioengineering and Biotechnology*, *8*, 515146.

Xu, C., Li, C., Chen, J., Xiong, Y., Qiao, Z., Fan, P., Li, C., Ma, S., Liu, J., Song, A., Tao, B., Xu, T., Xu, W., Chi, Y., Xue, J., Wang, P., Ye, D., Gu, H., Zhang, P., … Chen, F. X. (2023a). R-loop-dependent promoter-proximal termination ensures genome stability. *Nature 2023 621:7979*, *621*(7979), 610–619.

Xu, C., Li, C., Chen, J., Xiong, Y., Qiao, Z., Fan, P., Li, C., Ma, S., Liu, J., Song, A., Tao, B., Xu, T., Xu, W., Chi, Y., Xue, J., Wang, P., Ye, D., Gu, H., Zhang, P., … Chen, F. X. (2023b). R-loop-dependent promoter-proximal termination ensures genome stability. *Nature*, *621*(7979), 610–619.

Yamamoto, J., Hagiwara, Y., Chiba, K., Isobe, T., Narita, T., Handa, H., & Yamaguchi, Y. (2014). DSIF and NELF interact with Integrator to specify the correct post-transcriptional fate of snRNA genes. *Nature Communications 2014 5:1*, *5*(1), 1–10.

Yang, G., Xin, Q., & Dean, J. (2024). Degradation and translation of maternal mRNA for embryogenesis. *Trends in Genetics*, *40*(3), 238–249.

Yang, X. C., Purdy, M., Marzluff, W. F., & Dominski, Z. (2006). Characterization of 3'hExo, a 3' exonuclease specifically interacting with the 3' end of histone mRNA. *Journal of Biological Chemistry*, *281*(41), 30447–30454.

Yang, X.-C., Sabath, I., Dębski, J., Kaus-Drobek, M., Dadlez, M., Marzluff, W. F., & Dominski, Z. (2013). A complex containing the CPSF73 endonuclease and other polyadenylation factors associates with U7 snRNP and is recruited to histone pre-mRNA for 3'-end processing. *Molecular and Cellular Biology*, *33*(1), 28–37.

Yang, X. C., Sabath, I., Kunduru, L., Van Wijnen, A. J., Marzluff, W. F., & Dominski, Z. (2014). A conserved interaction that is essential for the biogenesis of histone locus bodies. *The Journal of Biological Chemistry*, *289*(49), 33767–33782.

Yang, Y., Wang, L., Han, X., Yang, W. L., Zhang, M., Ma, H. L., Sun, B. F., Li, A., Xia, J., Chen, J., Heng, J., Wu, B., Chen, Y. S., Xu, J. W., Yang, X., Yao, H., Sun, J., Lyu, C., Wang, H. L., … Yang, Y. G. (2019). RNA 5-Methylcytosine Facilitates the Maternal-to-Zygotic Transition by Preventing Maternal mRNA Decay. *Molecular Cell*, *75*(6), 1188-1202.e11.

Ye, X., Wei, Y., Nalepa, G., & Harper, J. W. (2003). The cyclin E/Cdk2 substrate p220(NPAT) is required for S-phase entry, histone gene expression, and Cajal body maintenance in human somatic cells. *Molecular and Cellular Biology*, *23*(23), 8586–8600.

Yuan, Y. R., Pei, Y., Ma, J. B., Kuryavyi, V., Zhadina, M., Meister, G., Chen, H. Y., Dauter, Z., Tuschl, T., & Patel, D. J. (2005). Crystal Structure of A. aeolicus Argonaute, a Site-Specific DNA-Guided Endoribonuclease, Provides Insights into RISC-Mediated mRNA Cleavage. *Molecular Cell*, *19*(3), 405–419.

Yu, S., & Kim, V. N. (2020). A tale of non-canonical tails: gene regulation by post-transcriptional RNA tailing. *Nature Reviews Molecular Cell Biology*, *21*(9), 542–556.

Zaborowska, J., Egloff, S., & Murphy, S. (2016). The pol II CTD: new twists in the tail. *Nature Structural & Molecular Biology*, *23*(9), 771–777.

Zeng, C., Weng, C., Wang, X., Yan, Y. H., Li, W. J., Xu, D., Hong, M., Liao, S., Dong, M. Q., Feng, X., Xu, C., & Guang, S. (2019). Functional Proteomics Identifies a PICS Complex Required for piRNA Maturation and Chromosome Segregation. *Cell Reports*.

Zhang, C., Montgomery, T. A., Gabel, H. W., Fischer, S. E. J., Phillips, C. M., Fahlgren, N., Sullivan, C. M., Carrington, J. C., & Ruvkun, G. (2011). mut-16 and other mutator class genes modulate 22G and 26G siRNA pathways in Caenorhabditis elegans. *Proceedings of the National Academy of Sciences of the United States of America*, *108*(4), 1201–1208.

Zhang, F., Ma, T., & Yu, X. (2013). A core hSSB1-INTS complex participates in the DNA damage response. *Journal of Cell Science*, *126*(Pt 21), 4850–4855.

Zhang, J. M., Hou, W. B., Du, J. W., Zong, M., Zheng, K. L., Wang, W. J., Wang, J. Q., Zhang, H., Mu, Y. S., Yin, Z., Ding, C. M., Sun, Q. Y., Liu, Z. H., & Kong, Q. R. (2020). Argonaute 2 is a key regulator of maternal mRNA degradation in mouse early embryos. *Cell Death Discovery*, *6*(1), 133.

Zhang, M., Kothari, P., Mullins, M., & Lampson, M. A. (2014). Regulation of zygotic genome activation and DNA damage checkpoint acquisition at the mid-blastula transition. *Cell Cycle*, *13*(24), 3828–3838.

Zhang, M., Lam, T. T., Tonelli, M., Marzluff, W. F., & Thapar, R. (2012). Interaction of the histone mRNA hairpin with stem-loop binding protein (SLBP) and regulation of the SLBP-RNA complex by phosphorylation and proline isomerization. *Biochemistry*, *51*(15), 3215–3231.

Zhao, B. S., Wang, X., Beadell, A. V., Lu, Z., Shi, H., Kuuspalu, A., Ho, R. K., & He, C. (2017). m6A-dependent maternal mRNA clearance facilitates zebrafish maternal-to-zygotic transition. *Nature 2017 542:7642*, *542*(7642), 475–478.

Zhao, C., & Emmons, S. W. (1995). A transcription factor controlling development of peripheral sense organs in C. elegans. *Nature*, *373*(6509), 74–78.

Zhao, J., Kennedy, B. K., Lawrence, B. D., Barbie, D. A., Gregory Matera, A., Fletcher, J. A., & Harlow, E. (2000). NPAT links cyclin E-Cdk2 to the regulation of replication-dependent histone gene transcription. *Genes and Development*, *14*(18), 2283–2297.

Zhao, X., McKillop-Smith, S., & Müller, B. (2004). The human histone gene expression regulator HBP/SLBP is required for histone and DNA synthesis, cell cycle progression and cell proliferation in mitotic cells. *Journal of Cell Science*, *117*(Pt 25), 6043–6051.

Zheng, H., Qi, Y., Hu, S., Cao, X., Xu, C., Yin, Z., Chen, X., Li, Y., Liu, W., Li, J., Wang, J., Wei, G., Liang, K., Chen, F. X., & Xu, Y. (2020). Identification of Integrator-PP2A complex (INTAC), an RNA polymerase II phosphatase. *Science*, *370*(6520).

Zheng, L., Dominski, Z., Yang, X.-C., Elms, P., Raska, C. S., Borchers, C. H., & Marzluff, W. F. (2003). Phosphorylation of stem-loop binding protein (SLBP) on two threonines triggers degradation of SLBP, the sole cell cycle-regulated factor required for regulation of histone mRNA processing, at the end of S phase. *Molecular and Cellular Biology*, *23*(5), 1590–1601.